

SATURN

MPR-SAT-FE-73-4

AUGUST 1, 1973

(NASA-TM-X-69537) SATURN 5 LAUNCH
VEHICLE FLIGHT EVALUATION REPORT, SA-513,
SKYLAB 1 (NASA) 255 p HC \$14.75

N73-33848

CSC L 22B

Unclas

G3/31 19843

SATURN V LAUNCH VEHICLE FLIGHT EVALUATION REPORT-SA-513 SKYLAB 1



PREPARED BY
SATURN FLIGHT EVALUATION WORKING GROUP



NATIONAL AERONAUTICS AND SPACE ADMINISTRATION

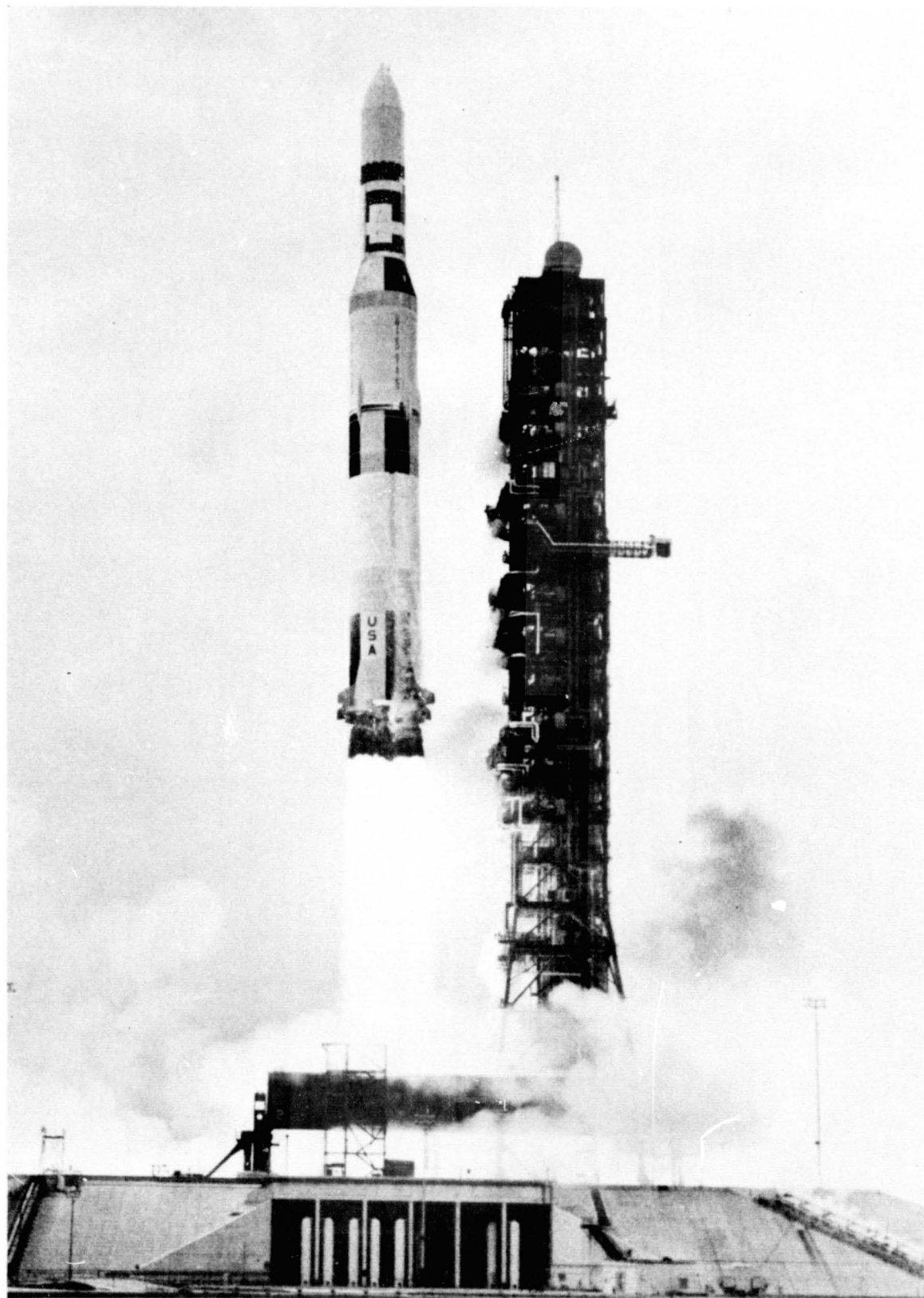
GEORGE C. MARSHALL SPACE FLIGHT CENTER

MPR-SAT-FE-73-4

AUGUST 1, 1973

**SATURN V LAUNCH VEHICLE
FLIGHT EVALUATION
REPORT-SA-513
SKYLAB-1**

PREPARED BY
SATURN FLIGHT EVALUATION
WORKING GROUP



MPR-SAT-FE-73-4

SATURN V LAUNCH VEHICLE FLIGHT EVALUATION REPORT - SA-513

SKYLAB-1

BY

Saturn Flight Evaluation Working Group

George C. Marshall Space Flight Center

ABSTRACT

Saturn V SA-513 (Skylab-1) was launched at 13:30:00 Eastern Daylight Time (EDT) on May 14, 1973, from Kennedy Space Center, Complex 39, Pad A. The vehicle lifted off on a launch azimuth of 90 degrees east of north and rolled to a flight azimuth of 40.88 degrees east of north. The launch vehicle successfully placed the Saturn Work Shop in the planned earth orbit.

All launch vehicle objectives were accomplished. No launch vehicle failures or anomalies occurred that seriously affected the mission.

Any questions or comments pertaining to the information contained in this report are invited and should be directed to:

Director, George C. Marshall Space Flight Center
Huntsville, Alabama 35812
Attention: Chairman, Saturn Flight Evaluation Working
Group, SAT-E (Phone 205-453-1030)

TABLE OF CONTENTS

	Page		Page
TABLE OF CONTENTS	iii	SECTION 5 - S-IC PROPULSION	
LIST OF ILLUSTRATIONS	vii	5.1 Summary	5-1
LIST OF TABLES	xi	5.2 S-IC Ignition Transient Performance	5-1
ACKNOWLEDGEMENT	xiii	5.3 S-IC Mainstage Performance	5-4
ABBREVIATIONS	xiv	5.4 S-IC Engine Shutdown Transient Performance	5-6
MISSION PLAN	xvii	5.5 S-IC Stage Propellant Management	5-6
FLIGHT SUMMARY	xix	5.6 S-IC Pressurization Systems	5-8
MISSION OBJECTIVES ACCOMPLISHMENT	xxv	5.6.1 S-IC Fuel Pressurization System	5-8
FAILURES AND ANOMALIES	xxvii	5.7 S-IC Pneumatic Control Pressure System	5-10
SECTION 1 - Introduction		5.8 S-IC Purge System	5-10
1.1 Purpose	1-1	5.9 S-IC POGO Suppression System	5-10
1.2 Scope	1-1	5.10 S-IC Hydraulic System	5-10
1.3 Performance Predictions Baseline	1-1	SECTION 6 - S-II PROPULSION	
SECTION 2 - EVENT TIMES		6.1 Summary	6-1
2.1 Summary of Events	2-1	6.2 S-II Chilldown and Buildup Transient Performance	6-2
2.2 Variable Time and Commanded Switch Selector Events	2-2	6.3 S-II Mainstage Performance	6-3
SECTION 3 - LAUNCH OPERATIONS		6.4 S-II Shutdown Transient Performance	6-7
3.1 Summary	3-1	6.5 S-II Stage Propellant Management System	6-8
3.2 Prelaunch Milestones	3-1	6.6 S-II Pressurization System	6-10
3.3 Terminal Countdown	3-1	6.6.1 S-II Fuel Pressurization System	6-10
3.4 Propellant Loading	3-1	6.6.2 S-II LOX Pressurization System	6-13
3.4.1 RP-1 Loading	3-1	6.7 S-II Pneumatic Control Pressure System	6-13
3.4.2 LOX Loading	3-3	6.8 S-II Helium Injection System	6-16
3.4.3 LH ₂ Loading	3-3	6.9 POGO Suppression System	6-16
3.5 Ground Support Equipment	3-3	6.10 S-II Orbital Safing Operations	6-18
3.5.1 Ground/Vehicle Interface	3-3	6.10.1 Fuel Tank Safing	6-18
3.5.2 MSFC Furnished Ground Support Equipment	3-4	6.10.2 LOX Tank Safing	6-18
SECTION 4 - TRAJECTORY		6.10.3 Engine Start Sphere Safing	6-18
4.1 Summary	4-1	6.10.4 Engine Control Sphere Safing	6-20
4.2 Trajectory Evaluation	4-1	6.11 S-II Hydraulic System	6-20
4.2.1 Ascent Phase	4-1	SECTION 7 - STRUCTURES	
4.2.2 Earth Orbit Phase	4-2	7.1 Summary	7-1
4.2.3 Meteoroid Shield Debris Impact Trajectory	4-11		
4.2.4 Spent S-II Orbit	4-11		

TABLE OF CONTENTS (CONTINUED)

		Page			Page
7.2	Total Vehicle Structures Evaluation	7-1		SECTION 11 - VEHICLE PRESSURE ENVIRONMENT	
7.2.1	Longitudinal Loads	7-1		11.1	Summary 11-1
7.2.2	Bending Moments	7-3		11.2	Base Pressures 11-1
7.2.3	Combined Loads	7-3		11.2.1	S-IC Base Pressures 11-1
7.2.4	Vehicle Dynamic Characteristics	7-4		11.2.2	S-II Base Pressures 11-1
7.2.5	Vibration Evaluation	7-9		11.3	S-II Forward Skirt Pressures 11-4
7.3	POGO Limiting Backup Cutoff System	7-9		11.4	S-IC/S-II Separation Pressure 11-8
SECTION 8 - GUIDANCE AND NAVIGATION				SECTION 12 - VEHICLE THERMAL ENVIRONMENT	
8.1	Summary	8-1		12.1	Summary 12-1
8.2	Guidance Comparisons	8-1		12.2	S-IC Base Heating 12-1
8.3	Navigation and Guidance Scheme Evaluation	8-6		12.3	S-II Base Heating 12-4
8.3.1	Major Differences From Past Schemes	8-6		12.4	Vehicle Aeroheating Thermal Environment 12-9
8.3.2	Guidance Event Times	8-7		12.5	S-IC/S-II Separation Thermal Environment 12-11
8.3.3	Yaw (Z) Axis Resolver Unreasonable Indication	8-7		SECTION 13 - ENVIRONMENTAL CONTROL SYSTEMS	
8.3.4	Pitch Axis Resolver Switchover	8-8		13.1	Summary 13-1
8.3.5	Attitude Commands	8-8		13.2	S-IC Environmental Control System 13-1
8.3.6	Terminal Conditions	8-9		13.3	S-II Environmental Control 13-2
8.3.7	Orbiter Phase	8-9		13.4	IU Environmental Control 13-2
8.4	Navigation and Guidance System Components	8-10		13.4.1	Thermal Conditioning System (TCS) 13-2
8.4.1	Stabilized Platform System	8-11		13.4.2	Gas Bearing System Performance 13-8
8.4.2	Guidance and Navigation Computer	8-11		13.4.3	Component Temperatures 13-8
SECTION 9 - CONTROL AND SEPARATION				SECTION 14 - DATA SYSTEMS	
9.1	Summary	9-1		14.1	Summary 14-1
9.2	S-IC Control System Evaluation	9-1		14.2	Vehicle Measurement Evaluation 14-1
9.2.1	Liftoff	9-1		14.3	Airborne VHF Telemetry Systems Evaluation 14-1
9.2.2	Inflight Dynamics	9-1		14.4	C-Band Radar System Evaluation 14-2
9.2.3	63-Second Anomaly	9-8		14.5	Secure Range Safety Command Systems 14-10
9.3	S-II Control System Evaluation	9-15		14.6	Command and Communications System Evaluation 14-11
9.4	Instrument Unit Control Components Evaluation	9-18		14.6.1	Summary of Performance 14-11
9.5	Separation	9-18		14.7	Ground Engineering Cameras 14-11
9.5.1	S-IC/S-II Separation	9-18		SECTION 15 - MASS CHARACTERISTICS	
9.5.2	S-II Second Plane Separation Evaluation	9-18		15.1	Summary 15-1
9.5.3	S-II/SWS Separation	9-23		15.2	Mass Evaluation 15-1
SECTION 10 - ELECTRICAL NETWORKS AND EMERGENCY DETECTION SYSTEM				SECTION 16 - SATURN WORK SHOP SUMMARY 16-1	
10.1	Summary	10-1		SECTION 17 - 63 AND 593 SECOND ANOMALIES	
10.2	S-IC Stage Electrical System	10-1		17.1	Summary 17-1
10.3	S-II Stage Electrical System	10-2		17.2	63 Second Anomaly 17-1
10.4	Instrument Unit Electrical Systems	10-3		17.2.1	Initial Vehicle Response 17-1
10.5	Saturn V Emergency Detection System (EDS)	10-4		17.2.2	Initial Orbital Work Shop (OWS) Measurement Response 17-2
				17.2.3	Meteoroid Shield Structural Failure 17-2

TABLE OF CONTENTS (CONTINUED)

		Page
17.3	593 Second Disturbance	17-12
17.4	Meteoroid Shield Failure	17-22
17.5	Conclusions	17-26
17.6	Impact of Anomalies on Launch Vehicle	17-27
17.7	Investigating Committee	17-27

APPENDIX A - ATMOSPHERE

A.1	Summary	A-1
A.2	General Atmospheric Conditions at Launch Time	A-1
A.3	Surface Observations at Launch Time	A-1
A.4	Upper Air Measurements	A-1
A.4.1	Wind Speed	A-1
A.4.2	Wind Direction	A-6
A.4.3	Pitch Wind Component	A-6
A.4.4	Yaw Wind Component	A-6
A.4.5	Component Wind Shears	A-6
A.4.6	Extreme Wind Data in the High Dynamic Region	A-6
A.5	Thermodynamic Data	A-14
A.5.1	Atmospheric Temperature	A-14
A.5.2	Atmospheric Pressure	A-14
A.5.3	Atmospheric Density	A-14
A.5.4	Optical Index of Refraction	A-14
A.6	Comparison of Selected Atmospheric Data for Saturn V Launches	A-14

APPENDIX B - SL-1/SA-513 SIGNIFICANT CONFIGURATION CHANGES

B.1	Introduction	B-1
B.2	S-IC Stage	
B.2.1	S-IC Configuration	B-1
B.2.2	S-IC Systems	B-1
B.3	S-II Stage	B-4
B.3.1	S-II Configuration	B-4
B.3.2	S-II Systems	B-5
B.4	Instrument Unit (IU)	B-7
B.4.1	IU Configuration	B-7
B.4.2	IU Systems	B-9
B.5	Saturn Work Shop (SWS)	B-9
B.5.1	SWS Configuration	B-9

LIST OF ILLUSTRATIONS

Figure		Page	Figure		Page
2-1	SA-513 LVDC Clock/Ground Time Difference	2-2	6-8	S-II LOX Tank Ullage Pressure	6-14
4-1	SA-513 Ascent Trajectory Position Comparison	4-3	6-9	S-II LOX Pump Inlet Conditions	6-15
4-2	SA-513 Ascent Trajectory Space-Fixed Velocity and Flight Path Angle Comparisons	4-4	6-10	S-II Center Engine LOX Feedline Accumulator Bleed System Performance	6-17
4-3	SA-513 Ascent Trajectory Acceleration Comparison	4-5	6-11	S-II Center Engine LOX Feedline Accumulator Fill Transient	6-17
4-4	SA-513 Dynamic Pressure and Mach Number Comparisons	4-6	6-12	S-II Center Engine LOX Feedline Accumulator Helium Supply System Performance	6-18
4-5	SA-513 Launch Vehicle Groundtrack	4-13	6-13	S-II Fuel Tank Ullage Pressure During Safing	6-19
4-6	Impact Footprints for SL-1 Meteoroid Shield Debris	4-14	6-14	S-II LOX Tank Ullage Pressure During Safing	6-19
5-1	S-IC LOX Start Box Requirements	5-2	6-15	S-II Engine GH ₂ Start Tank Safing	6-20
5-2	S-IC Engines Thrust Buildup	5-3	6-16	S-II Engine Helium Tank Safing	6-21
5-3	S-IC Stage Propulsion Performance	5-5	7-1	SA-513 Longitudinal Acceleration at IU During S-IC Thrust Buildup and Launch	7-2
5-4	S-IC Outboard Engine Thrust Decay	5-7	7-2	SA-513 Longitudinal Acceleration at IU at Time of S-IC Engine Cutoff	7-2
5-5	S-IC Fuel Tank Ullage Pressure	5-8	7-3	SA-513 Longitudinal Acceleration at IU During S-II Thrust Decay and S-II/SWS Separation	7-3
5-6	S-IC LOX Tank Ullage Pressure	5-9	7-4	SA-513 Longitudinal Load Distribution at Time of Maximum Bending Moment, CECO and OECO	7-4
6-1	S-II Engine Start Tank Performance	6-2	7-5	SA-513 Maximum Bending Moment	7-5
6-2	S-II Engine Pump Inlet Start Requirements	6-4	7-6	SA-513 Lateral Acceleration During Thrust Buildup and Launch	7-5
6-3	S-II Engine Thrust Buildup Transients	6-5	7-7	SA-513 Envelope of Maximum Combined Loads	7-6
6-4	S-II Steady State Operation	6-6	7-8	SA-513 Modal Activity (Longitudinal)	7-7
6-5	S-II Outboard Engines Thrust Decay	6-8	7-9	SA-513 Modal Activity (Lateral)	7-8
6-6	S-II Fuel Tank Ullage Pressure	6-11	7-10	IU, Upper Mounting Ring Data PSD Comparison	7-10
6-7	S-II Fuel Pump Inlet Conditions	6-12	8-1	SA-513 Trajectory and ST-124M Platform Velocity Comparisons, Boost-to-Orbit Insertion (Trajectory Minus LVDC)	8-2

LIST OF ILLUSTRATIONS (CONTINUED)

Figure		Page	Figure		Page
8-2	SA-513 Actual and Predicted Velocity Gained After GCS	8-5	11-4	S-II Heat Shield Aft Face Pressure	11-6
8-3	Attitude Commands	8-9	11-5	S-II/OWS Interstage Pressure	11-7
9-1	Pitch Plane Dynamics During S-IC Burn	9-3	12-1	S-IC Base Region Total Heating Rate	12-2
9-2	Yaw Plane Dynamics During S-IC Burn	9-4	12-2	S-IC Base Region Gas Temperature	12-3
9-3	Roll Dynamics During S-IC Burn	9-5	12-3	S-IC Thermal Environments Ambient Gas Temperature Under Engine Cocoon	12-4
9-4	Pitch and Yaw Plane Free Stream Angle of Attack During S-IC Burn	9-6	12-4	S-II Heat Shield Aft Heat Rate	12-5
9-5	SA-513 LH ₂ Peak-to-Peak Slosh Mass Displacement	9-9	12-5	S-II Heat Shield Recovery Temperature	12-5
9-6	Pitch Plane Dynamics During 63-Second Anomaly	9-10	12-6	S-II Heat Shield Aft Radiation Heat Rate	12-7
9-7	Yaw Plane Dynamics During 63-Second Anomaly	9-11	12-7	S-II Thrust Cone Forward Surface Temperature	12-7
9-8	Roll Plane Dynamics During the 63-Second Anomaly	9-12	12-8	Estimate of Maximum Predicted S-II Thrust Cone Temperatures	12-8
9-9	Lateral IU Acceleration During 63-Second Anomaly	9-13	12-9	S-II Engine Compartment Gas Temperature (C674-206)	12-8
9-10	Pitch and Yaw Plane Free Stream Angle of Attack During 63-Second Anomaly	9-14	12-10	S-II Engine Compartment Gas Temperature (C676-206)	12-9
9-11	Pitch Plane Dynamics During S-II Burn	9-16	12-11	S-II Engine Actuation System Reservoir Oil Temperature (Engine 4 Typical)	12-10
9-12	Yaw Plane Dynamics During S-II Burn	9-17	12-12	SA-513 Predicted Location of Separated Flow	12-11
9-13	SA-513 S-II Base Region Pressures	9-20	13-1	IU Sublimator Start-Up Parameters (Initial Cycle)	13-3
9-14	SA 513 S-II Thrust Cone Forward Surface Temperature	9-21	13-2	IU TCS Coolant Control Parameters	13-5
9-15	S-II Interstage Separation Diagram	9-24	13-3	IU TCS Hydraulic Performance	13-6
9-16	S-II-13 Interstage Station 196 Tension Strap Analysis	9-25	13-4	IU TCS GN ₂ Sphere Pressure (D25-603)	13-7
9-17	Attitude Errors at S-II/SWS Staging	9-26	13-5	IU Inertial Platform GN ₂ Pressures	13-9
9-18	S-II Distance Relative to Skylab at S-II Safing	9-27	13-6	IU GBS GN ₂ Sphere Pressure (D10-603)	13-10
10-1	IU 6D10 Battery Parameters	10-5	13-7	IU Selected Component Temperatures	13-11
10-2	IU 6D20 Battery Parameters	10-6	13-8	IU Selected Component Temperatures	13-12
10-3	IU 6D30 Battery Parameters	10-7	14-1	S-II Stage VHF Telemetry Ground Station Coverage Time	14-4
10-4	IU 6D40 Battery Parameters	10-8	14-2	Instrument Unit VHF Telemetry Ground Station Coverage Time	14-5
11-1	S-IC Base Heat Shield Differential Pressure	11-2	14-3	C-Band Acquisition and Loss Times	14-6
11-2	S-II Heat Shield Forward Face Pressure	11-3	14-4	CCS Coverage (Sheet 1 of 3)	14-7
11-3	S-II Thrust Cone Pressure	11-5	17-1	Propagation of the 63-Second Transient	17-3
			17-2	SA-513 R 11 Inertial Attitude Angle Transients During 63-Second Anomaly	17-4
			17-3	OWS Instrumentation Timeline for 63-Second Anomaly	17-5

LIST OF ILLUSTRATIONS (CONTINUED)

Figure		Page	Figure		Page
17-4	OWS Instrumentation Location	17-6	A-7	Pitch (S_x) and Yaw (S_z) Component Wind Shears at Launch Time of SA-513 (SL-1)	A-11
17-5	OWS Meteoroid Shield Instrumentation External View	17-7	A-8	Relative Deviation of Temperature and Pressure from the PRA-63 Reference Atmosphere, SA-513 (SL-1)	A-15
17-6	OWS Configuration During Meteoroid Shield Structure Failure (Artist Concept)	17-8	A-9	Relative Deviation of Density and Absolute Deviation of the Index of Refraction From the PRA-63 Reference Atmosphere, SA-513 (SL-1)	A-16
17-7	S-II Stage Engine No. 1 Actuator Response to the 63-Second Transient	17-10	B-1	Skylab Space Vehicle Configuration	B-2
17-8	OWS Exterior During SL-2 CSM Flyaround Inspection	17-11	B-2	S-IC Stage Configuration	B-3
17-9	Simulated Force and Total Impulse	17-17	B-3	S-II Stage Configuration	B-6
17-10	Comparison of Actual and Simulated Lateral IU Acceleration During 63-Second Anomaly	17-18	B-4	Instrument Unit Configuration	B-8
17-11	Comparison of Actual and Simulated Roll Rate During 63-Second Anomaly	17-19	B-5	Saturn Work Shop (SWS) in Orbital Configuration	B-11
17-12	SAS Wing 2 Instrumentation Timeline for 593 Second Anomaly	17-21	B-6	Saturn Work Shop Habitable Area	B-13
17-13	Instrumentation Location and OWS Configuration Near 593 Seconds	17-23			
17-14	Interpretation of IU Control Measurements During 593-Second Period	17-24			
17-15	Meteoroid Shield-Flow Through Auxiliary Tunnel	17-25			
17-16	Meteoroid Shield Response	17-25			
17-17	SL-1 Auxiliary Tunnel Calculated Pressure Distribution at 63 Seconds	17-26			
A-1	Surface Weather Map Approximately 5 1/2 Hours Before Launch of SA-513	A-2			
A-2	500 Millibar Map Approximately 5 1/2 Hours Before Launch of SA-513	A-4			
A-3	Scalar Wind Speed at Launch Time of SA-513 (SL-1)	A-7			
A-4	Wind Direction at Launch Time of SA-513 (SL-1)	A-8			
A-5	Pitch Wind Velocity Component (W_x) at Launch Time of SA-513 (SL-1)	A-9			
A-6	Yaw Wind Velocity Component (W_z) at Launch Time of SA-513 (SL-1)	A-10			

LIST OF TABLES

Table		Page	Table		Page
1	Mission Objective Accomplishments	xxv	8-3	SA-513 Navigation Comparisons (PACSS-13)	8-5
2-1	Time Base Summary	2-1	8-4	SA-513 Start Times for IGM Guidance Commands	8-7
2-2	Significant Event Times Summary	2-3	8-5	SA-513 End Conditions	8-10
2-3	Variable Time and Commanded Switch Selector Events	2-7	8-6	SA-513 Orbital-Phase Commanded Attitude Angles	8-10
3-1	SA-513/SL-1 Prelaunch Milestones	3-2	9-1	SA-513 Liftoff Conditions Misalignment Summary	9-2
4-1	Comparison of Significant SA-513 Trajectory Events	4-7	9-2	Maximum Control Parameters During S-IC Burn	9-7
4-2	Comparison of SA-513 S-IC Cutoff Events	4-8	9-3	Maximum Control Parameters During S-II Burn	9-15
4-3	Comparison of SA-513 S-II Cutoff Events	4-9	10-1	S-IC Stage Battery Power Consumption	10-1
4-4	Comparison of SA-513 Separation Events	4-10	10-2	S-II Stage Battery Power Consumption	10-2
4-5	Comparison of SA-513 Earth Orbit Insertion Conditions	4-12	10-3	IU Battery Power Consumption	10-4
4-6	SA-513 Comparison of Spent S-II Stage Orbital Parameters at 2 Hours Range Time	4-15	14-1	SA-513 Measurement Summary	14-2
4-7	SA-513 Spent S-II Stage Orbital Parameters on Sixth Revolution	4-16	14-2	SA-513 Flight Measurements Waived Prior to Flight	14-3
5-1	F-1 Engine Systems Buildup Times	5-2	14-3	SA-513 Measurement Malfunctions	14-3
5-2	S-IC Individual Standard Sea Level Engine Performance	5-4	14-4	SA-513 Questionable Flight Measurements	14-3
5-3	S-IC Propellant Mass History	5-7	14-5	SA-513 Launch Vehicle Telemetry Links	14-10
6-1	S-II Engine Performance	6-7	14-6	Command and Communication System Command History, SA-513	14-12
6-2	SA-513 Flight Flight S-II Propellant Mass History	6-9	15-1	Total Vehicle Mass - S-IC Burn Phase - Kilograms	15-3
8-1	SA-513 Inertial Platform Velocity Comparisons	8-3	15-2	Total Vehicle Mass - S-IC Burn Phase - Pounds	15-3
8-2	SA-513 Velocity Gain After Guidance Cutoff Signal	8-4	15-3	Total Vehicle Mass - S-II Burn Phase - Kilograms	15-4
			15-4	Total Vehicle Mass - S-II Burn Phase - Pounds	15-4

LIST OF TABLES (CONTINUED)

Table		Page
15-5	Flight Sequence Mass Summary	15-5
15-6	Mass Characteristics Comparison	15-6
17-1	Meteoroid Shield Failure Event Correlation	17-9
17-2	OWS Meteoroid Shield Torsion Rod Indicated Positions	17-13
17-3	Sequential Summary of Events Related to 63-Second Anomaly	17-14
17-4	Sequential Summary of Events Related to 593-Second Anomaly	17-20
A-1	Surface Observations at SA-513 Launch Time	A-3
A-2	Systems Used to Measure Upper Air Wind Data for SA-513	A-5
A-3	Maximum Wind Speed in High Dynamic Pressure Region for Apollo/Saturn 501 through Saturn 513 Vehicles	A-12
A-4	Extreme Wind Shear Values in the High Dynamic Pressure Region for Apollo/Saturn 501 through Saturn 513 Vehicles	A-13
A-5	Selected Atmospheric Observations for Apollo/Saturn 501 through Saturn 513 Vehicle Launches at Kennedy Space Center, Florida	A-17
B-1	S-IC Significant Configuration Changes	B-5
B-2	S-II Significant Configuration Changes	B-7
B-3	IU Significant Configuration Differences Between IU-512 and IU-513	B-10

ACKNOWLEDGEMENT

This report is published by the Saturn Flight Evaluation Working Group, composed of representatives of Marshall Space Flight Center, Kennedy Space Center, and MSFC's prime contractors, and in cooperation with the Johnson Space Center. Significant contributions to the evaluation have been made by:

George C. Marshall Space Flight Center

Science and Engineering

Aero-Astroynamics Laboratory

Astrionics Laboratory

Computation Laboratory

Astronautics Laboratory

Saturn Program Office

Skylab Program Office

John F. Kennedy Space Center

The Boeing Company

International Business Machines Corporation

Rockwell International/Space Division

Rockwell International/Rocketdyne Division

General Electric Company

ABBREVIATIONS

ACN	Ascension Island	DAC	Data Acquisition Camera
ACS	Alternating Current Power Supply	DDAS	Digital Data Acquisition System
AM	Airlock Module	DEE	Digital Events Evaluator
ANT	Antigua	EBW	Exploding Bridge Wire
AOS	Acquisition of Signal	ECO	Engine Cutoff
ARIA	Apollo Range Instrument Aircraft	ECP	Engineering Change Proposal
ATM/DA	Apollo Telescope Mount Deployment Assembly	ECS	Environmental Control System
ATM	Apollo Telescope Mount	EDS	Emergency Detection System
BDA	Bermuda	EDT	Eastern Daylight Time
CCS	Command and Communications System	EMR	Engine Mixture Ratio
CCW	Counter Clockwise	ESC	Engine Start Command
CDDT	Countdown Demonstration Test	EST	Eastern Standard Time
CECO	Center Engine Cutoff	FAS	Fixed Airlock Shroud
CIF	Central Instrumentation Facility	FCC	Flight Control Computer
CG	Center of Gravity	FM/FM	Frequency Modulation/ Frequency Modulation
CM	Command Module	FRT	Flight Readiness Test
CNV	Cape Kennedy	FWD	Forward
CRO	Carnarvon	GBI	Grand Bahama Island
CRP	Computer Reset Pulse	GBS	Gas Bearing System
CSM	Command and Service Module	GCS	Guidance Cutoff Signal
CT4	Cape Telemetry 4	GDS	Goldstone
CVS	Continuous Vent System	GG	Gas Generator
CW	Clockwise	GOX	Gaseous Oxygen
CYI	Canary Island	GRR	Guidance Reference Release
		GSCU	Ground Service Cooling Unit

ABBREVIATIONS (CONTINUED)

GSE	Ground Support Equipment	MAD	Madrid
GTK	Grand Turk Island	MAP	Message Acceptance Pulse
GWM	Guam	MDA	Multiple Docking Adapter
HAW	Hawaii	MILA	Merritt Island Launch Area
HDA	Holddown Arm	ML	Mobile Launcher
HE	Helium	MLC	Mobile Launcher Computer
HFCV	Helium Flow Control Valve	MR	Mixture Ratio
HSK	Honeysuckle Creek	MRCV	Mixture Ratio Control Valve
ICD	Interface Control Document	MS	Meteoroid Shield
IGM	Iterative Guidance Mode	MSFC	Marshall Space Flight Center
IMU	Inertial Measurement Unit	MSFN	Manned Space Flight Network
IS	Interstage	MTG	Mounting
IU	Instrument Unit	NASA	National Aeronautics and Space Administration
JSC	Johnson Space Center	NFL	Newfoundland
KSC	Kennedy Space Center	NPSP	Net Positive Suction Pressure
KW	Kilowatt	NPV	Nonpropulsive Vent
LH ₂	Liquid Hydrogen	OA	Orbital Assembly (SWS Plus A CSM)
LMR	Launch Mission Rule	OAT	Overall Test
LOR	Lunar Orbit Rendezvous	OECO	Outboard Engine Cutoff
LOS	Loss of Signal	OI	Orbit Insertion
LOX	Liquid Oxygen	OMPT	Observed Mass Point Trajectory
LSC	Linear Shaped Charge	OT	Operational Trajectory
LUT	Launch Umbilical Tower	OWS	Orbital Work Shop (A Modified S-IVB Stage)
LV	Launch Vehicle		
LVDA	Launch Vehicle Data Adapter		
LVDC	Launch Vehicle Digital Computer		
LVGSE	Launch Vehicle Ground Support Equipment		

ABBREVIATIONS (CONTINUED)

PACSS	Project Apollo Coordinate System Standards	SL	Skylab
PAFB	Patrick Air Force Base	SM	Service Module
PCB	Printed Circuit Board	SRSCS	Secure Range Safety Command System
PCM	Pulse Code Modulation	STDV	Start Tank Discharge Valve
PCM/FM	Pulse Code Modulation/Frequency Modulation	SV	Space Vehicle
PIO	Process Input/Output	SWS	Saturn Work Shop (OWS, AM, MDA, ATM, PS and IU)
PRA	Patrick Reference Atmosphere	TACS	Thruster Attitude Control System
PS	Payload Shroud	TCS	Thermal Conditioning System
PTCS	Propellant Tanking Computer System	TCS	Terminal Countdown Sequencer
PU	Propellant Utilization	TEX	Corpus Christi (Texas)
PWM	Pulse Width Modulator	TM	Telemetry
q	Free Stream Dynamic Pressure	TSM	Tail Service Mast
RACS	Remote Automatic Calibration System	TVC	Thrust Vector Control
RF	Radio Frequency	USB	Unified S-Band
RP-1	Hydrocarbon Fuel (S-IC Stage)	UT	Universal Time
SA	Saturn	VA	Volt Amperes
SA	Service Arm	VAN	Vanguard (Ship)
SACS	Service Arm Control Switches	VDC	Volts Direct Current
SAS	Solar Array System	VHF	Very High Frequency
SC	Spacecraft	VIB	Vibration
SCFM	Standard Cubic Feet per Minute	WLP	Wallops Island
SCIM	Standard Cubic Inch per Minute		

MISSION PLAN

The Saturn V SA-513 (Skylab-1) is to place the Saturn Work Shop (SWS) in a nearly circular earth orbit at an altitude of 234 n. mi. and inclined 50° to the equator. SA-513 is comprised of the S-IC-13, S-II-13, and the Instrument Unit (IU)-513. This is the first flight in the Skylab Program and the only planned flight incorporating the SWS payload.

Launch is scheduled to occur on the 14th of May 1973 from Launch Complex 39, Pad A of the Kennedy Space Center (KSC) at 1:30 p.m., EDT. The vehicle is aligned along a 90° azimuth at liftoff. Following liftoff the vehicle rolls to a flight azimuth of approximately 41° measured east of north. Vehicle weight at ignition is nominally 6,297,336 lbm.

The S-IC stage powered flight lasts approximately 158 seconds. The S-II stage provides powered flight for approximately 430 seconds inserting the SWS into its circular orbit. Separation of the SWS from the S-II will be accomplished through the use of retro-motors located on the S-II stage whose thrust places the S-II into an elliptical orbit of 234 x 197 n. mi. altitude. Vehicle weight at Guidance Cutoff Signal (GCS) is nominally 319,129 lbm. SWS weight after separation is nominally 197,180 lbm.

A maneuver of the SWS to the local vertical attitude will be commanded from the IU at 599 seconds. The payload shroud (nominally 25,640 lbm) will be jettisoned from this attitude at approximately 908 seconds.

The next planned attitude change will place the SWS into a solar inertial body attitude with the positive Z body axis pointed at the center of the sun and the X body axis in the orbital plane and pointing in the direction of the sunset terminator. This orientation is to be maintained until control is transferred to the Apollo Telescope Mount (ATM).

ATM and associated solar array deployment are accomplished under the direction of the IU nominally at 998 and 1492 seconds, respectively. ATM telemetry is activated at approximately 2208 seconds.

Orbital Work Shop (OWS) solar arrays are to be deployed at 2463 seconds, and the meteoroid shield is to be deployed at 5763 seconds to provide OWS thermal control capability. Command of the Thruster Attitude Control System is transferred to the ATM digital computer at 17,400 seconds.

No experiments are assigned to the SA-513 launch vehicle.

FLIGHT SUMMARY

The first launch vehicle of the Skylab series, SA-513 (Skylab-1), was launched at 13:30:00 Eastern Daylight Time (EDT) on May 14, 1973, from Pad 39A of the Kennedy Space Center. The performance of the launch vehicle was satisfactory and all MSFC objectives were accomplished.

The ground systems supporting the SA-513/Skylab-1 countdown and launch performed satisfactorily except for the occurrence of LVGSE Mobile Launcher computer drum read errors. This malfunction caused no launch delay. There were no unscheduled holds in the countdown. Damage to the pad, Launch Umbilical Tower (LUT) and support equipment was considered minimal.

The vehicle was launched on an azimuth 90 degrees east of north. A roll maneuver was initiated at 12.2 seconds that placed the vehicle on a flight azimuth of 40.880 degrees east of north. The trajectory parameters were close to nominal except the S-IC velocity which was 18.0 meters per second greater than nominal at the outboard engine cutoffs. The largest contributors to this velocity have been identified as the tailwind and higher stage specific impulse. S-II stage performance deviated from nominal because the aft interstage failed to separate. The Saturn Work Shop (SWS) insertion conditions were achieved 0.64 second later than nominal with altitude nominal and velocity 0.6 meter per second greater than nominal. Orbital insertion parameters of the spent S-II stage deviated slightly from nominal but recontact with the SWS was precluded for at least eight months.

All S-IC propulsion systems performed satisfactorily. The propulsion performance was very close to the predicted nominal. Overall stage site thrust was 0.07 percent higher than predicted. Total propellant consumption rate was 0.11 percent lower than predicted and the total consumed mixture ratio was 0.46 percent higher than predicted. Specific impulse was 0.18 percent higher than predicted. Total propellant consumption from Holddown Arm release to Outboard Engines Cutoff (OECO) was low by 0.18 percent. The F-1 engine model specification LOX pump inlet total pressure upper limit of 150 psia was exceeded by all engines at Center Engine Cutoff (CECO) as predicted. Engine 5 exceeded the specification by 4 psia and Engines 1, 2, 3, and 4 by 2 psia. The higher pressures are attributed to the higher boost acceleration schedule for the Skylab mission than for Apollo and caused no problem for flight. The F-1 engine shutdown sequence was changed from the 1-4 sequence used on previous flights to a 1-2-2 sequence (Engines 5, 1-3, 2-4) to reduce vehicle dynamics. CECO was initiated by the Instrument Unit (IU) at 140.72 seconds, 0.02 seconds later than planned. OECO was initiated by the LOX depletion sensors for engine pair 1-3 at 158.16

seconds and for engine pair 2-4 at 158.23 as predicted. At OECO of engine pair 1-3, the LOX residual was 30,582 lbm compared to the predicted 37,175 lbm and the fuel residual was 27,727 lbm compared to the predicted 31,337 lbm. The S-IC hydraulic system performed satisfactorily.

The S-II propulsion systems performed satisfactorily throughout the flight. The S-II Engine Start Command (ESC), as sensed at the engines, occurred at 160.61 seconds. CECO was initiated by the Instrument Unit (IU), based on characteristics velocity, at 314.05 seconds. OECO, initiated by an IU velocity signal, occurred at 588.99 seconds giving an outboard engine operating time of 428.38 seconds or 0.7 seconds longer than predicted. Engine mainstage performance was satisfactory throughout flight. The total stage thrust at the standard time slice (61 seconds after S-II ESC) was 0.13 percent below predicted. Total propellant flowrate, including pressurization flow, was 0.18 percent below predicted, and the stage specific impulse was 0.05 percent above predicted at the standard time slice. Stage propellant mixture ratio was 0.54 percent below predicted. Engine thrust buildup and cutoff transients were within the predicted envelopes. The propellant management system performance was satisfactory throughout loading and flight, and all parameters were nominal. Propellant residuals at OECO were 16,616 lbm LOX, 2319 lbm less than predicted and 5878 lbm LH₂, 319 lbm less than predicted. Control of Engine Mixture Ratio (EMR) was accomplished with the two-position pneumatically operated mixture ratio control valves. The low EMR step occurred 1.1 seconds later, relative to ESC, than predicted. The performance of the LOX and LH₂ tank pressurization systems were satisfactory. Ullage pressure in both tanks was adequate to meet or exceed engine inlet net positive suction pressure minimum requirements throughout mainstage. The engine servicing, recirculation, helium injection, and valve actuation systems performed satisfactorily. All orbital safing operations were performed satisfactorily. Safing of the LH₂ and LOX propellant tanks was verified by ullage pressures which decayed to less than 50% of design burst values. The engine helium and hydrogen pressure spheres were safed successfully when the vent valves were opened at 805.1 seconds. S-II hydraulic system performance was normal throughout the flight.

Evaluation of the structural performance of the launch vehicle shows no area of concern for the SA-513 vehicle, and all conditions were well within the envelope observed on recent Apollo flights. The maximum structural loads were experienced during the S-IC boost phase and were below the design values. The maximum bending moment was 82×10^6 lbf-in at the S-IC LOX tank (approximately 40 percent of the design value). The maximum longitudinal transient responses at the IU were +0.15 g and +0.05 g and occurred at S-IC CECO and OECO, respectively. These values are lower than those observed on recent flights. During S-IC boost phase the expected small oscillatory response in the first longitudinal mode (6 Hz) was observed from approximately 95 seconds until CECO. The Instrument Unit sensors reached +0.06 g just prior to CECO. This is the

same level experienced on AS-512 and AS-511. POGO did not occur during S-II boost. The SA-513 vibration levels were similar at liftoff and lower during subsequent flight as compared to those experienced on previous missions.

The Guidance and Navigation System successfully supported the accomplishment of all guidance and navigation mission objectives with no discrepancies in performance of the hardware. The end conditions at orbit insertion were attained with insignificant error. An anomaly related to the flight program occurred at 3805 seconds, during the first orbital revolution. This was a switch from the inertial platform pitch axis gimbal fine resolver to the backup gimbal resolver. A single test failure of the yaw axis gimbal resolver "Zero Reasonableness Test" occurred at 190 seconds. Guidance and navigation system components responded to the physical excitations experienced by the vehicle at 63 and 593 seconds. A change in the navigation scheme was instituted on this flight to avoid the possibility of introducing significant errors because of lateral accelerometer pickups limiting against their mechanical stops during liftoff. However, telemetry data indicated that no limiting occurred. The guidance scheme was modified to include inertially-referenced pitch, as well as yaw, commands for the tower clearance maneuver because of the orientation of the platform coordinate system, required by the northerly flight azimuth. A yaw steering command profile based on increased anticipated cross-wind components was added to the atmospheric-boost phase of guidance.

The control systems functioned correctly throughout the flight of SA-513. Engine gimbal deflections were nominal. Bending and slosh dynamics were adequately stabilized. No undue dynamics accompanied any separation, however, the S-IC/S-II interstage failed to separate and caused high temperature and pressures in the S-II thrust cone region during the S-II burn. The failure is attributed to damage to the linear shaped charge or its cover resulting from Orbital Work Shop (OWS) meteoroid shield debris.

The SA-513 launch vehicle electrical systems performed satisfactorily. The emergency detection system, in an open loop configuration, functioned properly. The operation of the batteries, power supplies and switch selectors was normal. All exploding bridge wire firing units performed normally including the S-II second plane separation EBW firing units.

The SA-513 base pressures were similar to Apollo flights except for the effect of the S-II second plane separation failure. The S-IC base heat shield was instrumented with two differential pressure measurements. The S-IC flight data show trends and magnitudes similar to the Apollo flight data. The S-II base region contained three absolute pressure measurements. The measurement on the aft face of the heat shield showed a similar trend and magnitude to Apollo flight data. Measurements on the

forward face of the heat shield and thrust cone surface agreed with Apollo flight data up to the time of second plane separation. Following the time of second plane separation, however, the data from these measurements remain at a higher level than that seen during the Apollo flights. These higher levels, along with other anomalous data led to the conclusion that the S-IC/S-II interstage had failed to separate. S-II forward skirt pressure showed a more rapid decrease in pressure than was expected after 67 seconds, indicating a leak in that area probably caused by damage from meteoroid shield debris.

The thermal environments of the base regions of the SA-513 stages were nominal except for the effect of S-II stage second plane separation failure. The S-II base region thermal environment was expected to be about the same as that experienced on Apollo flights. However, the S-IC/S-II interstage failed to separate; consequently, the thrust cone region temperatures following scheduled time of separation were greater than experienced during Apollo flights. Aerodynamic heating environments were not measured on SA-513. Since the S-IC/S-II separation dynamics for SA-513 were nominal, the heating rates to the S-IC forward dome and S-II base area during separation were well below maximum allowable values.

Environmental control system performance was satisfactory. The S-IC stage forward compartment and aft compartment thermal environments were adequately maintained throughout the launch countdown and S-IC boost phase. The S-II stage engine compartment conditioning system maintained the ambient temperature and thrust cone surface temperatures within design ranges throughout the launch countdown. The system also maintained an inert atmosphere within the compartment. The IU stage environmental control system maintained coolant temperatures, pressures, and flowrates continuously within the required ranges and design limits.

All data systems performed satisfactorily throughout the flight. Flight measurements from onboard telemetry were 99.7 percent reliable. Telemetry performance was satisfactory and no hardware anomalies were observed. Radio Frequency (RF) propagation was satisfactory, though the usual interference due to flame effects and staging were experienced. Usable Very High Frequency (VHF) data were received until 67,620 seconds (18:47:00). The Secure Range Safety Command Systems (SRSCS) on the S-IC and S-II stages were ready to perform their functions properly, on command, if flight conditions during launch phase had required destruct. The system properly safed the S-II destruct system on a command transmitted shortly after completion of powered flight (589 seconds). The performance of the Command Communications System (CCS) was satisfactory from liftoff through 151,200 seconds (42:40:45. Good tracking data were received from the C-Band radar, with Hawaii (HAW) indicating last record of interrogation at 16,915 seconds (4:41:55). In general, ground engineering camera coverage was good; however, there was no coverage of the 63 second anomaly because of cloud cover.

Total vehicle mass, determined from post-flight analysis, was within 1.91 percent of prediction from ground ignition through S-II stage shutdown. This larger than anticipated difference was due mainly to the S-IC/S-II interstage not separating as expected. Had the S-II stage residuals and OWS not been 4900 pounds less than predicted, this percentage would have been greater.

Skylab-1 launch vehicle instrumentation recorded unusual disturbances at approximately 63 and 593 seconds during flight. The first evidence of anomalous behavior was an increase in S-II stage antenna reflected power beginning at 59.87 seconds. At 62.76 seconds the Work Shop film vault vibration measurement recorded a structural transient which propagated up and down the space vehicle. At approximately 593 seconds, immediately after S-II/OWS separation, another transient was recorded on the IU and Orbital Work Shop (OWS) instrumentation. The cause of the transient at 63 seconds was structural failure and release of the Orbital Work Shop (OWS) meteoroid shield, and premature fracture of the OWS Solar Array System (SAS) Wing No. 2 tie down fittings, permitting Wing No. 2 to partially deploy. The 593 second transient was caused by the partially deployed SAS Wing No. 2 being rotated past its fully deployed position and torn from its hinges by impingement of the S-II retro plume. The vehicle reacted properly to the disturbances originating at the OWS. The origin of this anomaly was in a unique payload and external to the launch vehicle; therefore, no launch vehicle corrective action is planned. The only significant effect was the damage causing the S-II second plane separation failure.

The planned Saturn Work Shop (SWS) activation and deployment functions occurred as scheduled except for the solar array wing problems, with transfer of attitude control from the IU to the ATM at approximately 4 hours and 50 minutes. The payload shroud was jettisoned, and the Apollo Telescope Mount (ATM) and its solar array were deployed as planned during the first orbit. The OWS solar array Wing No. 1 released as planned during the first orbit but stopped after only a few degrees of movement. This array was restrained from further movement by debris from the meteoroid shield.

The first astronaut crew arrived at the SWS on May 25, 1973. After a flyaround inspection and a soft docking, the crew undocked and attempted to free the solar array Wing No. 1 using special tools while standing in the open command module hatch. This activity was not successful. A later attempt on mission day 14 using Skylab extravehicular activity facilities was successful in deploying the wing which subsequently operated normally.

The crew completed the deactivation procedures and left the SWS on June 22, 1973, after a stay of 28 days.

MISSION OBJECTIVES ACCOMPLISHMENT

Table 1 presents the Marshall Space Flight Center (MSFC) launch vehicle objectives for Skylab 1 as defined in the "Saturn Mission Implementation Plan SL-1/SA-513," MSFC Document PM-SAT-8010.21, Revision A, dated March 30, 1973. An assessment of the degree of accomplishment of each objective is shown. Discussion supporting the assessment can be found in other sections of this report as shown in Table 1.

Table 1. Mission Objective Accomplishments

NO.	LAUNCH VEHICLE OBJECTIVES	DEGREE OF ACCOMPLISHMENT	DISCREPANCIES	SECTION IN WHICH DISCUSSED
1	Boost and insert the Saturn Work Shop (SWS) into a circular earth orbit of about 234 n mi. altitude at an inclination of 50° with a descending node of 153.25°.	Complete	None	4
2	After earth orbit insertion, separate the S-II stage from the SWS so as to preclude recontact with the SWS for at least eight months.	Complete	None	4
3	After separation, vent the S-II stage residual propellants and pressurants to make the stage safe from explosive overpressure.	Complete	None	6
4	Provide attitude control signals to the Thruster Attitude Control System (TACS) until SWS attitude control is switched to the Apollo Telescope Module Digital Computer (ATMDC).	Complete	None	9
5	Provide switch selector commands to initiate SWS deployment operations.	Complete	None. Orbital Work Shop deployment problems were not related to switch selector commands.	2 and 17

FAILURES AND ANOMALIES

Evaluation of the Skylab-1 launch vehicle and Launch Vehicle Ground Support Equipment data revealed the four failures and/or anomalies summarized below, the first and fourth of which are considered significant.

ITEM	VEHICLE SYSTEM	ANOMALY OR FAILURE (CAUSE)	SIGNIFICANCE (CLASSIFICATION)	CORRECTIVE ACTION	SECTION REFERENCE
1	S-II SECOND PLANE SEPARATION	AFT INTERSTAGE FAILED TO SEPARATE WHEN COMMANDED AT 189.9 SECONDS. (INCOMPLETE PROPAGATION OF THE LINEAR SHAPED CHARGE DUE TO DAMAGE FROM OWS DEBRIS.)	NONE ON THIS MISSION. HOWEVER, SIMILAR OCCURRENCE ON MANNED MISSION COULD RESULT IN CATASTROPHIC FAILURE IF NOT DETECTED OR MANDATORY ABORT IF DETECTED. (APD 19C SIGNIFICANT FAILURE, APD 44 NON-CONFORMANCE CATEGORY [NCC] 1)	ENGINEERING CHANGE PROPOSAL (ECP) 7129 ACTION PENDING.	9.5.2 10.3 11.0 12.0
2	LVGSE/ESE	ERRONEOUS READOUTS FROM THE MOBILE LAUNCHER COMPUTER MAGNETIC STORAGE DRUM STARTING AT T-1 HOUR 58 MINUTES. (IMPROPER SEATING OF PRINTED CIRCUIT BOARD.)	PRECLUDED EXECUTION OF FOUR NON-CRITICAL LAUNCH FUNCTIONS. (APD 19C FAILURE, APD 44 NCC 4)	NONE.	3.3
3	GUIDANCE & NAVIGATION	INERTIAL PLATFORM PITCH AXIS GIMBAL FINE RESOLVER SWITCHED TO THE BACKUP RESOLVER AT 3805 SECONDS. (IMPROPER SETTING OF TEST CONSTANT AND NULL SHIFT IN CONTROL SIGNAL PROCESSOR, EITHER SUFFICIENT TO CAUSE FAILURE OF ZERO REASONABLENESS TEST IN CONTROL DEADBAND.)	LOSS OF REDUNDANCY. (APD 19C ANOMALY, APD 44 NCC 4)	REASONABLENESS TEST CONSTANT WILL BE CHANGED FROM 1.4° TO 2.0° FOR SL-3 AND SL-4. CHANGED TEST CONSTANT PROHIBITS ZERO REASONABLENESS TEST FAILURE WITHIN THE MEASURED CONTROL SYSTEM DEADBAND. IN THE EVENT ANOTHER MISSION SIMILAR TO SL-1 WERE PLANNED, CONSIDERATION WOULD BE GIVEN TO INHIBITING THE TEST DURING ORBITAL OPERATIONS.	8.0
4	LAUNCH VEHICLE	LAUNCH VEHICLE INSTRUMENTATION RECORDED UNUSUAL DISTURBANCE AT APPROXIMATELY 63 AND 593 SECONDS DURING FLIGHT. (AT APPROXIMATELY 63 SECONDS THE ORBITAL WORK SHOP (OWS) METEOROID SHIELD STRUCTURALLY FAILED AND OWS SOLAR ARRAY SYSTEM (SAS) WING NO. 2 UNLATCHED PREMATURELY. AT APPROXIMATELY 593 SECONDS, THE PARTIALLY DEPLOYED SAS WING NO. 2 WAS TORN OFF AT THE HINGE, APPARENTLY BY IMPINGEMENT FROM THE S-II RETRO PLUME.)	THE LAUNCH VEHICLE REACTED PROPERLY TO THE EXTERNAL DISTURBANCES WITH NO SIGNIFICANT EFFECT ON LAUNCH VEHICLE PERFORMANCE EXCEPT SECOND PLANE SEPARATION FAILURE. (APD 19C SIGNIFICANT ANOMALY)	NO CORRECTIVE ACTION PLANNED FOR THE LAUNCH VEHICLE SYSTEMS.	17.0

SECTION 1

INTRODUCTION

1.1 PURPOSE

This report provides the National Aeronautics and Space Administration (NASA) Headquarters, and other interested agencies, with the launch vehicle evaluation results of the SA-513 flight (Skylab-1). The basic objective of flight evaluation is to acquire, reduce, analyze, evaluate and report on flight data to the extent required to assure future mission success and vehicle reliability. To accomplish this objective, actual flight problems are identified, their causes determined, and recommendations made for appropriate corrective action.

1.2 SCOPE

This report contains the performance evaluation of the major launch vehicle systems, with special emphasis on problems. Summaries of launch operations and Saturn Work Shop performance are included.

The official George C. Marshall Space Flight Center (MSFC) position at this time is represented by this report. It will not be followed by a similar report unless continued analysis or new information should prove the conclusions presented herein to be significantly incorrect.

1.3 PERFORMANCE PREDICTIONS BASELINE

Unless otherwise noted, all performance predictions quoted herein for comparison purposes are based on the SL-1 Launch Vehicle Operational Trajectory Data for May 14 launch, transmitted by S&E-AERO-MFT-59-73, dated May 3rd.

SECTION 2

EVENT TIMES

2.1 SUMMARY OF EVENTS

Range zero occurred at 13:30:00 Eastern Daylight Time (EDT) (17:30:00 Universal Time [UT]) May 14, 1973. Range time is the elapsed time from range zero, and is the time used throughout this report unless otherwise noted. Time from base time is the elapsed time from the start of the indicated time base. Table 2-1 presents the time bases used in the flight sequence program.

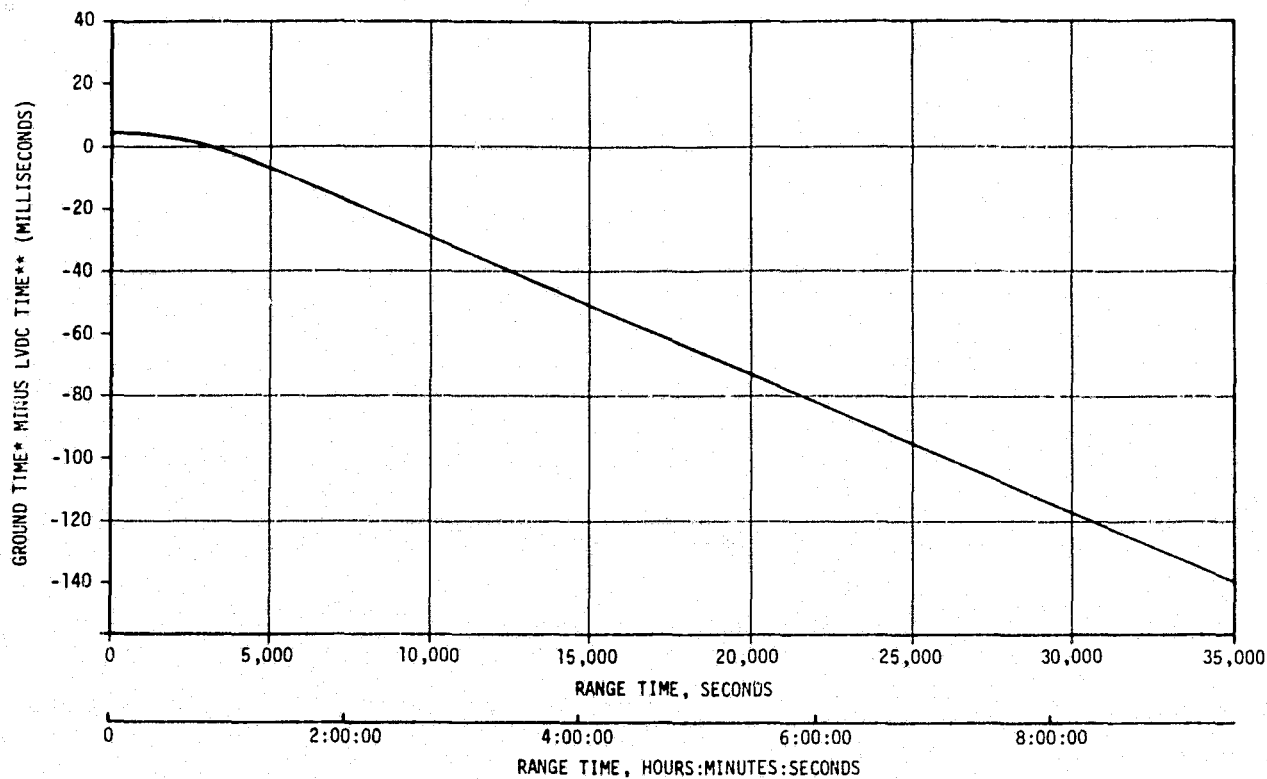
Table 2-1. Time Base Summary

TIME BASE	VEHICLE TIME* SECONDS	GROUND TIME** SECONDS	SIGNAL START
T ₀	-16.95	-16.95	Guidance Reference Release
T ₁	0.59	0.59	IU Umbilical Disconnect Sensed by LVDC
T ₂	140.79	140.79	Initiated by LVDC 0.1 Seconds after S-IC CECO Command
T ₃	158.25	158.25	S-IC OECO Sensed by LVDC
T ₄	589.17	589.17	S-II OECO Sensed by LVDC
T _{4A}	919.27	919.27	Vehicle Achieved Gravity Gradient Attitude Within 5°
T ₅	29,399.53	29,399.42	First Computation Cycle After T ₄ + 28810 Seconds

*Range Time of occurrence as indicated by uncorrected LVDC clock, i.e., the time of event as tagged onboard, converted to range time.

**Range Time of ground receipt of telemetered signal from vehicle. Includes telemetry transmission time and LVDC clock correction. See Figure 2-1.

The start of time bases T₀, T₁, T₂ and T₃ were nominal. T₄ was initiated approximately 0.7 seconds late, after receiving the S-II velocity cutoff and S-II engines out interrupt as discussed in Sections 6 and 9 of this document. Start time of T_{4A} was approximately 13.1 seconds earlier than predicted, initiated when the vehicle achieved an attitude within 5° of being parallel with the local vertical. Time base T₅ was initiated by the Launch Vehicle Digital Computer (LVDC) during the first computation cycle to exceed T₄ + 28,810 seconds and was approximately 0.9 seconds later than predicted.



* RANGE TIME OF GROUND RECEIPT OF TELEMETERED SIGNAL FROM VEHICLE.

** LVDC TIME OF OCCURRENCE.

Figure 2-1. SA-513 LVDC Clock/Ground Time Difference

Figure 2-1 shows the difference between telemetry signal receipt at a ground station and time of occurrence of an event as indicated by the LVDC clock. This curve includes the adjustments for LVDC clock speed.

A summary of significant event times for SA-513 is given in Table 2-2. The preflight predicted times have been adjusted to match the actual first motion time. The predicted times for establishing actual minus predicted times in Table 2-2 were taken from 40M33633B, "Interface Control Document Definition of Saturn SA-513/Skylab 1 Flight Sequence Program" and from the Skylab-1 Launch Vehicle Operational Trajectory Data for May 14 launch as transmitted by S&E-AERO-MFT-59-73, dated May 3, 1973.

2.2 VARIABLE TIME AND COMMANDED SWITCH SELECTOR EVENTS

Table 2-3 lists the switch selector events which were issued during the flight, but were not programmed for specific times.

Table 2-2. Significant Event Times Summary

ITEM	EVENT DESCRIPTION	RANGE TIME		TIME FROM BASE	
		ACTUAL SEC	ACT-PRED SEC	ACTUAL SEC	ACT-PRED SEC
1	GUIDANCE REFERENCE RELEASE (GRR)	-17.0	0.0	-17.5	0.1
2	S-IC ENGINE START SEQUENCE COMMAND (GROUND)	-8.9	0.0	-9.5	-0.1
3	S-IC ENGINE NO.5 START	-6.8	0.1	-7.3	0.1
4	S-IC ENGINE NO.1 START	-6.5	0.0	-7.0	0.0
5	S-IC ENGINE NO.3 START	-6.7	0.0	-7.2	0.0
6	S-IC ENGINE NO.2 START	-6.7	0.0	-7.2	0.0
7	S-IC ENGINE NO.4 START	-6.3	0.0	-6.8	0.0
8	ALL S-IC ENGINES THRUST OK	-1.8	-0.3	-2.4	-0.3
9	RANGE ZERO	0.0		-0.6	
10	ALL HCLDDOWN ARMS RELEASED (FIRST MOTION)	0.2	0.0	-0.4	-0.1
11	IU UMBILICAL DISCONNECT, START OF TIME BASE 1 (T1)	0.6	0.1	0.0	0.0
12	BEGIN TOWER CLEARANCE PITCH AND YAW MANEUVER	1.6	0.1	1.0	0.0
13	END PITCH MANEUVER	5.8	0.1	5.2	0.0
14	BEGIN PITCH AND ROLL MANEUVER	12.2	1.0	11.6	0.9
15	S-IC OUTBOARD ENGINE CANT ON 'A'	20.5	0.0	20.0	0.0
16	MACH 1	61.1	-0.4	60.5	-0.4
17	END ROLL MANEUVER	63.5	0.0	62.9	0.0
18	MAXIMUM DYNAMIC PRESSURE (MAX Q)	73.5	-1.5	72.9	-1.5
19	FLIGHT CONTROL COMPUTER SWITCH POINT NO. 1	105.5	0.0	105.0	0.0
20	FLIGHT CONTROL COMPUTER SWITCH POINT NO. 2	130.6	0.1	130.0	0.0
21	S-IC CENTER ENGINE CUTOFF COMMAND	140.7	0.1	140.1	0.0
22	S-IC CENTER ENGINE CUTOFF (CECO)	140.72	0.02	140.14	-0.04

Table 2-2. Significant Event Times Summary (Continued)

ITEM	EVENT DESCRIPTION	RANGE TIME		TIME FROM BASE	
		ACTUAL SEC	ACT-PRED SEC	ACTUAL SEC	ACT-PRED SEC
23	START OF TIME BASE 2 (T2)	140.8	0.1	0.0	0.0
24	S-IC OUTBOARD ENGINES CUTOFF ENABLE COMMAND	152.5	0.1	11.7	0.0
25	BEGIN TILT ARREST	158.1	1.0	17.3	0.9
26	S-IC OUTBOARD ENGINE CUTOFF (OECC)	158.16	0.01	17.37	-0.05
27	S-IC ENGINES NO. 1 & 3 CUTOFF	158.16	0.00	17.37	-0.07
28	S-IC ENGINES NO. 2 & 4 CUTOFF	158.23	0.00	17.44	-0.07
29	START OF TIME BASE 3 (T3)	158.2	0.0	0.0	0.0
30	START S-II LH2 TANK HIGH PRESSURE VENT MODE	158.3	0.0	0.1	0.0
31	S-II LH2 RECIRCULATION PUMPS OFF	158.4	0.0	0.2	0.0
32	S-IC/S-II SEPARATION COMMAND TO FIRE SEPARATION DEVICES AND RETRO MOTORS	159.9	0.0	1.6	-0.1
33	S-IC RETRO MOTOR EBW FIRE SIGNAL	159.9	-0.1	1.7	0.0
34	SEPARATION STRUCTURE COMPLETELY SEVERED	159.9	-0.1	1.7	-0.1
35	S-II ENGINE START SEQUENCE COMMAND (ESC)	160.6	0.0	2.4	0.0
36	S-II ENGINE SOLENOID ACTIVATION (AVERAGE OF FIVE)	160.6	0.0	2.4	0.0
37	S-II IGNITION-STDV OPEN	161.6	0.0	3.4	0.0
38	S-II CHILLDOWN VALVES CLOSE	163.5	0.0	5.3	0.0
39	S-II MAINSTAGE 3 SEC AFTER ESC	163.6	0.0	5.4	0.0
40	S-II HIGH (5.5) EMR NO. 1 ON	166.1	0.0	7.9	0.0
41	S-II HIGH (5.5) EMR NO. 2 ON	166.3	0.0	8.1	0.0
42	S-II AFT INTERSTAGE SEPARATION ARM NO. 1	183.2	0.0	25.0	0.0
43	ARM NO. 2	183.3	0.0	25.1	0.0
44	S-II SECOND PLANE SEPARATION COMMAND (JETTISON S-II AFT INTERSTAGE SEPARATION # 1)	189.9	0.0	31.7	0.0

Table 2-2, Significant Event Times Summary (Continued)

ITEM	EVENT DESCRIPTION	RANGE TIME		TIME FROM BASE	
		ACTUAL SEC	ACT-PRED SEC	ACTUAL SEC	ACT-PRED SEC
45	S-II SECOND PLANE SEPARATION EBW FIRE SIGNAL #1 (M86-206)	190.0	0.1	31.8	0.1
46	S-II SECOND PLANE SEPARATION COMMAND (JETTISON S-II AFT INTERSTAGE SEPARATION # 2)	190.0	0.0	31.8	0.0
47	S-II SECOND PLANE SEPARATION EBW FIRE SIGNAL #2 (M87-206)	—	—	—	—
48	ITERATIVE GUIDANCE MODE (IGM) PHASE 1 INITIATED	197.1	0.9	38.8	0.8
49	STEERING MISALIGNMENT (SMC) INITIATION	216.4	-0.4	58.1	-0.5
50	FLIGHT CONTROL COMPUTER SWITCH POINT #3	220.6	0.0	62.4	0.0
51	S-II CENTER ENGINE CUTOFF COMMAND VELOCITY DEPENDENT EVENT	314.0	-0.2	155.8	-0.2
52	S-II CENTER ENGINE CUTOFF (CECO)	314.05	-0.19	155.79	-0.21
53	START OF TRANSITIONAL TAU MODE BEGIN IGM PHASE 2	315.1	0.8	156.8	0.7
54	FLIGHT CONTROL COMPUTER SWITCH POINT #4	350.6	0.0	192.4	0.0
55	S-II LOW ENGINE MIXTURE RATIO (EMR) SHIFT (ACTUAL) VELOCITY DEPENDENT EVENT	403.7	1.1	245.4	1.0
56	START OF ARTIFICIAL TAU MODE BEGIN IGM PHASE 3	404.5	2.0	246.3	2.1
57	BEGIN TERMINAL STEERING	568.8	5.1	410.6	5.1
58	GUIDANCE CUTOFF SIGNAL (GCS)	588.96	0.64	430.71	0.63
59	S-II OUTBOARD ENGINE CUTOFF (OECO)	588.99	0.67	430.74	0.66
60	START OF TIME BASE 4	589.2	0.7	0.0	0.0
61	S-II/SWS SEPARATION COMMAND TO FIRE SEPARATION DEVICES AND RETRO MOTORS # 1	591.1	0.6	2.0	0.0
62	S-II/SWS SEPARATION COMMAND TO FIRE SEPARATION DEVICES AND RETRO MOTORS # 2	591.2	0.6	2.1	0.0

Table 2-2. Significant Event Times Summary (Continued)

ITEM	EVENT DESCRIPTION	RANGE TIME		TIME FROM BASE	
		ACTUAL SEC	ACT-PRED SEC	ACTUAL SEC	ACT-PRED SEC
63	S-II RETRO MOTOR EBW FIRE SIGNAL (M84-206, M85-206)	591.1	0.6	2.0	0.0
64	SEPARATION EBW FIRE SIGNAL (M101-206, M102-206)	591.2	0.7	2.1	0.1
65	SEPARATION STRUCTURE COMPLETELY SEVERED	591.1	0.5	2.0	-0.1
66	INITIATE S-II TIMER	591.2	0.6	2.0	-0.1
67	S-II NPV FIRING UNIT CHARGED	592.0	-0.1	2.8	-0.8
68	ORBIT INSERTION	599.0	0.7	9.8	0.0
69	BEGIN MANEUVER TO LOCAL VERTICAL ATTITUDE	599.6	1.1	10.4	0.4
70	**INITIATE ALL SII SAFING VENT **SEQUENCED BY S-II ONBOARD CONTROL AFTER SEPARATION	805.1	4.5	216.0	3.9
71	START OF TIME BASE NO 4A (T4A)	919.2	-13.1	0.0	0.0
72	PAYLOAD SHROUD JETTISON	920.4	-13.6	1.2	-0.5
73	INITIATE MANEUVER TO SOLAR INERTIAL ATTITUDE	958.8	-13.5	369.6	-14.2
74	INITIATE ATM DEPLOYMENT	999.1	0.6	410.0	0.0
75	INITIATE ATM SOLAR ARRAYS DEPLOYMENT	1492.3	0.6	903.2	0.0
76	ATM TELEMETRY ON	2209.1	0.6	1620.0	0.0
77	INITIATE OWS SOLAR ARRAYS DEPLOYMENT	2465.7	0.6	1876.6	0.0
78	INITIATE METEOROID SHIELD DEPLOYMENT	5764.1	0.6	5175.0	0.0
79	TACS COMM TRANSFER IU TO ATM	17400.7	0.6	16811.6	-0.1
80	START TIME BASE NO. 5 (T5)	29399.4	0.8	0.0	0.0

Table 2-3. Variable Time and Commanded Switch Selector Events

FUNCTION	STAGE	RANGE TIME (SEC)	TIME FROM BASE (SEC)	REMARKS
Telemetry Calibrator In-Flight Calibrate ON	IU	672.4	T ₄ +83.3	Newfoundland
Telemetry Calibrator In-Flight Calibrate OFF	IU	677.4	T ₄ +88.3	Newfoundland
Water Coolant Valve CLOSED	IU	949.2	T ₄ +360.1	Newfoundland
Water Coolant Valve CLOSED	IU	3349.2	T ₄ +2760.0	Newfoundland
Telemetry Calibrator In-Flight Calibrate ON	IU	3360.5	T ₄ +2771.3	Carnarvon Revolution 1
Telemetry Calibrator In-Flight Calibrate OFF	IU	3365.5	T ₄ +2776.3	Carnarvon Revolution 1
Telemetry Calibrator In-Flight Calibrate ON	IU	5704.5	T ₄ +5115.3	Texas
Telemetry Calibrator In-Flight Calibrate OFF	IU	5709.5	T ₄ +5120.3	Texas
Water Coolant Valve OPEN	IU	5749.2	T ₄ +5160.0	Texas
Water Coolant Valve CLOSED	IU	6049.2	T ₄ +5460.1	Texas
AM Deploy Buses OFF	SWS	11,038.7	T ₄ +10,449.5	LVDC Command
Telemetry Calibrator In-Flight Calibrate ON	IU	11,096.5	T ₄ +10,507.3	Hawaii
Telemetry Calibrator In-Flight Calibrate OFF	IU	11,101.5	T ₄ +10,512.3	Hawaii
Water Coolant Valve CLOSED	IU	12,949.2	T ₄ +12,360.1	Madrid Revolution 3
Telemetry Calibrator In-Flight Calibrate ON	IU	15,480.5	T ₄ +14,896.3	Honeysuckle Revolution 3
Telemetry Calibrator In-Flight Calibrate OFF	IU	15,485.5	T ₄ +14,896.3	Honeysuckle Revolution 3
Telemetry Calibrator In-Flight Calibrate ON	IU	17,384.5	T ₄ +16,795.3	Goldstone Revolution 3
Telemetry Calibrator In-Flight Calibrate OFF	IU	17,389.5	T ₄ +16,800.3	Goldstone Revolution 3

Table 2-3. Variable Time and Commanded Switch Selector Events
(Continued)

FUNCTION	STAGE	RANGE TIME (SEC)	TIME FROM BASE (SEC)	REMARKS
Water Coolant Valve OPEN	IU	17,749.3	T ₄ +17,160.1	Goldstone Revolution 3
Telemetry Calibrator In-Flight Calibrate ON	IU	18,688.5	T ₄ +18,099.3	Canary Revolution 4
Telemetry Calibrator In-Flight Calibrate OFF	IU	18,693.5	T ₄ +18,104.3	Canary Revolution 4
Water Coolant Valve OPEN	IU	25,249.3	T ₄ +24,660.1	Ascension Revolution 5
Telemetry Calibrator In-Flight Calibrate ON	IU	29,216.5	T ₄ +28,627.3	Goldstone Revolution 5
Telemetry Calibrator In-Flight Calibrate OFF	IU	29,221.5	T ₄ +28,632.3	Goldstone Revolution 5
Command Rate Measurement Switch	IU	34,986.2	T ₅ +5586.7	LVDC Command Goldstone Revolution 6
Water Coolant Valve OPEN	IU	35,449.3	T ₅ +6049.7	LVDC Command Goldstone Revolution 6
Telemetry Calibrator In-Flight Calibrate ON	IU	35,728.5	T ₅ +6329.0	Texas Revolution 6
Telemetry Calibrator In-Flight Calibrate OFF	IU	35,733.5	T ₅ +6334.0	Texas Revolution 6

SECTION 3

LAUNCH OPERATIONS

3.1 SUMMARY

The ground systems supporting the SA-513/Skylab 1 countdown and launch performed satisfactorily with the exception of the Launch Vehicle Ground Support Equipment (LVGSE) Mobile Launcher computer drum read errors. This malfunction, which is discussed in paragraph 3.5.2 caused no launch delay. The space vehicle was launched at 13:30:00 Eastern Daylight Time (EDT) (17:30:00 UT) on May 14, 1973, from Pad 39A of the Kennedy Space Center, Saturn Complex. There were no unscheduled holds in the countdown. Damage to the pad, Launch Umbilical Tower (LUT) and support equipment was considered minimal.

3.2 PRELAUNCH MILESTONES

A chronological summary of prelaunch milestones for the SA-513 launch is contained in Table 3-1. All stages, S-IC, S-II, and IU, performed normally during the countdown except during S-IC LOX loading, when the vent valves were being cycled to maintain a 2-4 psig ullage pressure, the open position switch on the LOX vent valve exhibited intermittent pickup or chatter. This occurred on the middle 4 of 6 valve cycles, and did not occur during the remainder of the countdown. It is believed that the chatter was due to the effect of the higher vent flowrates during this period when only one vent is used to vent the tank at 4 psig. This chatter has occurred during this same time period on previous countdowns. The chatter did not cause any problem nor affect valve operation.

3.3 TERMINAL COUNTDOWN

The SA-513/Skylab 1 terminal countdown was picked up at T-123 hours on May 9, 1973. Scheduled holds were initiated at T-7 hours for a duration of 30 minutes, and at T-2 hours for a duration of 1 hour. The space vehicle was launched at 13:30:00 EDT on May 14, 1973.

At T-1 hour 58 minutes, it was determined that the readout of the Mobile Launcher Computer (MLC) magnetic drum during the execution of the SE89 "Alternate Memory Checker Program" was erroneous. This is discussed in paragraph 3.5.2.

3.4 PROPELLANT LOADING

3.4.1 RP-1 Loading

The RP-1 system successfully supported countdown and launch without incident. Tail Service Mast (TSM) 1-2 fill and replenish was accom-

Table 3-1. SA-513/SL-1 Prelaunch Milestones

DATE	ACTIVITY OR EVENT
January 1, 1971	S-II-13 Stage Arrival
July 26, 1972	S-IC-13 Stage Arrival
August 2, 1972	S-IC Erection on Mobile Launcher (ML) - 2
September 20, 1972	S-II Erection
September 29, 1972	Saturn Work Shop (SWS) Erection
October 27, 1972	Instrument Unit (IU) - 513 Arrival
November 1, 1972	IU Erection
January 3, 1973	Launch Vehicle (LV) Electrical Systems Test Completed
February 6, 1973	LV Propellant Dispersion/Malfunction Overall Test (OAT) Complete
February 28, 1973	LV Service Arm OAT Complete
March 21, 1973	Space Vehicle (SV) OAT No. 1 (Plugs In) Complete
March 26, 1973	SV Electrical Mate
March 30, 1973	SV Flight Readiness Test (FRT) Completed
April 26, 1973	SV/ML Transfer to Pad 39A
April 26, 1973	RP-1 Loading
May 2, 1973	Countdown Demonstration Test (CDDT) Completed (Wet)
May 3, 1973	CDDT Completed (Dry)
May 9, 1973	SV Terminal Countdown Started (T-123 Hours)
May 14, 1973	SV Launch

plished at T-50 hours and S-IC level adjust and fill line inert occurred at about T-30 minutes. Both operations were satisfactory, there were no failures or anomalies. Launch countdown support consumed 211,373 gallons of RP-1.

3.4.2 LOX Loading

The LOX system supported countdown and launch satisfactorily. The fill sequence began with S-II chilldown at 7:02 EDT, May 14, 1973, and was completed 2 hours 5 minutes later with S-IC main fill complete at 9:07 EDT. Replenishment was automatic through the Terminal Countdown Sequence without incident. LOX consumption during launch countdown was 532,000 gallons.

3.4.3 LH₂ Loading

The LH₂ system successfully supported countdown and launch. The fill sequence began at 9:21 EDT, May 14, 1973, and was completed 45 minutes later when normal replenish was established at 10:06 EDT. S-II replenish was automatic until terminated at initiation of the Terminal Countdown Sequencer. Launch countdown support consumed approximately 335,000 gallons of LH₂.

3.5 GROUND SUPPORT EQUIPMENT

3.5.1 Ground/Vehicle Interface

In general, performance of the ground service systems supporting all stages of the launch vehicle was satisfactory. Overall damage to the pad, LUT, and support equipment from blast and flame impingement was considered minimal.

The Propellant Tanking Computer System (PTCS) adequately supported all countdown operations and there was no damage or system failures.

The Environmental Control System (ECS) successfully supported the SA-513 countdown. All specifications for ECS flow rates, temperatures, and pressures were met and flow/pressure criteria were satisfactory during the air to GN₂ changeover.

The Holddown Arms and Service Arm Control Switches (SACS) satisfactorily supported countdown and launch. All Holddown Arms released pneumatically within a 12 millisecond period. The retraction and explosive release lanyard pull was accomplished in advance of ordnance actuation with a 33 millisecond margin. Pneumatic release valves 1 and 2 opened within 18 milliseconds after SACS armed signal. The SACS primary switches closed at 399 and 387 milliseconds after commit. SACS secondary switches closed 963 and 966 milliseconds after commit.

Overall performance of the Tail Service Masts and Hydraulic Charging Unit was satisfactory. Mast retraction times were nominal; 2.163 seconds for TSM 1-2, 2.625 seconds for RSM 3-2 and 2.522 seconds for TSM 3-4, measured from umbilical plate separation to mast retracted.

The preflight and inflight Service Arms (S/A's 1 through 6, 6A, 7 and 8) supported the countdown in a satisfactory manner. Performance was nominal during terminal count and liftoff.

The primary damping system was retracted before propellant loading as a precautionary measure to preclude occurrence of a ruptured hose problem similar to that on SA-206 during Countdown Demonstration Test (CDDT). It was maintained in operational status so reconnect could be accomplished should it be needed before the completion of propellant loading. The requirement for the Auxiliary Damping System was deleted for SL-1 launch countdown.

The Digital Events Evaluation (DEE)-3 and DEE-6 systems satisfactorily supported all countdown operations. There were no system failures and no launch damage.

3.5.2 MSFC Furnished Ground Support Equipment

MSFC furnished electrical and mechanical ground support equipment successfully supported the Skylab 1 launch.

At T-1 hour 58 minutes, it was determined that the readout of the Mobile Launcher Computer (MLC) magnetic drum during the execution of the SE89 "Alternate Memory Checker Program" was erroneous. A subsequent drum-read incorrectly altered the MLC alternate memory. The MLC alternate memory was restored successfully by operator intervention. Drum-read problems were then experienced during the S-IC propellant monitor program. At T-1 hour 30 minutes, a decision was made to continue the countdown without the use of the MLC magnetic drum. This decision precluded further execution of the following non-critical launch functions:

FT49/FE50	ST-124M Accelerometer Monitor Programs
BE01	S-IC Propellant Temperature Monitor
BE02	S-IC Propellant Level Monitor
SE89	Alternate Memory Checker

Real time work-arounds utilizing telemetry and Digital Data Acquisition System data were implemented to provide equivalent monitoring functions.

During postlaunch trouble shooting a failed diode in a flip-flop circuit in the MLC drum address circuitry was found. However, analysis showed this failure was probably not related to the observed erroneous drum-read symptoms. During further trouble shooting, a printed circuit board (PCB) in the MLC drum address

circuitry was removed and reinserted, clearing the failure and indicating that the cause was improper seating. Additional site testing verified that no intermittent component failure was involved and confirmed improper seating of the PCB as the cause of the anomaly.

Computer test and maintenance procedures were reviewed and determined to be adequate. Improperly seated printed circuit boards are an infrequent occurrence, and are normally revealed in early testing so that the countdown is not materially affected. Therefore, no corrective action was taken.

SECTION 4

TRAJECTORY

4.1 SUMMARY

The vehicle was launched on an azimuth 90 degrees east of north. A roll maneuver was initiated at 12.2 seconds that placed the vehicle on a flight azimuth of 40.880 degrees east of north. The trajectory parameters were generally close to nominal except the S-IC velocity which was 18.0 meters per second greater than nominal at the outboard engine cutoffs. The largest contributors to this velocity have been identified as the tailwind and higher stage specific impulse. The Saturn Work Shop (SWS) insertion conditions were achieved 0.64 second later than nominal with altitude nominal and velocity 0.6 meter per second greater than nominal. S-II stage performance deviated from nominal in large part because the aft interstage failed to separate.

Orbital insertion parameters of the spent S-II stage deviated slightly from nominal but recontact with the SWS was precluded for at least eight months.

A study to determine the impact footprint of the meteoroid shield's debris is reported herein. Also, the orbital parameters of the spent S-II stage are provided.

4.2 TRAJECTORY EVALUATION

The reconstructed trajectory was generated by merging the ascent phase and the orbit phase trajectory segments. The analysis for each phase was conducted separately with appropriate end point constraints to provide trajectory continuity. Available C-band radar and USB tracking data plus telemetered guidance velocity data were used in the trajectory reconstruction.

4.2.1 Ascent Phase

The ascent phase spans the interval from guidance reference release through earth orbit insertion. The ascent trajectory was established by using telemetered guidance velocity data as generating parameters to fit tracking data from three C-band stations (Merritt Island, Patrick Air Force Base, and Bermuda FPQ-6) and one S-band station (Bermuda). Approximately 22 percent of the C-band tracking data and 31 percent of the S-band tracking data were eliminated due to inconsistencies. The launch phase portion of the ascent phase (liftoff to approximately 20 seconds) was established by constraining integrated telemetered navigation data to the best estimate trajectory.

Actual and nominal altitude, surface range, and crossrange for the ascent phase are presented in Figure 4-1. Actual and nominal space-fixed velocity and flight path angle during ascent are shown in Figure 4-2. Actual and nominal comparisons of total non-gravitational accelerations are shown in Figure 4-3. The maximum acceleration during S-IC burn was 4.45 g.

Mach number and dynamic pressure are shown in Figure 4-4. These parameters were calculated using meteorological data measured to an altitude of 62.5 kilometers (33.7 nmi). Above this altitude, the measured data were merged into the US Standard Reference Atmosphere.

Actual and nominal values of parameters at significant trajectory event times, S-IC and S-II cutoff events, and separation events are shown in Tables 4-1, 4-2, 4-3 and 4-4, respectively.

The S-IC velocity at cutoff, although well within the 3σ limits, was noticeably higher than predicted. A limited investigation as to possible causes yielded the following information: The winds on launch day were higher than the prediction used in the Operational Trajectory. Being principally tailwinds, this would effectively improve S-IC performance and add approximately 8 m/s to the S-IC velocity at cutoff. It was also found that increasing the S-IC stage specific impulse used in the Operational Trajectory by approximately 0.2% would produce an additional 6 m/s in velocity. Other contributors, which were not simulated but would result in increased S-IC performance are: lower-than-predicted RP-1 density, lower S-II weight (propellant and payload), unpredicted S-II insulation ablation, and the separation of the meteoroid shield.

From extensive data evaluation and flight radar observations it was concluded that the S-II aft interstage failed to separate completely when commanded at 189.9 seconds. A discussion of these analyses is presented in paragraph 9.5.2.

4.2.2 Earth Orbit Phase

Orbital tracking was conducted by the NASA Spacecraft Tracking and Data Network. Two C-band stations (Merritt Island and Bermuda) provided two data passes at the beginning of the first orbit. Ten S-band stations (Merritt Island, Bermuda, Canary, Ascension, Madrid, Carnarvon, Honeysuckle, Hawaii, Goldstone and Texas) furnished twenty additional tracking passes during the first three revolutions.

Telemetered guidance velocity data were used to derive the orbital non-gravitational acceleration (venting) model. The orbit trajectory was obtained by integrating a comprehensive force model (gravity plus venting) with corrected insertion conditions forward to 16,200 seconds (4:30:00) which is near Transfer to ATM Control. The insertion conditions were obtained by using the force model and a differential correction procedure to fit the available tracking data.

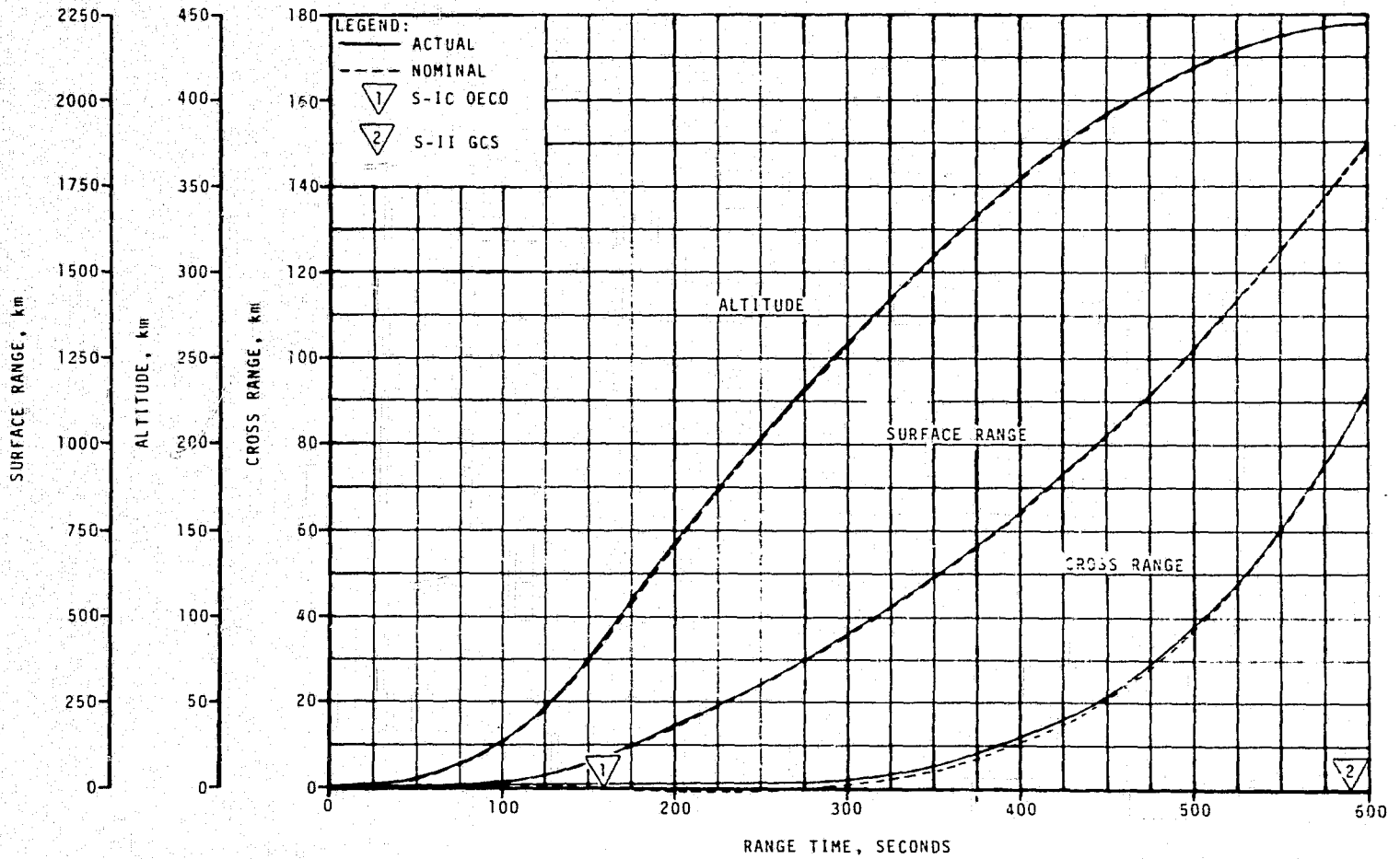


Figure 4-1. SA-513 Ascent Trajectory Position Comparison

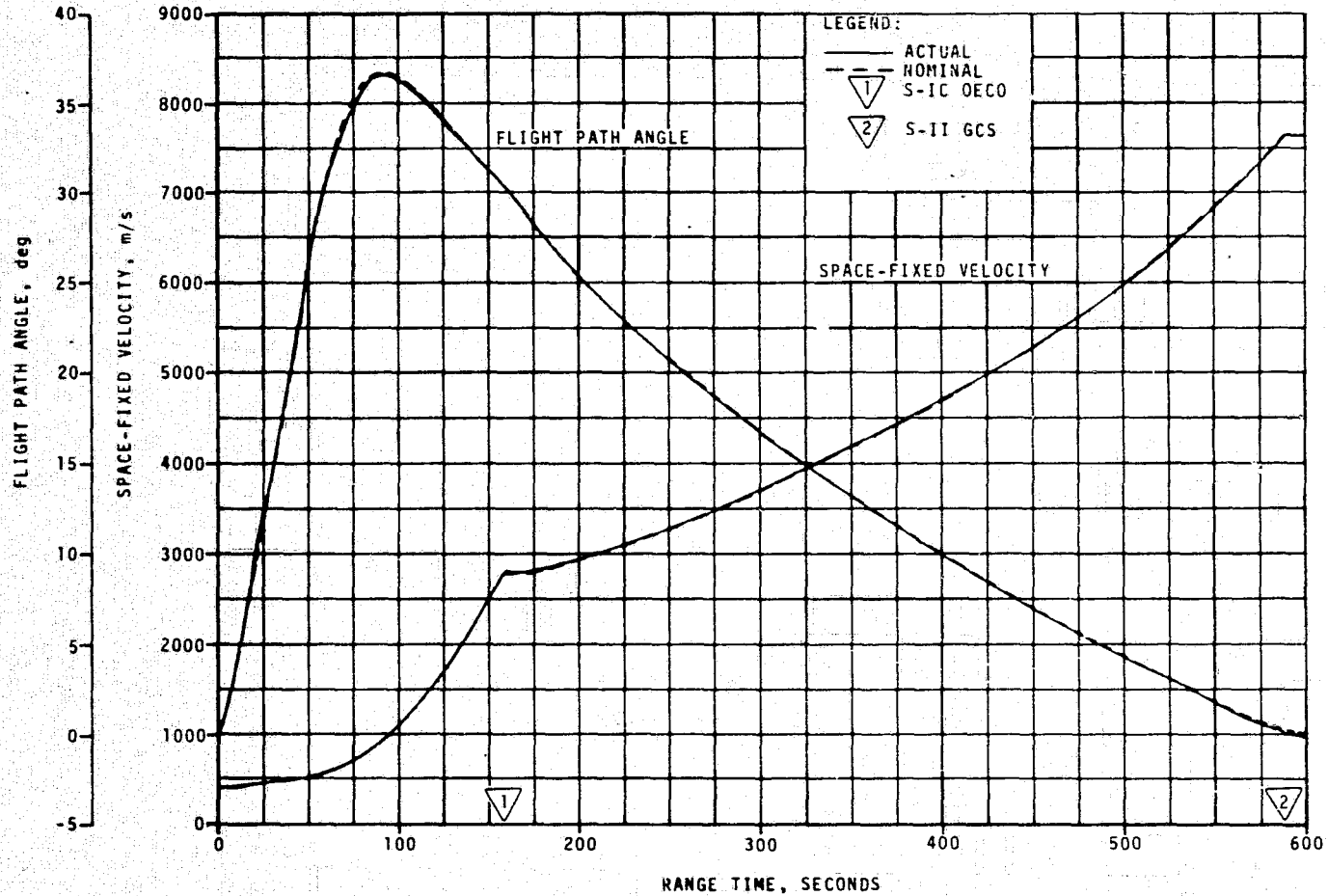


Figure 4-2. SA-513 Ascent Trajectory Space-Fixed Velocity and Flight Path Angle Comparisons

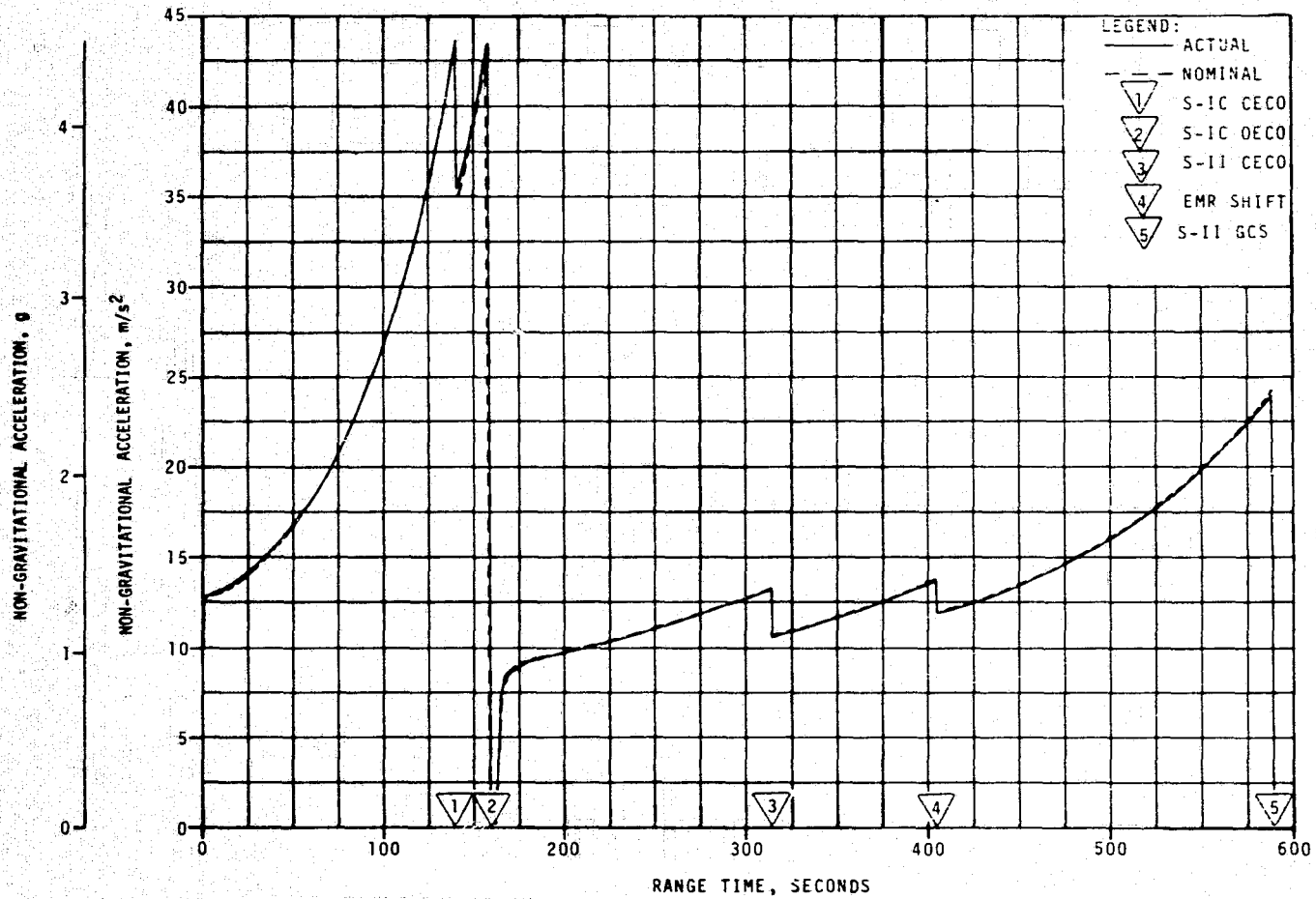


Figure 4-3. SA-513 Ascent Trajectory Acceleration Comparison

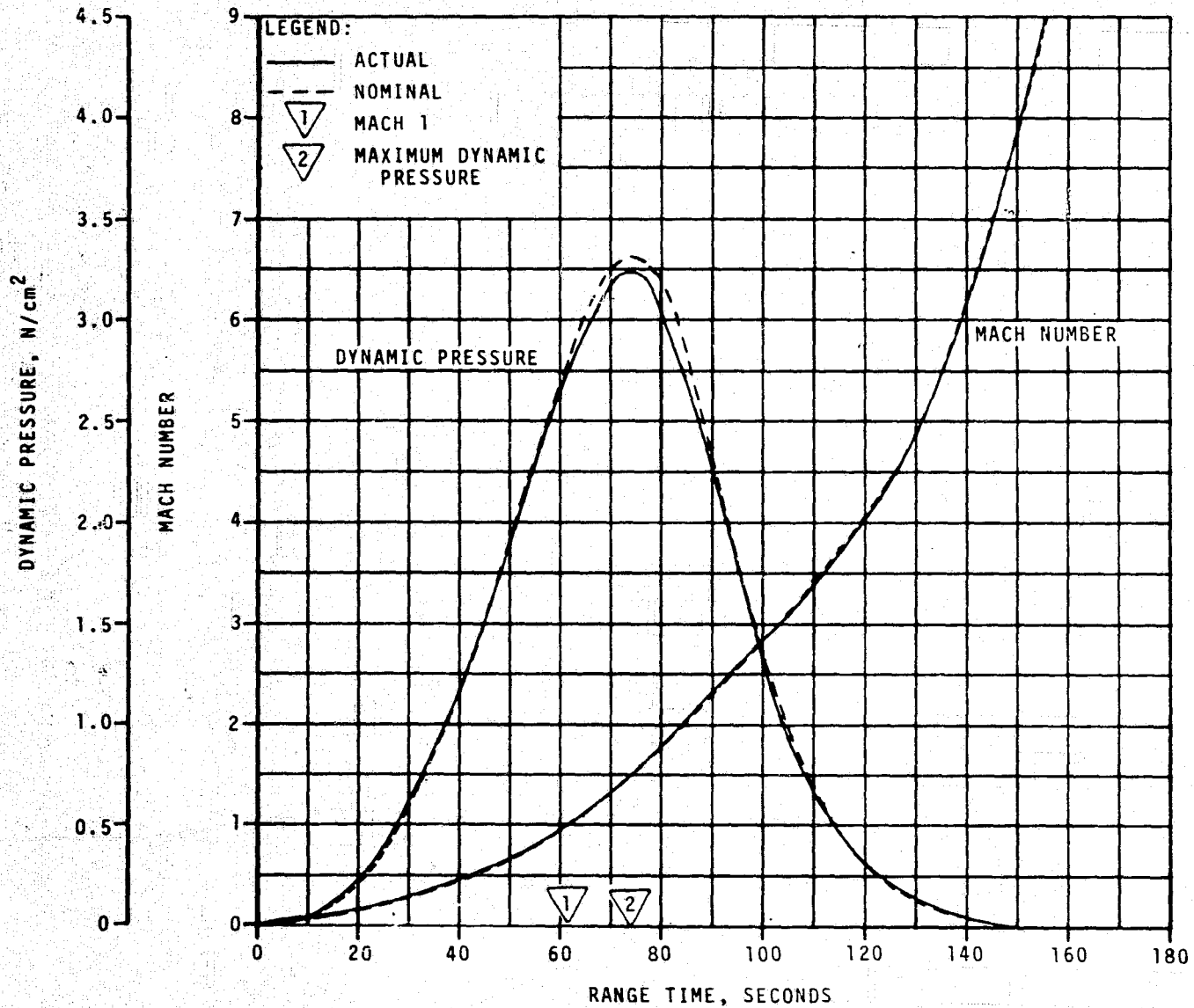


Figure 4-4. SA-513 Dynamic Pressure and Mach Number Comparisons

Table 4-1. Comparison of Significant SA-513 Trajectory Events

EVENT	PARAMETER	ACTUAL	NOMINAL	ACT - NOM	
First Motion	Range Time, sec	0.22	0.22	0.00	
	Total Non-Gravitational Acceleration, m/s^2 (ft/s^2) (g)	11.24 (36.88) (1.15)	10.97 (35.99) (1.12)	0.27 (0.89) (0.03)	
	MACH 1	Range Time, sec	61.0	61.5	-0.5
MACH 1	Altitude, km (nmi)	7.7 (4.2)	7.6 (4.1)	0.1 (0.1)	
	Maximum Dynamic Pressure	Range Time, sec	73.5	75.0	-1.5
Maximum Dynamic Pressure	Dynamic Pressure, n/cm^2 (lbf/ft^2)	3.25 (670.78)	3.33 (695.48)	-0.08 (-16.70)	
	Altitude, km (nmi)	12.0 (6.5)	12.3 (6.6)	-0.3 (-0.1)	
	*Maximum Total Non-Gravitational Acceleration:	S-IC	Range Time, sec	140.72	140.62
		Acceleration, m/s^2 (ft/s^2) (g)	43.66 (143.24) (4.45)	43.60 (143.04) (4.45)	0.06 (0.20) (0.00)
S-II		Range Time, sec	589.00	588.32	0.68
		Acceleration, m/s^2 (ft/s^2) (g)	23.97 (78.64) (2.44)	24.35 (79.89) (2.48)	-0.38 (-1.25) (-0.04)
*Maximum Earth-Fixed Velocity:	S-IC	Range Time, sec	159.00	159.22	-0.22
		Velocity, m/s (ft/s)	2,565.3 (8,416.3)	2,547.0 (8,356.3)	18.3 (60.0)
	S-II	Range Time, sec	590.50	590.53	-0.03
		Velocity, m/s (ft/s)	7,333.3 (24,059.4)	7,332.1 (24,055.4)	1.2 (4.0)

*Nearest Time Point Available

Table 4-2. Comparison of SA-513 S-IC Cutoff Events

PARAMETER	ACTUAL	NOMINAL	ACT-NOM
	S-IC CECO (ENGINE SOLENOID)		
Range Time, sec	140.72	140.62	0.10
Altitude, km (nmi)	62.4 (33.7)	61.9 (33.4)	0.5 (0.3)
Space-Fixed Velocity, m/s (ft/s)	2,214.4 (7,265.1)	2,201.1 (7,221.5)	13.3 (43.6)
Flight Path Angle, deg	32.446	32.589	-0.143
Heading Angle, deg	50.494	50.393	0.101
Surface Range, km (nmi)	54.1 (29.2)	53.1 (28.7)	1.0 (0.5)
Cross Range, km (nmi)	0.4 (0.2)	0.1 (0.1)	0.3 (0.1)
Cross Range Velocity, m/s (ft/s)	-1.4 (-4.6)	-6.9 (-22.6)	5.5 (18.0)
	S-IC OECO (ENGINE SOLENOID)		
Range Time, sec	158.16	158.16	0.00
Altitude, km (nmi)	85.2 (46.0)	84.7 (45.7)	0.5 (0.3)
Space-Fixed Velocity, m/s (ft/s)	2,800.5 (9,188.0)	2,782.5 (9,128.9)	18.0 (59.1)
Flight Path Angle, deg	30.581	30.697	-0.116
Heading Angle, deg	48.443	48.302	0.141
Surface Range, km (nmi)	85.7 (46.3)	84.7 (45.7)	1.0 (0.6)
Cross Range, km (nmi)	0.4 (0.2)	0.0 (0.0)	0.4 (0.2)
Cross Range Velocity, m/s (ft/s)	-1.7 (-5.6)	-9.8 (-32.2)	8.1 (26.6)

Table 4-3. Comparison of SA-513 S-II Cutoff Events

PARAMETER	ACTUAL	NOMINAL	ACT-NOM
	S-II CECS (ENGINE SOLENOID)		
Range Time, sec	314.05	314.24	-0.19
Altitude, km (nmi)	273.2 (147.5)	272.4 (147.1)	0.8 (0.4)
Space-Fixed Velocity, m/s (ft/s)	3,860.6 (12,666.0)	3,849.9 (12,630.9)	10.7 (35.1)
Flight Path Angle, deg	15.759	15.791	-0.032
Heading Angle, deg	48.111	48.107	0.004
Surface Range, km (nmi)	493.5 (266.5)	490.1 (264.6)	3.4 (1.9)
Cross Range, km (nmi)	2.5 (1.3)	1.1 (0.6)	1.4 (0.7)
Cross Range Velocity, m/s (ft/s)	55.2 (181.1)	54.6 (179.1)	0.6 (2.0)
	S-II GUIDANCE CUTOFF SIGNAL		
Range Time, sec	588.96	588.32	0.64
Altitude, km (nmi)	442.1 (238.7)	442.0 (238.7)	0.1 (0.0)
Space-Fixed Velocity, m/s (ft/s)	7,641.9 (25,071.9)	7,642.2 (25,072.8)	-0.3 (-0.9)
Flight Path Angle, deg	0.013	0.013	0.000
Heading Angle, deg	56.383	56.329	0.054
Surface Range, km (nmi)	1,810.7 (977.7)	1,801.6 (972.8)	9.1 (4.9)
Cross Range, km (nmi)	84.5 (45.6)	83.6 (45.1)	0.9 (0.5)
Cross Range Velocity, m/s (ft/s)	709.9 (2,329.1)	709.1 (2,326.4)	0.8 (2.7)
Inclination, deg	50.029	50.030	-0.001
Descending Node, deg	153.249	153.252	-0.003
Eccentricity	0.0021	0.0020	0.0001
$C_3, \frac{m^2}{s^2}$ ($\frac{ft^2}{s^2}$)	-58,638,675 (-631,181,445)	-58,635,937 (-631,151,973)	-2,738 (-29,472)

Table 4-4. Comparison of SA-513 Separation Events

PARAMETER	ACTUAL	NOMINAL	ACT-NOM
	S-IC/S-II SEPARATION		
Range Time, sec	159.9	159.9	0.0
Altitude, km (nmi)	87.7 (47.4)	87.3 (47.1)	0.4 (0.3)
Space-Fixed Velocity, m/s (ft/s)	2,807.0 (9,209.3)	2,789.1 (9,150.6)	17.9 (58.7)
Flight Path Angle, deg	30.344	30.451	-0.107
Heading Angle, deg	48.422	48.278	0.144
Surface Range, km (nmi)	89.4 (48.3)	88.4 (47.7)	1.0 (0.6)
Cross Range, km (nmi)	0.4 (0.2)	0.0 (0.0)	0.4 (0.2)
Cross Range Velocity, m/s (ft/s)	-1.7 (-5.6)	-9.8 (-32.2)	8.1 (26.6)
Geodetic Latitude, deg N	29.213	29.210	0.003
Longitude, deg E	-80.001	-80.010	0.009
	S-II/SWS SEPARATION		
Range Time, sec	591.1	590.5	0.6
Altitude, km (nmi)	442.1 (238.7)	442.0 (238.7)	0.1 (0.0)
Space-Fixed Velocity, m/s (ft/s)	7,648.2 (25,092.5)	7,648.2 (25,092.5)	0.0 (0.0)
Flight Path Angle, deg	0.003	0.002	0.001
Heading Angle, deg	56.480	56.429	0.051
Surface Range, km (nmi)	1,825.4 (985.6)	1,816.7 (980.9)	8.7 (4.7)
Cross Range, km (nmi)	86.0 (46.4)	85.1 (46.0)	0.9 (0.4)
Cross Range Velocity, m/s (ft/s)	712.1 (2,336.3)	711.5 (2,334.3)	0.6 (2.0)
Geodetic Latitude, deg N	39.772	39.732	0.040
Longitude, deg E	-66.000	-66.076	0.076

A comparison of actual and nominal earth orbit insertion parameters is presented in Table 4-5. The groundtrack from insertion to near Transfer to ATM Control near the end of the third orbit is given in Figure 4-5.

4.2.3 Meteoroid Shield Debris Impact Trajectory

A three degree of freedom simulation was used to model the probable impact trajectory of the meteoroid shield debris (see Section 17) and the resulting impact footprints are shown in Figure 4-6. The following items characterize the essential elements used for the simulation:

- a. Initial velocities and positions were taken from the 7-Day Observed Mass Point Trajectory (OMPT) data.
- b. The Cape Kennedy wind data from the SA-513 postflight meteorological data tape was used to represent the winds acting on the debris.
- c. A mass of 270 kg with an area of 70 m² (mass per unit area = 3.86 kg/m²) was taken to represent the aluminum shield.
- d. Impact footprints were determined parametrically assuming drag varying from 5 percent to 100 percent of flat plate drag, and time of separation varying from 60 to 65 seconds.

The 70 percent flat plate drag case is estimated to be the best representation of the falling meteoroid shield, and the associated point for the 63-second separation represents the most likely impact point.

4.2.4 Spent S-II Orbit

Skin tracking data of the spent S-II stage were received from the Merritt Island, Bermuda and Carnarvon C-band radars for portions of the second and sixth orbits. Separate orbit solutions were done on the second and sixth orbits using a gravity-only model. Comparisons of the actual and nominal orbits at two hours range time are presented in Table 4-6. At two hours, the SWS and S-II are in the same orbital plane and the SWS trails the S-II by three degrees; the separation distance is 298 kilometers. Table 4-7 presents the spent S-II stage orbital parameters at the midpoint of the sixth orbit. A comparison of these parameters to the mission plan show that the apogee altitude was actually 239.5 rather than 234 n.mi. and the perigee altitude was 201.0 instead of 197 n. mi. The differences are a result of vehicle attitude errors during separation and are discussed in paragraph 9.5.3. Recontact with the SWS has been precluded for at least eight months by the phasing relationship between the orbits, the trim burns raising the orbit of the SWS, and the more rapid decay of the S-II orbit due to the smaller ballistic coefficient of the S-II stage.

Table 4-5. Comparison of SA-513 Earth Orbit Insertion Conditions

PARAMETER	ACTUAL	NOMINAL	ACT-NOM
Range Time, sec	598.96	598.32	0.64
Altitude, km (nmi)	442.2 (238.8)	442.1 (238.7)	0.1 (0.1)
Space-Fixed Velocity, m/s (ft/s)	7,649.3 (25,096.1)	7,648.7 (25,094.2)	0.6 (1.9)
Flight Path Angle, deg	-0.007	0.001	-0.008
Heading Angle, deg	56.827	56.777	0.050
Inclination, deg	50.030	50.028	0.002
Descending Node, deg	153.252	153.248	0.004
Eccentricity	0.0002	0.0003	-0.0001
Apogee Altitude, km * (nmi)	433.8 (234.2)	433.3 (234.0)	0.5 (0.2)
Perigee Altitude, km * (nmi)	431.5 (233.0)	429.5 (231.9)	2.0 (1.1)
Period, min	93.23	93.21	0.02
Geodetic Latitude, deg N	40.051	40.009	0.042
Longitude, deg E	-65.484	-65.564	0.080

*Based on a Spherical Earth with Radius = 6,378.165 km.

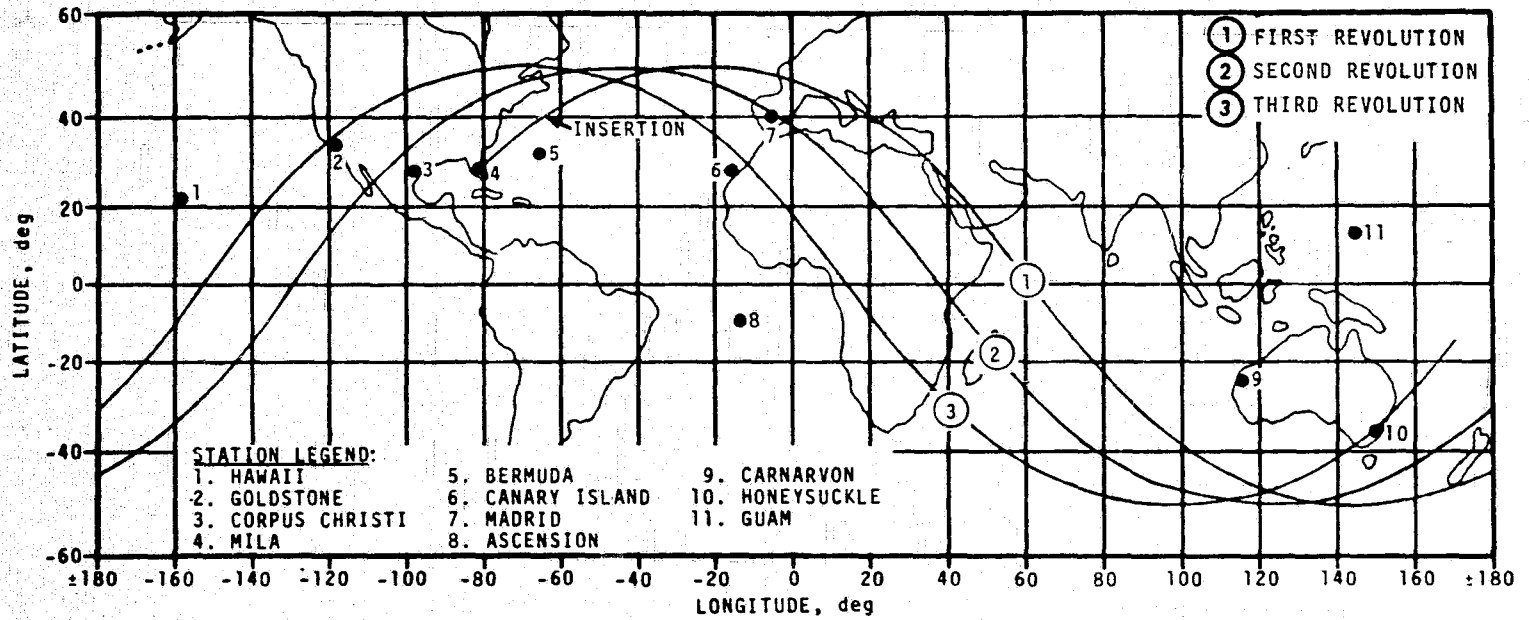


Figure 4-5. SA-513 Launch Vehicle Groundtrack

4-14

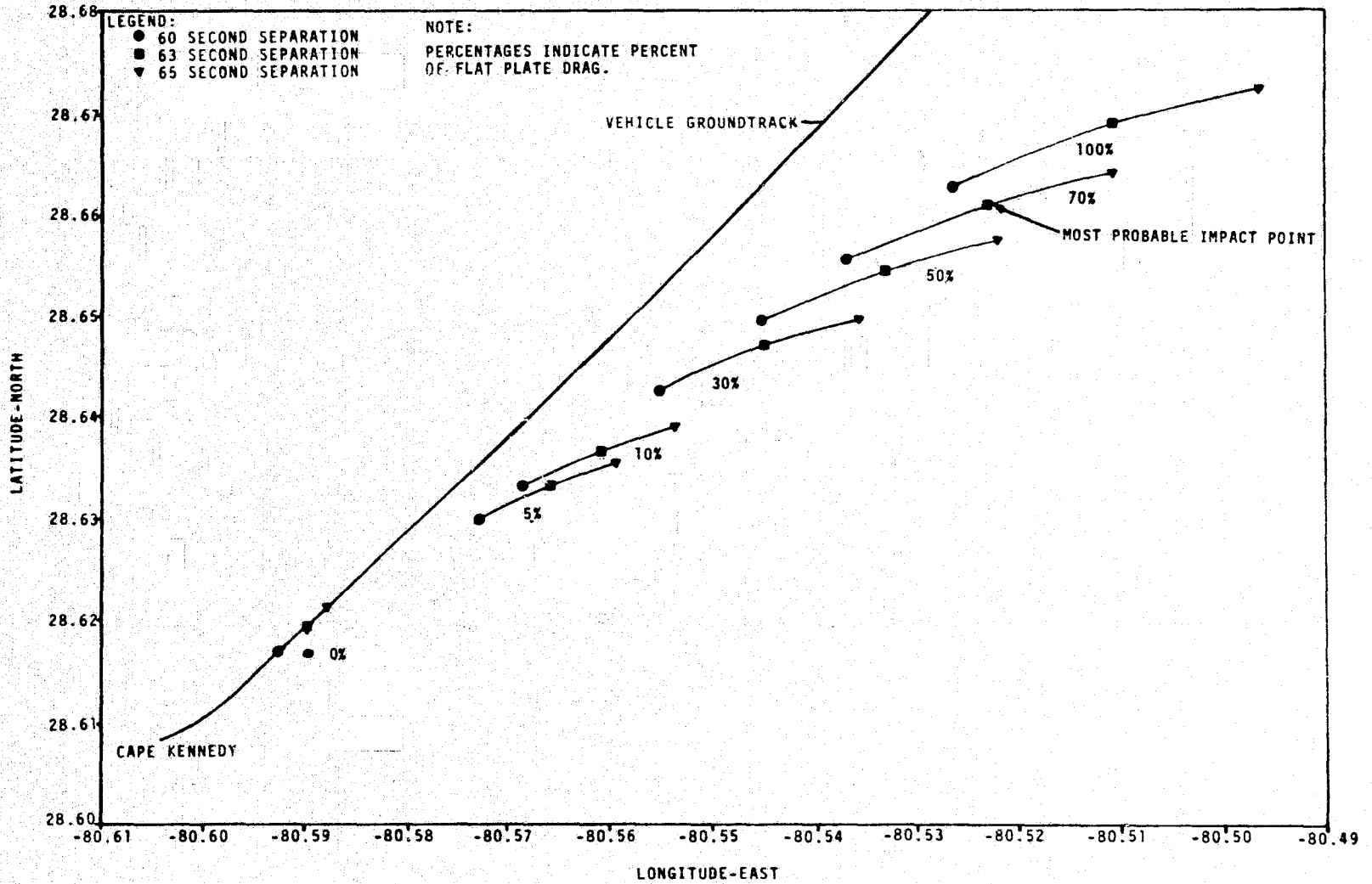


Figure 4-6. Impact Footprints for SL-1 Meteoroid Shield Debris

Table 4-6. SA-513 Comparison of Spent S-II Stage Orbital Parameters at 2 Hours Range Time

PARAMETER	ACTUAL	NOMINAL	ACT-NOM
Radius, km (n mi)	6,796.713 (3,669.931)	6,795.679 (3,669,373)	1.034 (0.558)
Velocity, m/s (ft/s)	7,648.6 (2,331.3)	7,648.2 (2,331.2)	0.4 (0.1)
Right Ascension - True of Date (deg)	163.696	163.755	-0.059
Declination (deg)	39.276	39.239	0.037
Heading (deg)	123.929	123.696	-0.040
Path Angle (deg)	-0.217	-0.231	0.014
C3 km ² /s ² (n mi ² /s ²)	-58.791200 (-17.140791)	-58.815334 (-17.147828)	0.024134 (0.007037)
Period (min)	92.58	92.52	0.06
Apogee Radius km (n mi)	6,810.6 (3,677.4)	6,810.1 (3,677.1)	0.5 0.3
Perigee Radius km (n mi)	6,749.4 (3,644.4)	6,744.3 (3,641.6)	5.1 2.8
Semi-Major Axis km (n mi)	6,780.0 (3,660.9)	6,777.2 (3,659.4)	2.8 (1.5)
Eccentricity	0.004517	0.004860	-0.000343
Inclination (deg)	50.037	50.034	0.003
Right Ascension of Node - True of Date (deg)	26.957	26.950	0.007
Argument of Perigee	-112.352	-111.263	-1.089
True Anomaly (deg)	-123.333	-124.360	1.027

4-15

Table 4-7. SA-513 Spent S-II Stage Orbital Parameters on Sixth Revolution

PARAMETER	SIXTH REVOLUTION MIDPOINT
Time (GMT)	May 15 1:54:24
C ₃ km ² /s ² (n mi ² /s ²)	-58.738148 (-17.125324)
Period (min)	92.70
Apogee Radius km (n mi)	6,821.7 (3,683.4)
Perigee Radius km (n mi)	6,750.5 (3,645.0)
Semi-Major Axis km (n mi)	6,786.1 (3664.2)
Eccentricity	0.005247
Inclination (deg)	50.068
Right Ascension of Node - True of Date (deg)	25.605
Argument of Perigee (deg)	-122.180
True Anomaly (deg)	-57.820

SECTION 5

S-IC PROPULSION

5.1 SUMMARY

All S-IC propulsion systems performed satisfactorily. The propulsion performance was very close to the predicted nominal. Overall stage site thrust was 0.07 percent higher than predicted. Total propellant consumption rate was 0.11 percent lower than predicted and the total consumed mixture ratio was 0.46 percent higher than predicted. Specific impulse was 0.18 percent higher than predicted. Total propellant consumption from Holddown Arm (HDA) release to Outboard Engines Cutoff (OECO) was low by 0.18 percent.

The F-1 Engine model specification LOX pump inlet total pressure upper limit of 150 psia was exceeded by all engines at Center Engine Cutoff (CECO) as predicted. Engine 5 exceeded the specification by 4 psia and Engines 1, 2, 3, and 4 by 2 psia. The higher pressures are attributed to a higher boost acceleration schedule for the Skylab mission than for Apollo and caused no problem for flight.

The F-1 engine shutdown sequence was changed from the 1-4 sequence used on previous flights to a 1-2-2 sequence (Engines 5, 1-3, 2-4) to reduce vehicle dynamics. CECO was initiated by the Instrument Unit (IU) at 140.72 seconds, 0.02 seconds later than planned. OECO was initiated by the LOX depletion sensors for engine pair 1-3 at 158.16 seconds and for engine pair 2-4 at 158.23 as predicted. At OECO of engine pair 1-3, the LOX residual was 30,582 lbm compared to the predicted 37,175 lbm and the fuel residual was 27.727 lbm compared to the predicted 31,337 lbm.

The S-IC hydraulic system performed satisfactorily.

5.2 S-IC IGNITION TRANSIENT PERFORMANCE

The fuel pump inlet prestart pressure of 45.0 psia was within the F-1 engine acceptable starting range of 43.3 to 110 psia.

The LOX pump inlet prestart pressure and temperature were 80.4 psia and -285.5°F and were within F-1 engine acceptable starting region, as shown by Figure 5-1.

The planned 1-2-2 F-1 engine start sequence (Engines 5, 3-1, 4-2) was not achieved. Two engines are considered to start together if both thrust chamber pressures reach 100 psig within 100 milliseconds. By this definition, the starting order was 1-1-1-1-1 (Engines 5-3-1-2-4). The buildup times of all five engines as measured from engine control valve open signal to 100 psig chamber pressure, Table 5-1, were less than predicted, although within specifications. The 1-1-1-1-1 start sequence had no adverse affect on either propulsion system performance or on the structure.

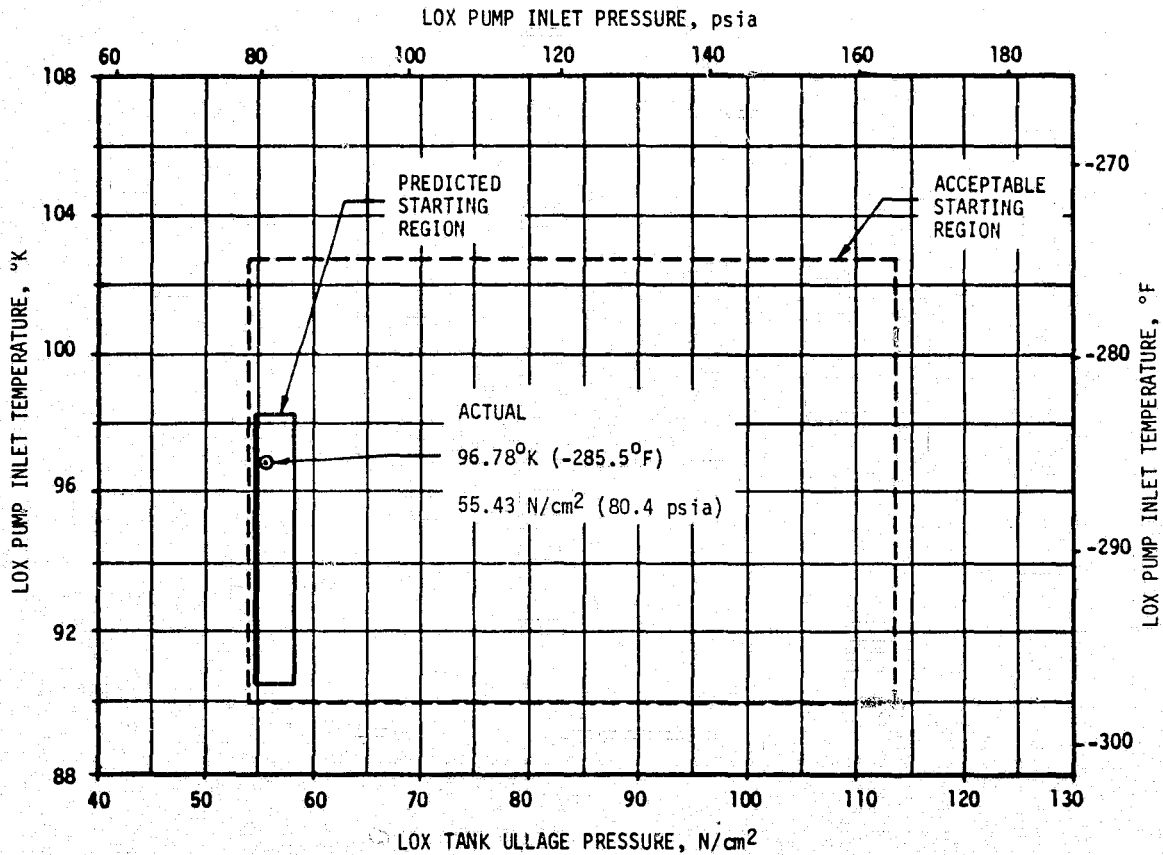


Figure 5-1. S-IC LOX Start Box Requirements

Table 5-1. F-1 Engine Systems Buildup Times

	BUILDUP TIME, SECONDS				
	ENGINE 1	ENGINE 2	ENGINE 3	ENGINE 4	ENGINE 5
Predicted*	3.822	4.287	4.004	3.899	3.873
Actual*	3.539	3.913	3.565	3.613	3.476
Difference	0.283	0.374	0.439	0.286	0.397
Direction	Fast	Fast	Fast	Fast	Fast

*Time from 4-way control valve open signal to 100 psig combustion chamber pressure. All times corrected to nominal prestart conditions.

The reconstructed propellant consumption during holddown (from ignition command to holddown arm release) was 77,099 lbm LOX (67,550 lbm predicted) and 22,337 lbm fuel (18,674 lbm predicted). The greater than predicted propellant consumption during holddown was due to the faster engine start and longer burn before holddown release. The reconstructed propellant load at holddown arm release was 3,232,480 lbm LOX (3,240,147 lbm predicted) and 1,383,759 lbm fuel (1,394,378 lbm predicted).

Thrust buildup rates were as expected, as shown in Figure 5-2. The shift in thrust buildup near the 1100 Klbf level on the outboard engines is attributed to ingestion of helium from the LOX prevalues during startup and is a normal occurrence. The thrust shift is absent on the inboard engine (Engine 5) since the POGO suppression helium injection system is not used on this engine.

The engine main oxidizer valve, main fuel valve, and gas generator ball valve opening times were nominal.

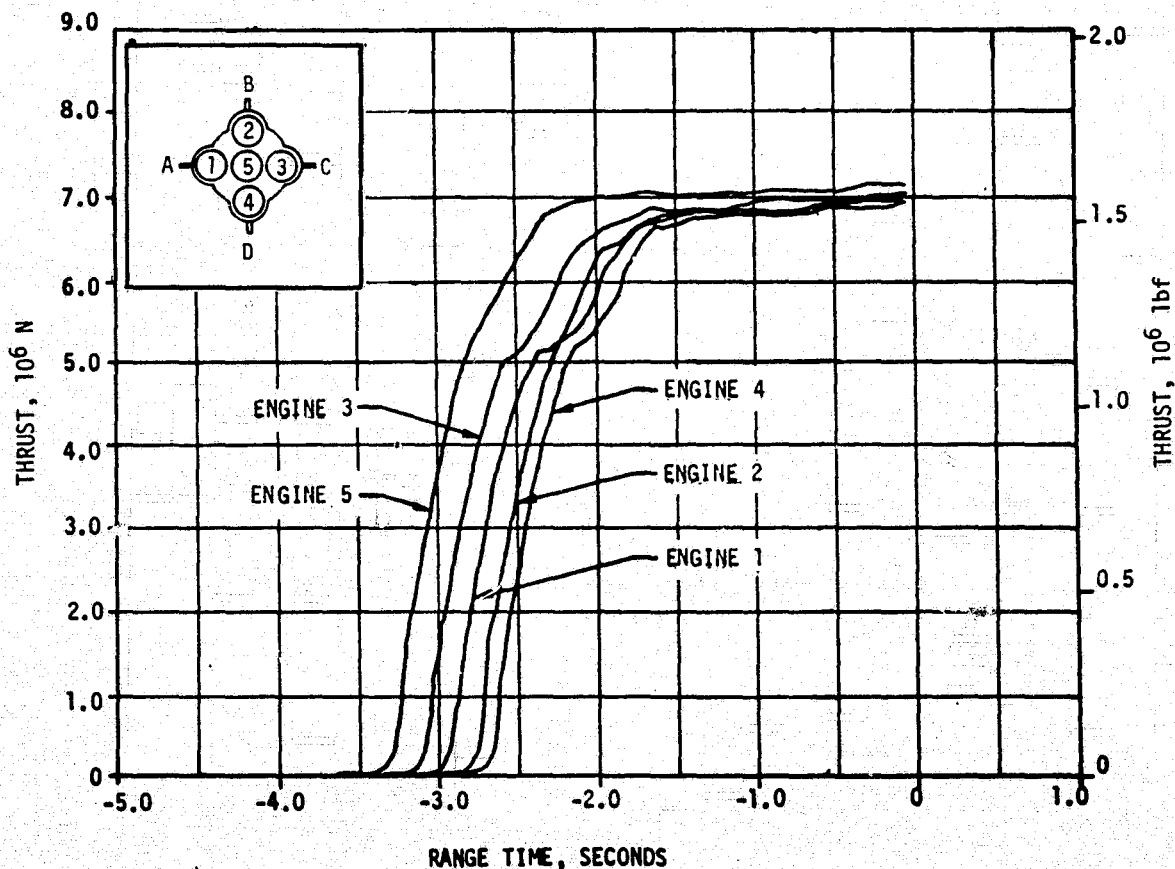


Figure 5-2. S-IC Engines Thrust Buildup

5.3 S-IC MAINSTAGE PERFORMANCE

S-IC stage propulsion performance was satisfactory. Stage thrust, specific impulse, mixture ratio, and propellant flowrate were well within operating limits as shown in Figure 5-3. The stage site thrust (averaged from time zero to OECO) was 0.07 percent higher than predicted. Total propellant consumption rate was 0.11 percent lower than predicted and the total consumed mixture ratio was 0.46 percent higher than predicted. The specific impulse was 0.18 percent higher than predicted. Total propellant consumption from HDA release to OECO was low by 0.18 percent.

For comparison of F-1 engine flight performance with predicted performance, the flight performance has been analytically reduced to standard conditions and compared to the predicted performance which is based on ground firings and also reduced to standard conditions. These comparisons are shown in Table 5-2 for the 35 to 38-second time slice. The largest thrust deviation from the predicted value was -10 Klbf for Engine 5. The 1498 Klbf thrust of Engine 5 was below the minimum value of 1500 Klbf. This caused no problem for flight. Engines 1, 2, 3, and 4 had lower thrusts than predicted by 1, 9, 3, and 6 Klbf, respectively. Total stage thrust was 29 Klbf lower than predicted for an average of -5.8 Klbf/engine. These performance values are derived from a reconstruction math model that uses a chamber pressure and pump speed match.

Table 5-2. S-IC Individual Standard Sea Level Engine Performance

PARAMETER	ENGINE	PREDICTED	RECONSTRUCTION ANALYSIS	DEVIATION PERCENT	STAGE DEVIATION PERCENT
Thrust 10 ³ lbf	1	1510	1509	-0.066	-0.383
	2	1516	1507	-0.594	
	3	1530	1527	-0.196	
	4	1516	1510	-0.396	
	5	1508	1498	-0.663	
Specific Impulse, lbf-s/lbm	1	265.1	265.0	-0.038	-0.060
	2	264.9	264.7	-0.076	
	3	265.9	265.8	-0.038	
	4	265.7	265.6	-0.038	
	5	264.4	264.1	-0.113	
Total Flowrate lbm/s	1	5698	5695	-0.053	-0.329
	2	5723	5692	-0.542	
	3	5755	5745	-0.174	
	4	5703	5686	-0.298	
	5	5704	5671	-0.579	
Mixture Ratio LOX/Fuel	1	2.297	2.294	-0.131	-0.132
	2	2.268	2.265	-0.132	
	3	2.260	2.257	-0.132	
	4	2.294	2.291	-0.131	
	5	2.271	2.268	-0.132	

NOTE: Performance levels were reduced to standard sea level and pump inlet conditions. Data were taken from the 35 to 38-second time slice.

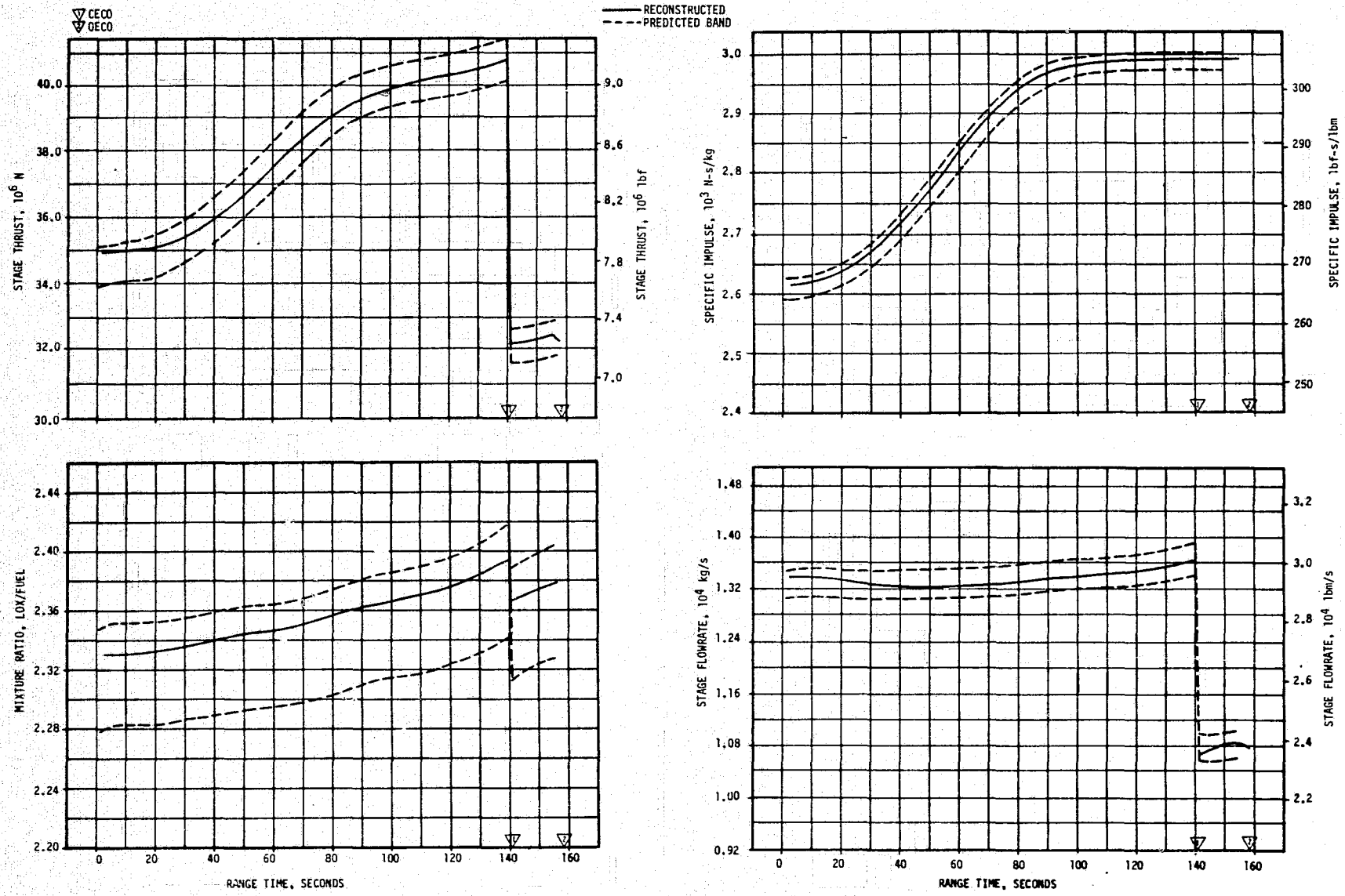


Figure 5-3. S-IC Stage Propulsion Performance

The Rocketdyne F-1 engine model specification LOX pump inlet total pressure upper limit of 150 psia was exceeded during S-IC-13 flight. The maximum value of 154 psia occurred on the center engine just before CECO at maximum longitudinal acceleration. Similarly, maximum pressure for the outboard engines was 152 psia at the same flight time. Predicted pressures were 155 and 153 psi for the center engine and outboard engines, respectively. The higher pressures are attributed to the higher boost acceleration schedule for Skylab than for Apollo. LOX pump inlet pressures higher than the engine specification also occurred on the AS-502 flight which had a high acceleration at inboard engine cutoff. Maximum pressure for AS-502 was 150.5 psia. Analysis of engine operating parameters and structural loads as coordinated between Rocketdyne, MSFC, and Boeing indicated that the high inlet pressures would not cause a problem for AS-502 flight. Similarly for SA-513, the high inlet pressure caused no problem for flight.

5.4 S-IC ENGINE SHUTDOWN TRANSIENT PERFORMANCE

The F-1 engine thrust decay transient was nominal. The cutoff impulse, measured from cutoff signal to zero thrust, was 680,542 lbf-s for the center engine (0.4 percent less than predicted) and 3,104,683 lbf-s for all outboard engines (4.9 percent greater than predicted). The total stage cutoff impulse of 3,785,225 lbf-s was 3.9 percent greater than predicted.

Center engine (Engine 5) cutoff was initiated by the IU at 140.72 seconds, 0.02 second later than planned. Engines 1 and 3 were programmed to shutdown 0.070 second earlier than Engines 2 and 4. This 2-2 outboard engine shutdown was accomplished and stage shutdown dynamics were significantly reduced. Individual engine thrust decay plots indicating the 2-2 shutdown sequence are shown in Figure 5-4. Cutoff signal to the outboard engines was initiated by LOX depletion and occurred at 158.16 seconds for engine pair 1-3 and at 158.23 seconds for engine pair 2-4 as predicted.

5.5 S-IC STAGE PROPELLANT MANAGEMENT

The S-IC stage does not have an active propellant utilization system. Minimum residuals are obtained by attempting to load the mixture ratio expected to be consumed by the engines plus the predicted unusable residuals. An analysis of the residuals experienced during a flight is a good measure of the performance of the passive propellant utilization system.

The residual LOX at OECO (first engine pair) was 30,582 lbm compared to the predicted value of 37,175 lbm. The fuel residual at OECO (first engine pair) was 27,727 lbm compared to the predicted value of 31,337 lbm. A summary of the propellants remaining at major event times is presented in Table 5-3.

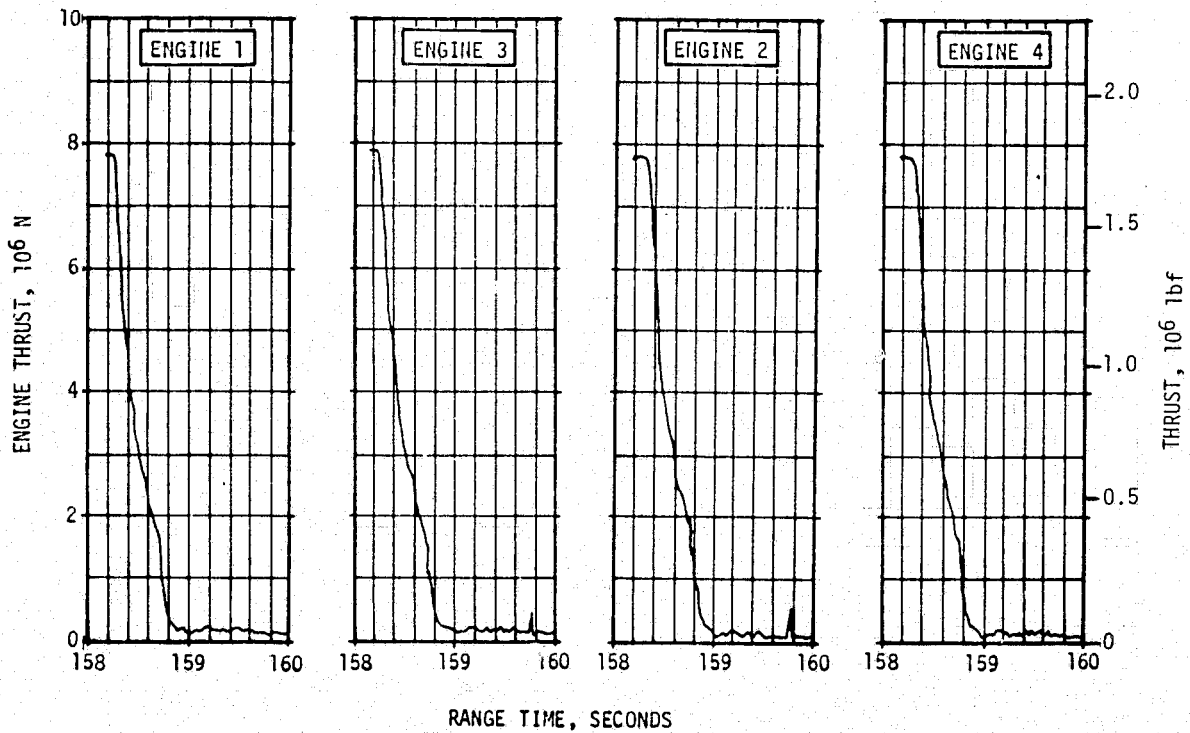


Figure 5-4. S-IC Outboard Engine Thrust Decay

Table 5-3. S-IC Propellant Mass History

EVENT	PREDICTED, LBM		LEVEL SENSOR DATA, LBM		RECONSTRUCTED, LBM (BEST ESTIMATE)	
	LOX	FUEL	LOX	FUEL	LOX	FUEL
Ignition Command	3,307,697	1,413,052	-----	1,406,109	3,309,579	1,406,096
Holddown Arm Release	3,240,147	1,394,378	3,225,467	1,382,988	3,232,480	1,383,759
CECO	332,664	156,010	325,264	152,019	325,140	151,624
OECO (First Pair)	37,175	31,337	30,893	28,533	30,582	27,727
Separation	31,067	28,141	-----	-----	24,211	24,355
Zero Thrust	30,957	28,064	-----	-----	24,090	24,271

Predicted and reconstructed values do not include pressurization gas so they will compare with level sensor data.

5.6 S-IC PRESSURIZATION SYSTEMS

5.6.1 S-IC Fuel Pressurization System

The fuel tank pressurization system performed satisfactorily, keeping ullage pressure within acceptable limits during flight. Helium Flow Control Valves (HFCV) No. 1 through 4 opened as planned and HFCV No. 5 was not required.

The low flow prepressurization system was commanded on at -97.0 seconds and was cycled on a second time at -3.1 seconds. High flow pressurization, accomplished by the onboard pressurization system, performed as expected. HFCV No. 1 was commanded on at -2.8 seconds and was supplemented by the ground high flow prepressurization system until umbilical disconnect.

Fuel tank ullage pressure was within the predicted limits throughout flight as shown by Figure 5-5. HFCV No.'s 2, 3, and 4 were commanded open during flight by the switch selector within acceptable limits. Helium bottle pressure was 3031 psia at -2.8 seconds and decayed to 550 psia at OECO. Total helium flowrate was as expected.

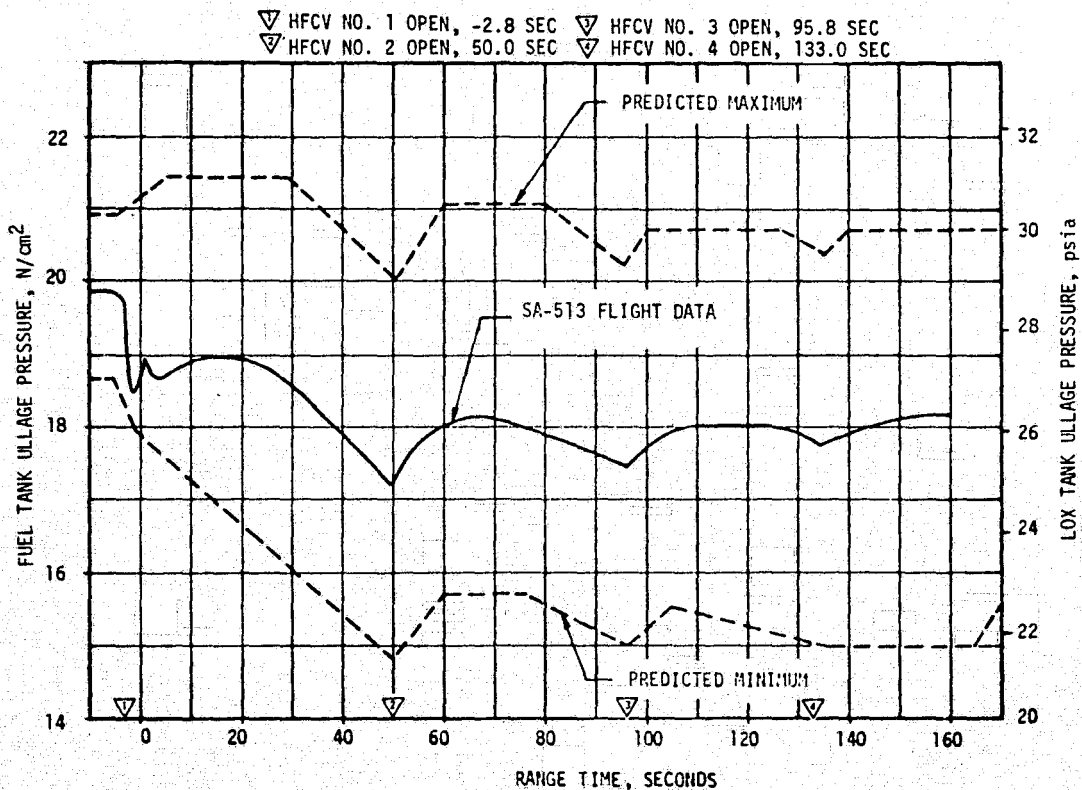


Figure 5-5. S-IC Fuel Tank Ullage Pressure

Fuel pump inlet pressure was maintained above the required minimum Net Positive Suction Pressure (NPSP) during flight.

5.6.2 S-IC LOX Pressurization System

The LOX pressurization system performed satisfactorily and all performance requirements were met. The ground prepressurization system maintained ullage pressure within acceptable limits until launch commit. The onboard pressurization system performed satisfactorily during flight.

The prepressurization system was initiated at -72.0 seconds. Ullage pressure increased to the prepressurization switch band and flow was terminated at -57.7 seconds. The low flow system was cycled on three additional times at -38.4, -12.1, and -4.7 seconds. At -4.7 seconds, the high flow system was commanded on and maintained ullage pressure within acceptable limits until launch commit.

Ullage pressure was within the predicted limits throughout flight as shown in Figure 5-6. GOX flowrate to the tank was as expected. The maximum GOX flowrate after the initial transient was 47.2 lbm/s at CECO.

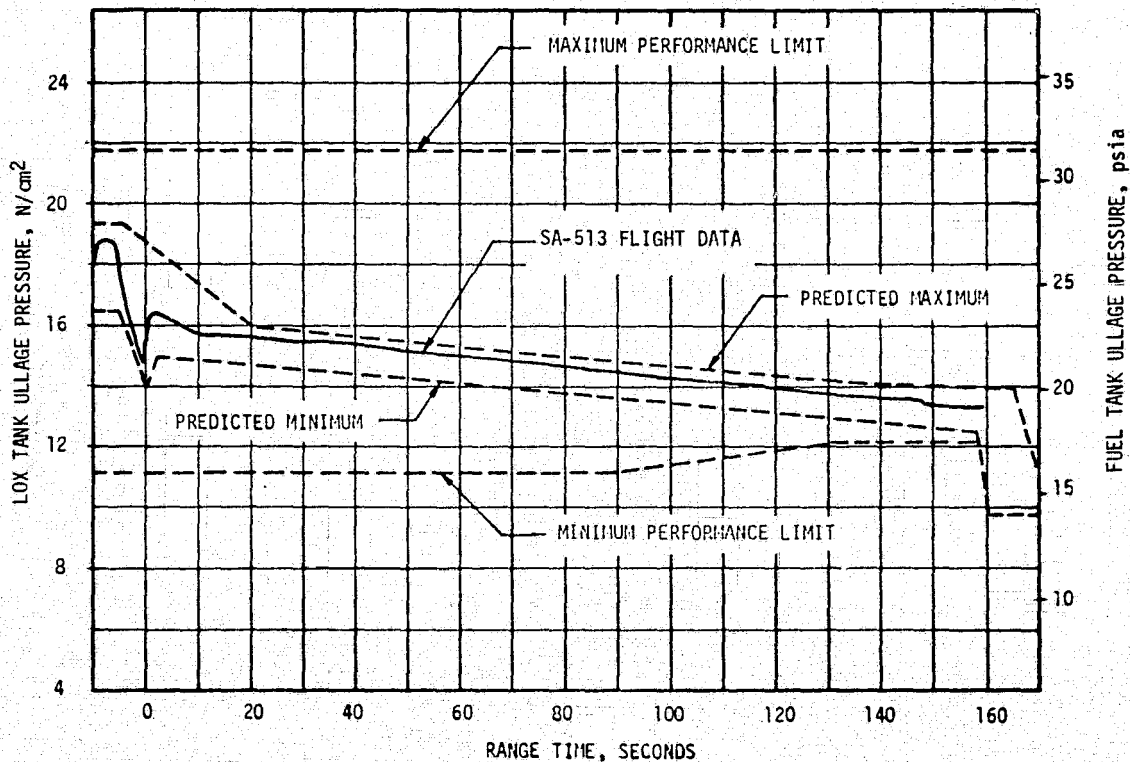


Figure 5-6. S-IC LOX Tank Ullage Pressure

The LOX pump inlet pressure met the minimum NPSP requirement throughout flight.

5.7 S-IC PNEUMATIC CONTROL PRESSURE SYSTEM

The control pressure system functioned satisfactorily throughout the S-IC flight.

Sphere pressure was 3040 psia at liftoff and remained steady until CECO when it decreased to 2926 psia. The decrease was due to center engine prevalve actuation. There was a further decrease to 2551 psia after OECO. Pressure regulator performance was within limits.

The engine prevalues were closed after CECO and OECO as required.

5.8 S-IC PURGE SYSTEMS

Performance of the purge systems was satisfactory during flight.

The turbopump LOX seal storage sphere pressure of 3032 psia at liftoff was within the prestart limits of 2700 to 3300 psia. Pressure was within the predicted envelope throughout flight and was 2744 psia at OECO.

The pressure regulator performance throughout the flight was within the 85 \pm 10 psig limits.

5.9 S-IC POGO SUPPRESSION SYSTEM

The POGO suppression system performed satisfactorily during S-IC flight.

Outboard LOX prevalve temperature measurements indicated that the prevalve cavities were filled with gas prior to liftoff as planned. The four resistance thermometers behaved during the SA-513 flight similarly to the flight of AS-512. The temperature measurements in the outboard LOX pre-valve cavities remained warm (off scale high) throughout flight, indicating helium remained in the prevalues as planned. The two thermometers in the engine prevalve were cold, indicating LOX in this valve as planned. The pressure and flowrate in the system were nominal.

5.10 S-IC HYDRAULIC SYSTEM

The performance of the S-IC hydraulic system was satisfactory. All servo-actuator supply pressures were within required limits.

Engine control system return pressures were within predicted limits and the engine hydraulic control system valves operated as planned.

SECTION 6

S-II PROPULSION

6.1 SUMMARY

The S-II propulsion systems performed satisfactorily throughout the flight. The S-II Engine Start Command (ESC), as sensed at the engines, occurred at 160.61 seconds. Center Engine Cutoff (CECO) was initiated by the Instrument Unit (IU), based on characteristic velocity, at 314.05 seconds. Outboard Engine Cutoff (OECO), initiated by an IU velocity signal, occurred at 588.99 seconds giving an outboard engine operating time of 428.38 seconds or 0.7 seconds longer than predicted.

Engine mainstage performance was satisfactory throughout flight. The total stage thrust at the standard time slice (61 seconds after S-II ESC) was 0.13 percent below predicted. Total propellant flowrate, including pressurization flow, was 0.18 percent below predicted, and the stage specific impulse was 0.05 percent above predicted at the standard time slice. Stage propellant mixture ratio was 0.54 percent below predicted. Engine thrust buildup and cutoff transients were within the predicted envelopes.

The propellant management system performance was satisfactory throughout loading and flight, and all parameters were nominal. Propellant residuals at OECO were 16,616 lbm LOX, 2319 lbm less than predicted and 5878 lbm LH₂, 319 lbm less than predicted. Control of Engine Mixture Ratio (EMR) was accomplished with the two-position pneumatically operated Mixture Ratio Control Valves (MRCV). The low EMR step occurred 1.1 seconds later relative to ESC, than predicted.

The performance of the LOX and LH₂ tank pressurization systems were satisfactory. Ullage pressure in both tanks was adequate to meet or exceed engine inlet Net Positive Suction Pressure (NPSP) minimum requirements throughout mainstage.

Performance of the center engine LOX feedline accumulator system for POGO suppression was satisfactory. The accumulator bleed and fill subsystems operations were within predictions.

The engine servicing, recirculation, helium injection, and valve actuation systems performed satisfactorily.

All orbital safing operations were performed satisfactorily. Safing of the LH₂ and LOX propellant tanks was verified by ullage pressures that decayed to less than 50% of design burst values. The engine helium and hydrogen pressure spheres were safed successfully when the vent valves were opened at 805.1 seconds.

S-II hydraulic system performance was normal throughout the flight.

6.2 S-II CHILLDOWN AND BUILDUP TRANSIENT PERFORMANCE

The engine servicing operations required to condition the engines prior to S-II engine start were satisfactorily accomplished. Thrust chamber jacket temperatures were within predicted limits at both prelaunch and S-II ESC. Thrust chamber chilldown requirements are -200°F maximum at prelaunch commit and -150°F maximum at ESC. Thrust chamber temperatures ranged between -256 and -287°F at prelaunch commit and between -205 and -232°F at ESC. Thrust chamber temperature warmup rates during S-IC boost agreed closely with those experienced on previous flights.

Start tank system performance was satisfactory. Both temperature and pressure conditions of the engine start tanks were within the required prelaunch and engine start boxes as shown in Figure 6-1. Start tank temperature and pressure increase rates were normal during prelaunch and S-IC boost and no indication of start tank relief valve operation was noted.

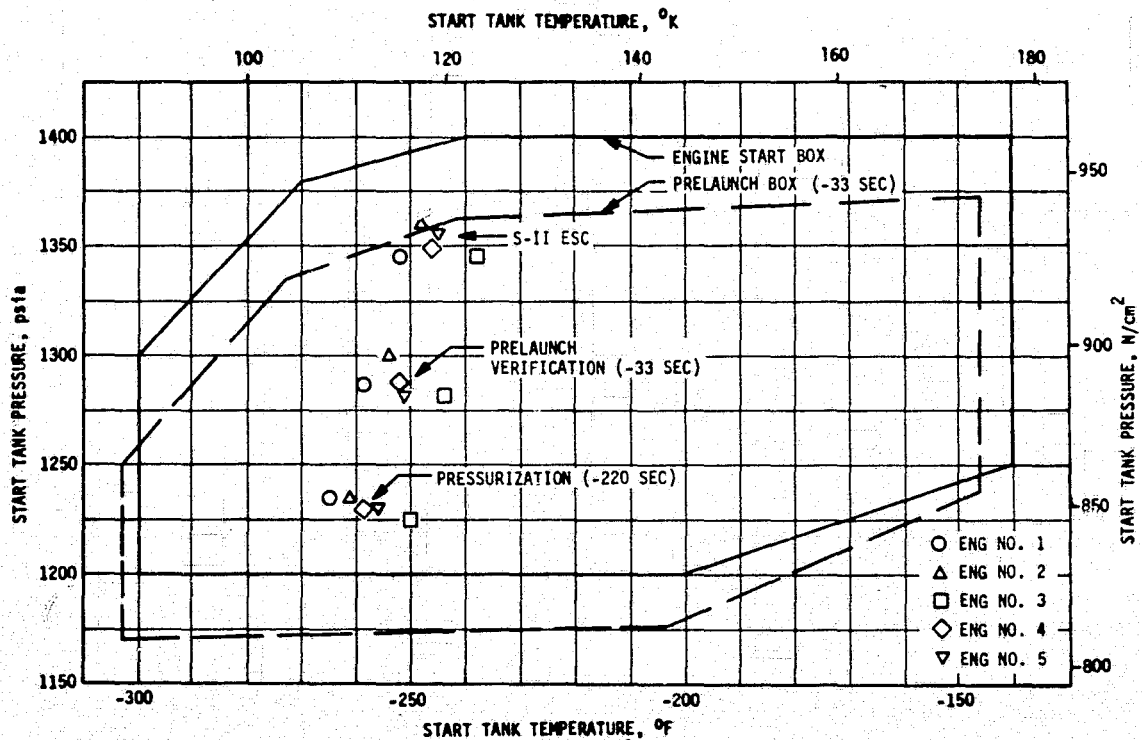


Figure 6-1. S-II Engine Start Tank Performance

All engine helium tank pressures were within the prelaunch limits of 2800 to 3350 psia and engine start limits of 2800 to 3500 psia. Engine helium tank pressures ranged between 3150 and 3245 psia at launch commit and between 3250 and 3375 psia at S-II ESC.

The LOX and LH₂ recirculation systems, used to chill the feed ducts, turbopumps, and other engine components performed satisfactorily during prelaunch and S-IC boost. Engine pump inlet temperatures and pressures at S-II ESC were well within the requirements as shown in Figure 6-2. The LOX pump discharge temperatures at S-II ESC were approximately 12.0°F subcooled, well below the 3°F subcooling requirement.

Prepressurization of the propellant tanks was accomplished satisfactorily. Tank ullage pressures at S-II ESC were 40.3 psia for LOX and 28.6 psia for LH₂, well above the minimum requirement of 33.0 and 27.0 psia, respectively.

S-II ESC was received at 160.61 seconds and the start tank discharge valve (STDV) solenoid activation signal occurred 1.0 seconds later. The engine thrust buildup was satisfactory with all engines reaching the 90 percent operating level within 3.4 seconds after S-II ESC. Engine 5 did momentarily exceed the predicted thrust buildup envelope as shown in Figure 6-3. This was attributed to a slow second stage ramp during main oxidizer valve opening. The predicted envelope was based upon the performance of those engines on AS-509 and AS-510 and allowable variations in other variables (i.e., valve timing) were not included.

6.3 S-II MAINSTAGE PERFORMANCE

The propulsion reconstruction analysis showed that stage performance during mainstage operation was satisfactory. A comparison of predicted and reconstructed thrust, specific impulse, total flowrate, and mixture ratio versus time is shown in Figure 6-4. Stage performance during the high EMR portion of flight (prior to CECO) was very close to predicted. At ESC +61 seconds, total stage thrust was 1,164,965 lbf which was 1483 lbf (0.13 percent) below the preflight prediction. Total propellant flowrate including pressurization flow, was 2760.7 lbm/s, 0.18 percent below predicted. Stage specific impulse, including the effect of pressurization gas flowrate, was 422.0 lbf-s/lbm, 0.05 percent above predicted. The stage propellant mixture ratio was 0.54 percent below predicted.

Center Engine Cutoff was initiated at ESC +153.44 seconds. This action reduced total stage thrust by 234,734 lbf to a level of 930,507 lbf. The EMR shift from high to low occurred 243.1 seconds after ESC and the reduction in stage thrust occurred as expected. At ESC +351 seconds, the total stage thrust was 795,491 lbf; thus, a decrease in thrust of 135,016 lbf was indicated between high and low EMR operation. S-II burn duration was 428.38 seconds, which was 0.7 seconds longer than predicted.

Individual J-2 engine data are presented in Table 6-1 for the ESC +61 second time slice. Good correlation exists between predicted and reconstructed flight performance. The performance levels shown in Table 6-1 have not been adjusted to standard J-2 altitude conditions and do not include the effects of pressurization flow.

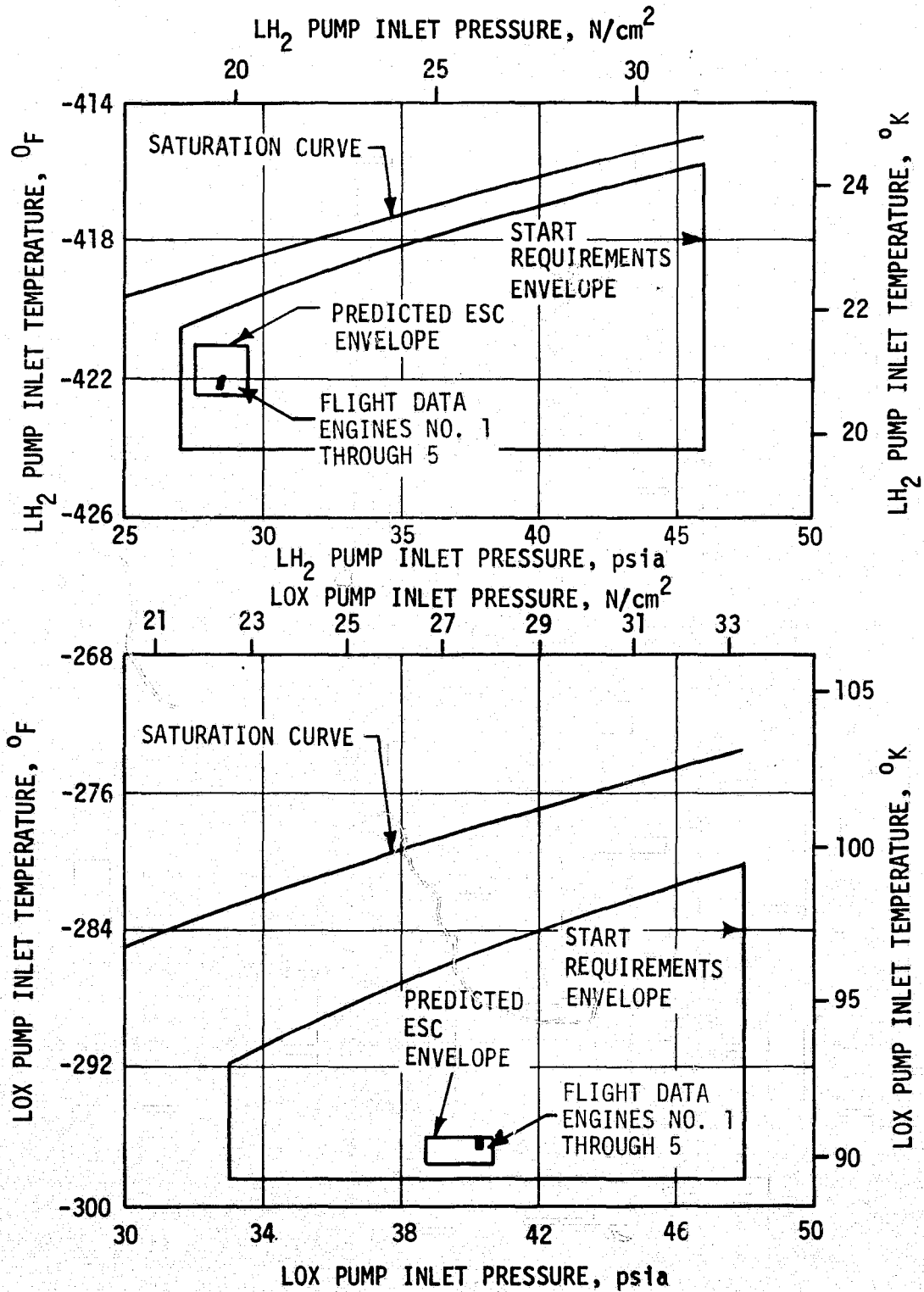


Figure 6-2. S-II Engine Pump Inlet Start Requirements

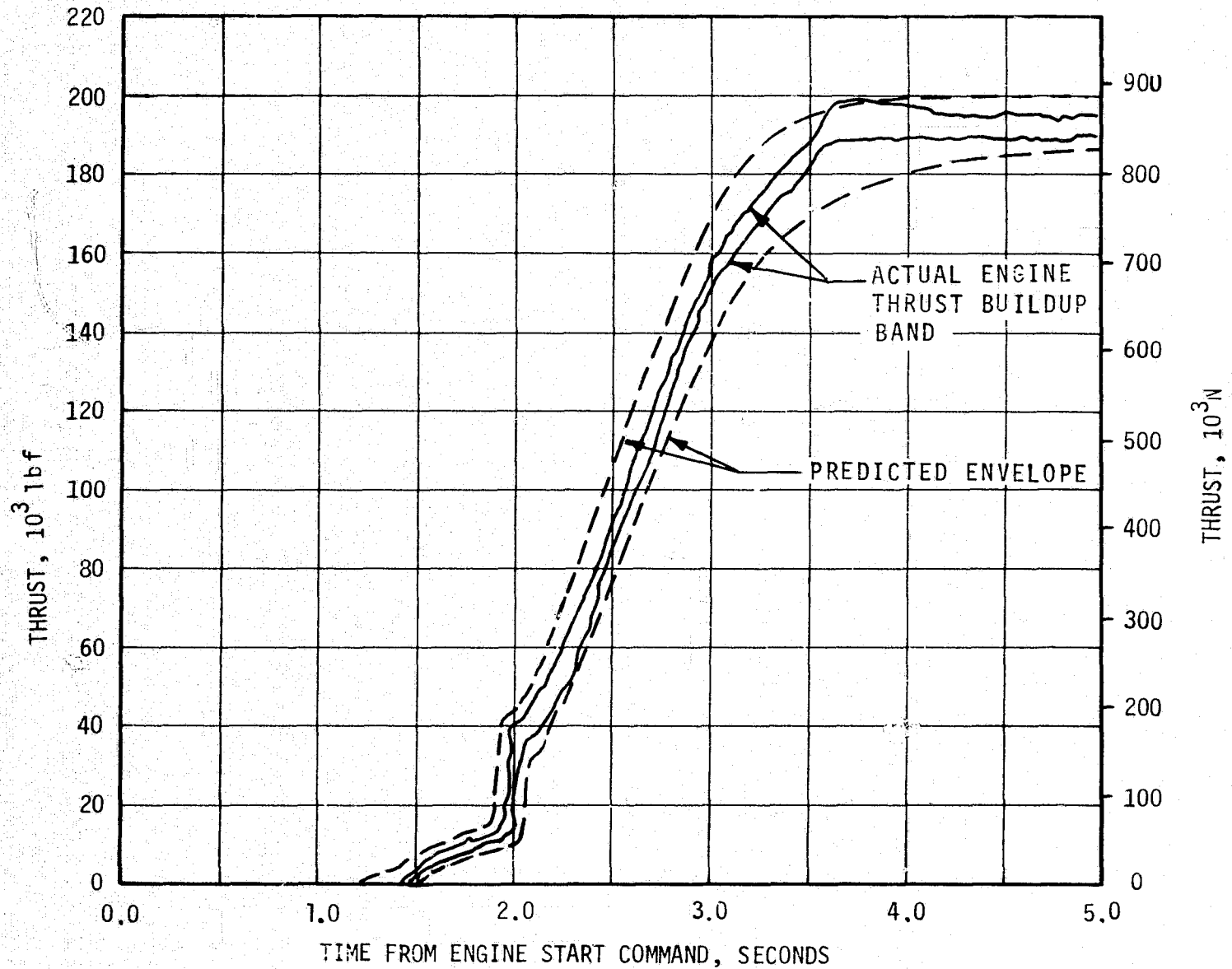


Figure 6-3. S-II Engine Thrust Buildup Transients

9-9

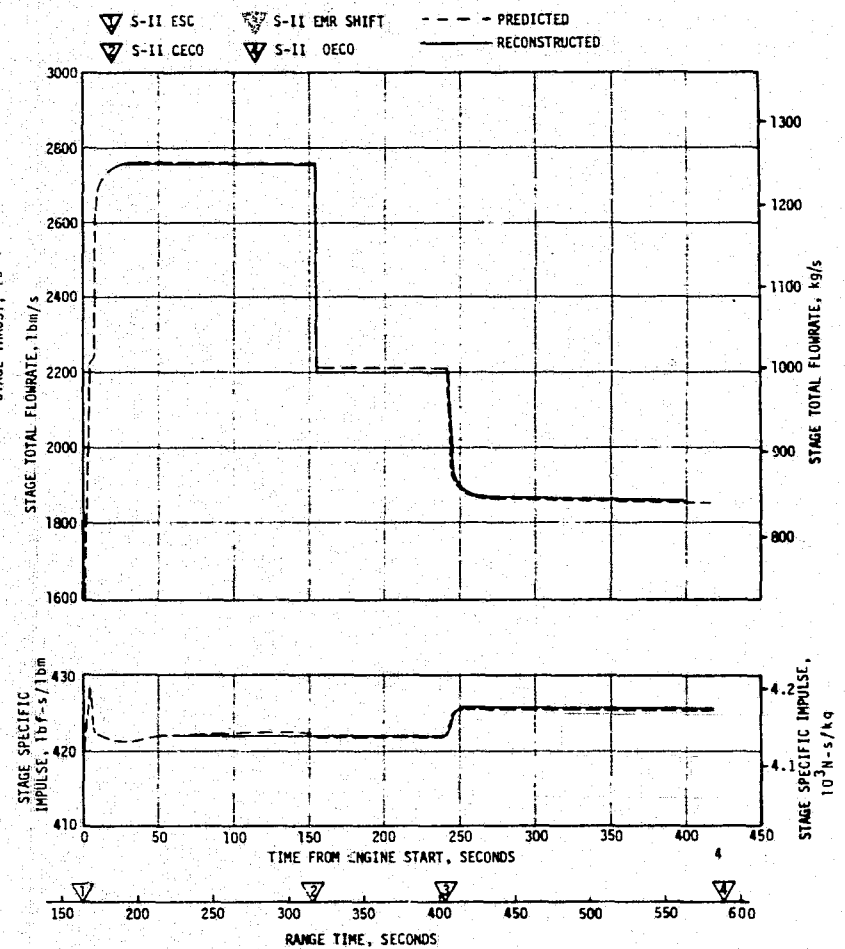
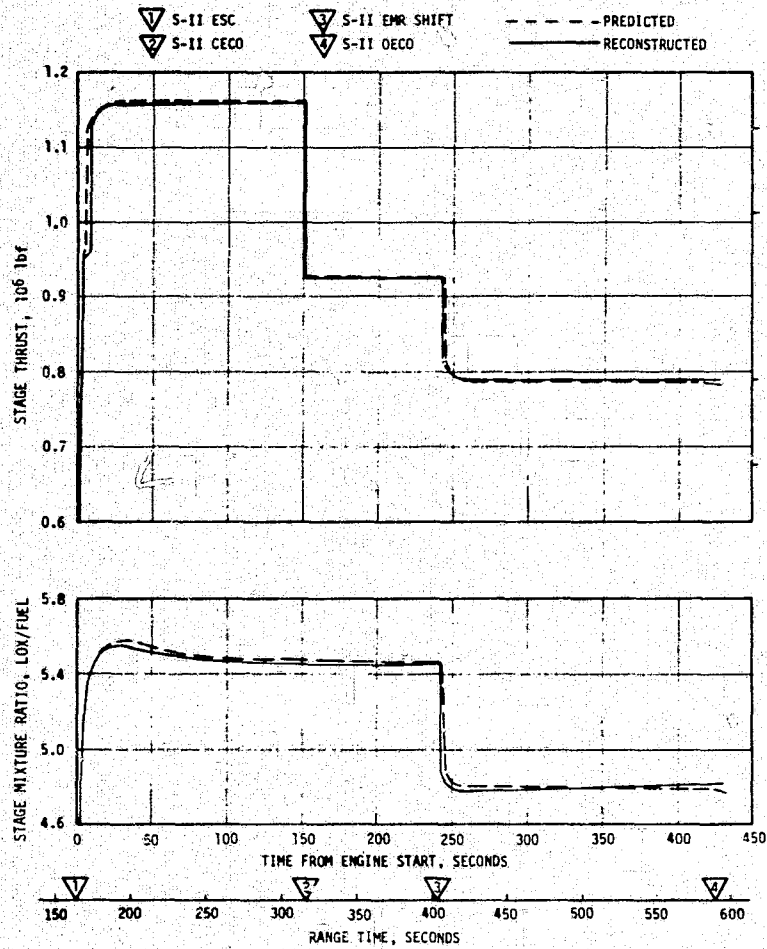


Figure 6-4. S-II Steady State Operation

Table 6-1. S-II Engine Performance

	ENGINE	PREDICTED	RECONSTRUCTION ANALYSIS	PERCENT INDIVIDUAL DEVIATION	PERCENT STAGE DEVIATION
Thrust, lbf	1	236,992	236,410	-0.25	-0.13
	2	231,320	232,278	+0.41	
	3	230,644	230,166	-0.21	
	4	232,180	231,660	-0.22	
	5	235,312	234,452	-0.36	
Specific Impulse, lbf - s/lbm	1	425.8	425.8	0	+0.057
	2	423.0	423.4	+0.095	
	3	423.2	423.5	+0.071	
	4	422.4	422.5	+0.024	
	5	425.0	425.4	+0.094	
Engine Flowrate, lbm/s	1	556.58	555.24	-0.24	-0.18
	2	546.91	548.61	+0.31	
	3	544.94	543.46	-0.27	
	4	549.62	548.27	-0.25	
	5	553.72	551.12	-0.47	
Engine Mixture Ratio, LOX/LH ₂	1	5.619	5.606	-0.23	-0.51
	2	5.599	5.563	-0.64	
	3	5.578	5.552	-0.47	
	4	5.589	5.570	-0.34	
	5	5.492	5.445	-0.86	

NOTE: Performance values at ESC +61 seconds. Values are site conditions and do not include effect of pressurization flow.

An in-run shift of -0.6°F over an 8 second period was exhibited in engine 4 fuel pump discharge temperature commencing at ESC +285 seconds. There were no corresponding changes in any other engine data and the temperature measurement was determined to be indicating warm between ESC and ESC +285 seconds. The measurement is considered questionable and no engine performance change was indicated by the flight data.

6.4 S-II SHUTDOWN TRANSIENT PERFORMANCE

The outboard engine thrust decay performance was within the predicted band as shown in Figure 6-5. As expected, outboard engine performance did not exhibit decay prior to cutoff as on previous flights. This is attributed to the higher propellant head and lower temperature propellant at the engine inlets due to the higher propellant reserves left in the tanks with the velocity signaled cutoff versus the previous mode of operating to oxidizer depletion.

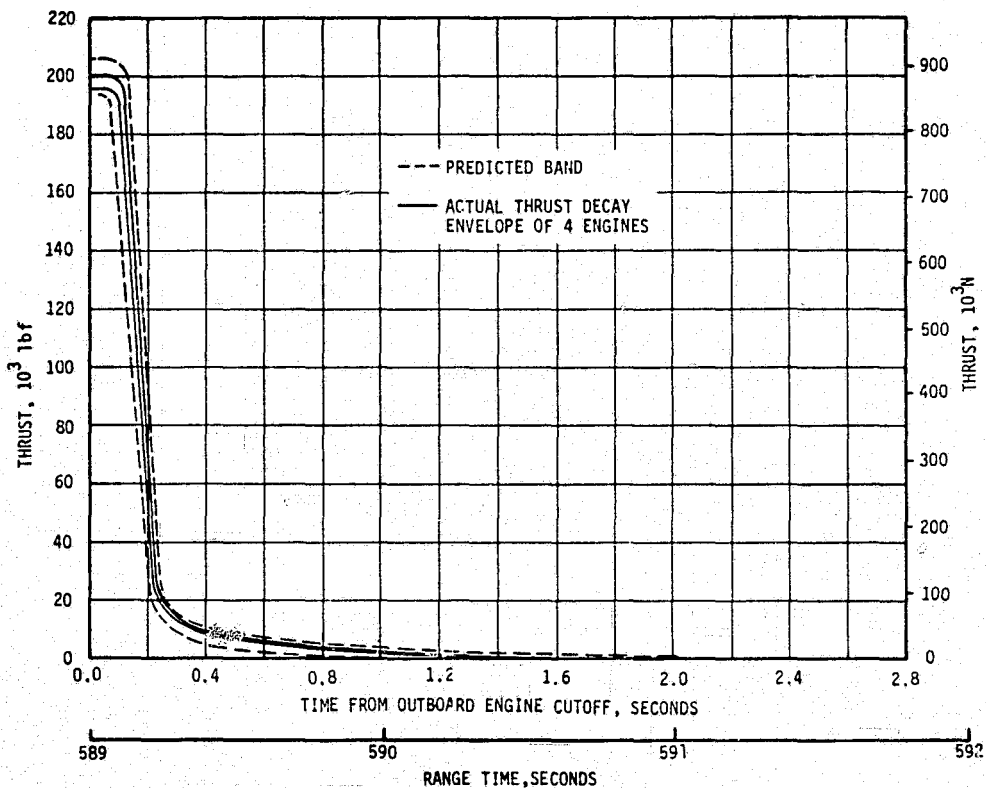


Figure 6-5. S-II Outboard Engines Thrust Decay

At S-II OECO, total thrust was down to 795,043 lbf. Stage thrust dropped to five percent of this level within 0.5 seconds. The stage cutoff impulse through the five percent thrust level is estimated to be 140,544 lbf-s.

6.5 S-II STAGE PROPELLANT MANAGEMENT SYSTEM

Ground loading and flight performance of the S-II stage propellant management system were nominal and all parameters were within normal ranges.

The Propellant Tanking Computer System (PTCS) and the stage propellant management system properly controlled S-II loading and replenishment. All S-II stage LOX and LH₂ liquid level point sensors and capacitance probes operated without any problems during the propellant loading. Both LOX and LH₂ point sensor percent wet indications were all within the loading redlines at -187 seconds.

Open loop control of EMR during flight was successfully accomplished through use of the engine two-position pneumatically operated Mixture Ratio Control Valves (MRCV). At ESC, helium pressure drove the valves to the engine start position corresponding to the 4.8 EMR. The high EMR (5.5) command was received at ESC + 5.5 seconds as expected, providing a nominal high EMR of 5.5 for the first phase of the Programmed Mixture Ratio (PMR).

The low EMR shift occurred at ESC +243.1 seconds, which is 1.1 seconds later than predicted. This time difference is attributed to either IU computational cycle time or the launch vehicle reaching the preset step command velocity at a later time than planned. The average EMR at the low step was 4.84 (4.80 predicted) which is well within the two sigma ± 0.06 mixture ratio tolerance.

Outboard Engine Cutoff (OECO) was initiated by the IU velocity signal at ESC + 428.38 seconds which was 0.7 seconds later than predicted, within tolerance. Based on the 5% point sensors and flowmeter data, propellant residuals (mass in tanks) at OECO were 16,616 lbm LOX and 5878 lbm LH₂ versus 18,935 lbm LOX, and 6197 lbm LH₂ predicted. The open-loop propellant utilization error at OECO was 22 lbm LH₂ which is within the estimated three sigma dispersion of ± 2500 lbm LH₂. open-loop PU error at OECO was 22 lbm LH₂ which is within the estimated three sigma dispersion of ± 2500 lbm LH₂.

Table 6-2 presents a comparison of propellant masses as measured by the PU probes and engine flowmeters. The best estimate of full load and cutoff masses was derived from the engine flowmeter integration and 5% point sensors.

Table 6-2. SA-513 Flight S-II Propellant Mass History

EVENT	PREDICTED, LBM		PU SYSTEM ANALYSIS, LBM		ENGINE FLOWMETER INTEGRATION, LBM, (BEST ESTIMATE)	
	LOX	LH ₂	LOX	LH ₂	LOX	LH ₂
Liftoff	822,200	160,170	822,200	160,134	820,596	160,266
S-II ESC	822,200	160,166	822,649	159,726	820,596	160,252
S-II Low EMR Step Command	306,699	65,951	307,002	65,620	303,909	65,626
5 Percent Point Sensor	75,940	16,818	78,467	16,826	75,940	16,818
S-II OECO	18,935	6,197	17,240	5,681	16,616	5,878
S-II Residual After Thrust Decay	18,715	6,081	DATA NOT USABLE	DATA NOT USABLE	16,331	5,777

NOTE: Table is based on mass in tanks and sump only. Propellant trapped external to tanks and LOX sump is not included. PU data are not corrected for tank/probe mismatch.

S-II LH₂ slosh amplitudes as indicated by the capacitance probes were nominal except for the time period between 60 and 90 seconds of S-IC boost when amplitudes were greater than predicted. Maximum amplitude reached at the probe was 14 inches peak-to-peak at 80 seconds, compared to 12 inches predicted. The cause of this difference is not fully resolved. Just prior to S-IC cutoff, indicated S-II slosh amplitudes were 4 inches peak-to-peak at the probe for LH₂ and 0.5 inches peak-to-peak for LOX. After S-II thrust buildup, the amplitudes were 9.5 inches peak-to-peak for LH₂ and 7.5 inches peak-to-peak for LOX. A full discussion of S-II slosh is given in paragraph 9.2.2.

6.6 S-II PRESSURIZATION SYSTEM

6.6.1 S-II Fuel Pressurization System

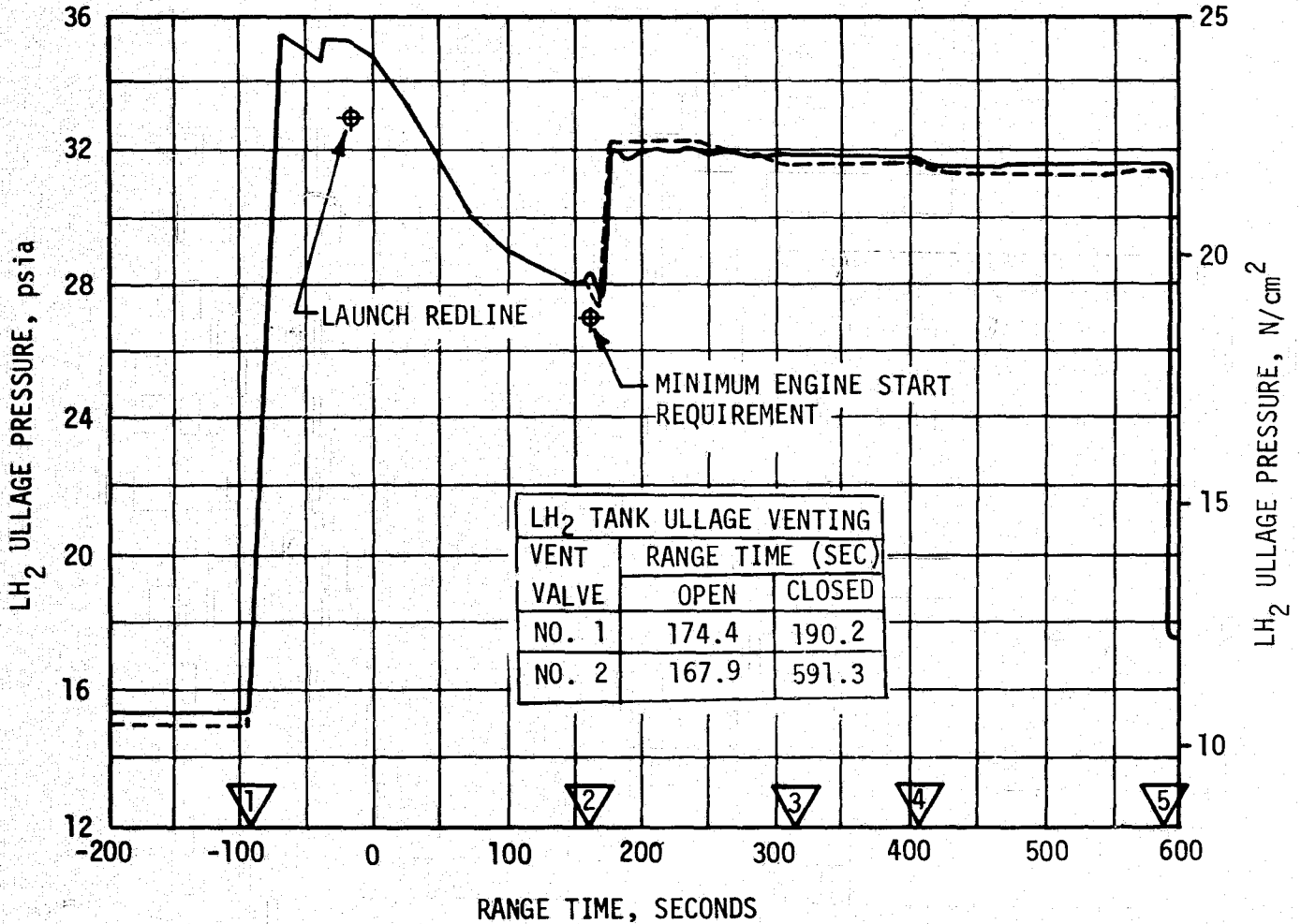
LH₂ tank ullage pressure, actual and predicted, is presented in Figure 6-6 for autosequence, S-IC boost, and S-II boost. The LH₂ vent valves were closed at -93.1 seconds and the ullage volume pressurized to 35.4 psia in 17.6 seconds. One make-up cycle was required at approximately -39 seconds and the ullage pressure was increased from 34.5 psia to 35.3 psia. Ullage pressure at -19 seconds (launch commit) was 35.3 psia which is within the redline limits of 33.0 to 38.0 psia. Ullage pressure decayed to 35.0 psia at S-IC ESC at which time the pressure decay rate increased for about 20 seconds. The increased decay rate was attributed to an increase in LH₂ surface agitation caused by S-IC engine firing and flight control maneuvers. This decay is normal and seen on previous launches.

During S-IC boost, the LH₂ tank pressure remained within the allowable low-mode band of 27.5 to 29.5 psi. Neither LH₂ vent valves opened during this boost mode. Ullage pressure at S-II engine start was 28.6 psia exceeding the minimum engine start requirement of 27 psia. The LH₂ vent valves were switched to the high vent mode (30.5 to 33.0 psia) prior to S-II engine start.

During S-II boost, the GH₂ for pressurizing the LH₂ tank was controlled by a flow control orifice in the LH₂ tank pressurization line with maximum tank pressure controlled by the LH₂ vent valves. For this flight, the ullage pressure remained within the 30.5 to 33 psia vent band. LH₂ vent valve No. 1 opened three (3) times during the first 29.6 seconds of S-II boost. LH₂ vent valve No. 2 opened at 167.9 seconds and remained open until 591.3 seconds. The LH₂ ullage pressure was within 0.3 psi of the predicted pressure during S-II boost.

Figure 6-7 shows LH₂ pump total inlet pressure, temperature, and Net Positive Suction Pressure (NPSP) for the J-2 engines. The parameters were in close agreement with the predicted values throughout the S-II flight period. NPSP remained above the minimum requirement throughout the S-II burn phase.

- 1 LH₂ PREPRESSURIZATION START
 - 2 S-II ESC
 - 3 S-II CECO
 - 4 S-II EMR SHIFT
 - 5 S-II OECS
- - - - PREDICTED
 ———— ACTUAL



6-11

Figure 6-6. S-II Fuel Tank Ullage Pressure

6.6.2 S-II LOX Pressurization System

LOX tank ullage pressure, actual and predicted, is presented in Figure 6-8 for autosequence, S-IC boost, and S-II burn. After a 107 second cold helium chilldown flow through the LOX tank, the chilldown flow was terminated at -200 seconds. The vent valves were closed at -184 seconds and the LOX tank was pressurized to the pressure switch setting of 38.6 psia in 50.6 seconds. One pressure make-up cycle was required at -103.2 seconds. The LOX tank ullage pressure increased to 39.7 psia because of common bulkhead flexure during LH₂ tank prepressurization. Ullage pressure at -19 seconds was 39.7 psia which is within the redline limits of 36 to 43 psia. The LOX vent valves performed satisfactorily during all prelaunch operations.

The LOX vent valves remained closed during S-IC boost and the LOX tank ullage pressure prior to S-II ESC was 40.3 psia. During S-II boost, the LOX tank pressure varied from a maximum of 41.3 psia at 180 seconds to a minimum of 39.6 psia at S-II OECO. The GOX for pressurizing the LOX tank was controlled by a flow control orifice in the LOX tank pressurization line with the LOX tank vent valves controlling excessive pressure buildup within a pressure range setting of 39.0 to 42.0 psia. LOX vent valve No. 2 remained closed during S-II boost. LOX vent valve No. 1 cracked open and reseated a total of 75 times between 161.7 seconds and 355.5 seconds. Frequent vent valve modulations indicate the valve was modulating within a narrow crack and reseat pressure band. This performance is acceptable since the ullage pressure was stable during this period.

The LOX tank ullage pressure was within 0.3 psi of the pressure predicted for S-II boost during high engine mixture ratio (EMR) and was greater than predicted during low EMR engine operation as shown in Figure 6-8. Comparisons of the LOX pump total inlet pressure, temperature, and NPSP are presented in Figure 6-9. Throughout S-II boost, the LOX pump NPSP was well above the minimum requirement.

This was the third flight using the LOX tank pressure switch purge. The purge system was incorporated to preclude a potential LOX/GOX incompatibility situation within the LOX pressure switch assembly. The purge is connected to the helium injection and accumulator fill helium supply system. No instrumentation is available to evaluate the purge system. However, since both the helium injection and accumulator fill systems operated successfully, it is concluded that the purge system also functioned properly.

6.7 S-II PNEUMATIC CONTROL PRESSURE SYSTEM

The pneumatic control system functioned satisfactorily throughout the S-IC and S-II boost periods. Bottle pressure was 2990 psia at -30 seconds and with normal valve activities during S-II burn, pressure decayed to approximately 2685 psia after S-II OECO.

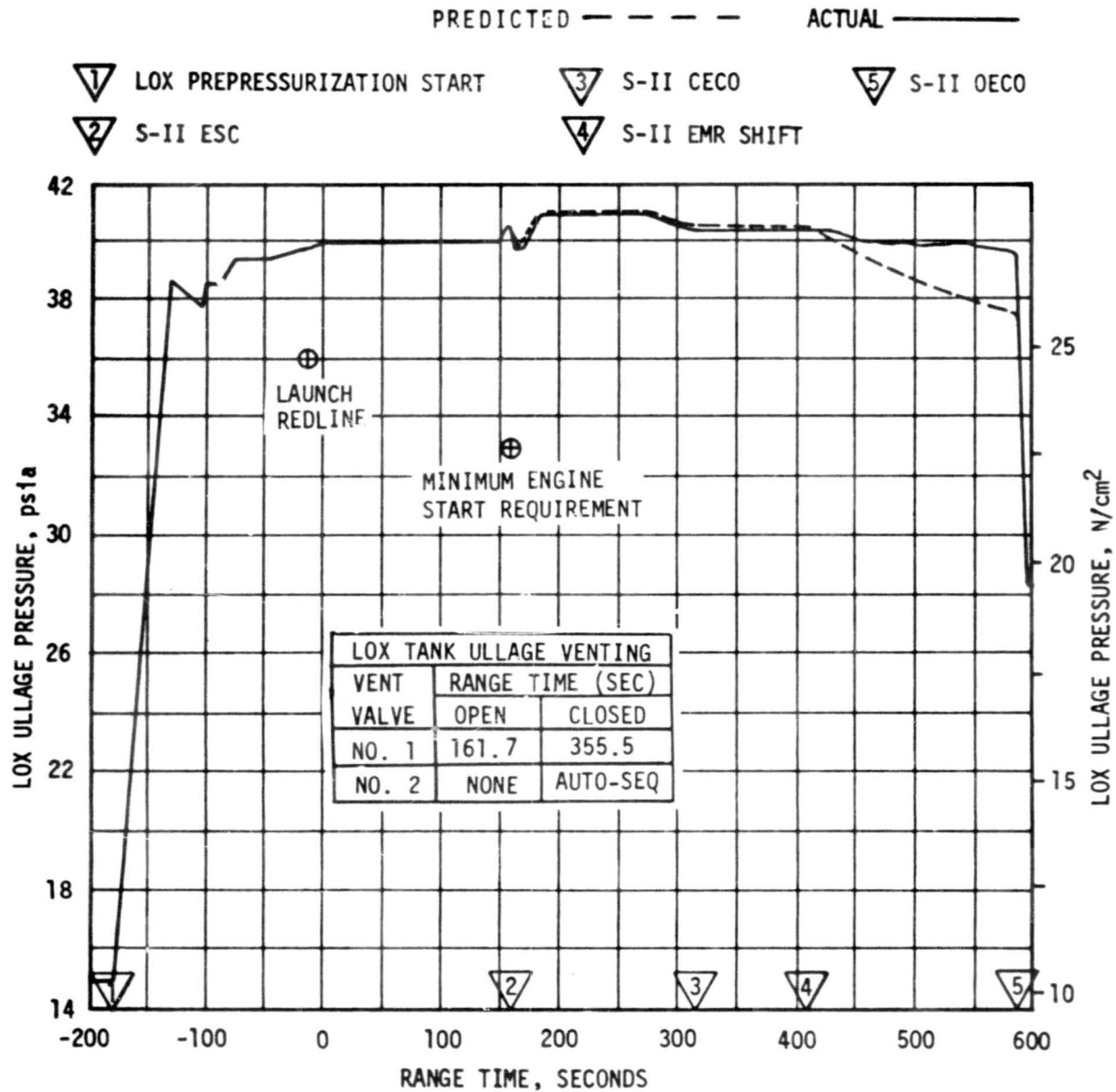


Figure 6-8. S-II LOX Tank Ullage Pressure

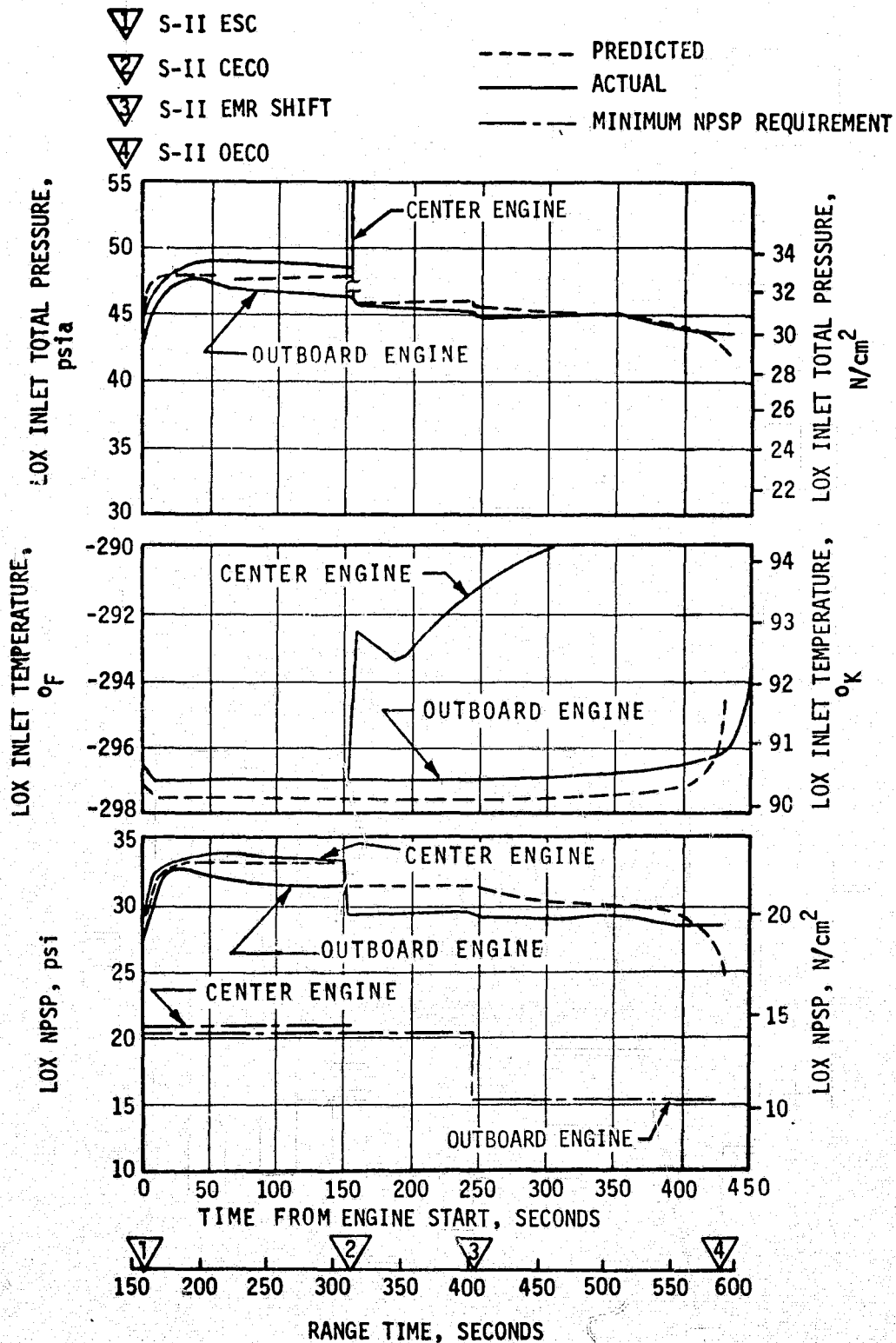


Figure 6-9. S-II LOX Pump Inlet Conditions

The pneumatic control system pressure regulator maintained the outlet pressure at 720 psia, except for the expected momentary pressure drops when the recirculation valves were actuated closed just after engine start, and when the pre valves were closed at CECO and OECO.

6.8 S-II HELIUM INJECTION SYSTEM

The performance of the helium injection system was satisfactory. The supply bottle was pressurized to 3000 psia prior to liftoff and by S-II ESC the pressure was 1755 psia. Helium injection average total flowrate during supply bottle blowdown (-30 to 158 seconds) was 70.3 SCFM. During the prelaunch countdown, the helium injection bottle decay test results indicated that no adverse trends existed.

6.9 POGO SUPPRESSION SYSTEM

A center engine LOX feedline accumulator was installed on the S-II stage as a POGO suppression device. Analysis indicates that there were no S-II POGO oscillations.

The accumulator system consists of (1) a bleed system to maintain sub-cooled LOX in the accumulator through S-IC boost and S-II engine start, and (2) a fill system to fill the accumulator with helium subsequent to engine start and maintain a helium filled accumulator through S-II CECO.

The accumulator bleed subsystem performance is satisfactory. Figure 6-10 shows the required accumulator temperature at engine start, the predicted temperatures during prelaunch and S-IC boost, and the actual temperatures experienced during AS-513 flight. The maximum allowable temperature of -281.5°F at engine start was adequately met (-294.4°F actual).

Accumulator fill was initiated 4.1 seconds after engine start. Figure 6-11 shows the accumulator LOX level versus time during accumulator fill. The fill time was 6.3 seconds, within the required 5 to 7 seconds. The helium fill flow rate, during the fill transient, was 0.0056 lbm/s and the accumulator pressure was 44.7 psia.

After the accumulator was filled with helium, it remained in that state until S-II CECO when the helium flow was terminated by closing the two fill solenoid valves. The accumulator bottom temperature measurement indicated there was liquid propellant splashing on the bottom temperature probe shortly after the accumulator was filled with helium gas. This type of phenomena was observed during the ground static firing test of the S-II-14 vehicle and the splashing presented no danger or problem to the success of the flight. Figure 6-12 shows the helium injection and accumulator fill supply bottle pressure during accumulator fill operation. The supply bottle pressure was within the predicted band, indicating that the helium usage rates were as predicted.

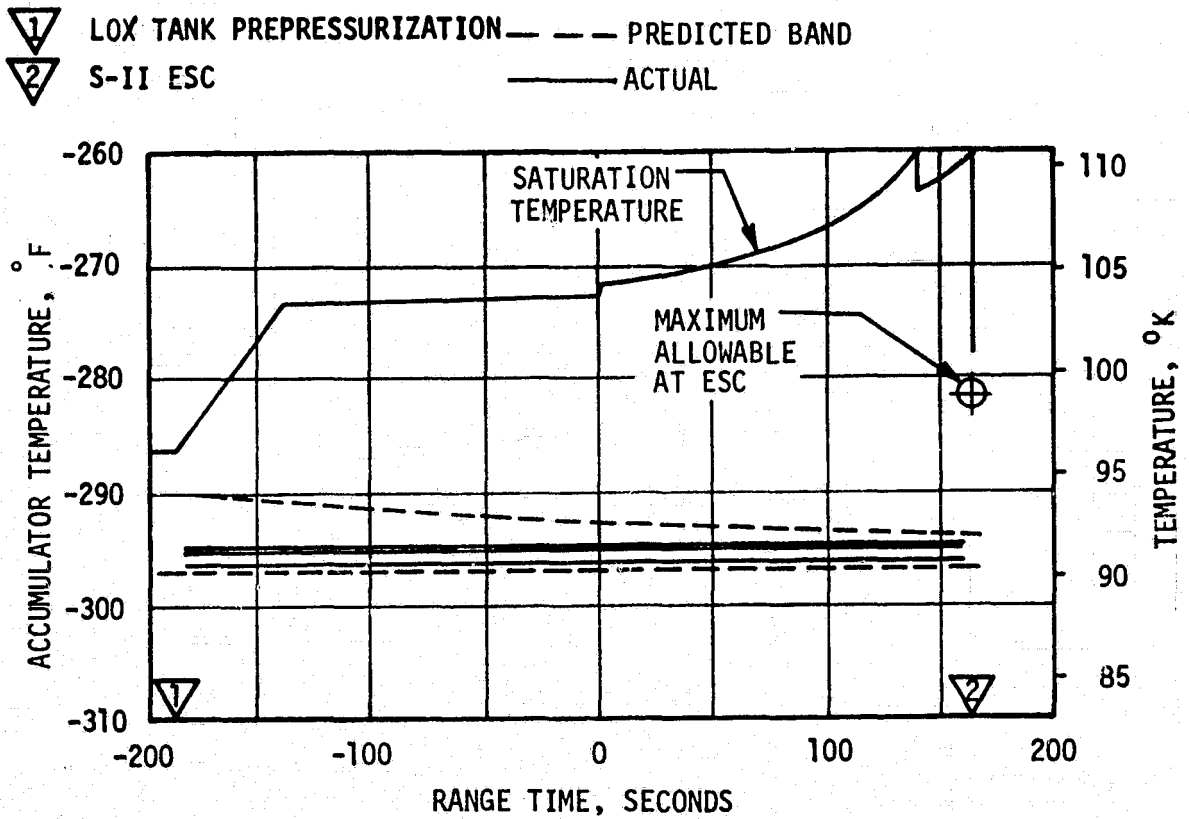


Figure 6-10. S-II Center Engine LOX Feedline Accumulator Bleed System Performance

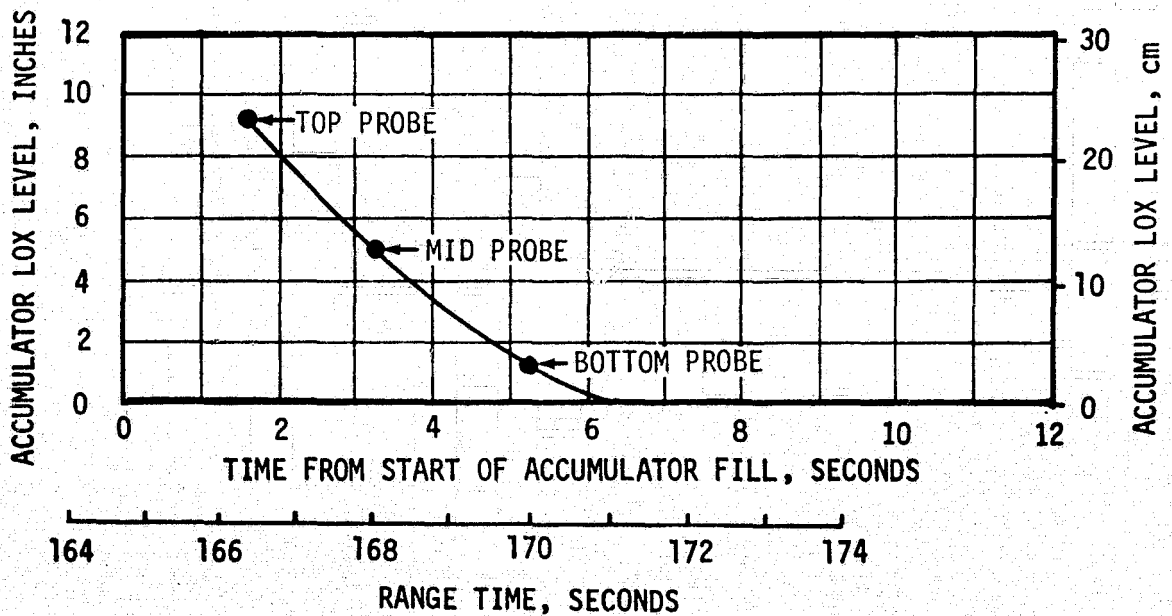


Figure 6-11. S-II Center Engine LOX Feedline Accumulator Fill Transient

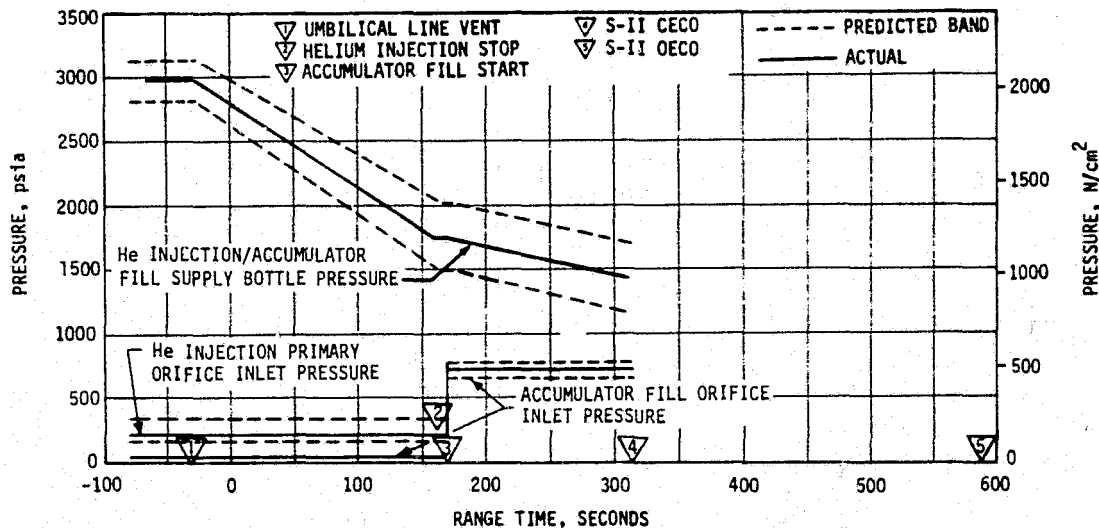


Figure 6-12. S-II Center Engine LOX Feedline Accumulator Helium Supply System Performance

6.10 S-II ORBITAL SAFING OPERATIONS

All orbital safing operations were performed satisfactorily. The engines hydrogen start tank pressures were slightly higher than expected at start of safing due to thermal warmup caused by the abnormally high aft inter-stage temperatures. The slightly higher pressures caused the pressure decay rate to be on the high side of the predicted band but safing was achieved successfully.

6.10.1 Fuel Tank Safing

S-II safing was initiated at 805.1 seconds and the two ordnance actuated fuel tank non-propulsive vent valves were opened at 805.2 seconds. The fuel tank ullage pressure subsequently decayed within the predicted band from 18.5 psia at the initiation of safing to 9.2 psia at 7200 seconds as shown in Figure 6-13. The differential pressure across the common bulkhead was at all times well below the maximum allowable collapse pressure of 14.6 psi.

6.10.2 LOX Tank Safing

The two ordnance actuated LOX tank non-propulsive vent valves were opened at 805.2 seconds. The LOX tank ullage pressure subsequently decayed within the predicted band from 29.7 psia at the start of safing to 9.2 psia at 7200 seconds as shown in Figure 6-14. Comparison of the LOX and LH₂ tank ullage pressures show that the differential pressure across the common bulkhead was well below the maximum allowable burst pressure of 17.5 psi.

6.10.3 Engine Start Sphere Safing

The hydrogen start tanks were safed by energizing the start tank emergency vent valves. This allows the tanks to vent overboard at umbilical panel

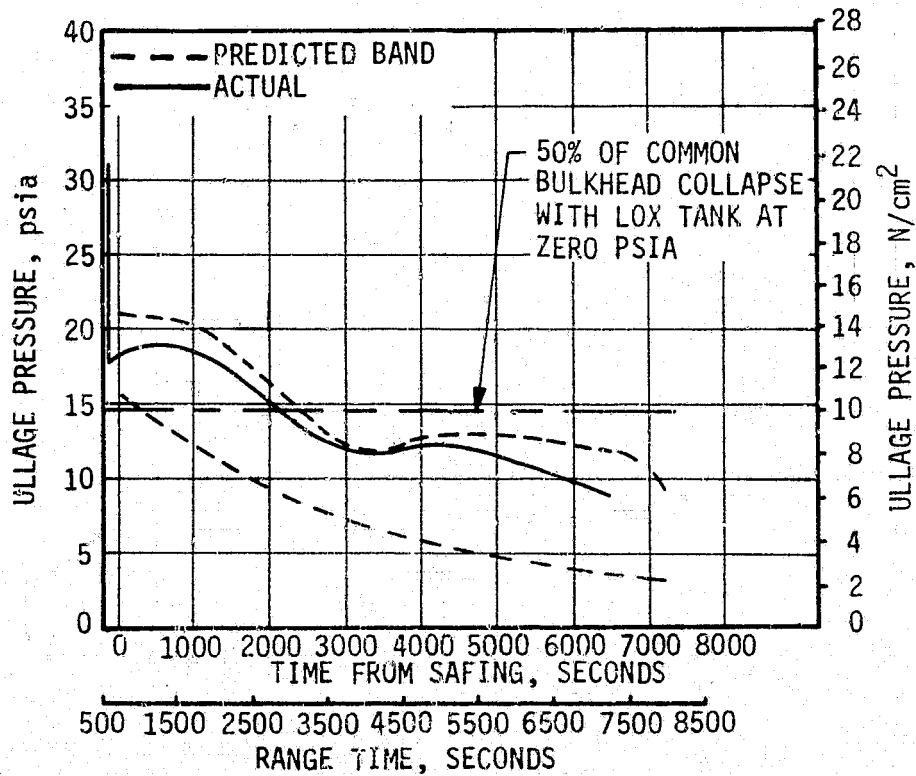


Figure 6-13. S-II Fuel Tank Ullage Pressure During Safing

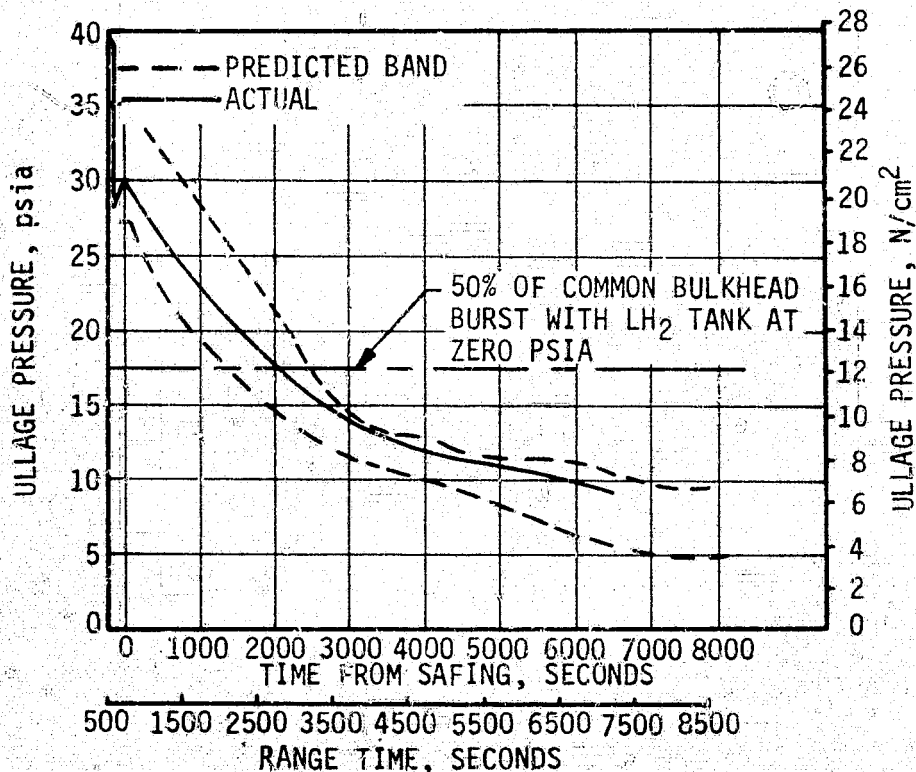


Figure 6-14. S-II LOX Tank Ullage Pressure During Safing

#3A through the LH₂ Pump Seal Drain System. The tanks were safed from a maximum pressure of 430 psia to 65 and 78 psia (Engines No.'s 3 and 4, respectively) in 855 seconds as shown in Figure 6-15. Data subsequent to the first revolution (5200 seconds from initiation of safing) indicated tank pressures of 12 and 18 psia. The tank pressures at the initiation of safing were slightly higher than predicted due to thermal warmup caused by the abnormally high aft interstage temperatures.

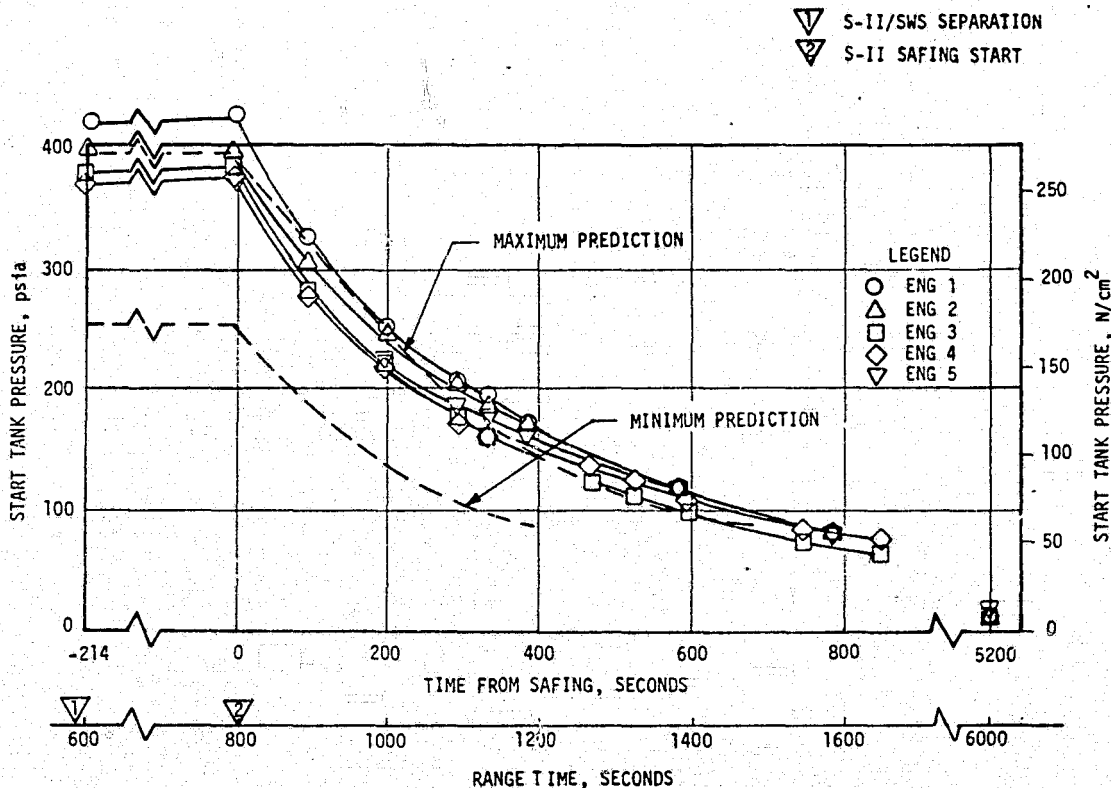


Figure 6-15. S-II Engine GH₂ Start Tank Safing

6.10.4 Engine Control Sphere Safing

The helium tanks were safed by energizing the engine helium control solenoid valves which initiates the engine purges (LOX dome, GG LOX injection and LOX pump intermediate seal) thus depleting the helium in the tanks. The tanks were safed from a maximum pressure of 2890 psia (Engine No. 5) down to 60 to 120 psia in 335 seconds as shown in Figure 6-16. Data subsequent to the first revolution (5200 seconds from initiation of safing) indicated tank pressures of 0 to 60 psia.

6.11 S-II HYDRAULIC SYSTEM

S-II hydraulic system performance was normal throughout the flight. Hydraulic pressures during the countdown and flight were normal. Accumulator gas pressures ranged between 3650 and 3800 psia compared to the redline of 3000 psia minimum. Accumulator pressures were between 3530 and 3630 psia, which is well within the predicted range of 3300 to 3800 psia. Reservoir pressures were between 98 and 100 psia compared to predicted values of 78 to 105 psia.

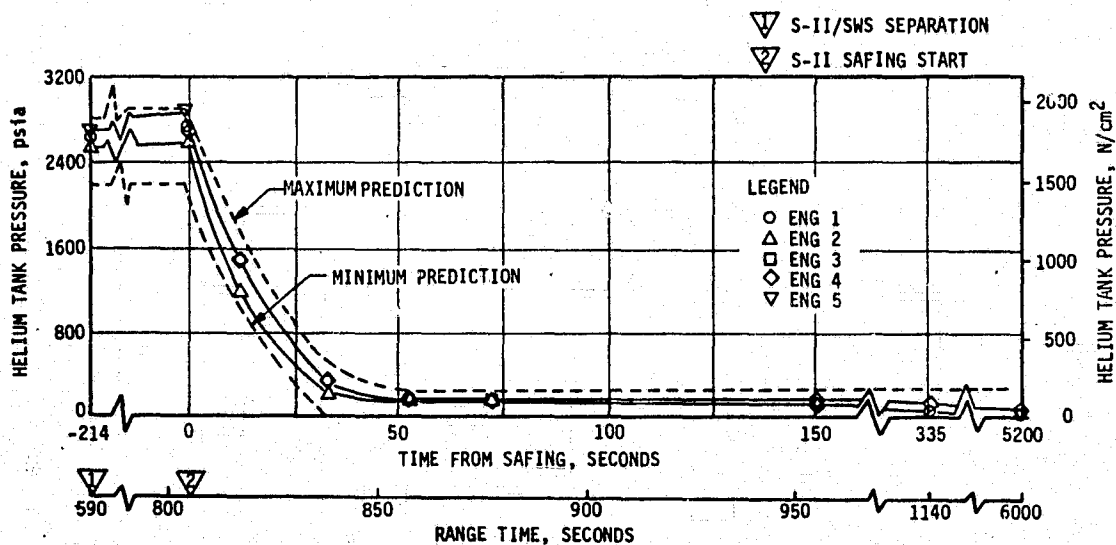


Figure 6-16. S-II Engine Helium Tank Safing

Servoactuator performance was normal. The servoactuator piston position was less than 0.25 degree compared to the redline of + 1.5 degrees. A maximum compressive force of 6500 lbs was exerted by the pitch actuator of Engine No. 1, well below the maximum predicted force of 19,000 lbs.

The fluid temperatures were nominal at liftoff and S-II ESC. However, during S-II boost the fluid temperatures increased more rapidly than on previous flights resulting in a maximum temperature of 198°F at engine cutoff compared to 120°F on other flights. The high temperatures are attributed to a high base heating condition in the engine compartment due to failure of the S-IC/S-II interstage to separate. (Discussed in paragraph 9.5.2)

The reservoir volumes during prelaunch and engine start were well above the minimum redline limit of 10 cubic inches. During S-II boost and at S-II OECO, the volumes were greater than on previous flights due to increased fluid thermal expansion caused by the unusually high base heating.

SECTION 7

STRUCTURES

7.1 SUMMARY

Evaluation of the structural performance of the launch vehicle shows no area of concern for the SA-513 vehicle, and all conditions were well within the envelope observed on recent Apollo flights.

The maximum structural loads were experienced during the S-IC boost phase and were below the design values. The maximum bending moment was 82×10^6 lbf-in at the S-IC LOX tank (approximately 40 percent of the design value). The maximum longitudinal transient responses at the Instrument Unit (IU) were $+0.15$ g and $+0.05$ g at S-IC Center Engine Cutoff (CECO) and Outboard Engine Cutoff (OECO), respectively. These values are lower than those observed on recent flights.

During S-IC boost phase the expected small oscillatory response in the first longitudinal mode (6 Hz) was observed from approximately 95 seconds until CECO. The Instrument Unit sensors reached $+0.06$ g just prior to CECO. This is the same level experienced on AS-5T2 and AS-511. POGO did not occur during S-IC boost.

The S-II stage center engine LOX feedline accumulator successfully inhibited the 16 Hz POGO oscillations. A peak response of $+0.2$ g was measured on engine No. 5 gimbal pad during steady state engine operation. As on previous Apollo flights, low amplitude 11 Hz oscillations were experienced near the end of S-II burn. Peak engine No. 1 gimbal pad response was $+0.04$ g. POGO did not occur during S-II boost.

The SA-513 vibration levels were similar at liftoff and lower during subsequent flights as compared to those experienced on previous missions.

7.2 TOTAL VEHICLE STRUCTURES EVALUATION

7.2.1 Longitudinal Loads

The structural loads experienced during SA-513 boost were well within design values. The steady state acceleration of 1.27 g at launch was slightly higher than predicted (1.25 g) resulting in slightly higher longitudinal loads but no associated problems. The maximum longitudinal dynamic response of $+0.20$ g (Figure 7-1) at the IU during thrust buildup is comparable to that experienced on previous Apollo flights.

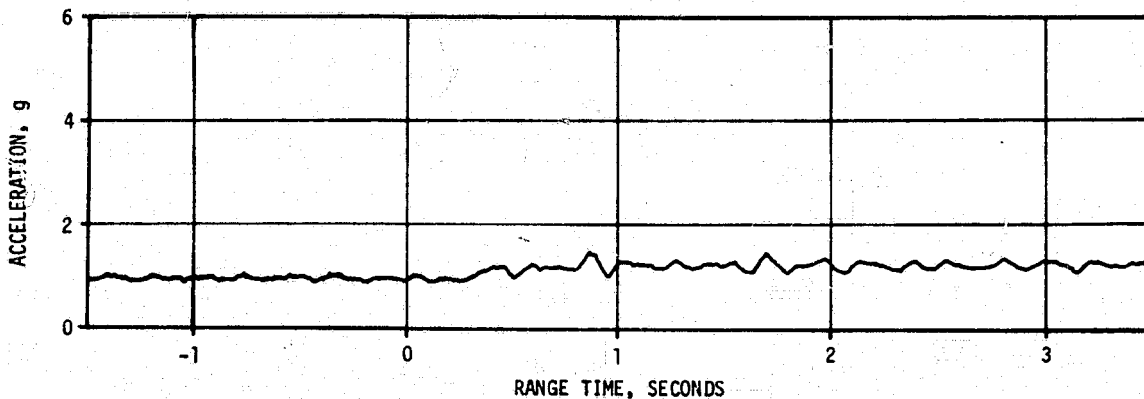


Figure 7-1. SA-513 Longitudinal Acceleration at IU During S-IC Thrust Buildup and Launch

The F-1 engine thrust buildup rates were normal. The ignition sequence was 1-1-1-1-1 with engines 2 and 3 igniting early relative to the center engine. While the planned 1-2-2 start sequence was not achieved (Reference Paragraph 5.2) the time deltas between pairs of diametrically opposed engines were within the 3σ dispersion (229 ms) used in the pre-flight loads analyses.

The maximum longitudinal dynamics resulting from CECO were $+0.15$ g at the IU as shown in Figure 7-2. This value was slightly lower than the $+0.25$ to $+0.20$ g which was experienced on previous flights.

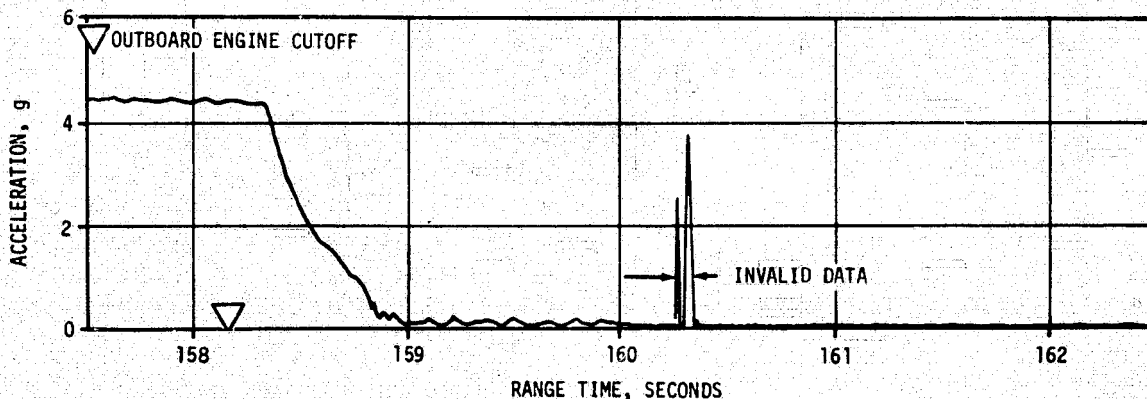
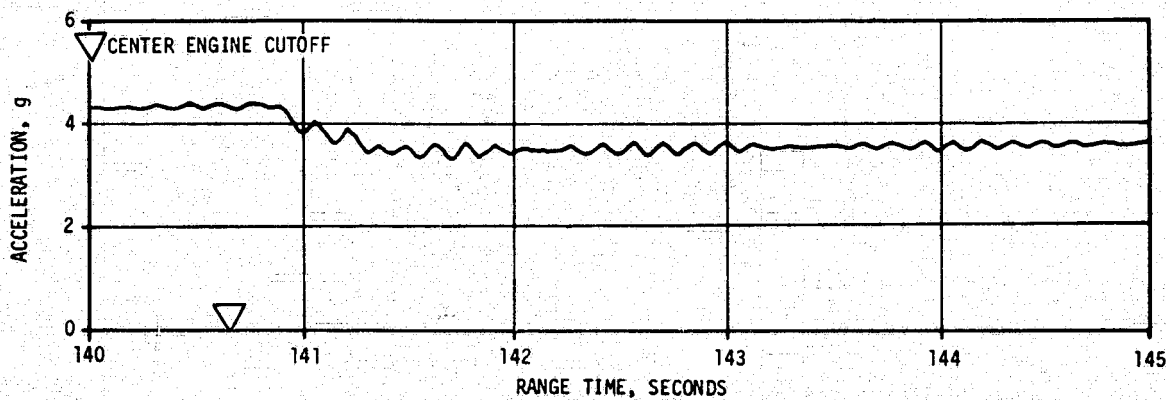


Figure 7-2. SA-513 Longitudinal Acceleration at IU at Time of S-IC Engine Cutoff

For OECO the maximum longitudinal dynamics at the IU were ± 0.05 g (Figure 7-2); previous flights were ± 0.27 to ± 0.32 g. The significantly lower dynamics at OECO are due to the staggered 2-2 outboard F-1 engine shutdown sequence.

Maximum IU longitudinal dynamics at S-II cutoff and S-II/SWS separation are shown in Figure 7-3. The dynamics of ± 0.1 g are significantly lower than the preflight prediction of ± 0.5 g.

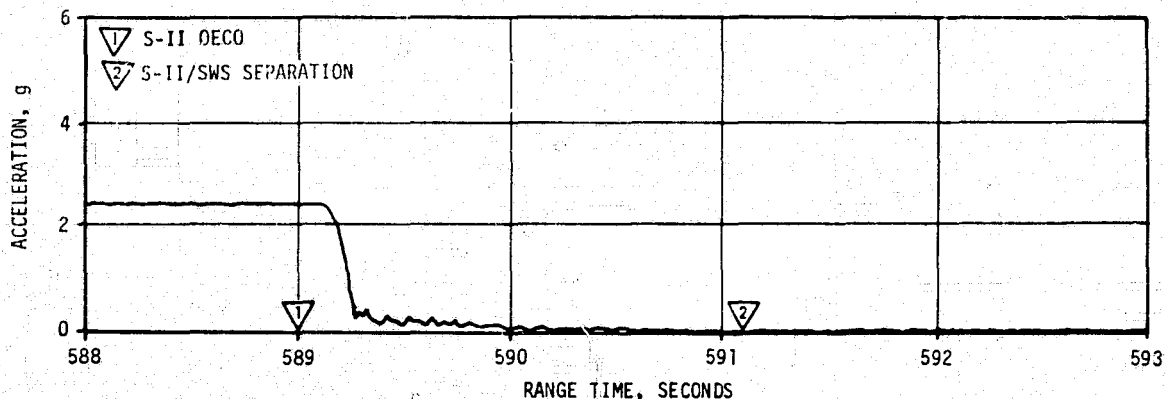


Figure 7-3. SA-513 Longitudinal Acceleration at IU During S-II Thrust Decay and S-II/SWS Separation

The longitudinal loads experienced at the time of maximum bending moment (66 seconds) were as expected and are shown in Figure 7-4. The steady state longitudinal acceleration was 1.9 g. Figure 7-4 also depicts that the maximum longitudinal loads imposed on the S-IC stage thrust structure, fuel tank, and intertank area occurred at S-IC CECE (140.5 seconds) at a longitudinal acceleration of 4.45 g.

7.2.2 Bending Moments

Peak bending moments occurring at 66 seconds are shown in Figure 7-5. Bending moment computations are based on measured flight parameters (gimbal angle and dynamic pressure) and reconstructed angle of attack. The maximum moment of 82×10^6 lbf-in at station 1156 was approximately 40 percent of design value.

The maximum lateral dynamics in the yaw direction at the IU during lift-off were ± 0.08 g (Figure 7-6). Accelerations in the pitch direction were of comparable amplitude. Predicted 3σ values during liftoff were ± 0.32 g at the IU.

7.2.3 Combined Loads

Combined compression and tension loads were computed for the maximum bending moment, CECE, and OECO conditions using the loads shown in Figures 7-4 and 7-5 and measured ullage pressures.

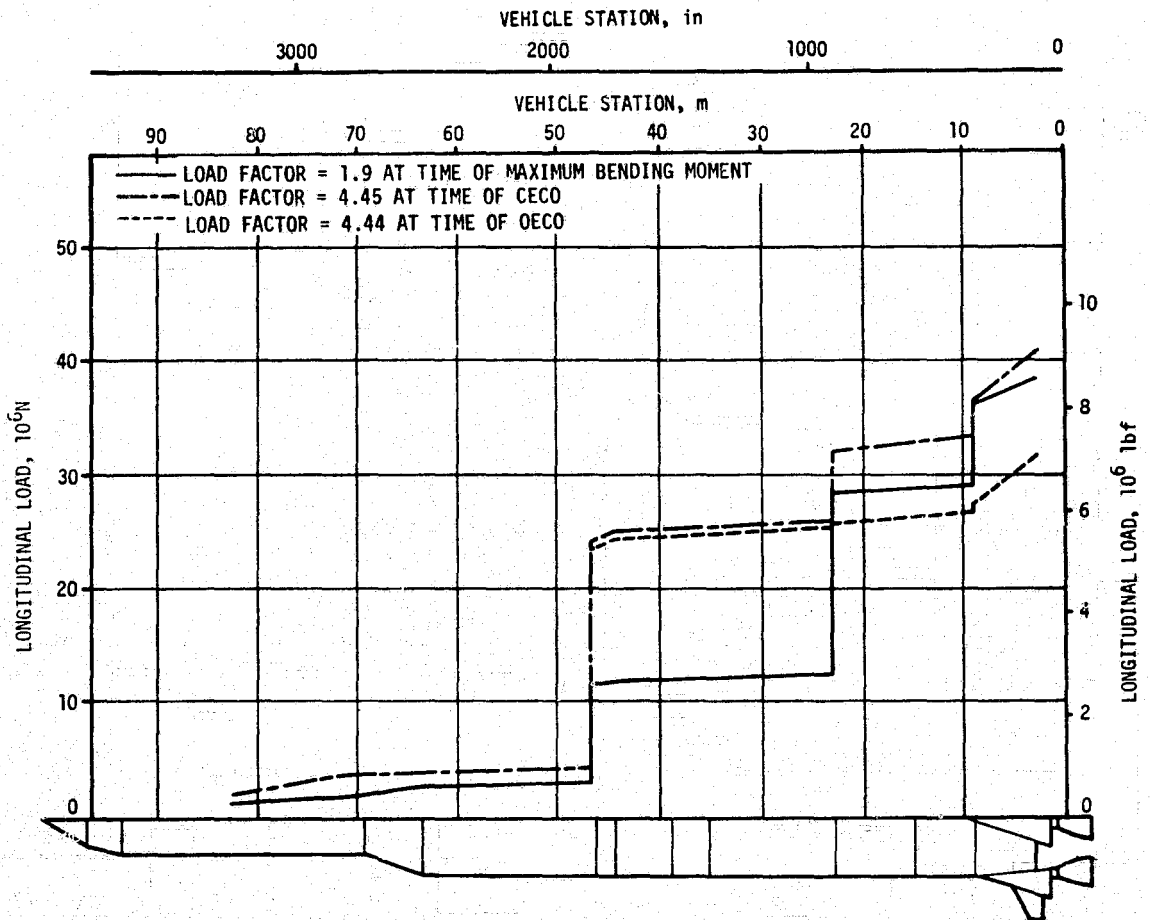


Figure 7-4. SA-513 Longitudinal Load Distribution at Time of Maximum Bending Moment, CECO and OECO

The envelope of combined loads experienced are shown for each vehicle station along with the associated capabilities in Figure 7-7. The minimum factor of safety (Ratio of capability to actual limit load) was 1.32 at Station 3258 for the CECO condition.

7.2.4 Vehicle Dynamic Characteristics

During S-IC stage boost, the significant vehicle response was in the expected 6 Hz first longitudinal mode. The IU sensor A2-603 reached ± 0.06 g near CECO. This is the same level experienced on AS-512 and AS-511. Spectral analysis of engine chamber pressure measurements shows no detectable buildup of structural/propulsion coupled oscillations. POGO did not occur during S-IC boost. Figure 7-8 shows the SA-513 longitudinal modal frequency correlation (analysis vs. measured). The analysis is in good agreement with the measured data as the vehicle responds in the first longitudinal mode (at low amplitudes) throughout the S-IC boost phase except for a few seconds after the 63-second anomaly (See Section 17). At this time, the accelerometer which is located on the IU skin senses longitudinal oscillations as the vehicle responds in

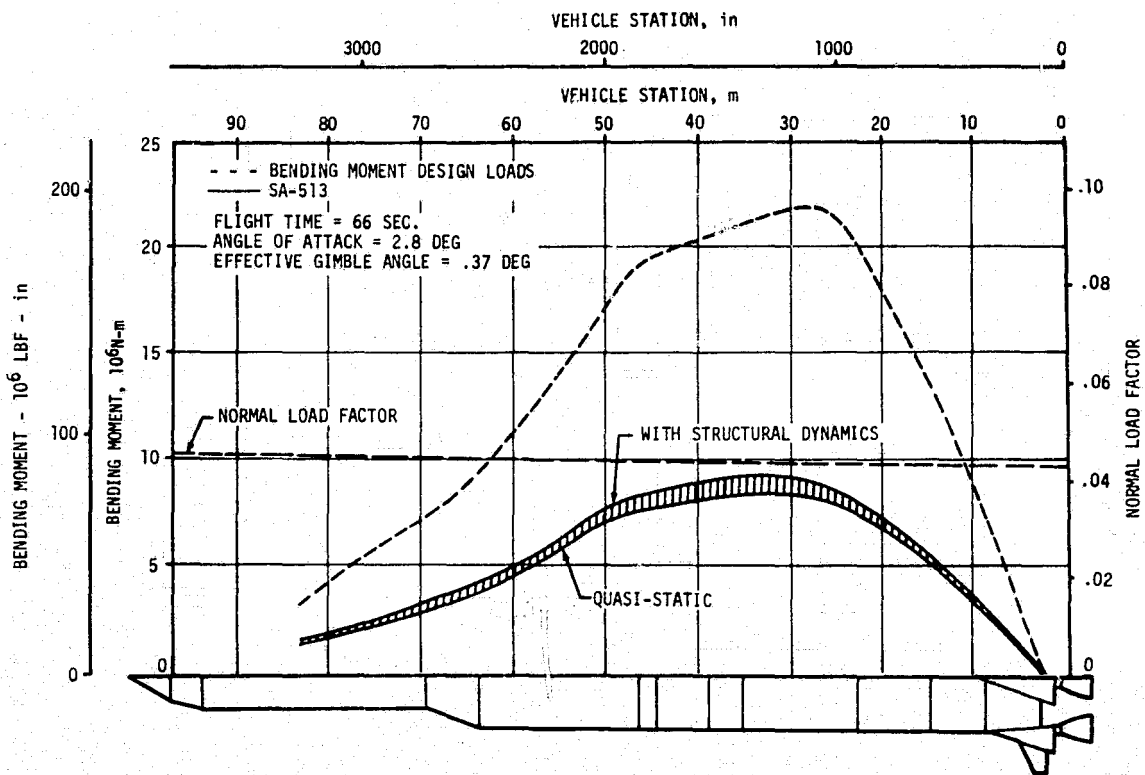


Figure 7-5. SA-513 Maximum Bending Moment

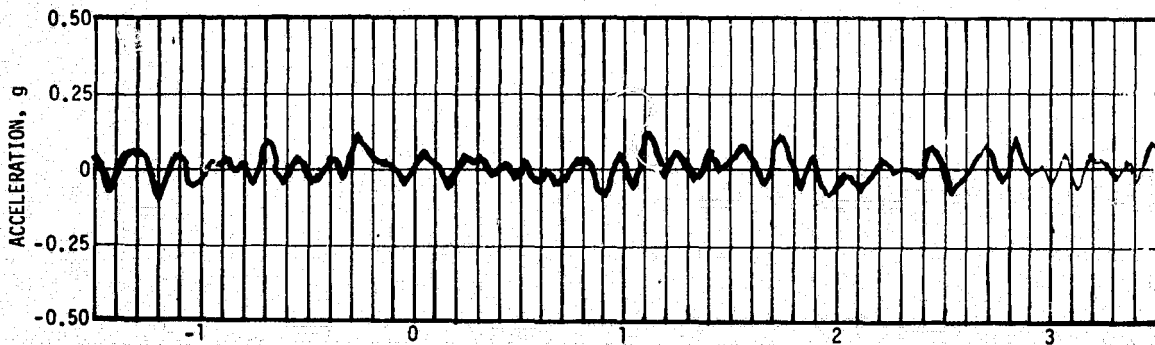


Figure 7-6. SA-513 Lateral Acceleration During Thrust Buildup and Launch

the third bending mode.

The SA-513 lateral modal frequency correlation (analysis vs. measured) shows the analysis to be in good agreement with the measured data (Figure 7-9). Early in the flight the vehicle responds in the third bending-mode. This mode can easily be excited by aerodynamic forces. Later in flight,

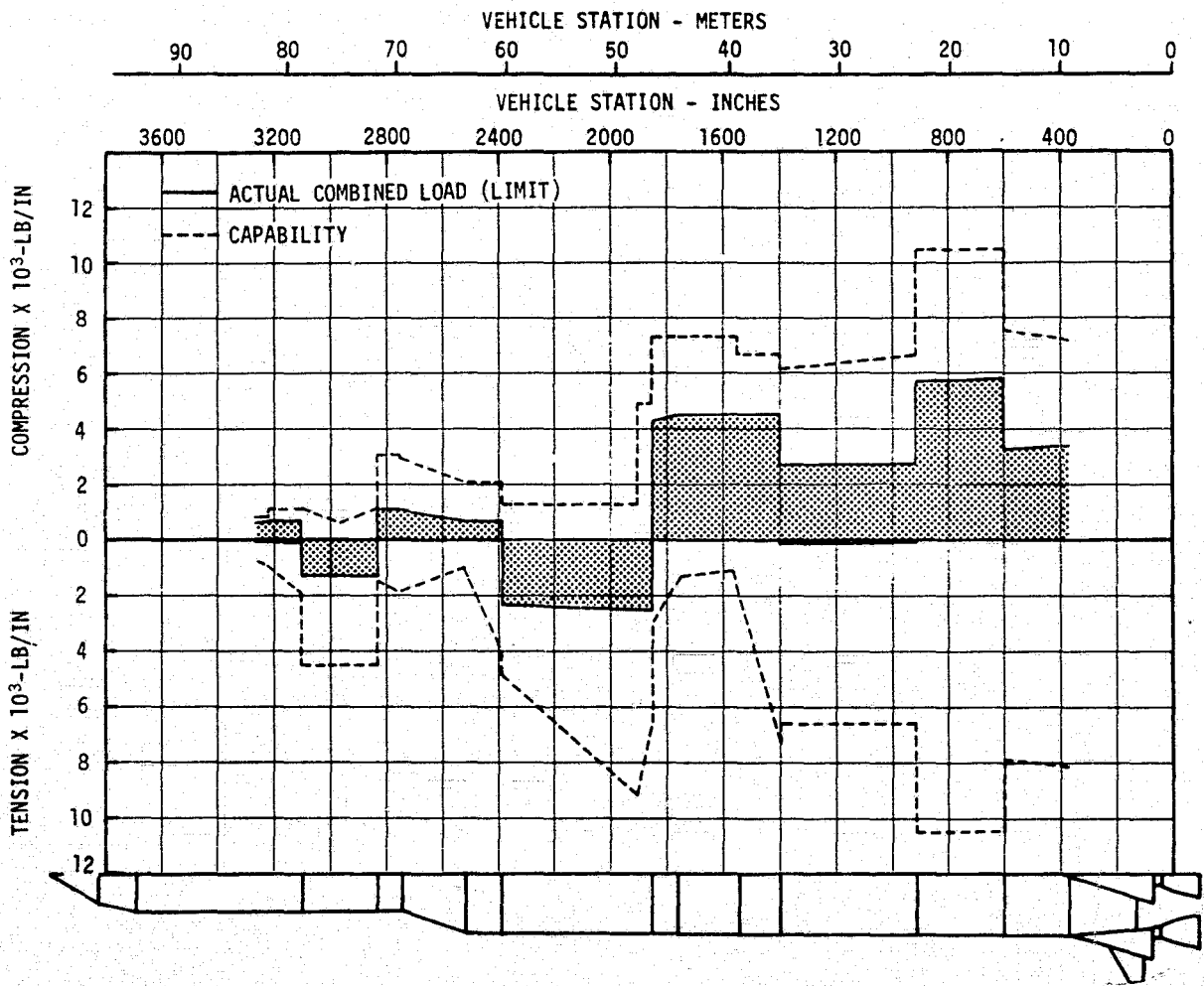


Figure 7-7. SA-513 Envelope of Maximum Combined Loads

when the aerodynamic forces diminish, the vehicle responds in the second mode which can be excited by engine perturbations. The maximum amplitude ($+0.4$ g) was recorded in the IU at the time of 63 seconds anomaly (reference Section 17) in the third bending mode which was excited externally at the OWS. This mode has its largest structural gain in this area and essentially zero gain at the engine gimbal pads.

The S-II stage center engine accumulator effectively suppressed the 16 Hz POGO phenomenon. The flight data show that the 16 Hz oscillations were inhibited with amplitudes generally less than those on recent Apollo flights. The peak center engine gimbal response was ± 0.2 g as compared to ± 0.4 g on AS-512. POGO did not occur.

Transients usually present in the center engine LOX pump inlet pressure during initiation of accumulator helium fill were not experienced during SA-513 flight.

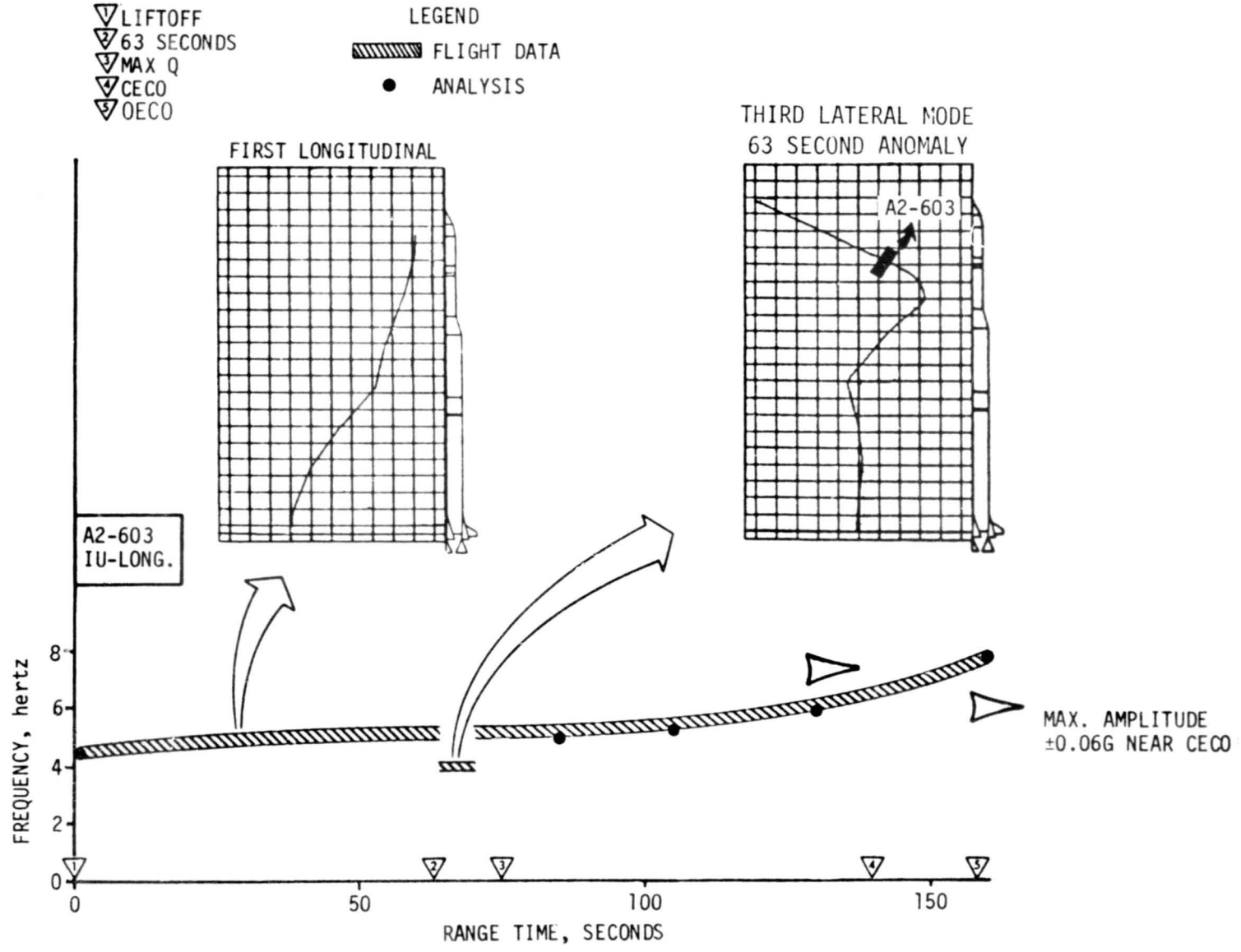


Figure 7-8. SA-513 Modal Activity (Longitudinal)

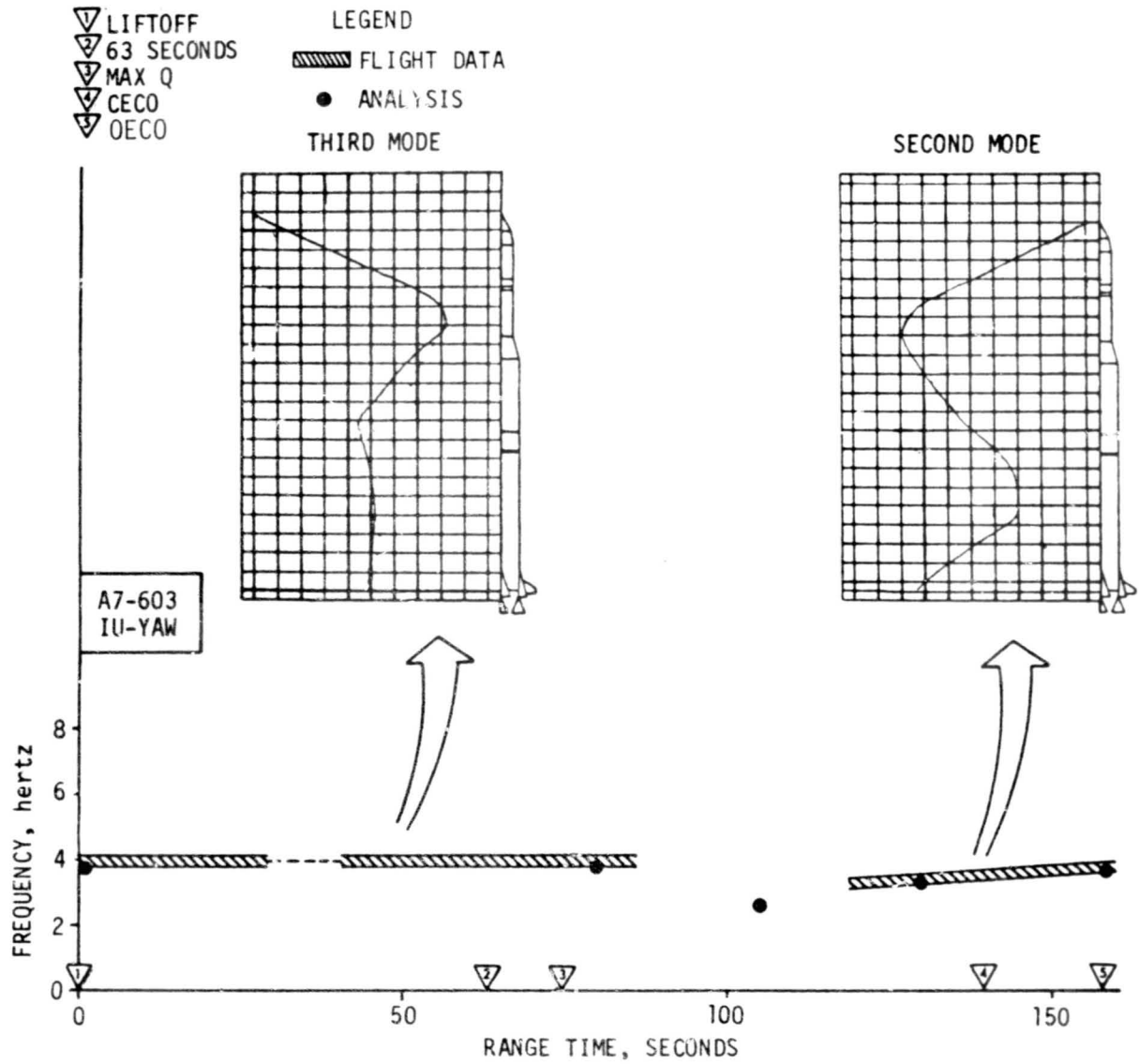


Figure 7-9. SA-513 Modal Activity (Lateral)

Late in S-II stage boost phase, the dynamic measurements displayed very low amplitude 11 Hz response. The Engine 1 thrust pad accelerometer (E361-206) data show a maximum level of ± 0.04 g at 9.8 Hz near 570 second.

7.2.5 Vibration Evaluation

The SA-513 vibration and acoustics data fall within the envelope of previous flight data indicating that these environments were as expected. Figure 7-10 depicts spectra for E0040-603 for AS-510, AS-511, AS-512 and SA-513 for liftoff, Mach 1 and Max q portions of the flight. The SA-513 data are comparable to previous vehicle levels at liftoff, and below these levels at subsequent flight times.

7.3 POGO LIMITING BACKUP CUTOFF SYSTEM

The POGO limiting backup cutoff system performed satisfactorily during the prelaunch and flight operations. The system did not produce any discrete outputs and should not have since there was no POGO.

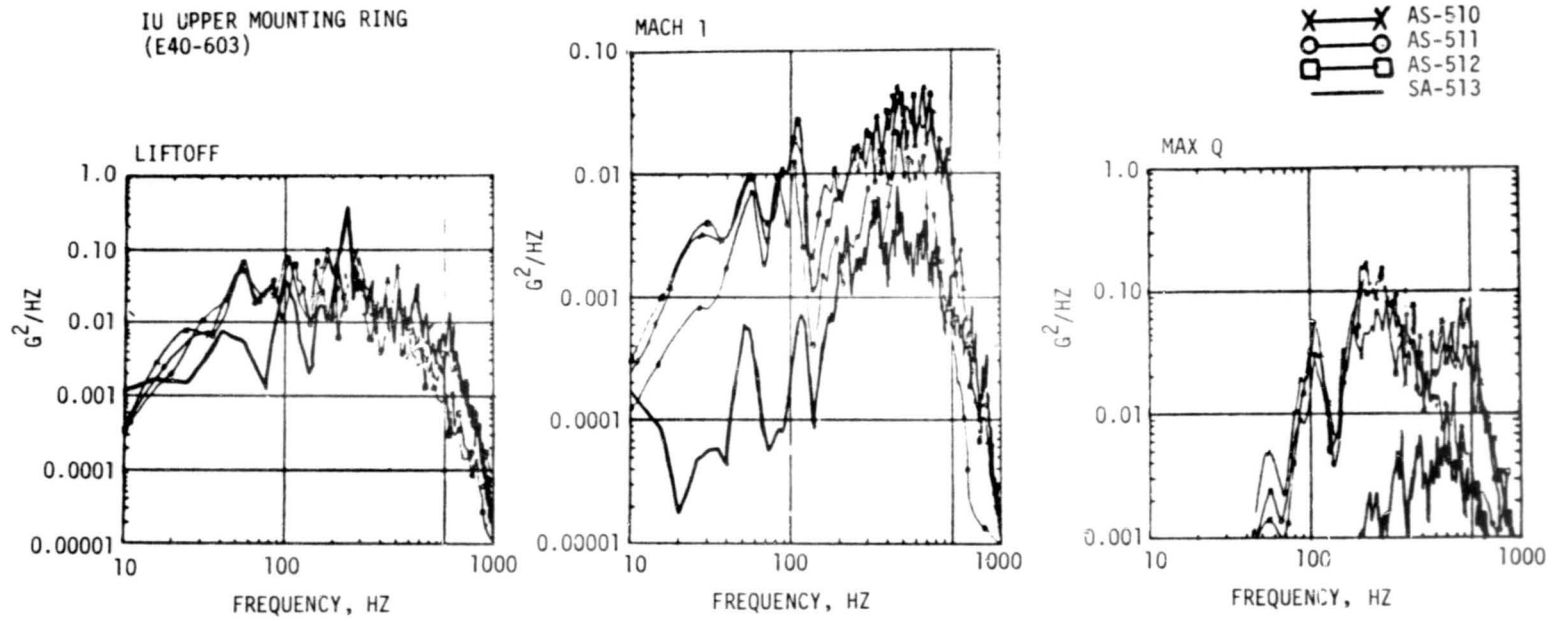


Figure 7-10. IU, Upper Mounting Ring Data PSD Comparison

SECTION 8

GUIDANCE AND NAVIGATION

8.1 SUMMARY

The Guidance and Navigation System successfully supported the accomplishment of all guidance and navigation mission objectives with no discrepancies in performance of the hardware. The end conditions at orbit insertion were attained with insignificant error.

An anomaly related to the flight program occurred at 3805 seconds, during the first orbital revolution. This was a switch from the inertial platform pitch axis gimbal fine resolver to the backup gimbal resolver, which is discussed in Paragraph 8.3.3.

A single test failure of the yaw axis gimbal resolver "Zero Reasonableness Test" occurred at 190 seconds. This event is discussed in Paragraph 8.3.2.

Guidance and navigation system components responded to the physical excitations experienced by the vehicle at 63 and 593 seconds (see Section 17).

A change in the navigation scheme was instituted on this flight due to the possibility of lateral accelerometer pickups limiting against their mechanical stops during liftoff. However, telemetry data indicated that no limiting occurred.

The guidance scheme was modified to include inertially-referenced pitch, as well as yaw, commands for the tower clearance maneuver because of the orientation of the platform coordinate system required by the northerly flight azimuth. A yaw steering command profile based on increased anticipated cross-wind components was added to the atmospheric-boost phase of guidance.

8.2 GUIDANCE COMPARISONS

The postflight guidance error analysis was based on the comparisons of position and velocity data generated by guidance system with corresponding values from the final postflight trajectory (21-Day Observed Mass Point Trajectory, OMPT) which was established by consideration of both tracking and guidance system data (see Section 4). Comparisons of the inertial platform measured velocities (Project Apollo Coordinate System Standard (PACSS) 12) with corresponding OMPT data from launch to Orbit Insertion (OI) are shown in Figure 8-1. The differences in vertical and cross range velocities are very small throughout the flight. The downrange differences may indicate, in addition to small platform hardware errors,

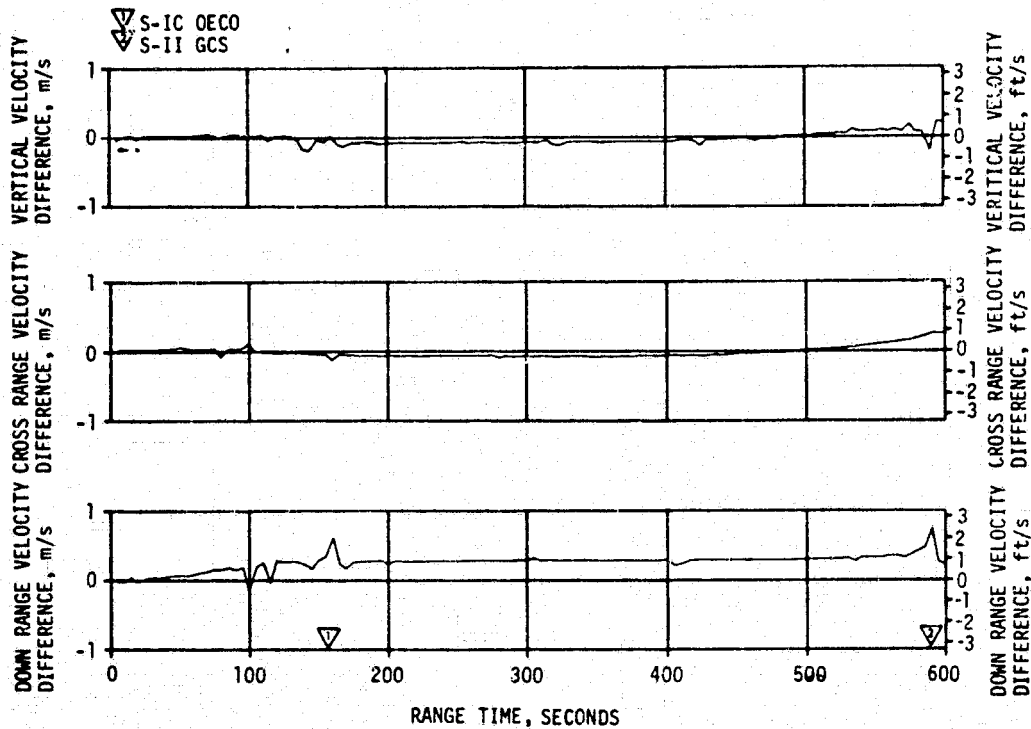


Figure 8-1. SA-513 Trajectory and ST-124M Platform Velocity Comparisons, Boost- to-Orbit Insertion (Trajectory Minus LVDC)

a small time bias, or angular error in the transformation of ground tracking data to the launch site and inertial coordinate system at the time of guidance reference release. However, the differences are within 3σ envelopes and well within the accuracy of the data compared.

The inertial platform velocity measurements at significant event times are shown in Table 8-1 along with corresponding data from the OMPT. The small differences between the telemetered and OMPT data reflect some combination of small guidance hardware errors and trajectory determination errors.

Velocity gain due to thrust decay and S-II retro-motor plume impingement after Guidance Cutoff Signal (GCS) was essentially as predicted until approximately 593 seconds. At that time the guidance and navigation system responded to the 593-second anomaly (see Section 17 for detailed discussion of this event). Measured and predicted velocity gains are summarized in Table 8-2 and shown in Figure 8-2. The velocity gain from GCS to S-II/SWS separation as sensed by the platform accelerometers, was 6.30 m/s (20.67 ft/s) or 0.10 m/s (0.33 ft/s) greater than the Operational Trajectory prediction. The measured velocity gain

Table 8-1. SA-513 Inertial Platform Velocity Comparisons

EVENT	DATA SOURCE	VELOCITY - PACSS 12		
		METERS/SECOND	(FEET/SECOND)	
		VERTICAL \dot{X}	CROSS RANGE \dot{Y}	DOWN RANGE \dot{Z}
S-IC	LVDC	3086.77 (10,127.20)	5.55 (18.21)	2162.82 (7095.87)
CECO	Postflight Trajectory	3086.17 (10,125.23)	5.24 (17.19)	2163.10 (7056.78)
S-II	LVDC	3179.80 (10,432.41)	517.78 (1698.75)	7501.07 (24,609.81)
GCS	Postflight Trajectory	3180.14 (10,433.53)	518.05 (1699.64)	7501.07 (24,609.81)
Orbital	LVDC	3174.85 (10,416.17)	518.85 (1702.26)	7506.95 (24,629.10)
Insertion	Postflight Trajectory	3175.28 (10,417.59)	518.28 (1700.39)	7507.39 (24,630.54)

from S-II/SWS separation to 593 seconds was slightly less than the OT values for the same time interval making the total velocity gain from GCS of 6.76 m/s (22.18 ft/s) for the Launch Vehicle Digital Computer (LVDC) compared to an OT value of 6.83 m/s (22.41 ft/s). The OT simulation assumed no thrust after this time period (approximately 4 seconds after GCS). However, the LVDC velocity accumulation indicated a 1.47 m/s (4.82 ft/sec) increase after 593.04 seconds. Since the LVDC reads the accumulated accelerometer outputs only at the beginning of a computation cycle (approximately 1 second) for navigation purposes, the velocity accumulations at approximately 593.71 seconds could be slightly in error. However, only one pulse (0.05 m/s) change in each component was noted over ten succeeding computation cycles. The accelerometer optisyn signals are in pairs and only one of each pair was telemetered which makes it impossible to actually reconstruct the accelerometer outputs during this transient period. The summation of the ΔV from point to point is shown in Table 8-2. The measured velocity gain from GCS to orbit insertion was 8.35 m/s (27.40 ft/s)

Table 8-2. SA-513 Velocity Gain After Guidance Cutoff Signal

TIME INTERVAL	DATA SOURCE	VELOCITY CHANGE - PACSS 12 - M/S (FT/S)				
		$\Delta\dot{X}$	$\Delta\dot{Y}$	$\Delta\dot{Z}$	ΔV^*	$\Sigma\Delta V$
From GCS to SWS Separation	LVDC	-3.25 (-10.66)	0.82 (2.69)	5.33 (17.49)	6.30 (20.67)	6.30 (20.67)
	OT	-3.21 (-10.53)	0.85 (2.79)	5.24 (17.19)	6.20 (20.34)	6.20 (20.34)
From SWS Separation to 593.04 sec.	LVDC	-0.20 (-0.66)	0.10 (0.33)	0.40 (1.31)	0.46 (1.51)	6.76 (22.18)
	OT	-0.33 (-1.08)	0.09 (0.30)	0.53 (1.74)	0.63 (2.07)	6.83 (22.41)
From 593.04 sec. to 593.71 sec.	LVDC	-1.45 (-4.76)	0.25 (0.82)	0.10 (0.33)	1.47 (4.82)	8.23 (27.00)
	OT	0	0	0	0	6.83 (22.41)
From 593.71 sec. to OI	LVDC	-0.05 (-0.16)	-0.10 (-0.33)	0.05 (0.16)	0.12 (0.39)	8.35 (27.40)
	OT	0	0	0	0	6.83 (22.41)

$$*\Delta V = (\Delta\dot{X}^2 + \Delta\dot{Y}^2 + \Delta\dot{Z}^2)^{1/2}$$

compared with the OT value of 6.83 m/s (22.41 ft/s). The LVDC total velocity at OI was 7649.22 m/s (25094.87 ft/s) which indicated an overspeed of 0.49 m/s (1.61 ft/s).

Comparisons of Navigation (PACSS #13) positions, velocities and flight path angle at significant event times are presented in Table 8-3. Differences between the LVDC and OT values reflect the normally encountered differences between actual and nominal flight environment and vehicle performance. At S-II stage cutoff the LVDC total velocity was 0.07 m/s (0.23 ft/s) less than the OT and the radius vector was 3.3 meters (11.0 feet) greater than the OT value. At OI the LVDC total velocity was 0.49 m/s (1.61 ft/s) greater than the OT value which was mostly due to the unexpected transient after S-II/SWS separation. The LVDC and OMPT data were in good agreement. The guidance system performed as expected from launch to OI.

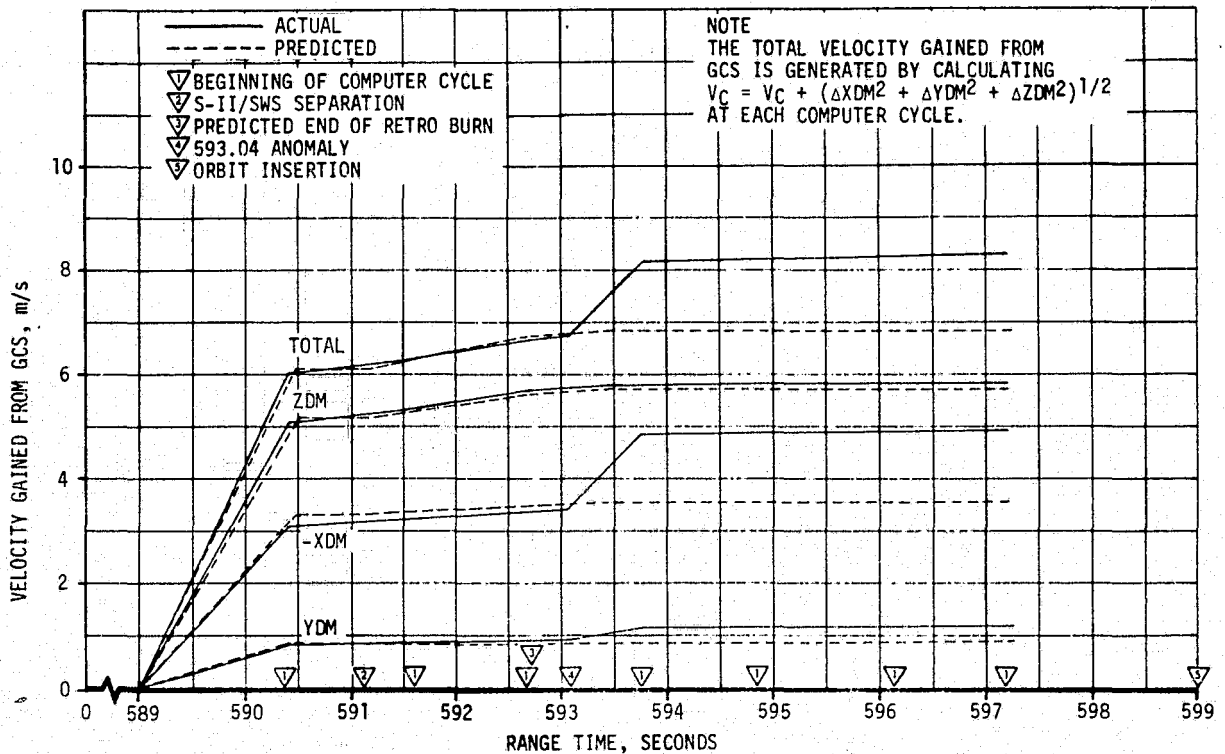


Figure 8-2. SA-513 Actual and Predicted Velocity Gained After GCS

Table 8-3. SA-513 Navigation Comparisons (PACSS 13)

EVENT	DATA SOURCE	POSITIONS METERS (FEET)				VELOCITIES METERS/SEC (FEET/SEC)				FLIGHT PATH ANGLE (DEG) (γ)
		X _S	Y _S	Z _S	R	X _S	Y _S	Z _S	V _S	
S-IC Engines Number 2 and 4 Cutoff	Navigator (LVDC)	6456954.3 (21184233.)	66287.8 (217480.)	120905.5 (396672.)	6458426.4 (21189063.)	1378.10 (4521.33)	305.63 (1002.72)	2421.90 (7945.87)	2803.24 (9196.98)	30.583306
	Postflight Trajectory	6456934.2 (21184167.)	66286.8 (217476.)	120905.5 (396672.)	6458406.3 (21188997.)	1377.67 (4519.91)	305.33 (1001.74)	2422.08 (7946.46)	2803.15 (9196.69)	30.57410
	Operational Trajectory	6456505. (21182759.)	65924. (216288.)	120046. (393852.)	6457957. (21187524.)	1374.14 (4508.33)	297.29 (975.36)	2404.49 (7888.74)	2785.35 (9138.30)	30.6885
	S-II GCS	Navigator (LVDC)	6486939.1 (21282609.)	245536.7 (805567.)	2062929.7 (6768142.)	6811486.3 (22347396.)	-2329.47 (-7642.62)	741.27 (2431.99)	7240.55 (23755.09)	7642.09 (25072.47)
	Postflight Trajectory	6486954.7 (21282660.)	245501.6 (805451.)	2063090.3 (6768669.)	6811548.5 (22347600.)	-2328.97 (-7640.98)	741.55 (2432.91)	7240.50 (23754.92)	7641.91 (25071.88)	0.01315
	Operational Trajectory	6489647. (21291492.)	244654. (802670.)	2054490. (6740452.)	6811483. (22347385.)	-2319.43 (-7609.68)	741.60 (2433.08)	7243.82 (23765.81)	7642.16 (25072.72)	0.0127
Orbit Insertion	Navigator (LVDC)	6463197.8 (21204717.)	252942.9 (829865.)	2135251.9 (7005420.)	6811476.1 (22347363.)	-2416.04 (-7926.64)	739.28 (2425.46)	7219.89 (23687.30)	7649.22 (25095.87)	-0.013267
	Postflight Trajectory	6463215.3 (21204775.)	252906.3 (829745.)	2135421.9 (7005977.)	6811544.6 (22347587.)	-2415.45 (-7924.70)	738.73 (2423.65)	7220.27 (23688.55)	7649.34 (25096.26)	-0.00707
	Operational Trajectory	6466005. (21213926.)	252065. (826986.)	2126861. (6977890.)	6811482. (22347382.)	-2404.62 (-7889.19)	739.50 (2426.19)	7223.15 (23698.01)	7648.73 (25094.25)	0.0008

8.3 NAVIGATION AND GUIDANCE SCHEME EVALUATION

The LVDC flight program performed all required functions properly. One anomaly occurred and is discussed in Paragraph 8.3.3. Several flight program changes from the Saturn V Apollo navigation and guidance scheme, as discussed below, were successfully instrumented. A minor discrepancy occurred and is discussed in Paragraph 8.3.2.

8.3.1 Major Differences From Past Schemes

Major differences between the SA-513 guidance scheme and that employed in recent Saturn V Apollo configurations consisted of the following: 1) inertially-referenced pitch commands to the tower clearance maneuver, 2) addition of yaw steering to the atmospheric boost time-tilt profile, 3) S-II stage CECO commanded as a function of vehicle characteristic velocity rather than burn duration, and 4) S-II stage OECO commanded on inertial velocity rather than depletion cutoff. The navigation scheme was altered to use pre-set accelerations in lieu of y and z accelerometer outputs until approximately 10 seconds.

The tower clearance maneuver consists of a rotation about the vehicle yaw axis. Past Saturn Apollo flights have been such that the inertial yaw axis was sufficiently parallel to the vehicle yaw axis so that only an inertial yaw steering command was necessary. Alignment of the Z inertial axis to the northerly flight azimuth of the SL-1 resulted in a change in the inertial axes to vehicle axes orientation such that an inertial pitch, as well as yaw, was required to obtain a rotation about the vehicle yaw axis.

Yaw steering as a function of time during atmospheric boost was added to minimize launch vehicle aerodynamic angle of attack and the attendant bending moment magnitude. This action was taken because of the increased magnitude of the anticipated crosswind component due to the more northerly launch azimuth coupled with the prevailing southwesterly winds in the launch area.

S-II CECO was commanded as a function of stage performance as keyed by a navigator-calculated accumulation of characteristic velocity. The change resulted in a more optimum S-II stage boost profile. S-II OECO was programmed as a guidance controlled event rather than a propellant depletion cutoff because the S-II was the terminal booster for the first time.

Modeled lateral acceleration inputs to the navigator in lieu of inertial Y and Z platform accelerometer outputs, were introduced into the flight program for the first ten seconds of flight. This change insured that if limiting did occur, no effect on the flight would result. Accelerometer limiting has in the case of three

previous flights been caused by the high level of acoustic energy that accompanies Saturn V liftoff. Limiting is due to the accelerometer pickup hitting their mechanical stop and cause biases to be introduced into the accelerometer values used in the onboard navigator. Prior studies showed that considerable degradation to the SWS orbit could result from the navigation errors associated with limiting. However, for this flight no limiting occurred. The modified scheme resulted in negligible error of -0.15 m/s downrange and -0.05 m/s crossrange.

8.3.2 Guidance Event Times

All guidance events scheduled at preset times occurred within acceptable tolerances. All flight program routines, including time-tilt, IGM, navigation and minor loop functions were accomplished properly. Times of occurrence of major navigation and guidance events are shown in Table 8-4.

Table 8-4. SA-513 Start Times for IGM Guidance Commands

EVENT	RANGE TIME - SECONDS		
	PREDICTED	ACTUAL	DELTA
IGM Initiation (Phase 1)	196.220	197.071	0.851
IGM Phase 2	314.345	315.089	0.744
IGM Phase 3	402.470	404.545	2.075
Terminal Steering	563.720	565.777	2.057

8.3.3 Yaw (Z) Axis Resolver Unreasonable Indication

A single instance of an unreasonable zero output by the yaw axis fine resolver was indicated at 190 seconds during the inertial attitude hold between S-II engine start and IGM initiation. The Zero Reasonableness Test is applied to distinguish between a normal electrical zero reading of the gimbal angle resolver, which can occur 64 times in a complete gimbal rotation (every 5.625 degrees), and a power supply failure which also would cause an electrical zero reading. When two successive zero readings occur and the attitude error is sufficiently

large to be causing control reaction, i.e., larger than a preset constant, the occurrence of successive zeros is considered unreasonable. Three unreasonable determinations in 0.8 seconds during boost (one second during orbit) initiates a switchover to the backup resolver. In this instance, only one unreasonable determination occurred.

Analysis of the fine gimbal angle data verified that the error word was proper and that the zero readings were expectable. The attitude error output was 0.24° and not changing. This offset in attitude error of greater than 0.06° resulted from a combination of rate gyro null offset and a stage thrust misalignment. It was determined, however, that the criteria should not be changed since the probability of three successive test failures without a real system failure is very low, and because the impact of inadvertent switchover to the backup resolver would only be loss of redundancy.

8.3.4 Pitch Axis Resolver Switchover

At 3805 seconds, during the first orbital revolution, the Y (pitch) fine gimbal angle was found unreasonable three times within one second causing switchover to the backup resolver. The unreasonable readings were determined by the Zero Reasonableness Test (see Paragraph 8.3.2). The resolver switchover had no effect on the mission and resulted only in loss of redundancy. The control system deadband used for orbital attitude control for the Saturn Work Shop has a larger attitude error limit deadband (2.0°) than in the Apollo system (1.0°). The computer test constant used to represent the deadband should, therefore, have been increased to reflect the increased attitude error limit. However, the test constant was set at 1.2° , the Apollo value. In addition, a null offset (within specification) in the Control Signal Processor effectively moved the control deadband so that an appropriately set test constant would not have properly represented the edge of the deadband. These two conditions, either of them sufficient, permitted the Zero Reasonableness Test to be failed in pitch when the vehicle pitch attitude was actually within the control deadband.

A repeat of this occurrence for either SL-3 or SL-4 is unlikely. However, the test constant values have been re-evaluated based on known rate-gyro null offsets. As a result of this re-evaluation, the test constant will be increased to 2.0° .

8.3.5 Attitude Commands

Vehicle attitude commands issued during boost are shown in Figure 8-3 along with the predicted values. Yaw steering commands are slightly different from those predicted due to larger than predicted steering misalignment corrections, and different-from-nominal initial conditions for IGM initiation.

8.3.6 Terminal Conditions

A comparison of desired and achieved guidance terminal conditions is shown in Table 8-5. The small error values indicate satisfactory performance by the guidance and navigation system.

8.3.7 Orbiter Phase

Orbital guidance and events sequencing were as specified. Commanded attitudes during the orbital phase are shown in Table 8-6.

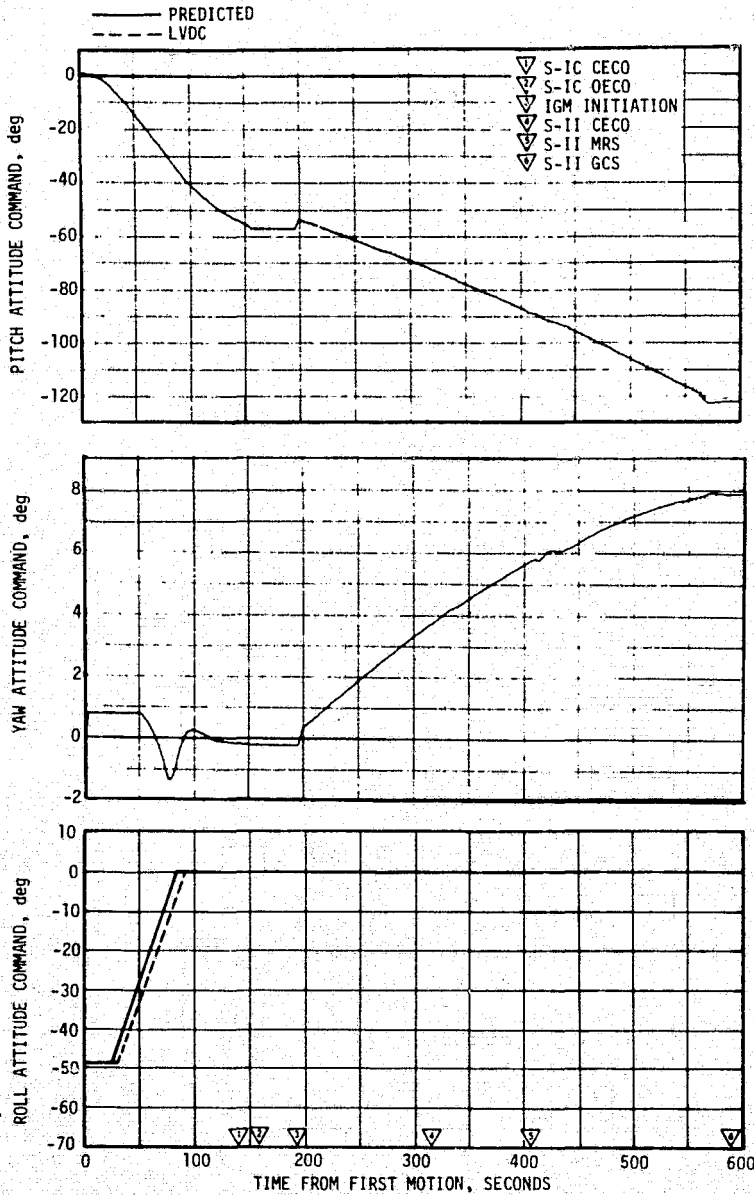


Figure 8-3. Attitude Commands

Table 8-5. SA-513 End Conditions

PARAMETER	DESIRED	ACHIEVED	ERROR (ACHIEVED- DESIRED)
Velocity, V_T (m/sec)	7648.7198	7648.6326	-.0872
Radius, R_T (meters)	6811534.0	6811492.5	-41.5
Path Angle, θ_T (deg)	+0.005	-.002905	-.007905
Inclination, I (deg)	50.029	50.0284	-.0006
Descending Node, λ (deg)	153.25	153.249	-.001

Table 8-6. SA-513 Orbital-Phase Commanded Attitude Angles

EVENT	TIME	COMMANDED ANGLE, DEGREE		
		ROLL (X)	PITCH (Y)	YAW (Z)
Attitude Hold	T4	+0.0335	-121.0352	+8.0524
Shroud Jettison and Initiate Orbital Guidance	T4 + 11.005 Sec	0.0	161.7026	-2.1296
Solar Attitude	T4 + 370.169	-175.1280	-81.1276	+5.6845

8.4 NAVIGATION AND GUIDANCE SYSTEM COMPONENTS

The navigation and guidance hardware satisfactorily supported the accomplishment of mission objectives.

8.4.1 Stabilized Platform System

All three gyro servo loops operated properly. Maximum deflections of the pickoffs at various event times are listed below:

	<u>Z Gyro</u>	<u>X Gyro</u>	<u>Y Gyro</u>
Liftoff	<+.05° -.05°	<+.05° <-.05°	<+.05° <-.05°
~ 63 Sec	+0.1° -0.1°	+0.1° -0.1°	+0.07° -.06°
~ 593 Sec	+0.08° -.07°	+2.7° -0.15°	+0.07° -0.1°
Payload Shroud Jettison	+0.07° <-.05°	<+.05° <-.05°	+0.1° -.05°

All three accelerometer servo loops responded properly to the vehicle accelerations. Maximum deflections of the pickoffs at various times are listed as follows:

	<u>Z Accel</u>	<u>X Accel</u>	<u>Y Accel</u>
Liftoff	+1.7° -1.9°	+1.1° -1.0°	+2.0° -2.0°
~ 63 Sec	+0.4° -0.4°	+0.5° -0.3°	+0.5° -0.6°
~ 593 Sec	+1.3° -1.4°	+4.5° -5.2°	+2.7° -2.9°
Payload Shroud	+2.0° -3.6°	+1.8° -1.4°	+1.7° -2.1°

8.4.2 Guidance and Navigation Computer

The LVDC and LVDA performed satisfactorily, and no hardware anomalies were observed during any phase of SL-1 flight.

SECTION 9

CONTROL AND SEPARATION

9.1 SUMMARY

The control systems functioned correctly throughout the flight of SA-513. Engine gimbal deflections were nominal. Bending and slosh dynamics were adequately stabilized. No undue dynamics accompanied any separation, however, the S-IC/S-II interstage failed to separate and caused high temperatures and pressures in the S-II thrust cone region during the S-II burn, as discussed in paragraph 9.5.2. The failure is attributed to damage to the Linear Shaped Charge (LSC) or the LSC cover resulting from Orbital Work Shop meteoroid shield debris.

9.2 S-IC CONTROL SYSTEM EVALUATION

9.2.1 Liftoff

The liftoff tower clearance maneuver occurred as planned. Table 9-1 summarizes liftoff misalignments and conditions.

9.2.2 Inflight Dynamics

The SA-513 control system performed as expected during S-IC boost except during the 63-second anomaly discussed in paragraph 9.2.3. Windsphere measurements indicate two significant wind peaks. The first wind peak was 29.5 meters per second at 9.25 kilometers altitude with an azimuth of 263 degrees. The second peak was 34.4 meters per second at 12.7 kilometers with an azimuth of 267 degrees. The first wind peak caused the maximum total angle of attack of 2.8 degrees. The control system adequately stabilized the vehicle in this wind. About 7% of the available pitch gimbal angle and 8% of the available yaw gimbal angle were used.

Time histories of pitch, yaw, and roll control parameters are shown in Figures 9-1 through 9-4. The peaks are summarized in Table 9-2. Dynamics in the region between liftoff and 40 seconds resulted primarily from guidance commands. Between 40 and 110 seconds vehicle dynamics were caused by the pitch and yaw guidance programs, the wind, and the 63-second anomaly. Dynamics from 110 seconds to S-IC outboard engine cutoff were caused by center engine shutdown, tilt arrest and high altitude winds. There is no evidence of a flow separation transient as experienced on Apollo flights.

The attitude errors indicate that the equivalent thrust vector misalignments were 0.05 and -0.05 degrees in pitch and yaw, respectively. Roll engine misalignment was zero degrees prior to outboard engine cant and 0.01 degree after cant. The attitude error transients at center engine cutoff

Table 9-1. SA-513 Liftoff Conditions Misalignment Summary

PARAMETER	PREDICTED 3 σ RANGE			LAUNCH		
	PITCH	YAW	ROLL	PITCH	YAW	ROLL
Thrust Misalignment, deg	± 0.31	± 0.31	± 0.37	0.05	-0.05	0.0
Center Engine Cant, deg	± 0.31	± 0.31	-	0.09	0.02	-
Vehicle Stacking and Pad Misalignment, deg	± 0.28	± 0.28	0.0	0.0	0.0	0.0
Attitude Error at Holddown Arm Release, deg	-	-	-	-0.06	-0.06	0.06
Peak Soft Release Force Per Slow Release Rod, N(1bf)	PREDICTED			ACTUAL		
	415,900 (93,500)			*		
	19.55 m/s (38 Knots) at 161.5 Meters (530 Feet)			5.1 m/s (10.0 Knots) at 161.5 Meters (530 Feet)		
Wind						
Thrust to Weight	1.240			1.263		
*Data not available						

indicate that the center engine misalignments were 0.09 and 0.02 degrees in pitch and yaw respectively.

All dynamics were within vehicle capability. The attitude errors required to trim out the effects of thrust unbalance, offset center of gravity, thrust vector misalignment and control system misalignments were within predicted envelopes. The peak angles of attack in the maximum dynamic pressure (Max q) region were -2.02 degrees in pitch and 1.96 degrees in yaw. The peak average engine deflections required to trim out the aerodynamic moments in this region were -0.34 degree in pitch and 0.39 degree in yaw.

- | | | | |
|-----|--------------------------------|------|------------------------|
| ▽ 1 | BEGIN TOWER CLEARANCE MANEUVER | ▽ 9 | MAX q |
| ▽ 2 | END PITCH MANEUVER | ▽ 10 | 1st GAIN SWITCH |
| ▽ 3 | BEGIN PITCH/ROLL MANEUVER | ▽ 11 | 2nd GAIN SWITCH |
| ▽ 4 | OUTBOARD ENGINE CANT | ▽ 12 | CENTER ENGINE CUTOFF |
| ▽ 5 | MACH 1 | ▽ 13 | TILT ARREST |
| ▽ 6 | END ROLL MANEUVER | ▽ 14 | OUTBOARD ENGINE CUTOFF |

— MEASURED (FILTERED TO 0.3 HZ)
 - - - SIMULATED

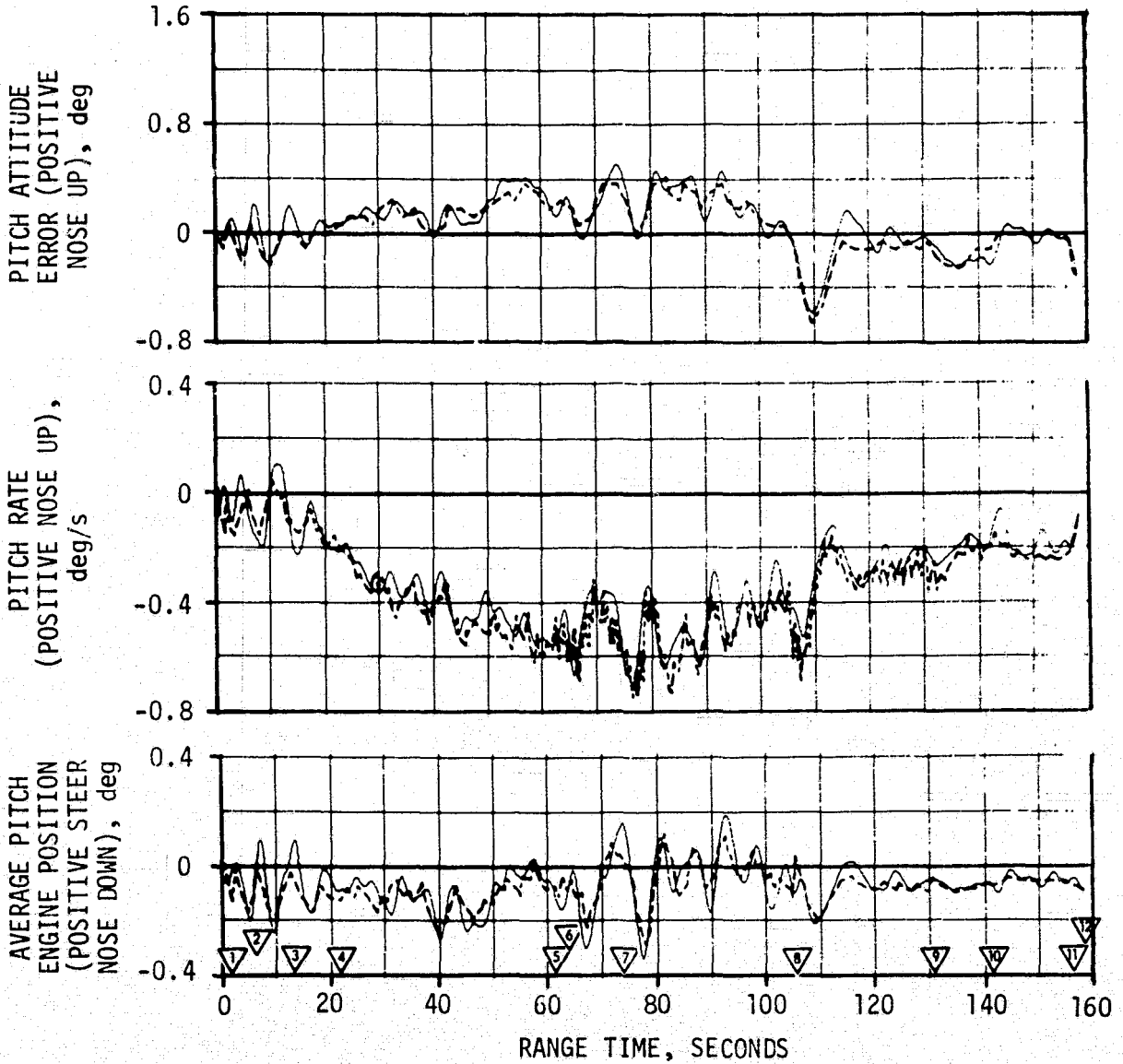


Figure 9-1. Pitch Plane Dynamics During S-IC Burn

- ▽ BEGIN TOWER CLEARANCE MANEUVER
- ▽ END PITCH MANEUVER
- ▽ BEGIN PITCH/ROLL MANEUVER
- ▽ OUTBOARD ENGINE CANT
- ▽ MACH 1
- ▽ END ROLL MANEUVER
- ▽ MAX q
- ▽ 1st GAIN SWITCH
- ▽ 2nd GAIN SWITCH
- ▽ CENTER ENGINE CUTOFF
- ▽ TILT ARREST
- ▽ OUTBOARD ENGINE CUTOFF

— MEASURED (FILTERED TO 0.3 HZ)
 - - - SIMULATED

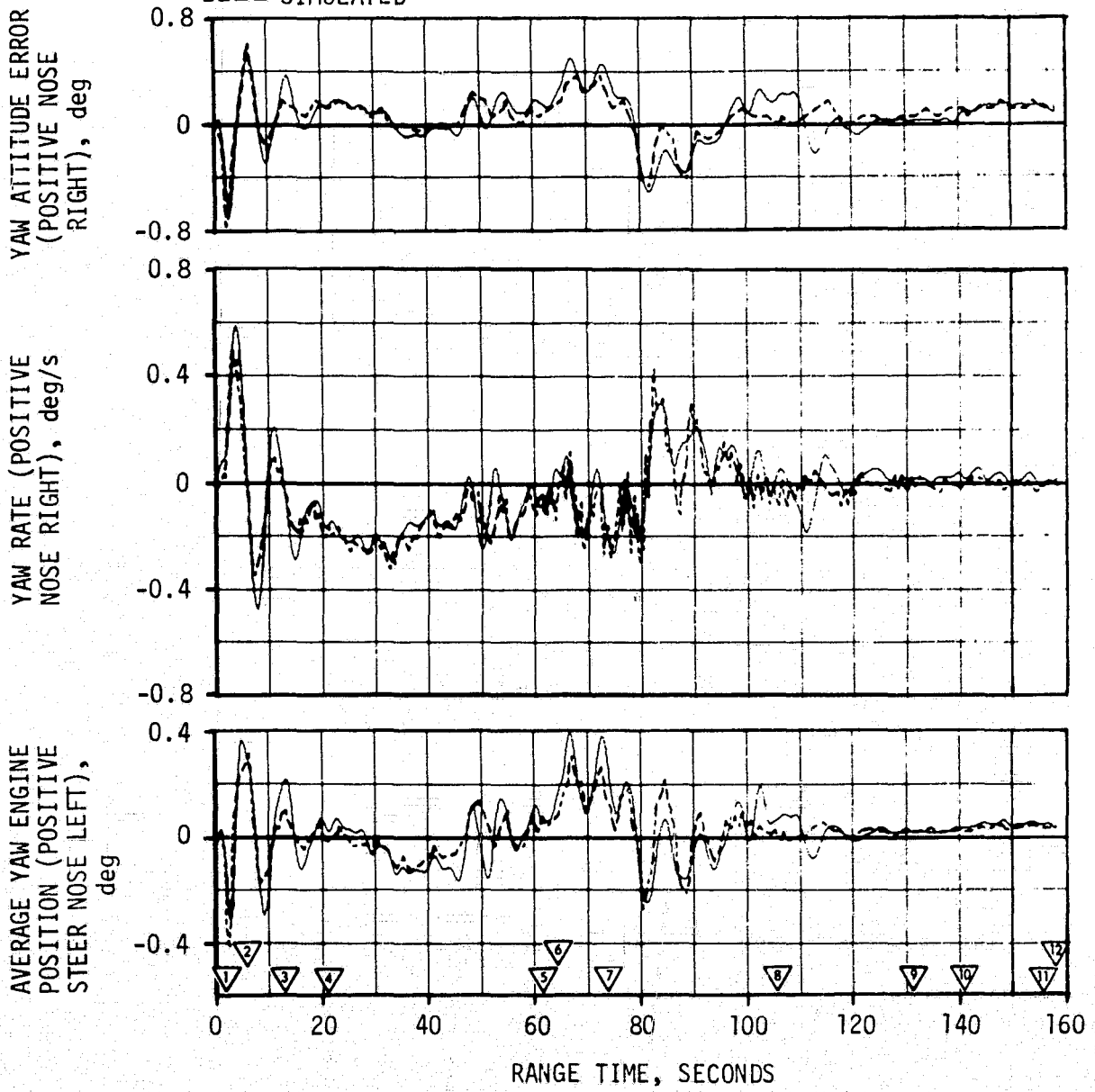


Figure 9-2. Yaw Plane Dynamics During S-IC Burn

- ▽ BEGIN TOWER CLEARANCE MANEUVER
- ▽ END PITCH MANEUVER
- ▽ BEGIN PITCH/ROLL MANEUVER
- ▽ OUTBOARD ENGINE CANT
- ▽ MACH 1
- ▽ END ROLL MANEUVER

- ▽ MAX q
- ▽ 1st GAIN SWITCH
- ▽ 2nd GAIN SWITCH
- ▽ CENTER ENGINE CUTOFF
- ▽ TILT ARREST
- ▽ OUTBOARD ENGINE CUTOFF

— MEASURED
 - - - SIMULATED

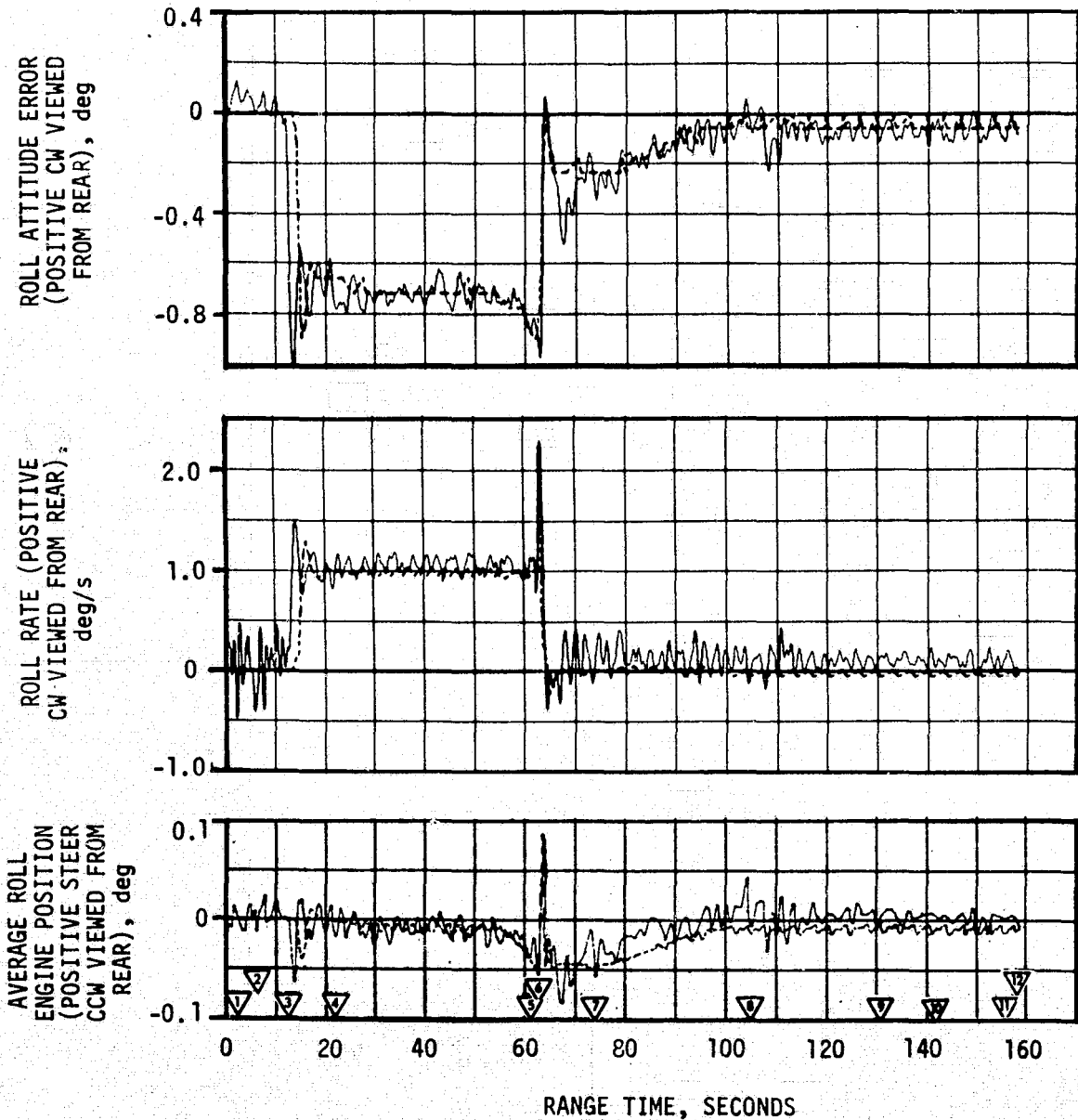


Figure 9-3. Roll Dynamics During S-IC Burn

- | | | | |
|---|--------------------------------|---|------------------------|
| ▽ | BEGIN TOWER CLEARANCE MANEUVER | ▽ | MAX q |
| ▽ | END PITCH MANEUVER | ▽ | 1st GAIN SWITCH |
| ▽ | BEGIN PITCH/ROLL MANEUVER | ▽ | 2nd GAIN SWITCH |
| ▽ | OUTBOARD ENGINE CANT | ▽ | CENTER ENGINE CUTOFF |
| ▽ | MACH 1 | ▽ | TILT ARREST |
| ▽ | END ROLL MANEUVER | ▽ | OUTBOARD ENGINE CUTOFF |

———— CALCULATED FROM OBSERVED VELOCITY AND WIND SPEED
 - - - - - SIMULATED

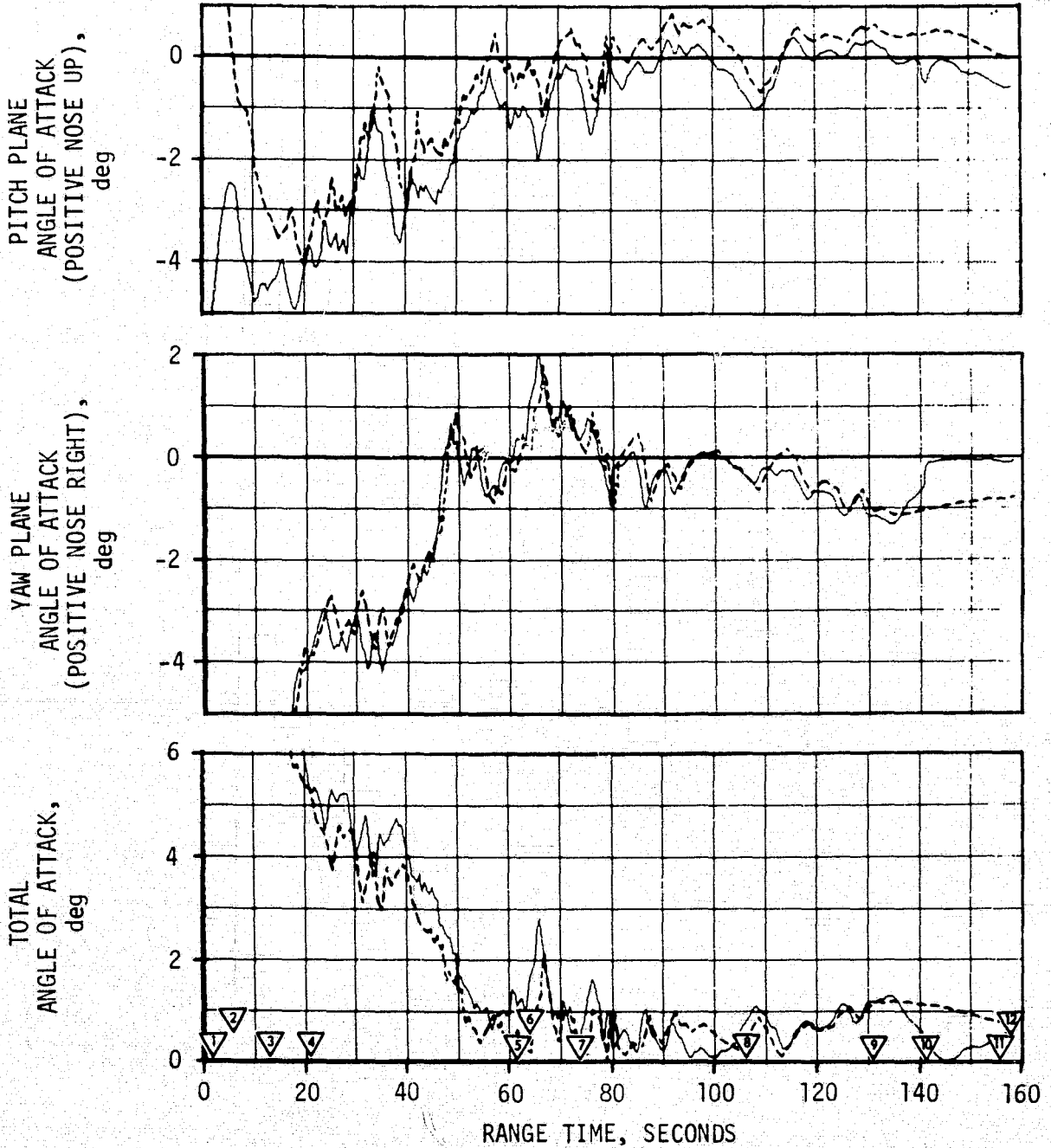


Figure 9-4. Pitch and Yaw Plane Free Stream Angle of Attack During S-IC Burn

Table 9-2. Maximum Control Parameters During S-IC Burn

PARAMETERS	PITCH PLANE*		YAW PLANE*		ROLL PLANE*	
	AMPLITUDE	RANGE TIME (SEC)	AMPLITUDE	RANGE TIME (SEC)	AMPLITUDE	RANGE TIME (SEC)
Attitude Error, deg	-0.60	109.0	-0.66	2.9	-1.02	13.5
Angular Rate, deg/s	-0.70	76.6	0.58	4.1	1.5 to 2.5**	63.0
Average Gimbal Angle, deg	-0.37	77.5	0.45	66.7	+0.09 -0.09	63.6 67.3
Angle of Attack, deg (During Max q)	-2.02	66.0	1.96	65.5		
Angle of Attack Dynamic Pressure Product, deg-N/CM ² (deg-lbf/ft ²)	5.98 (1250)	66.0	5.77 (1210)	65.5		
Normal Acceleration, m/s ² (ft/s ²)	0.27 (0.90)	76.9	0.31 (1.00)	65.6		

*Corrected for biases

**Caused by 63-second anomaly

No divergent bending dynamics were observed. Figure 9-5 shows LH2 slosh mass displacements measured during flight along with preflight predicted and postflight simulated displacements. The measured data shown has been reduced by 40% to account for amplification factors in the capacitance probe during S-IC flight. The deviation between measured and postflight simulated data may be due to: a) harmonic beating of the first slosh mode with higher modes not modeled in the simulation; or b) unpredictable slosh wave rotation out of the plane of the probe.

Vehicle dynamics prior to S-IC/S-II first plane separation were within staging requirements.

9.2.3 63-Second Anomaly

The SA-513 launch vehicle instrumentation indicated unusual disturbances at about 63-seconds. An external moment caused an increase in roll rate to about 2.2 degrees/second. Pitch and yaw rate transients also were observed, but the frequency of these transients (about 4 Hertz) indicate that these were structural responses. The pitch and yaw accelerometers in the IU also recorded structural motion.

An analysis has been made of the vehicle dynamics during the 63-second region of flight. It was found that the rigid-body and structural motion of the vehicle can be approximated by an external impulse of 26,100 newton-seconds applied in the region of Solar Array System (SAS) wing number 2. This impulse is produced by a force of 290,000 newtons acting for 0.09 seconds. The force is applied tangentially to the meteoroid shield (at vehicle station 75.34) at a point 30 degrees from position IV toward position I with pitch and yaw components of 251,000 and -145,000 newtons, respectively.

Figures 9-6 through 9-8 show the simulated dynamic responses to the external force compared with the measured responses. The measured error data shown is 100 sample-per-second data. However, the available measured rate data shown is sampled at 10 samples per second. This low sampling frequency significantly affects the quality of the rate measurements. Figure 9-9 shows the simulated and measured I.U. lateral accelerations. The angles of attack are shown in Figure 9-10.

A more complete discussion of the 63-second anomaly is contained in Section 17.

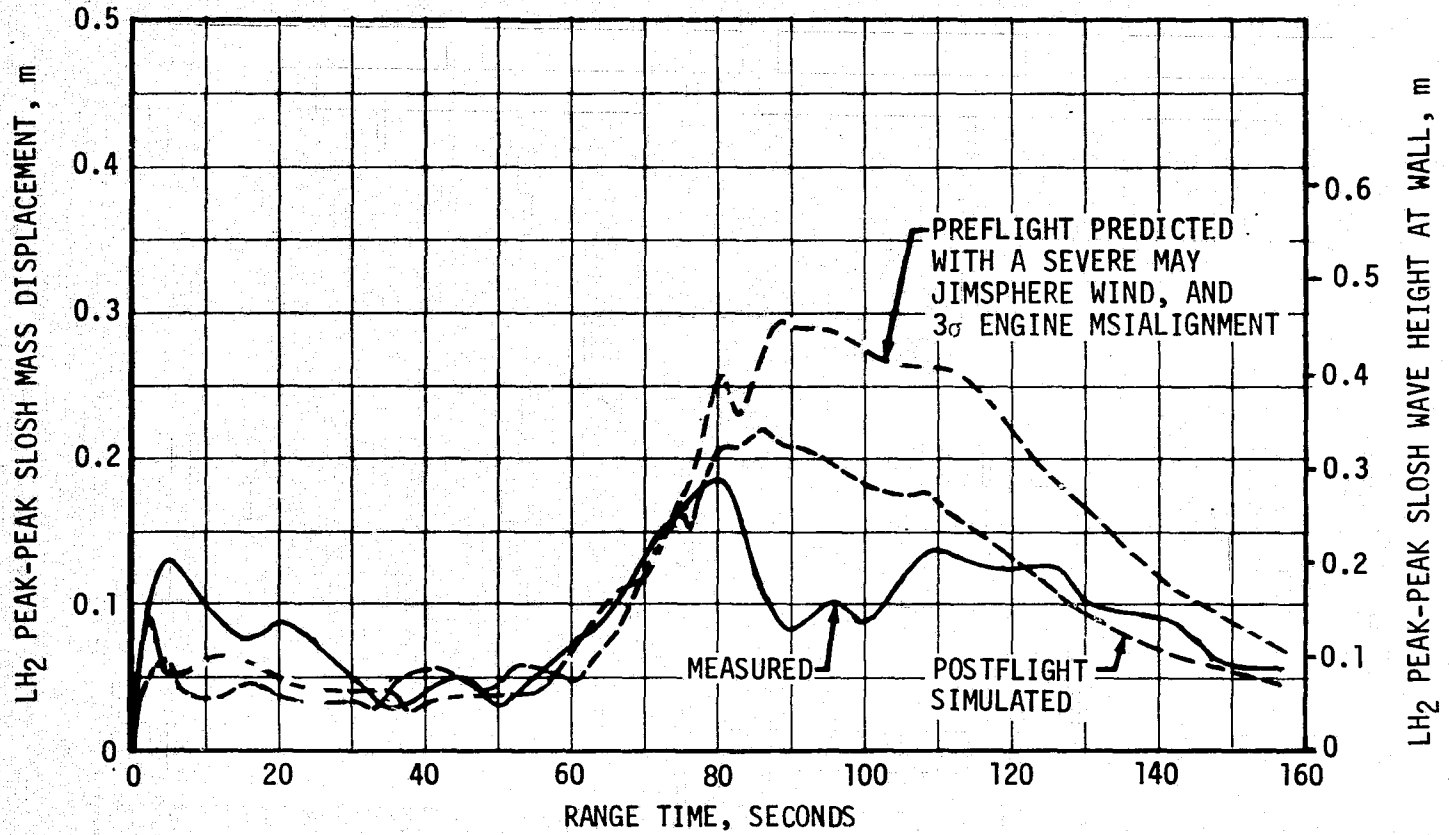


Figure 9-5. SA-513 LH₂ Peak-to-Peak Slosh Mass Displacement

▽ FORCE INTRODUCED, 62.88 SECONDS
 ▽ FORCE REMOVED, 62.98 SECONDS
 ▽ END ROLL MANEUVER

— MEASURED (RAW DATA WITH BIASES REMOVED)
 - - - MEASURED (FILTERED TO 1.5 HZ)
 - - - SIMULATED

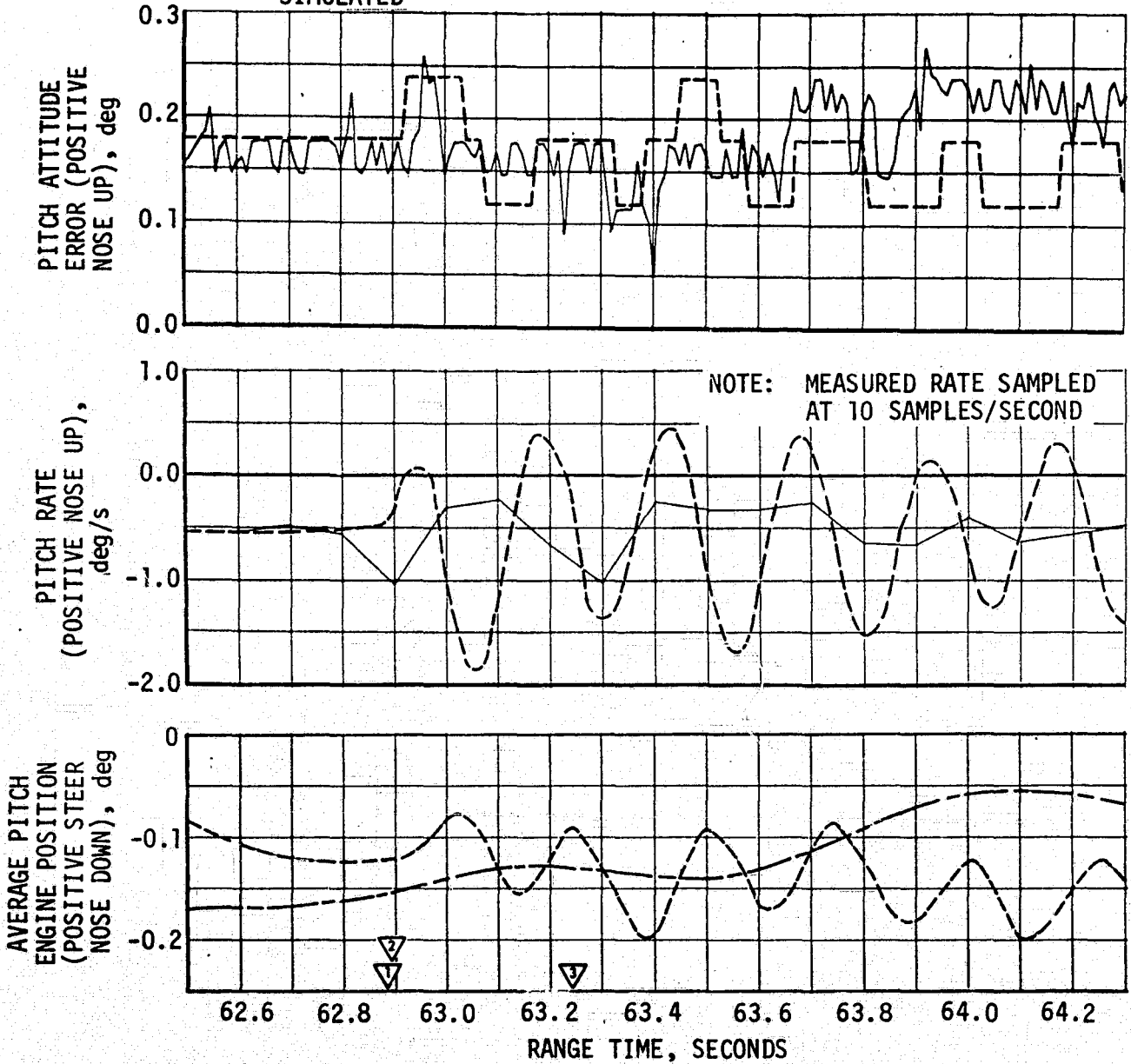


Figure 9-6. Pitch Plane Dynamics During 63-Second Anomaly

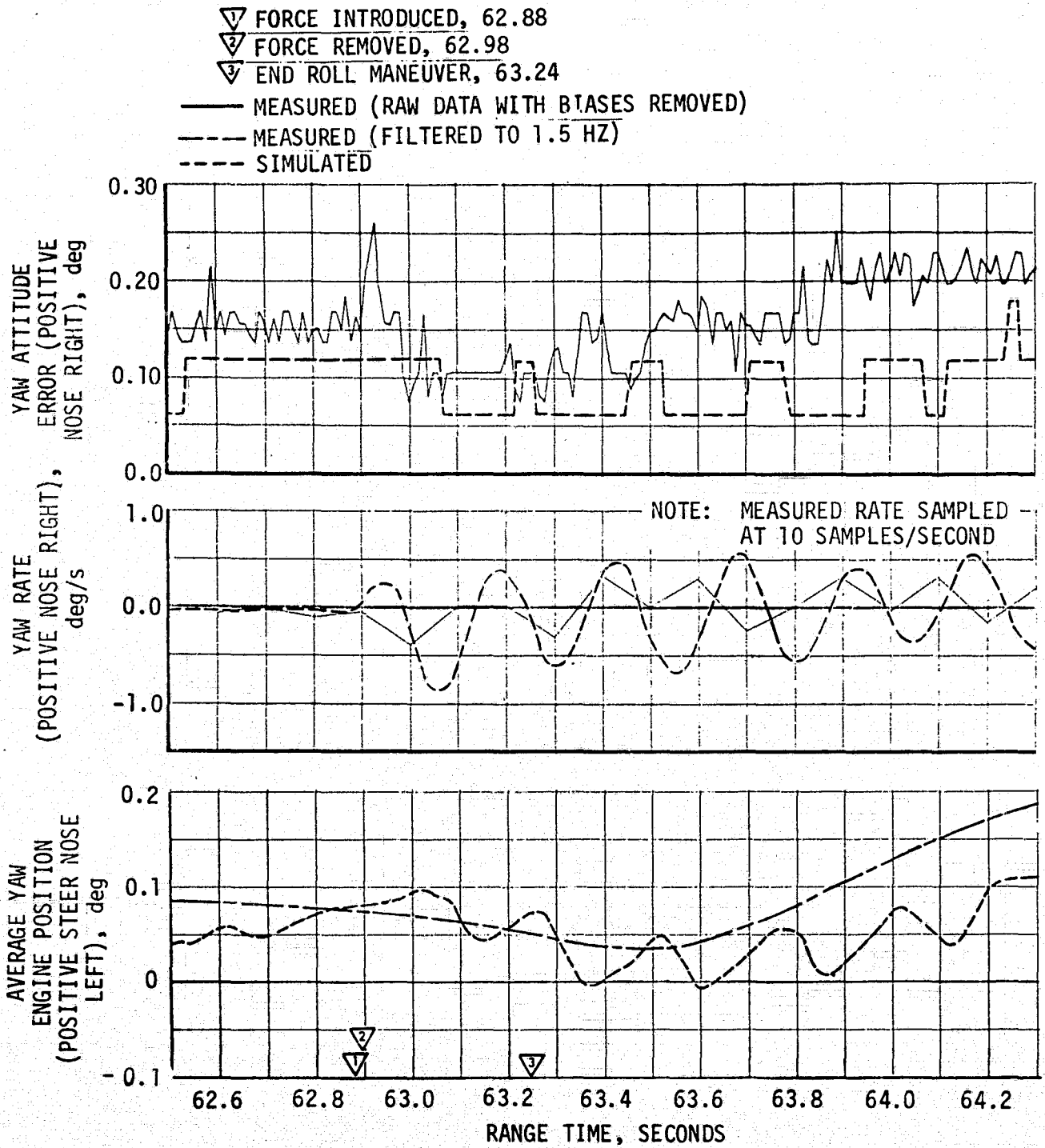


Figure 9-7. Yaw Plane Dynamics During 63-Second Anomaly

- ▽ FORCE INTRODUCED, 62.88
- ▽ FORCE REMOVED, 62.98
- ▽ END ROLL MANEUVER, 63.24

— MEASURED (RAW DATA WITH BIAS REMOVED)
 - - - MEASURED (RATE FILTERED TO 1.0 HZ,
 ENGINE DEFLECTION TO 1.5 HZ)
 - - - - SIMULATED

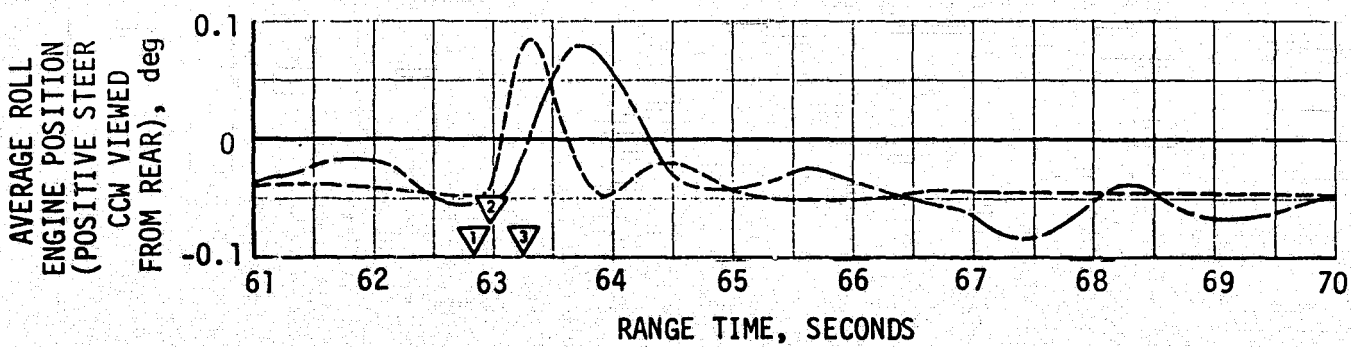
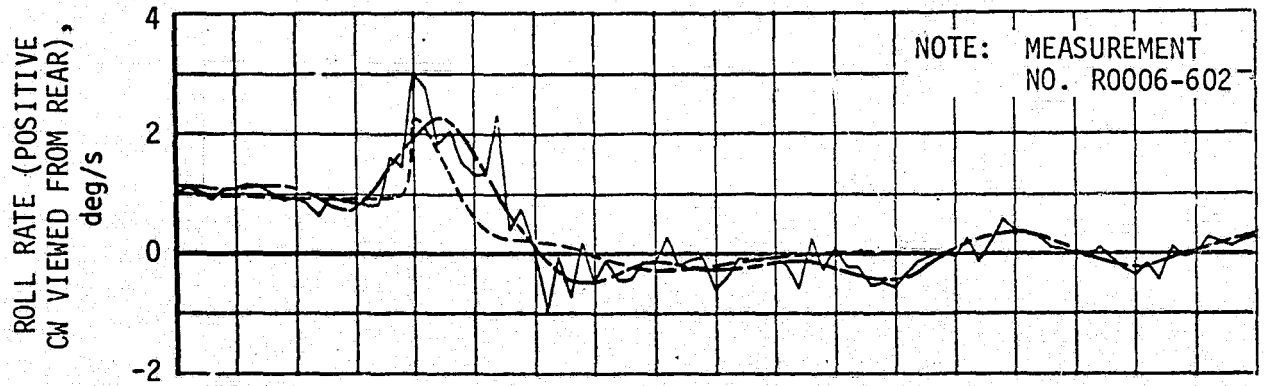
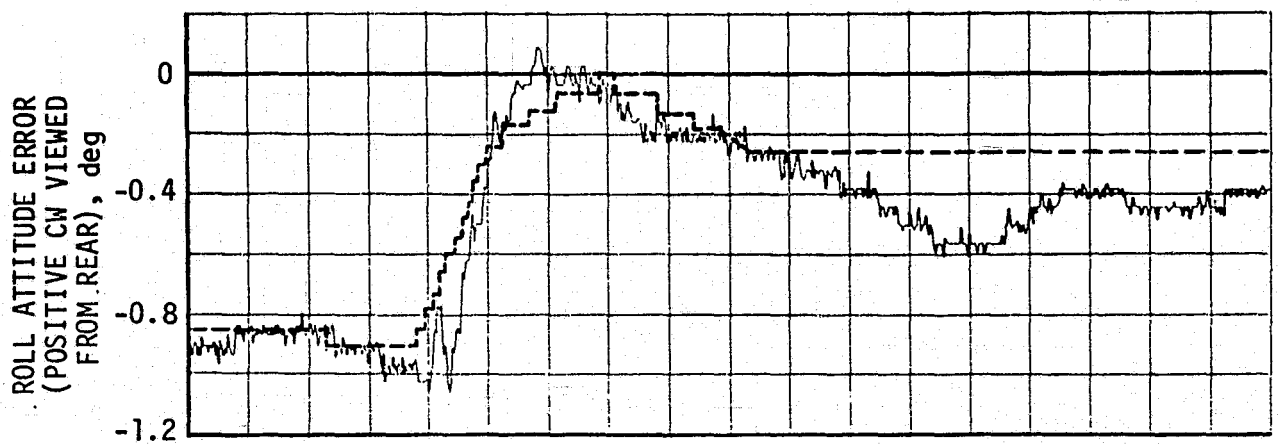


Figure 9-8. Roll Plane Dynamics During the 63-Second Anomaly

- ▽ FORCE INTRODUCED, 62.88
- ▽ FORCE REMOVED, 62.98
- ▽ END ROLL MANEUVER, 63.24

— MEASURED (RAW DATA WITH BIASES REMOVED)
 - - - SIMULATED

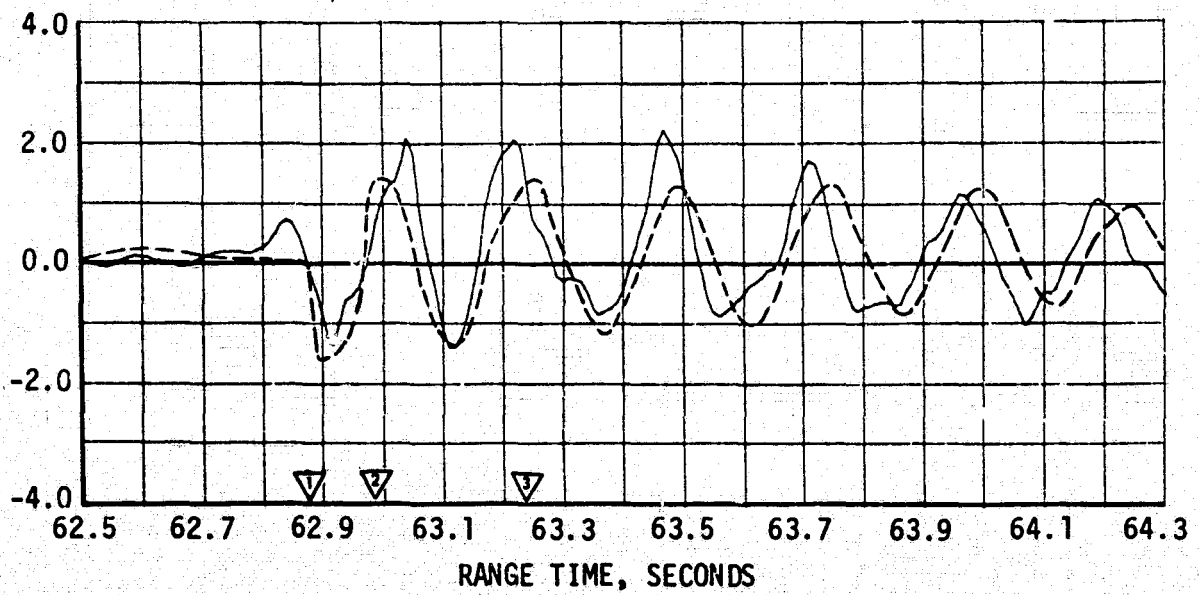
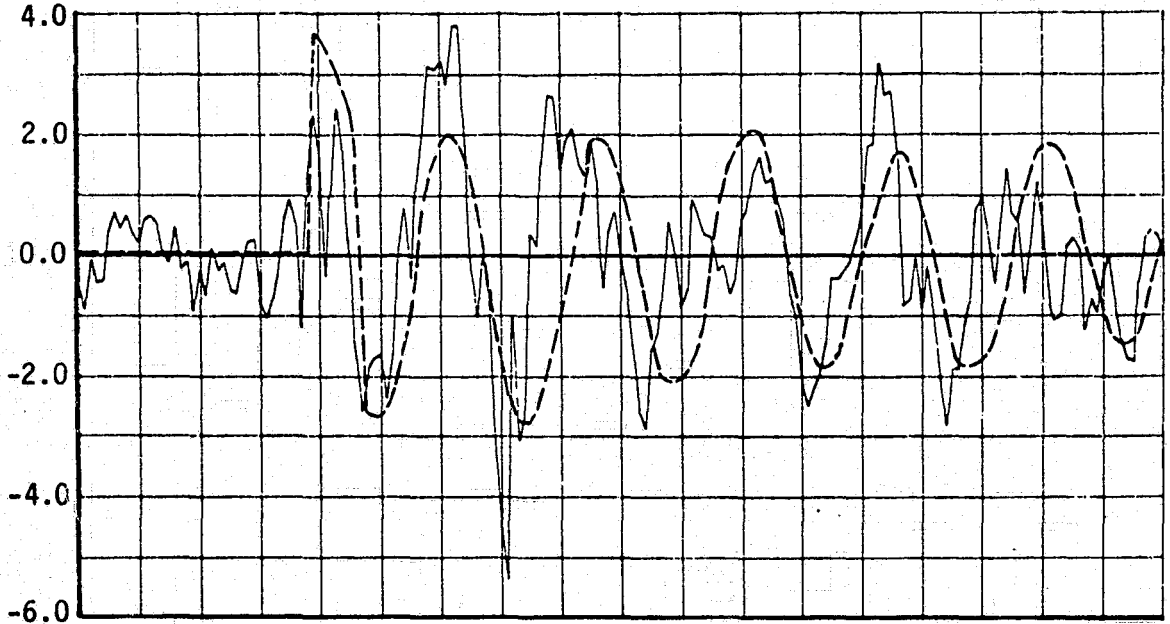


Figure 9-9. Lateral IU Acceleration During 63-Second Anomaly

▽ FORCE INTRODUCED, 62.88
 ▽ FORCE REMOVED, 62.98
 ▽ END ROLL MANEUVER, 63.24

— CALCULATED FROM OBSERVED VELOCITY AND WIND SPEED
 - - - SIMULATED

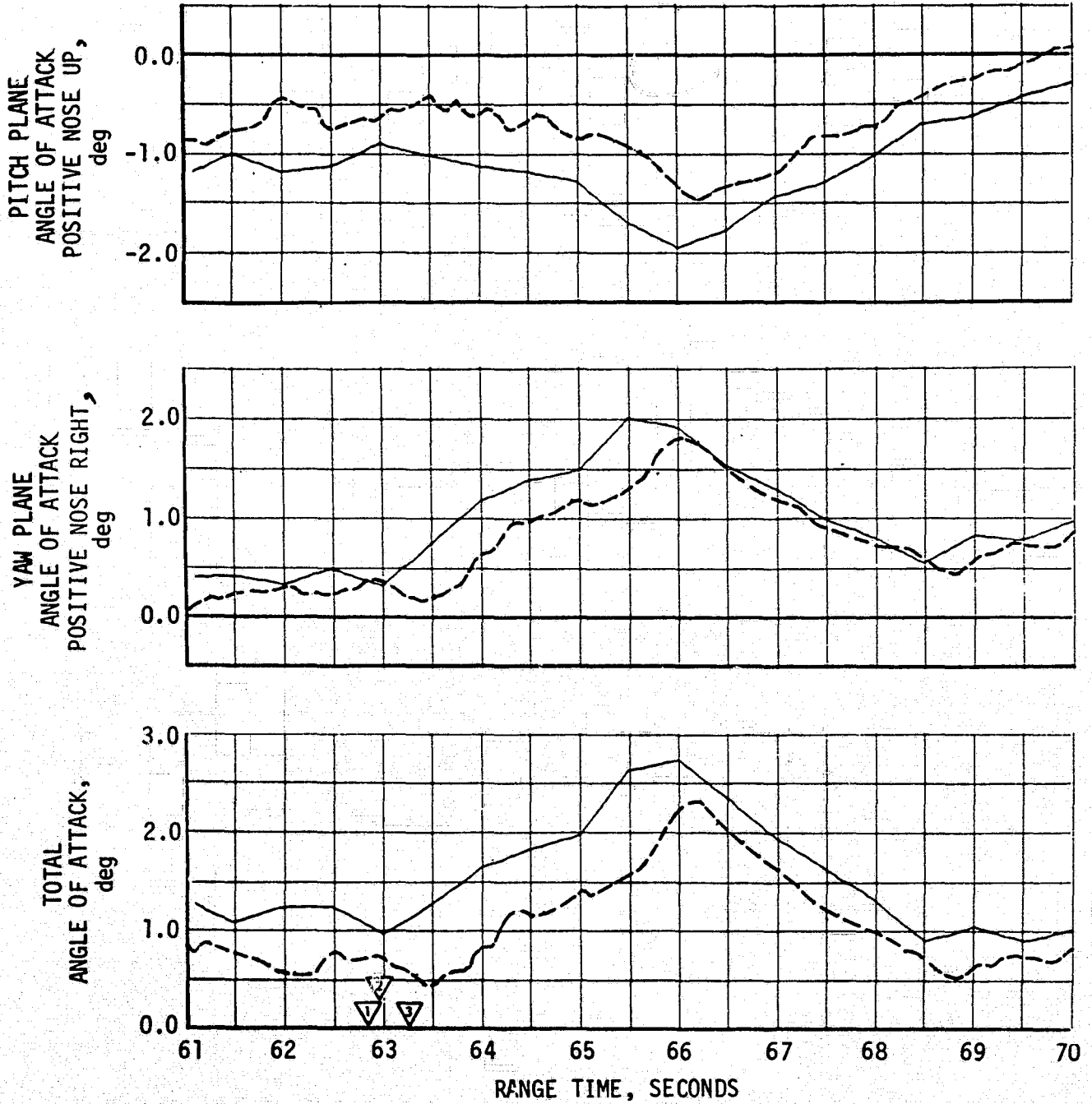


Figure 9-10. Pitch and Yaw Plane Free Stream Angle of Attack During 63-Second Anomaly

The S-II stage attitude control system performance was satisfactory. The vehicle dynamics were within expectations at all times. The maximum values of pitch parameters and yaw attitude error occurred in response to Iterative Guidance Mode (IGM) Phase 1 initiation. The maximum values of yaw gimbal angle and all roll control parameters occurred in response to S-IC/S-II separation conditions. The maximum control parameter values for the period of S-II burn are shown in Table 9-3.

Table 9-3. Maximum Control Parameters During S-II Burn

PARAMETER	PITCH PLANE*			YAW PLANE*		ROLL PLANE*	
	UNITS	MAGNITUDE	RANGE TIME (SEC)	MAGNITUDE	RANGE TIME (SEC)	MAGNITUDE	RANGE TIME (SEC)
Attitude Error	Deg	-1.7	199.5	0.4	226.5	-1.9	163.0
Attitude Rate	Deg/s	0.9	200.8	-0.1	166.0	1.8	164.1
Average Gimbal Angle	Deg	-1.2	162.8	0.4	163.2	-0.4	163.5
*All biases removed							

Between S-IC OECO and initiation of IGM Phase 1, commands were held constant. Significant events occurring during this interval were S-IC/S-II separation, and S-II stage J-2 engine start. Pitch and yaw dynamics during this interval indicated adequate control stability as shown in Figures 9-10 and 9-11, respectively. Steady state attitudes were achieved within 10 seconds from S-IC/S-II separation.

At IGM initiation, guidance commands caused the vehicle to pitch up. During IGM, the vehicle pitched down at a constant commanded rate of approximately -0.1 deg/s. The transient magnitudes experienced were similar to previous flights.

Other guidance command changes which caused dynamic changes were End Artificial Tau Mode and beginning of Terminal Steering. The engine deflections in yaw following CECO were the result of change of trim conditions. The center engine was not precanted to compensate for compliance deflection, and because of the location of fixed links this compliance effect occurred in the yaw plane as shown in the maximum yaw attitude rate in Table 9-3.

Flight and simulated data comparisons, Figures 9-11 and 9-12, show agreement at those events of greatest control system activity. Differences between the two can be accounted for largely by engine location misalignments, thrust vector misalignments and uncertainties in engine thrust buildup characteristics. The inflight thrust misalignments were found to be -0.1 degree about pitch and yaw axes.

- 1 S-IC/S-II SEPARATION
 - 2 INITIATION OF IGM
 - 3 CENTER ENGINE CUTOFF
 - 4 MIXTURE RATIO SHIFT, BEGIN ARTIFICIAL TAU MODE
 - 5 END ARTIFICIAL TAU MODE
 - 6 BEGIN TERMINAL STEERING
 - 7 OUTBOARD ENGINE CUTOFF
- MEASURED
 - - - - SIMULATED

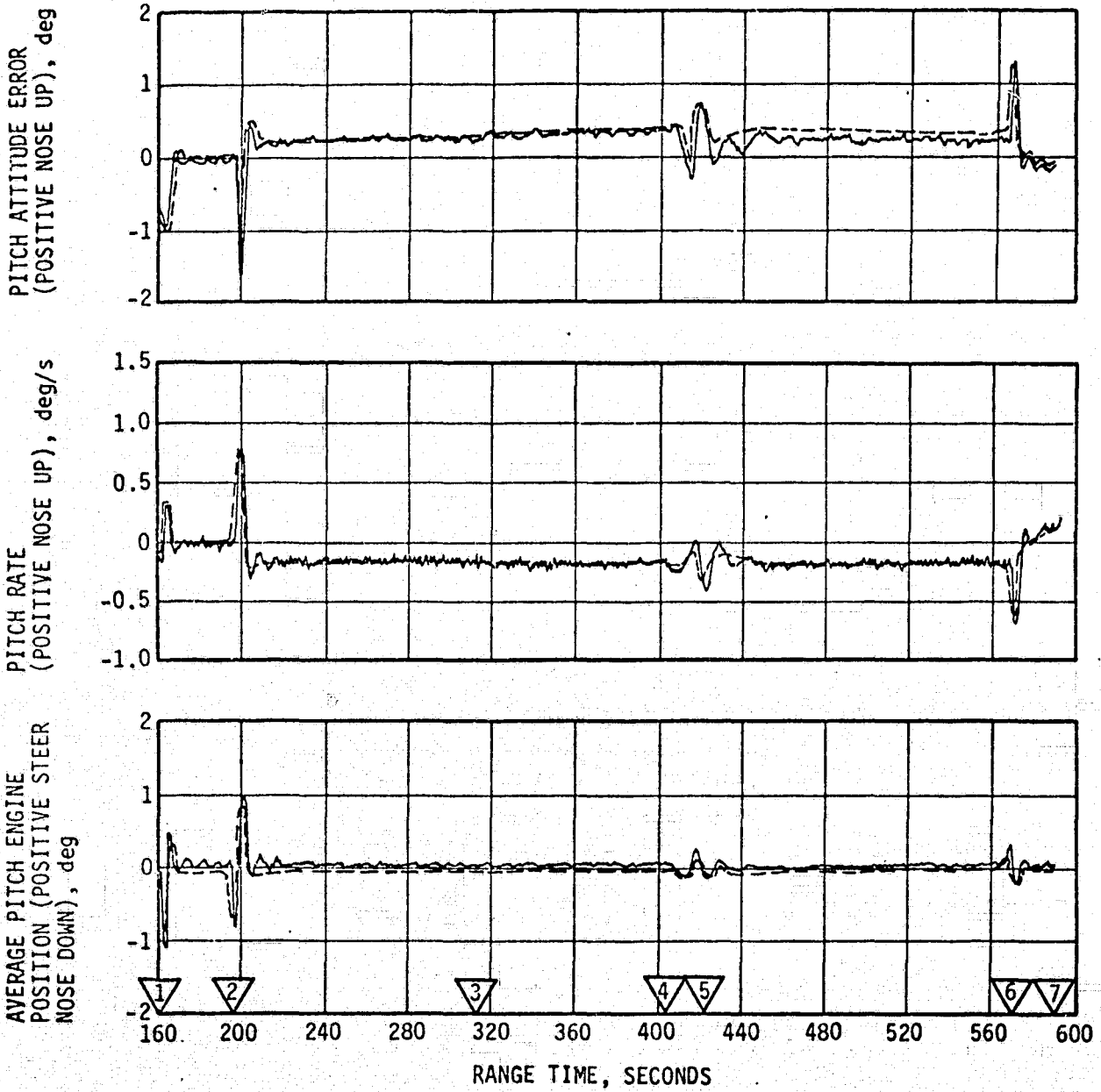


Figure 9-11. Pitch Plane Dynamics During S-II Burn

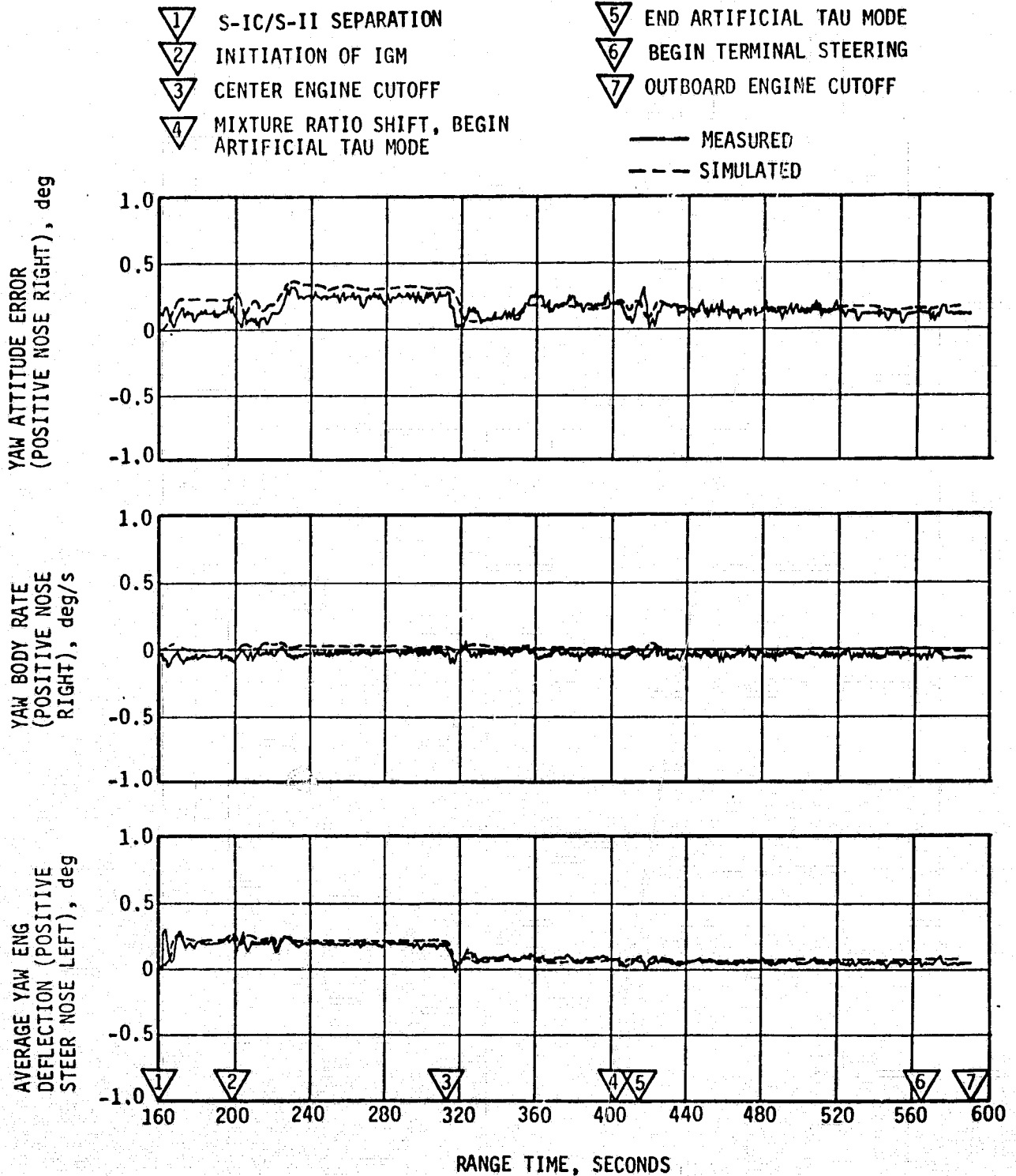


Figure 9-12. Yaw Plane Dynamics During S-II Burn

9.4 INSTRUMENT UNIT CONTROL COMPONENTS EVALUATION

All elements of the Control Subsystem functioned properly throughout the boost phase of the mission. During the coast phase of this flight, all error and error rate signals remained within the deadband. Attitude Control commands continued to be issued by the IU after S-II cutoff and vehicle responses indicated proper Thruster Attitude Control System function.

Discussion of a switch from the ST-124M inertial platform pitch axis gimbal angle fine resolver to the coarse (backup) resolver at 3805 seconds is presented in Section 8. Corrective action will be considered for any additional Orbital Work Shop launch vehicles.

9.5 SEPARATION

9.5.1 S-IC/S-II Separation

S-IC/S-II separation and associated sequencing were accomplished as planned with eight S-IC retro-motors providing the separation forces. S-IC and S-II stage clearance was 7 feet better than the 1 foot required when liquid hydrogen was dumped through the J-2 engines.

During the first plane separation period (159 to 161 seconds), the maximum S-II roll attitude error and angular rate were approximately -0.7 degree, and -0.4 deg/sec, respectively. Maximum S-II pitch and yaw attitude errors were -0.6 and 0.2 degree, respectively. Corresponding maximum pitch and yaw rates at this time were -0.1 and 0 deg/sec. These rates result in a lateral motion of the S-IC forward skirt relative to the J-2 engines. This motion is calculated to be 0.02 meters (0.6 inches), resulting in a clearance between J-2 engines and S-IC stage forward skirt of 0.9 meters (35 inches). In contrast, the clearance distance is typically 0.9 meters (36 inches) when pitch and yaw rates are zero. So the clearance in this case is normal.

Separation was completed when the J-2 engines main propellant ignition occurred at about 4.1 seconds from S-IC engines cutoff. At that time the stages are parted a distance of over 50 feet, and the distance continues to increase with time.

9.5.2 S-II Second Plane Separation Evaluation

The S-II Interstage failed to fully separate, causing elevated temperature and risk of structural failure as discussed below.

During S-II flight it was observed that the heat shield forward face and thrust cone pressure measurements, Figure 11-3; thrust cone forward

surface temperature measurements; Figure 12-7: heat shield curtain gas temperature measurements, Figures 12-9 and 12-10; and engine actuation system reservoir oil temperature measurements, paragraph 6.11; were much higher than measured on previous flights. The thrust cone temperature was seen to rise at a relatively rapid rate until CEEO instead of showing a distinct change at interstage separation so characteristic of all previous flights. At S-II OEEO, the measured SA-513 curtain gas temperatures were about 234°F higher than on previous flights. An analysis of the thermal environment indicates that thermally induced structural failure in the thrust structure area of the S-II stage was approached and would have been exceeded for a "one control engine out" condition.

In addition, it was observed that the S-II stage burn time was longer than nominal at velocity cutoff.

In order to determine the cause of the observed base region anomalies, the following three failure modes were considered and analyzed: a) flexible curtain failure, b) gas leak within the engine mounting circle forward of the heat shield, and c) failure of the S-II interstage to separate. The analysis clearly established that neither the flexible curtain failure mode nor the gas leak failure mode would have produced a condition which would result in a reasonable match of the observed data.

The pressure and thermal analysis based upon the failure of the S-II aft interstage to separate was based on these assumptions: a) flow field forward of the heat shield is fed by the reversed gases deflected by the aft surface of the heat shield, b) thrust cone and heat shield forward face pressures are proportional to the heat shield aft face pressure. The results are shown in Figures 9-13 through 9-14 which show that the predicted trends for both the heat shield forward face and thrust cone pressures and thrust cone temperatures are in agreement with the flight data.

Three other areas of investigation also provided supportive evidence that the interstage did not physically separate from the stage. These were: (1) radar observations, (2) vibration data, and (3) the S-II/SWS separation relative velocity.

On previous Saturn V flights, changes in the radar echo were correlatable with the events of first and second plane separation, initiation of IGM, etc. These same events were observed on the SL-1 flight with the exception of the second plane separation event. No change was observed in the radar pattern during the time frame in which second plane separation should have occurred.

Analysis of radial vibrations at the forward skirt stringer shows that on three previous flights (AS-510 through AS-512) the vibration sensor (flight measurement E0081-219) detected the Linear Shaped Charge (LSC) detonation, responding with a transient damped low frequency (15 to 17 Hz) wave shape modulating the characteristic (about 100 Hz) frequency. In each case the

- △ S-II IGNITION
- △ INTERSTAGE SEPARATION
- △ CECO
- △ EMR SHIFT
- △ S-II OECO

▨ PREDICTED - INTERSTAGE-ON

— ACTUAL
 - - - NOMINAL

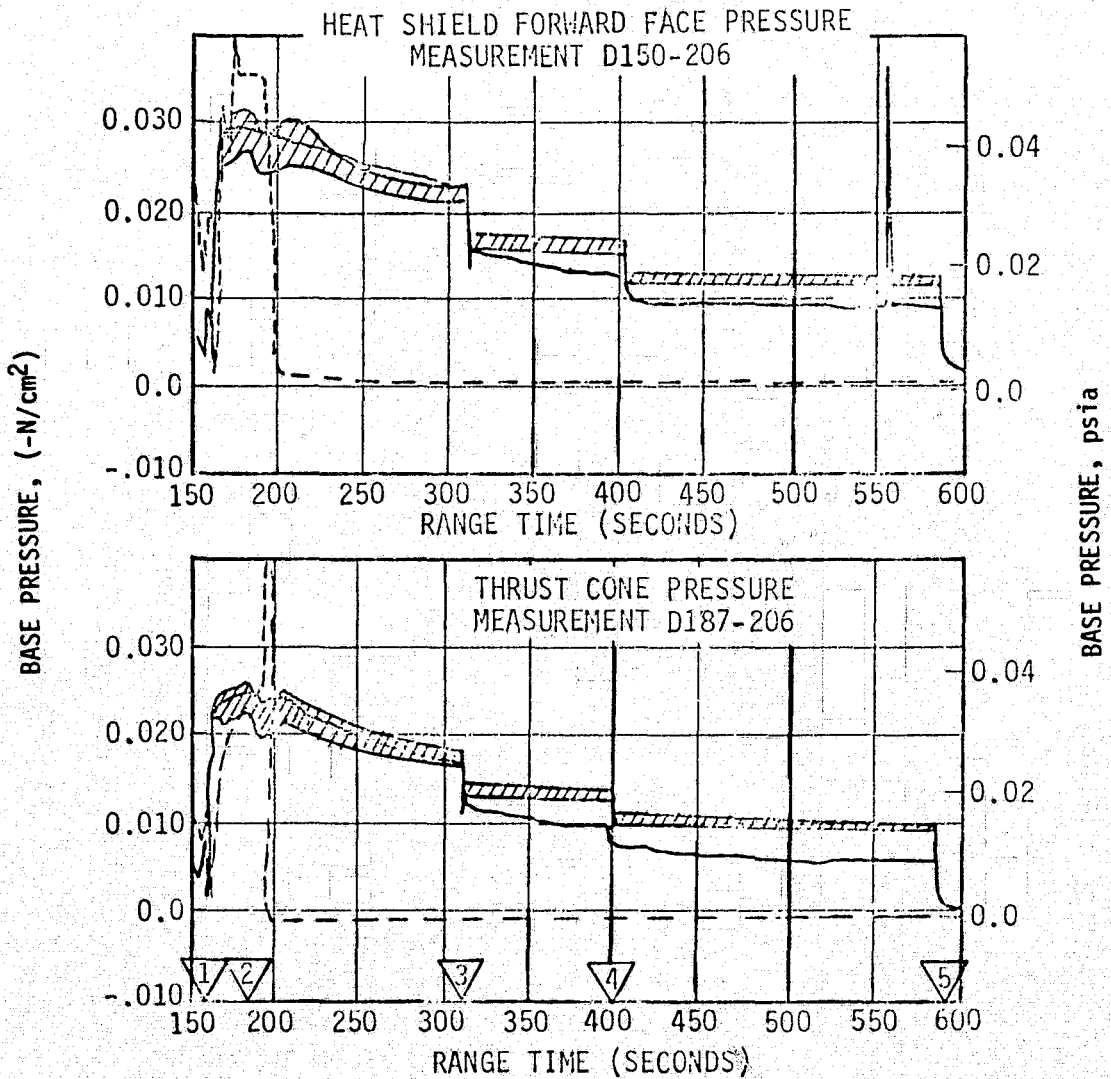


Figure 9-13. SA-513 S-II Base Region Pressures

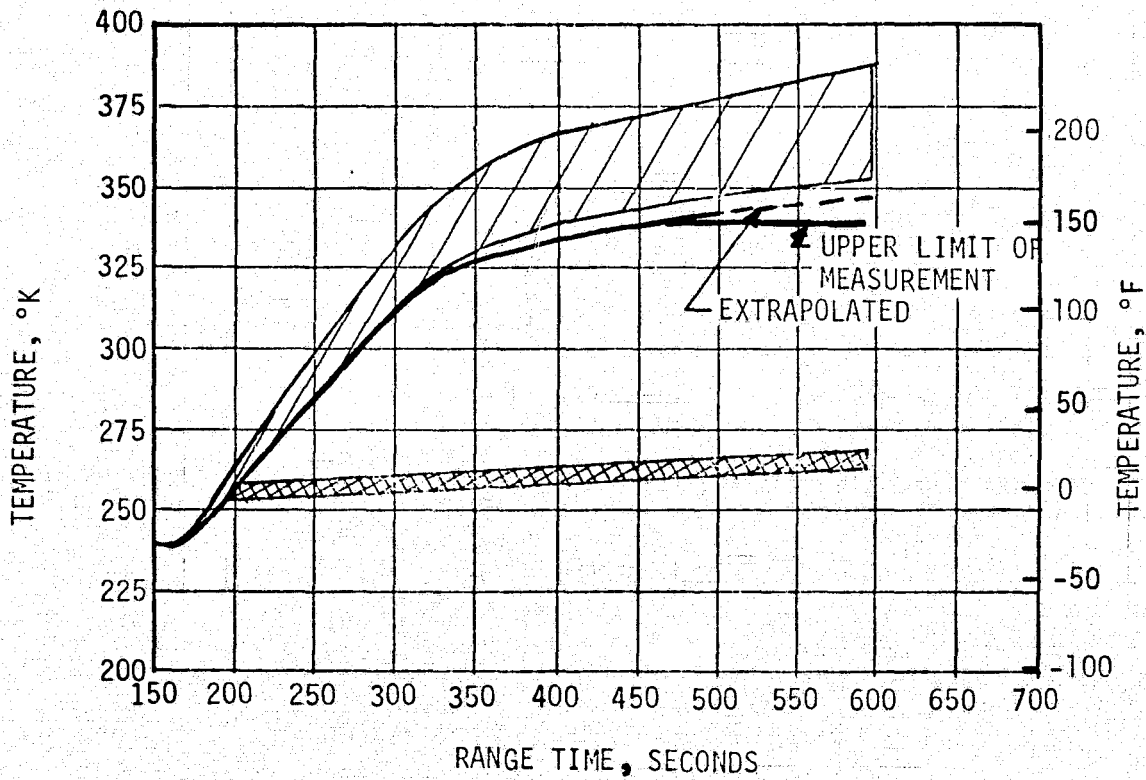
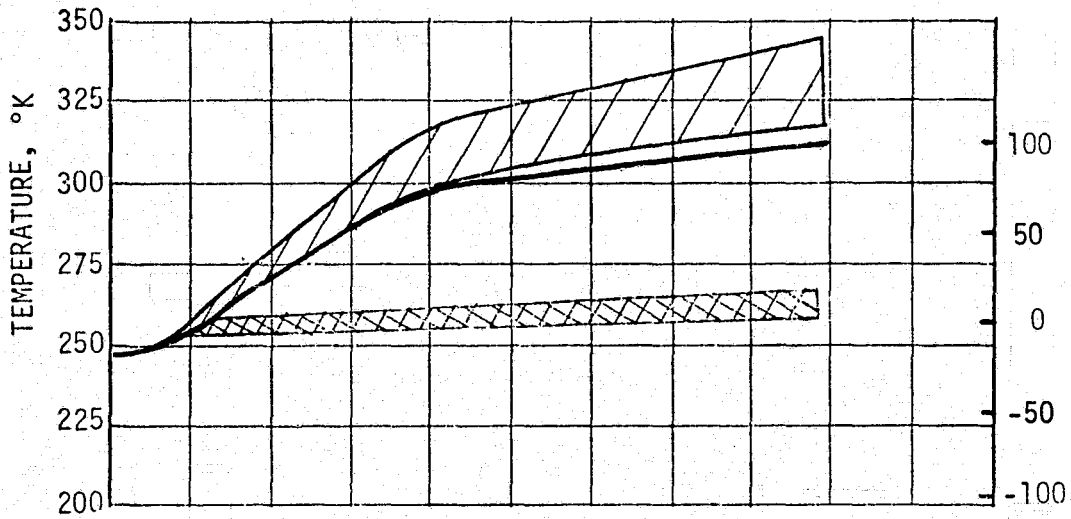
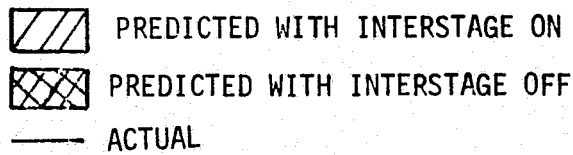


Figure 9-14. SA-513 S-II Thrust Cone Forward Surface Temperature

peak-to-peak amplitude of the transient is about four times the peak-to-peak amplitude of the residual vibrations and decays in about 0.5 seconds. The SA-513 vibration sensor responded to a disturbance at the time of second plane separation command; however, the transient response was only about twice the peak-to-peak amplitude of the residual vibrations and decays in about 0.2 second. The smaller response on SA-513 could indicate that the source of the disturbance was not as strong as on previous flights.

The actual S-II/SWS separation delta V was determined to be approximately 18.5 m/sec. This agrees closely with analysis of separation conditions when S-II aft interstage is attached.

The above evidence shows that the S-II Interstage failed to separate, however, the electrical data seemed to indicate that a normal separation had occurred. A detailed analysis was required to resolve this paradox.

The key elements of the second plane separation system are shown in Figure 9-15. Two Exploding Bridge Wire (EBW) units located near vehicle Position II, fire opposite ends of a Linear Shaped Charge (LSC) loop that passes completely around the vehicle in the separation plane. When the LSC is detonated by an EBW firing unit the tension straps (199 straps about the vehicle circumference) holding the interstage in place are severed and the interstage falls away. The normal sequence is for the EBW unit 1A to fire first with the detonation propagating around the entire LSC loop in approximately 4 ms, towards Position I. As a backup the second unit fires 100 ms later with the capability of detonating the entire LSC loop from the opposite direction. If separation is nominal, electrical disconnect between the S-II stage and the interstage occurs prior to the second firing command 100 ms later and since the EBW units are located on the interstage the backup EBW is not triggered. Electrical disconnect occurs when the S-II stage and the aft interstage are approximately 1/4 inch apart at the electrical connector panel.

Since the firing sequence occurred normally and electrical disconnect at the interstage electrical panel was indicated by the normal voltage decay transient of the EBW 1B voltage monitor and battery voltage of units located in the interstage at least partial separation was indicated. Partial separation indicates that some of the tension straps were severed. Assuming that detonation did not propagate completely around the LSC loop an analysis was conducted to show where detonation was interrupted. This analysis considered that a sufficient number of straps were severed to permit at least 1/4 inch separation at the electrical panel, but that a sufficient number of straps remained intact to hold the interstage on against inertial forces. The analysis shows that severing a 165° arc (89 tension straps) will provide 1/4 inch deflection for electrical connector demating and a minimum of 100° arc (55 tension straps) needed to hold the interstage. These results are shown in Figure 9-16 and indicate that propagation was interrupted between vehicle Position III

and 20° beyond vehicle Position IV towards Position I. This corresponds to a location between stringer 12 and stringer 162, Figure 9-15.

Five LSC failure modes were investigated. These included thermal damage, from aerodynamic heating, LSC failure to propagate, installation/operational damage, over-pressurization of the fairing, and debris damage. The most probable failure mechanism was identified to be debris damage from the OWS meteoroid shield which was lost at approximately 63 seconds (see Section 17).

An analysis was performed to determine if the debris could impact the S-II stage and, in particular, the S-II interstage separation plane LSC. The analysis determined that the debris could contact the S-II stage and data indicates it did damage the S-II forward skirt area increasing the vent area by approximately 108 in² as shown in Figure 11-5. The LH₂ tank sidewall was protected with spray foam insulation and probably incurred no damage from the passing debris. Traveling between 200 and 1000 ft/sec, the debris probably hit the LSC protective cover and damaged the LSC to interrupt subsequent propagation. Even if the debris had penetrated the LSC cover only, the resulting temperature of the LSC would increase to approximately 450 - 550°F because of aerodynamic heating and auto-ignite. This condition could burn rather than detonate a short length of the LSC and impair detonation propagation.

Vehicle operational or hardware corrective actions are still under investigation for future missions of either an Apollo or Skylab Program. The necessity for Apollo vehicle design changes and operational flight mission rule revisions will be assessed separately from Skylab mission applications, consistent with unique factors in each review.

9.5.3 S-II/SWS Separation

All of the S-II/SWS separation commands were issued and received properly. All expected responses from eight S-II stage vibration and acoustic measurements were received at the time of S-II/SWS separation verifying that separation had occurred at 591.1 seconds.

The attitude errors that occurred during S-II/SWS separation were larger than nominal, see Figure 9-17 for pitch, yaw and roll errors. These abnormally large values are a result of the 593-second anomaly. The corresponding attitude rates and accelerations are presented with a discussion of this anomaly in Section 17.

There is no flight data available to measure separation lateral clearance between the OWS radiator and the S-II/SWS interstage structure. A separation clearance analysis was performed based on the known rotation of the SWS vehicle after separation and the predicted S-II stage rotation due to center-of-gravity offsets. At the time when the OWS radiator had moved axially to the top of the S-II/SWS interstage, the lateral clearance was estimated to be 1.4 meters.

9-24

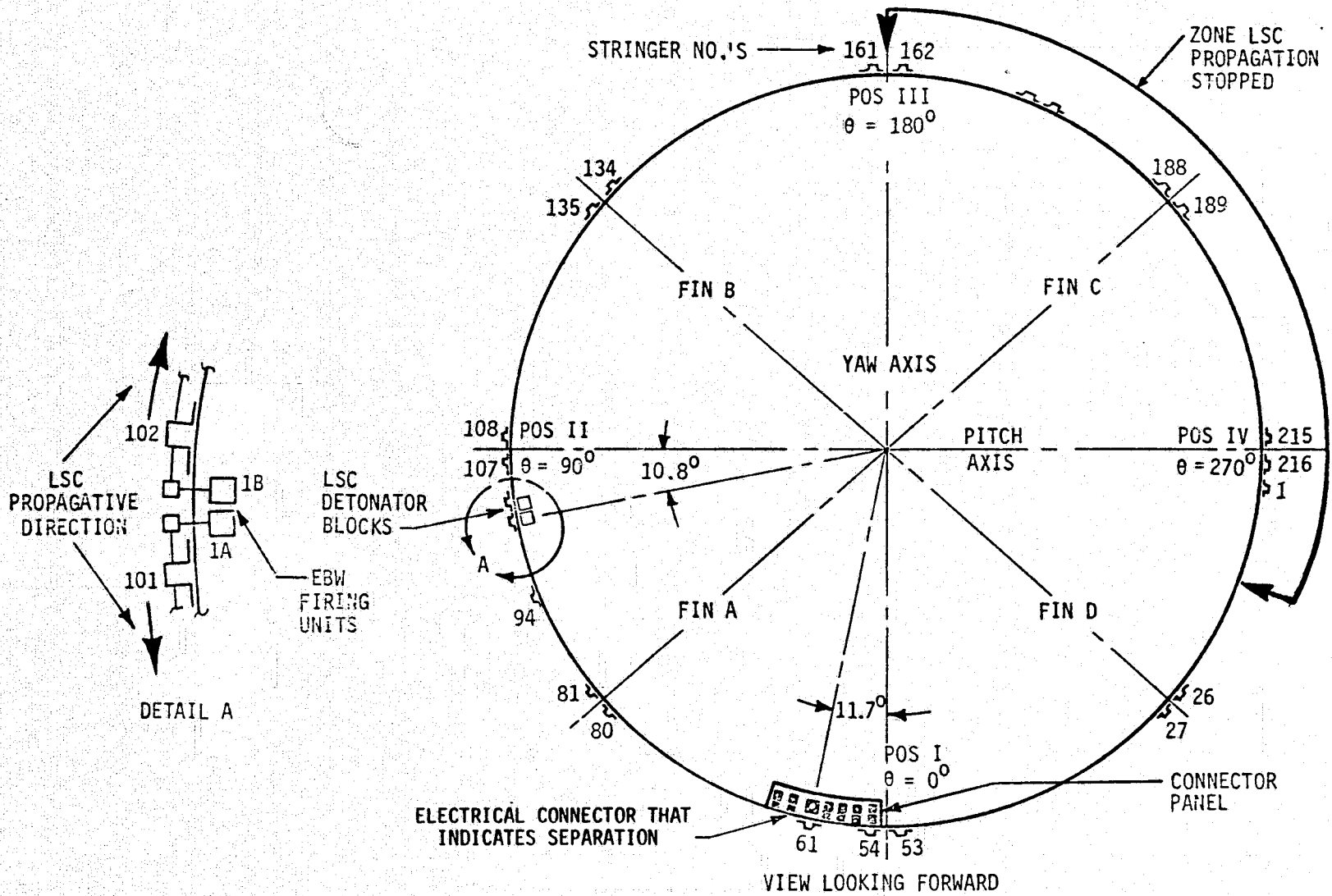


Figure 9-15. S-II Interstage Separation Diagram

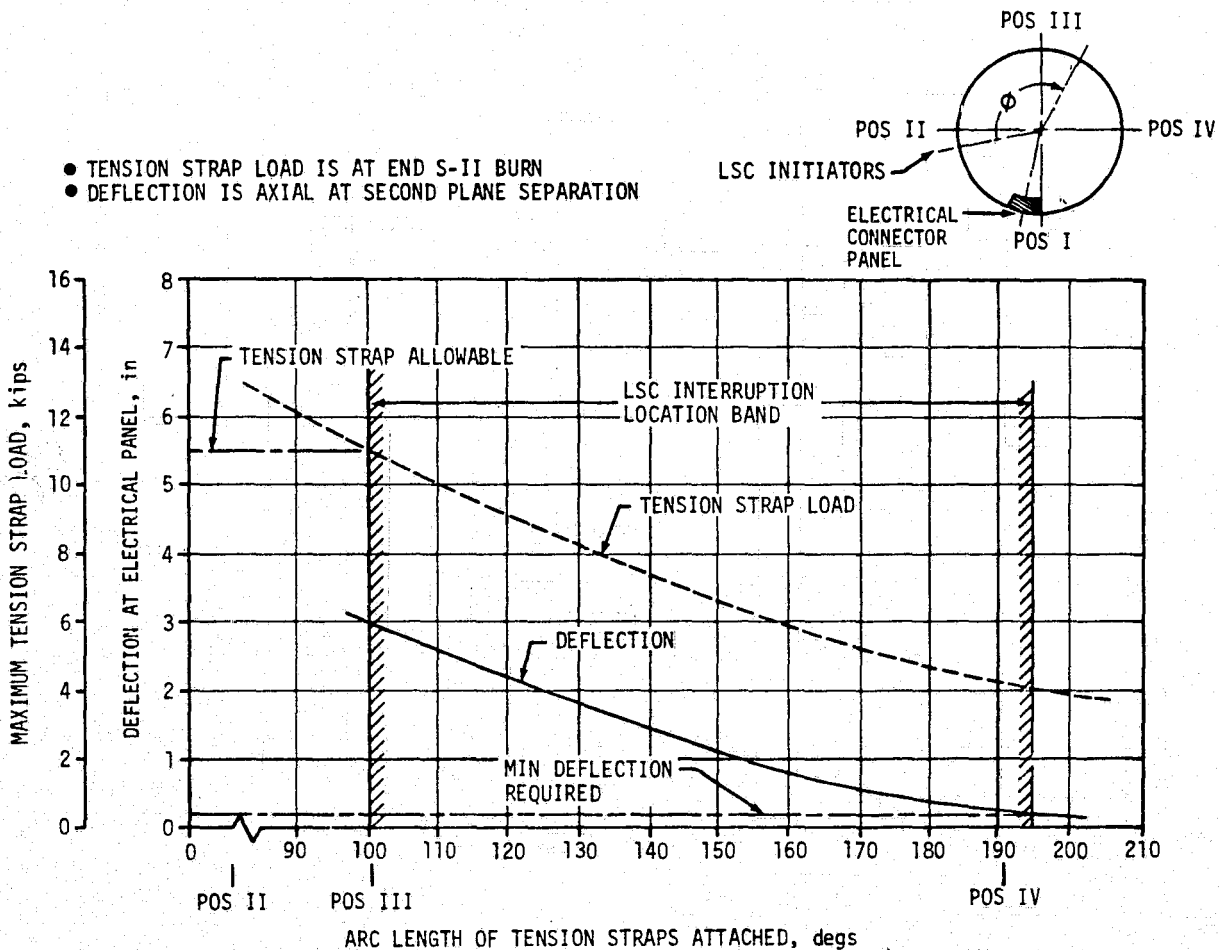


Figure 9-16. S-II-13 Interstage Station 196 Tension Strap Analysis

An analysis of the S-II/SWS separation velocity (ΔV) was made using S-II stage weight with and without the S-II interstage attached. If the S-II interstage had separated as scheduled then the S-II weight at S-II/SWS separation would have been 53,964 Kg and the separation ΔV would have been 20.3 m/sec. If the S-II interstage was still attached then the S-II stage would have been 5027 Kg heavier at S-II/SWS separation and the separation ΔV would have been 18.5 m/sec. The actual separation ΔV , as determined by tracking data, was 18.2 to 18.9 m/sec which agrees closely with separation velocity with the S-II interstage attached.

After successful S-II/SWS separation, the relative distance between the vehicle elements provided an adequate margin of safety when S-II stage pressure safing/venting was initiated. The safing sequence was scheduled at 210 seconds after S-II/SWS separation. As can be seen by the dotted line in Figure 9-18, this interval is sufficiently long to insure an adequate clearance distance during safing.

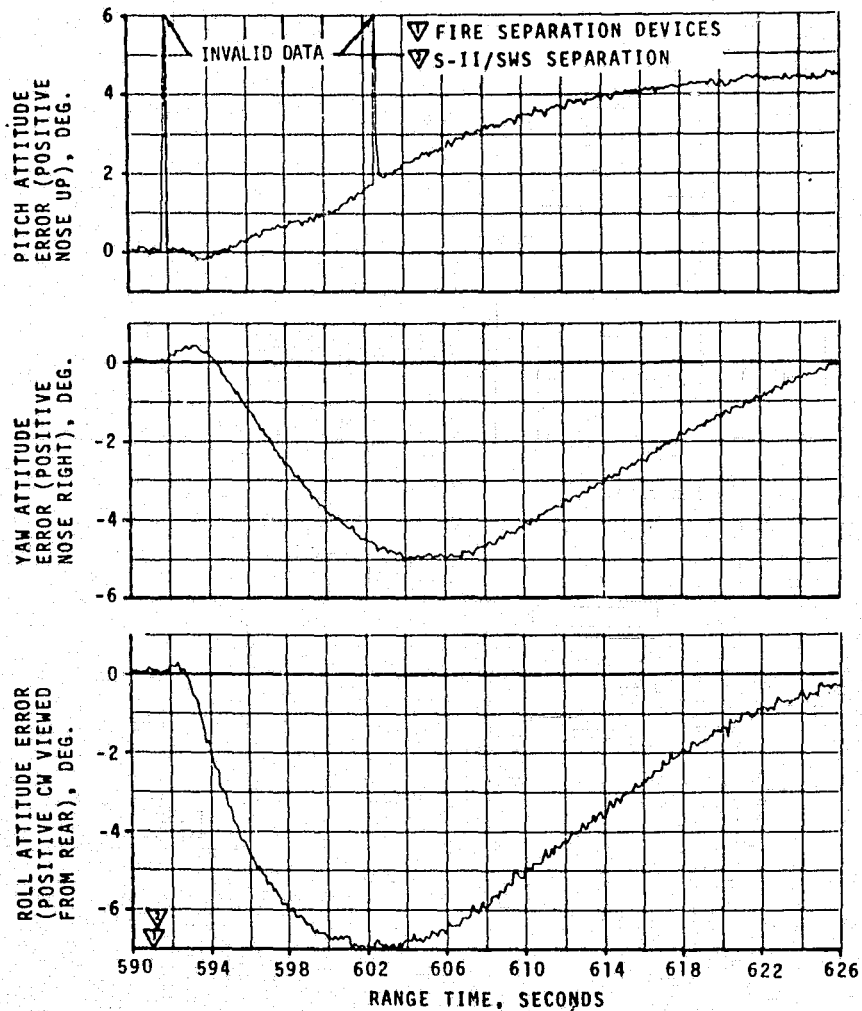


Figure 9-17. Attitude Errors at S-II/SWS Staging

Since the S-II/SWS has a nominal nosedown attitude with respect to the velocity vector at separation, the S-II stage initially moves upward and to the rear. Under nominal conditions the spent stage would have crossed the 2134 meter safe clearance distance at about 110 seconds after separation and it would have been 4118 meters from the SWS at the nominal safing time of 210 seconds.

The actual delta velocity of 18.82 m/s was about 1.1 meters/second less than the nominal value but the nominal safing time was about 4 seconds later than predicted. The net result as shown in Figure 9-18 was that the separation distance at the safing time was 3991 meters rather than the 4118 meter nominal value. In any case, there was an adequate margin of safety over the minimum allowable value of 2134 meters. If the S-II interstage had separated properly, the S-II/SWS separation distance at the safing time would have been 4364 meters using the actual retro motor performance and a safing time of 214 seconds after separation.

9-27/9-28

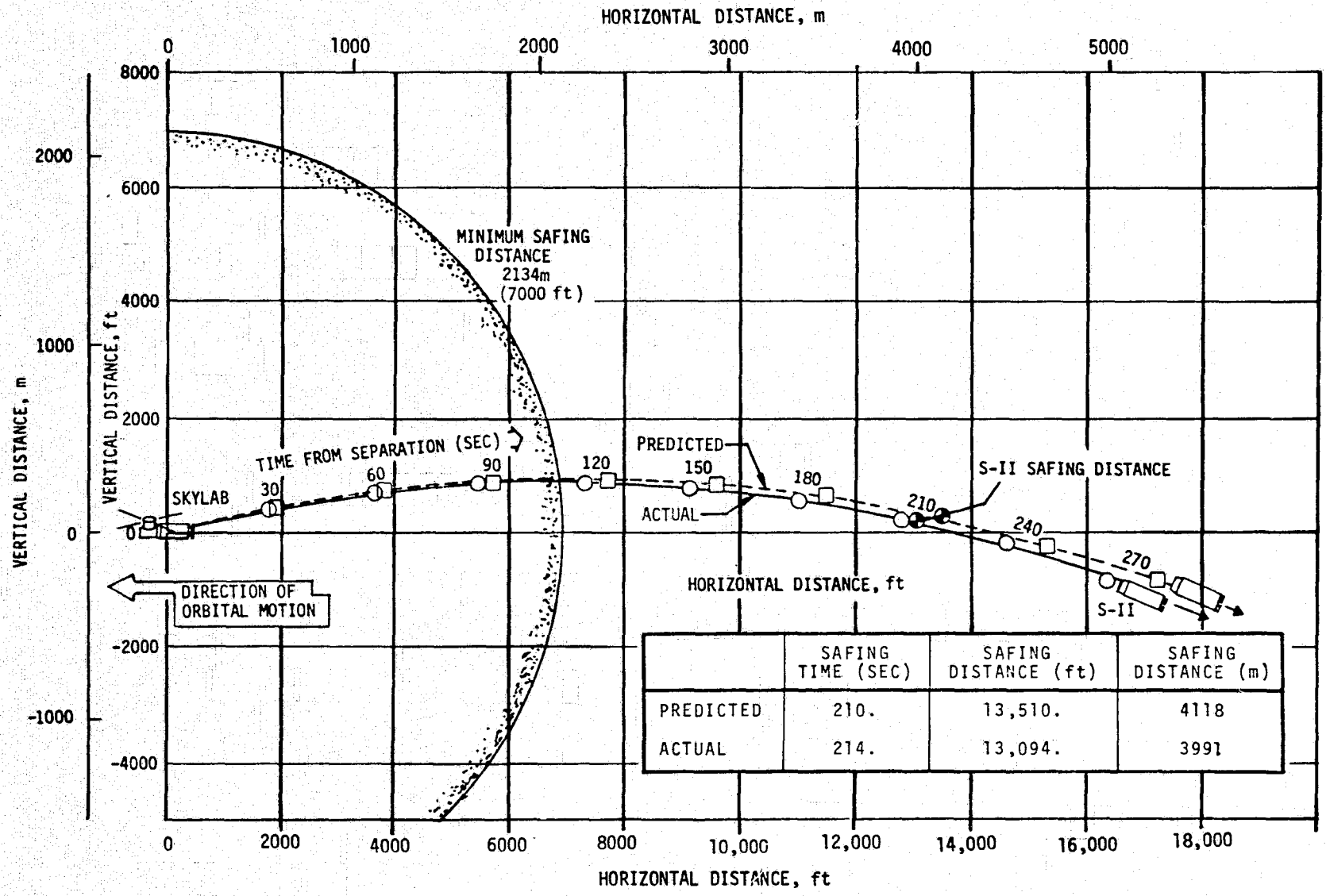


Figure 9-18. S-II Distance Relative to Skylab at S-II Safing

SECTION 10

ELECTRICAL NETWORKS AND EMERGENCY DETECTION SYSTEM

10.1 SUMMARY

The SA-513 launch vehicle electrical systems performed satisfactorily throughout the required boost and orbital phases. The Emergency Detection System (EDS), in an open loop configuration, functioned properly. The operation of the batteries, power supplies and switch selectors were normal. All Exploding Bridge Wire (EBW) firing units performed normally including the S-II second plane separation EBW firing units, which reacted as expected during the S-II interstage separation anomaly.

10.2 S-IC STAGE ELECTRICAL SYSTEM

The S-IC stage electrical system performance was satisfactory. Battery voltages were within performance limits of 26.5 to 32.0 V during powered flight. The battery currents were near predicted and below the maximum limits of 50 amperes for each battery. Battery power consumption was within the rated capacity of each battery, as shown in Table 10-1.

Table 10-1. S-IC Stage Battery Power Consumption

BATTERY	RATED CAPACITY (AMP-HR)	POWER CONSUMPTION*	
		AMP-HR	PERCENT OF CAPACITY
Operational	8.33	4.11	49.4
Instrumentation	8.33	5.68	68.1

*Calculated from battery activation to end of telemetry (at 517.4 seconds).

The two measuring power supplies remained within the required 5 ± 0.05 V. All switch selector channels functioned as commanded by the Instrument Unit (IU) and were within required time limits.

The separation and retro-motor EBW firing units were armed and triggered as programmed. Charging time and voltage characteristics were within performance limits.

The range safety command system EBW firing units were in a state-of-readiness for vehicle destruct, had it been necessary.

10.3 S-II STAGE ELECTRICAL SYSTEM

The stage electrical power system was unchanged from previous flights but electrical control circuits were incorporated for orbital safing of stage pressure vessels. Redundant switch selector commands were also added to increase the reliability of the separation systems (reference Appendix B).

The S-II stage electrical system performed satisfactorily. All battery and bus voltages remained within specified limits throughout the flight and safing operations. Instrumentation bus power was available well beyond the minimum predicted battery life to monitor S-II stage safing parameters. All bus currents remained within predicted limits. Main bus current averaged 30 amperes during S-IC boost and varied from 43 to 51 amperes during S-II boost. Instrumentation bus current averaged 22 amperes during S-IC and S-II boost. Recirculation bus current averaged 87 amperes during S-IC boost. Ignition bus current averaged 30 amperes during the S-II ignition sequence. All battery temperatures remained within predicted limits.

Battery power consumption and the rated capacity of each battery are shown in Table 10-2.

Table 10-2. S-II Stage Battery Power Consumption

BATTERY	RATED CAPACITY (AMP-HR)	POWER CONSUMPTION	
		AMP-HR	PERCENT OF CAPACITY
Main	35	50.30*	144
Instrumentation	35	51.80*	148
Recirculation #1	30	11.53**	38.4
Recirculation #2	30	11.57**	38.6

*Calculated from battery activation until end of data (at 3960 and 7440 seconds for Main and Instrumentation batteries, respectively).

**Calculated from battery activation until the batteries were electrically disconnected at time of S-II second plane separation.

All switch selector channels functioned as commanded by the IU. All stage safing functions were performed satisfactorily. The LH₂ recirculation pump inverters operated properly.

The range safety command system EBW firing units were in the required state-of-readiness for vehicle destruct, had it been necessary.

The non-propulsive vent EBW firing units which were added to SA-513 for S-II safing purposes performed satisfactorily.

All EBW firing units for the stage separation systems performed satisfactorily including the S-II second plane separation units (1A and 1B). Evaluation of the second plane separation EBW firing units arm and discharge characteristics has established that these units did not contribute to the interstage separation anomaly discussed in Section 9, Paragraph 9.5.2.

The primary EBW Unit 1A fired upon command resulting in only partial propagation due to the damaged Linear Shaped Charge. This propagation provided sufficient physical separation of the interstage to cause disconnect of the interstage interfacing connectors and interrupt of the firing command to the backup EBW Unit 1B. Thus, electrical signals were generated, which were typical of the normal separation sequence and gave no indication of an anomalous interstage separation.

The normal separation sequence was initiated with the charging of EBW firing unit 1A and 1B following switch selector commands at 183.217 and 183.317 seconds, respectively. Firing of aft interstage separation EBW Unit 1A was then commanded at 189.917 seconds. This firing resulted in electrical disconnect of the interfacing connectors at some time between 189.927 and 190.009 seconds. Firing command to the backup EBW firing unit 1B was issued by the switch selector at 190.017 seconds.

10.4 INSTRUMENT UNIT ELECTRICAL SYSTEMS

The IU electrical system remained essentially unchanged from previous flights except for the incorporation of a heater across the 6D20 battery to increase its load and thereby ensure its passivation (reference Appendix B, paragraph B.4.1).

The IU electrical system functioned normally. All battery voltages and currents remained in the nominal range until battery depletion. Battery temperature rise was nominal based on available data. Battery voltages, currents and temperatures are shown in Figures 10-1 through 10-4. Battery power consumption and rated capacity for each battery are shown in Table 10-3.

Current sharing of the 6D10 and 6D30 batteries, to provide redundant power to the ST-124M, was satisfactory throughout the flight. Current sharing reached a maximum of 22 amperes and 26 amperes from the 6D10 and 6D30 battery respectively during the S-IC burn as compared to an average of

Table 10-3. IU Battery Power Consumption

BATTERY	RATED CAPACITY (AMP-HR)	POWER CONSUMPTION	
		AMP-HR	PERCENT OF CAPACITY
6D10	350	231.84***	66.2
6D20	350	212.72*	60.1
6D30	350	381.52**	109.0
6D40	350	375.10**	102.8

*Calculated from activation to the loss of telemetry at 67,620 seconds).

**Calculated from activation until battery voltage decayed below 26.0 V (at 64,987 and 42,503 seconds for batteries 6D30 and 6D40, respectively.)

***Calculated from activation until loss of current data at 46,374 seconds. Battery voltage indicated depletion at 65,880 seconds (see Figure 10-1).

18 amperes and 21 amperes (see Figures 10-1 and 10-3).

The 56 volt power supply maintained an output voltage of 56.1 \pm 0.5 V which is well within the required tolerance of 56 \pm 2.5 V.

The 5 volt measuring power supply performed nominally, maintaining a constant voltage within specified tolerances.

The switch selector, electrical distributors and network cabling performed nominally during the boost and orbital phases.

10.5 SATURN V EMERGENCY DETECTION SYSTEM (EDS)

The EDS was flown in an open loop configuration with all abort signals being inhibited. The system was monitored for vehicle performance parameters during the boost phase. All discrete indications for EDS events functioned normally. The performance of all thrust OK pressure switches and associated voting logic which monitors engine status was nominal.

The Q-Ball, which sensed maximum dynamic pressure differences on previous Apollo flights, was not employed on this flight (see Appendix B). As noted in Section 9, none of the EDS rate gyros gave any indication of angular overrate in the pitch, yaw or roll axis.

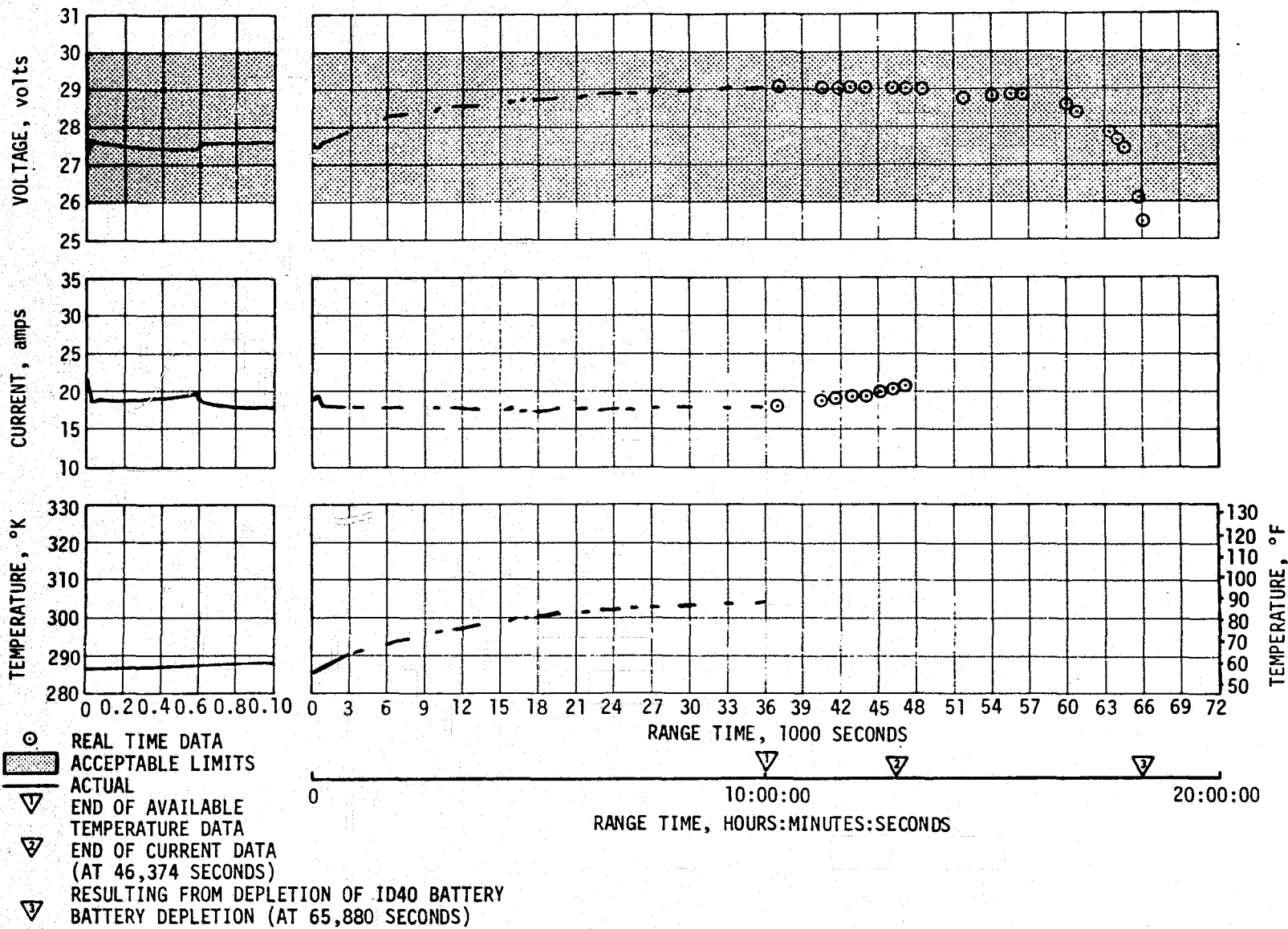


Figure 10-1. IU 6D10 Battery Parameters

9-01

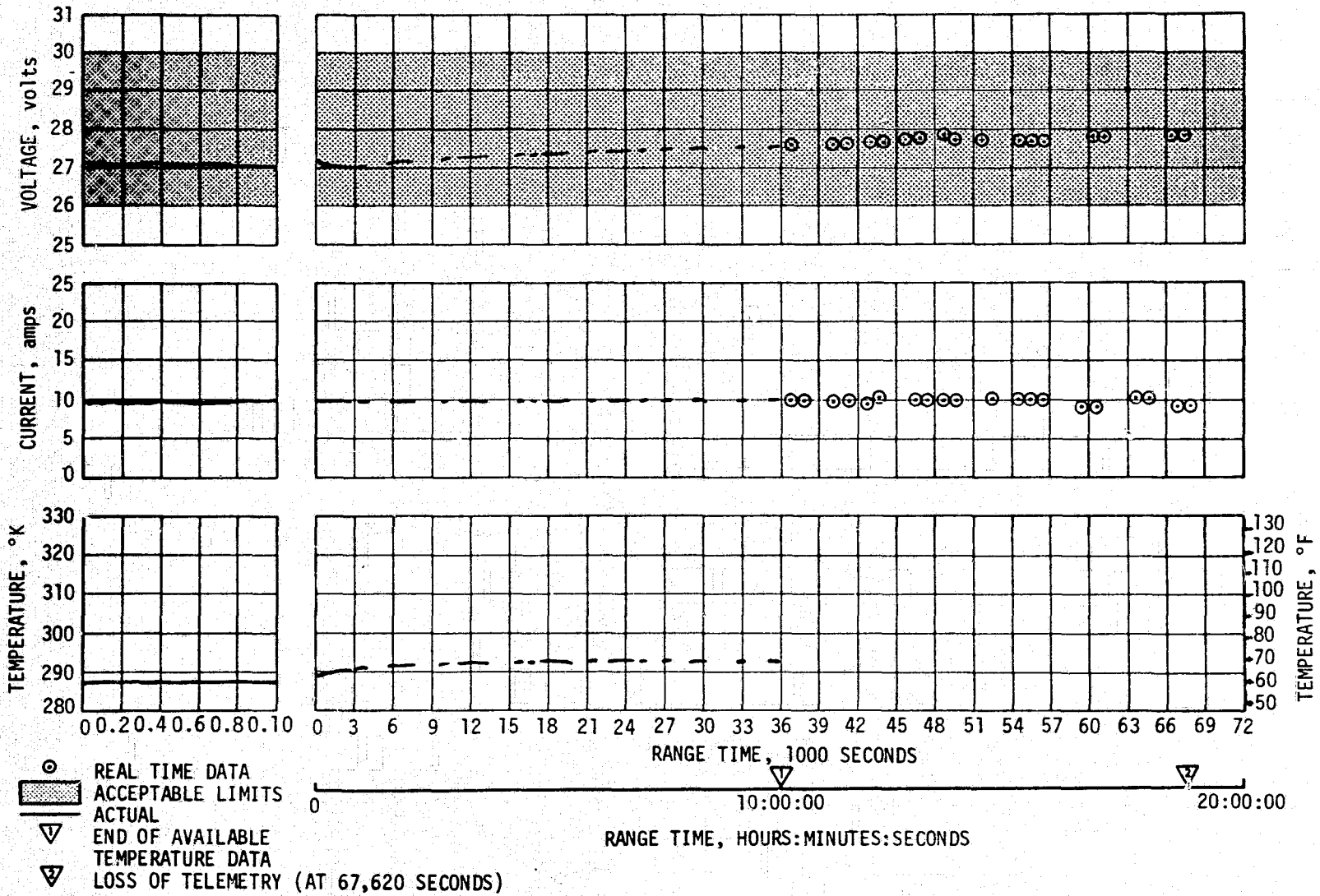


Figure 10-2. IU 6D20 Battery Parameters

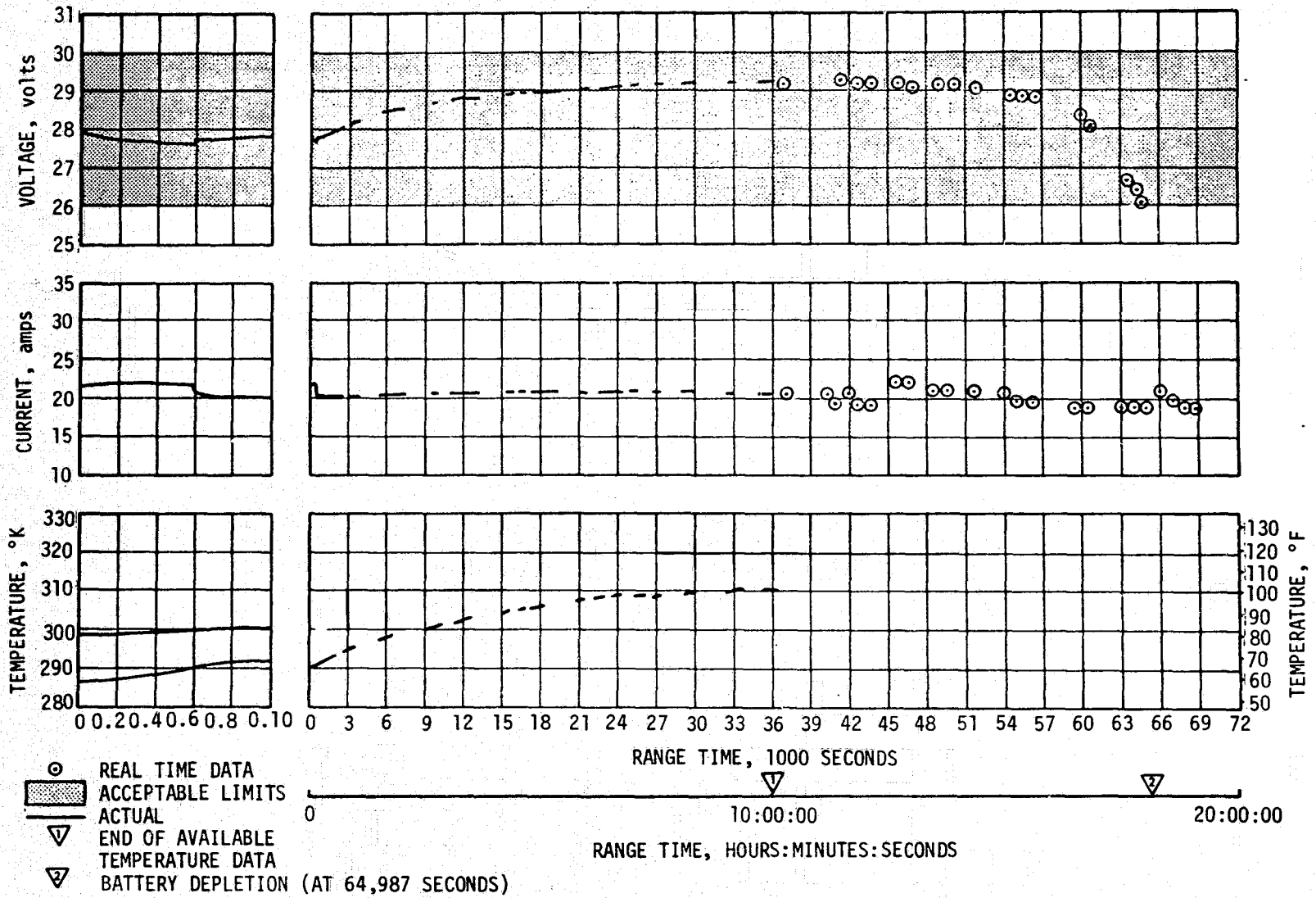


Figure 10-3. IU 6D30 Battery Parameters

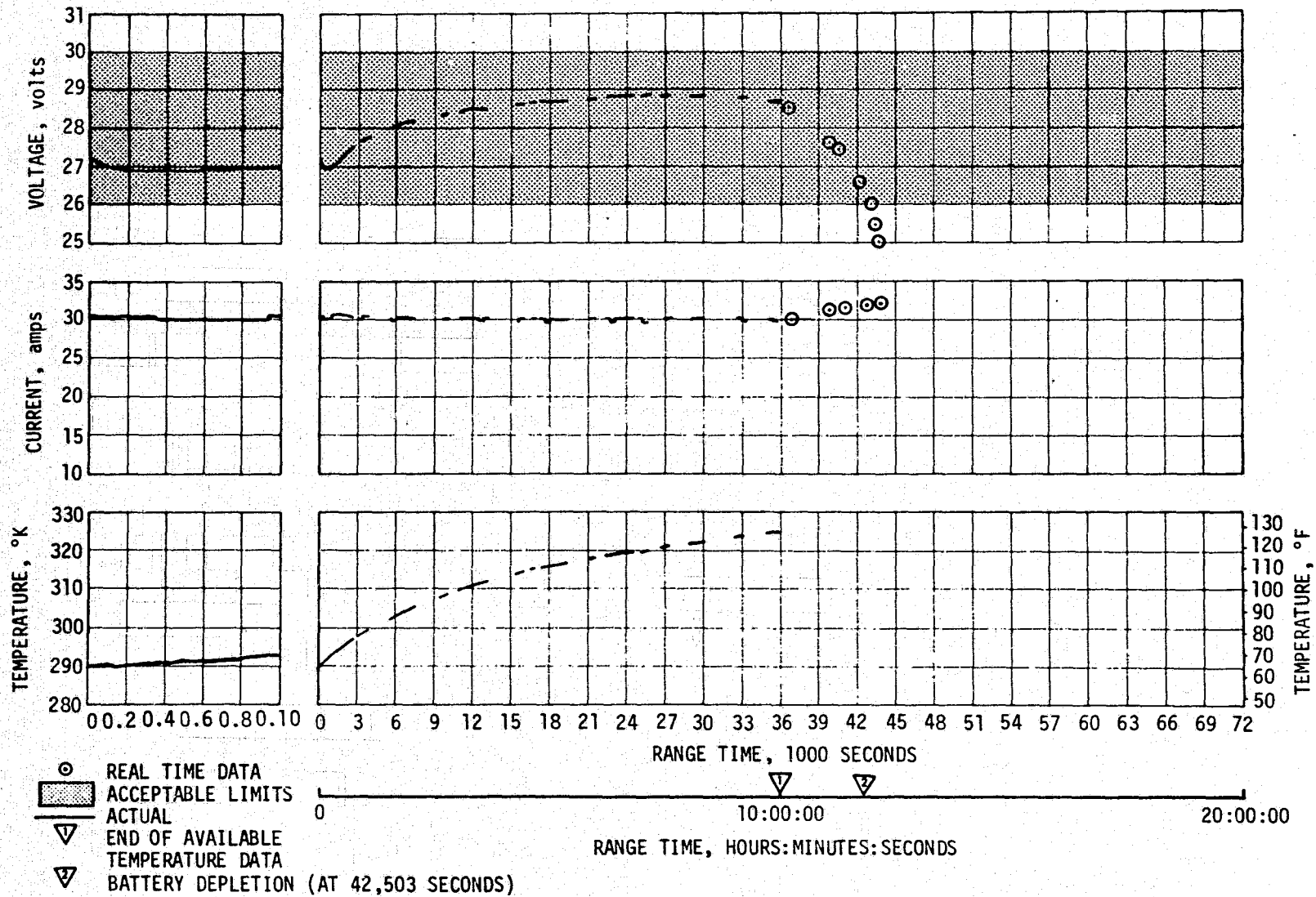


Figure 10-4. IU 6D40 Battery Parameters

SECTION 11

VEHICLE PRESSURE ENVIRONMENT

11.1 SUMMARY

The S-IC base heat shield was instrumented with two differential pressure measurements. The SA-513 flight data show trends and magnitudes similar to the Apollo flight data.

The SA-513 S-II base region contained three absolute pressure measurements. The measurement on the aft face of the heat shield showed a similar trend and magnitude to Apollo flight data. Measurements on the forward face of the heat shield and thrust cone surface agreed with Apollo flight data up to the time of second plane separation. Following the time of second plane separation, however, the data from these measurements remain at a higher level than that seen during the Apollo flights. These higher levels, along with other anomalous data led to the conclusion that the S-IC/S-II interstage had failed to separate.

S-II forward skirt pressure showed a more rapid decrease in pressure than was expected after 67 seconds, indicating a leak in that area probably caused by damage from debris resulting from the loss of the meteoroid shield.

11.2 BASE PRESSURES

11.2.1 S-IC Base Pressures

The base heat shield of the SA-513 S-IC was instrumented with two differential (internal minus external) pressure measurements, D0046-106 and D0047-106. The flight data, Figure 11-1, show similar trends and magnitudes to Apollo flight data. The maximum differential pressure was approximately 0.23 psi at an altitude of approximately 4 n. mi., which is well within the 2.50 psi burst and 2.75 psi crush design limits on the S-IC heat shield.

11.2.2 S-II Base Pressures

Figure 11-2 shows the S-II heat shield forward face pressure history (D0150-206), the postflight analytical values, and the data band from previous Apollo flights. The postflight analytical values assume the S-IC/S-II interstage remained on throughout the S-II flight, as discussed in Section 9.

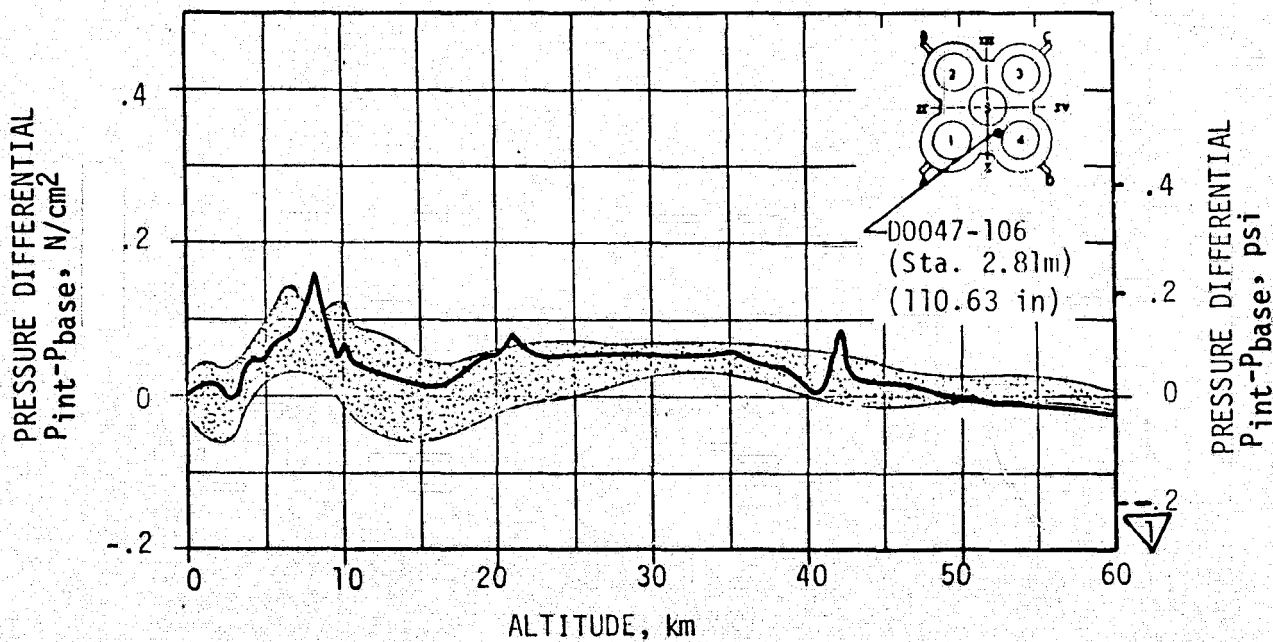
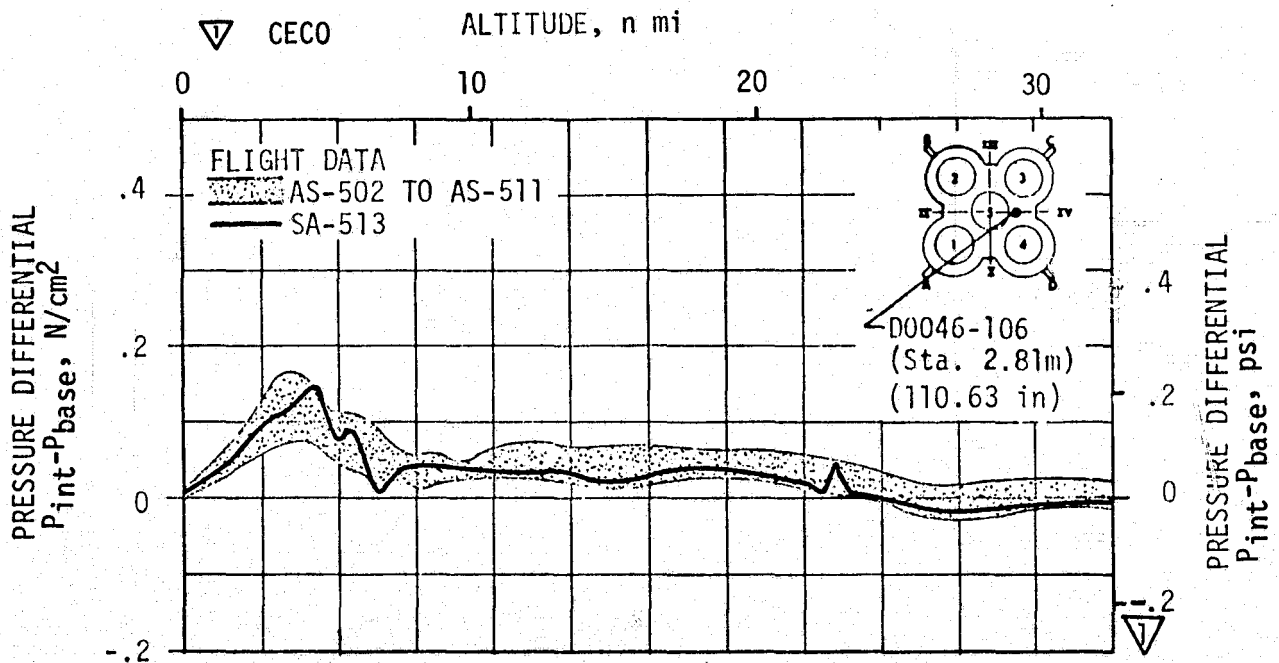


Figure 11-1. S-IC Base Heat Shield Differential Pressure

- 1 S-II IGNITION
- 2 INTERSTAGE SEPARATION
- 3 CECO
- 4 EMR SHIFT
- 5 S-II OEEO

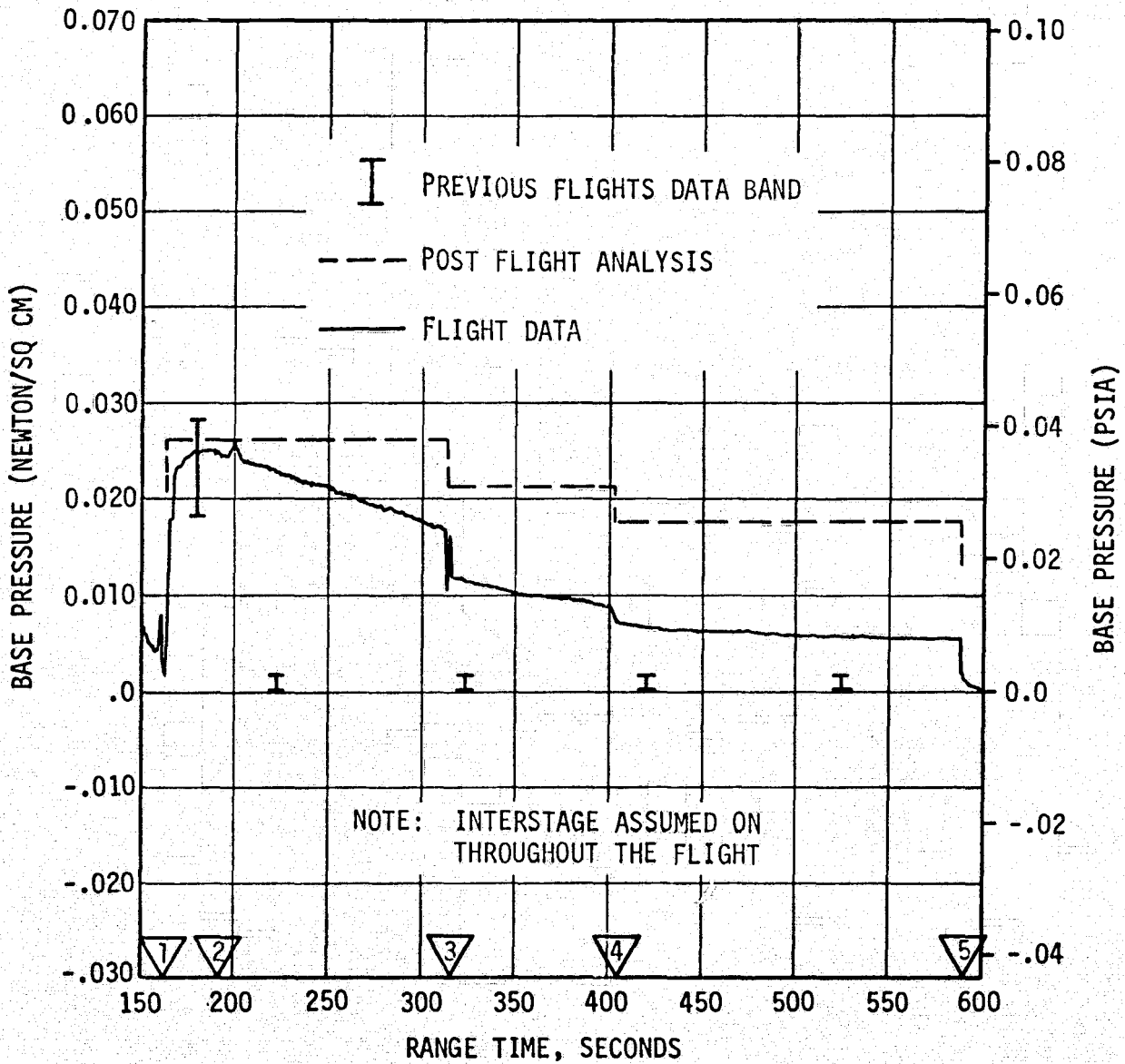
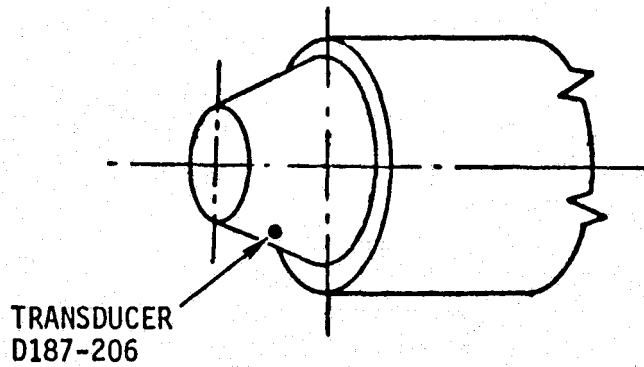


Figure 11-2. S-II Heat Shield Forward Face Pressure

From Figure 11-2, it is seen that no abrupt pressure drop occurs at the time of interstage separation and there is no characteristic pressure spike as has been observed on Apollo flights at the time of interstage separation. Also, the base pressures, following interstage separation time are an order of magnitude higher than corresponding Apollo flight values.

The gradual pressure decay of the heat shield forward face pressure measurement following separation time has not been seen previously because the pressure in this area has dropped abruptly following separation as shown in previous flight data (see Figure 11-2) and noted above. However, the aft face measurement has shown this decay on previous flights and it is probably caused by the reverse flow expansion process. This effect was not accounted for in the postflight analysis. The corresponding thrust cone pressure data (D0187-206) is presented in Figure 11-3. Again it is seen that the thrust cone pressures after interstage separation time are also an order of magnitude higher than the data band of previous Apollo flight data. Except for the gradual pressure decay in the flight data, the postflight analysis is in good agreement.

The heat shield aft face pressure history (D0158-206) is presented in Figure 11-4, together with the postflight analytical values, which are based on the S-IC/S-II interstage remaining on throughout flight, and the data band from previous Apollo flights. The analysis of the heat shield aft face pressures is developed using semi-empirical correlation between heat shield aft face static pressures and convective heating rates. These correlations are based on scale model hot flow test results and the data from previous flights. It is seen that the flight data fall within the data band of the previous flights as expected.

On previous flights the heat shield aft face pressure drops by approximately 0.01 psia after the time of interstage separation. This pressure drop did not occur during the SA-513 flight. The decay of the heat shield aft face pressure previously noted on Apollo flights appears to be more rapid during this flight. The postflight analytical pressure history is in agreement with the flight measured history except for the pressure decay effect which was not included in the analysis.

11.3 S-II FORWARD SKIRT PRESSURES

The S-II Orbital Work Shop interstage compartment pressure history during S-IC boost, which was measured by pressure transducer D0163-219, is shown in Figure 11-5. Also included in the figure is the analytically determined postflight prediction which is based on the postflight trajectory used in conjunction with a local flow properties program and a multiple chamber venting program.

- 1 S-II IGNITION
- 2 INTERSTAGE SEPARATION
- 3 CECO
- 4 EMR SHIFT
- 5 S-II OEEO

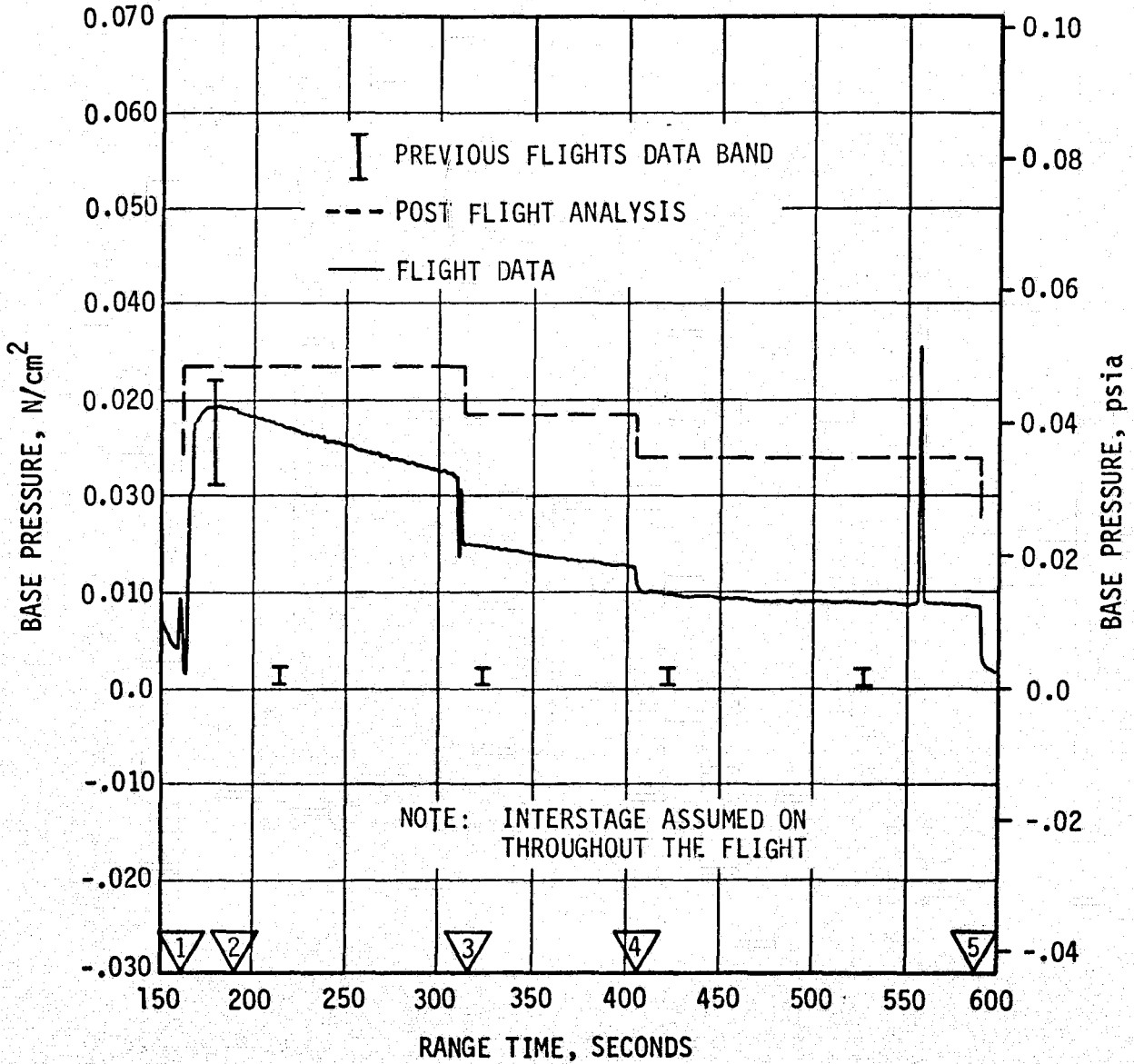
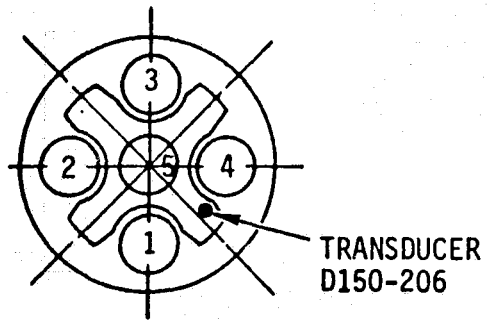


Figure 11-3. S-II Thrust Cone Pressure

- ▽ 1 S-II IGNITION
- ▽ 2 INTERSTAGE SEPARATION
- ▽ 3 CECO
- ▽ 4 EMR SHIFT
- ▽ 5 S-II OECO

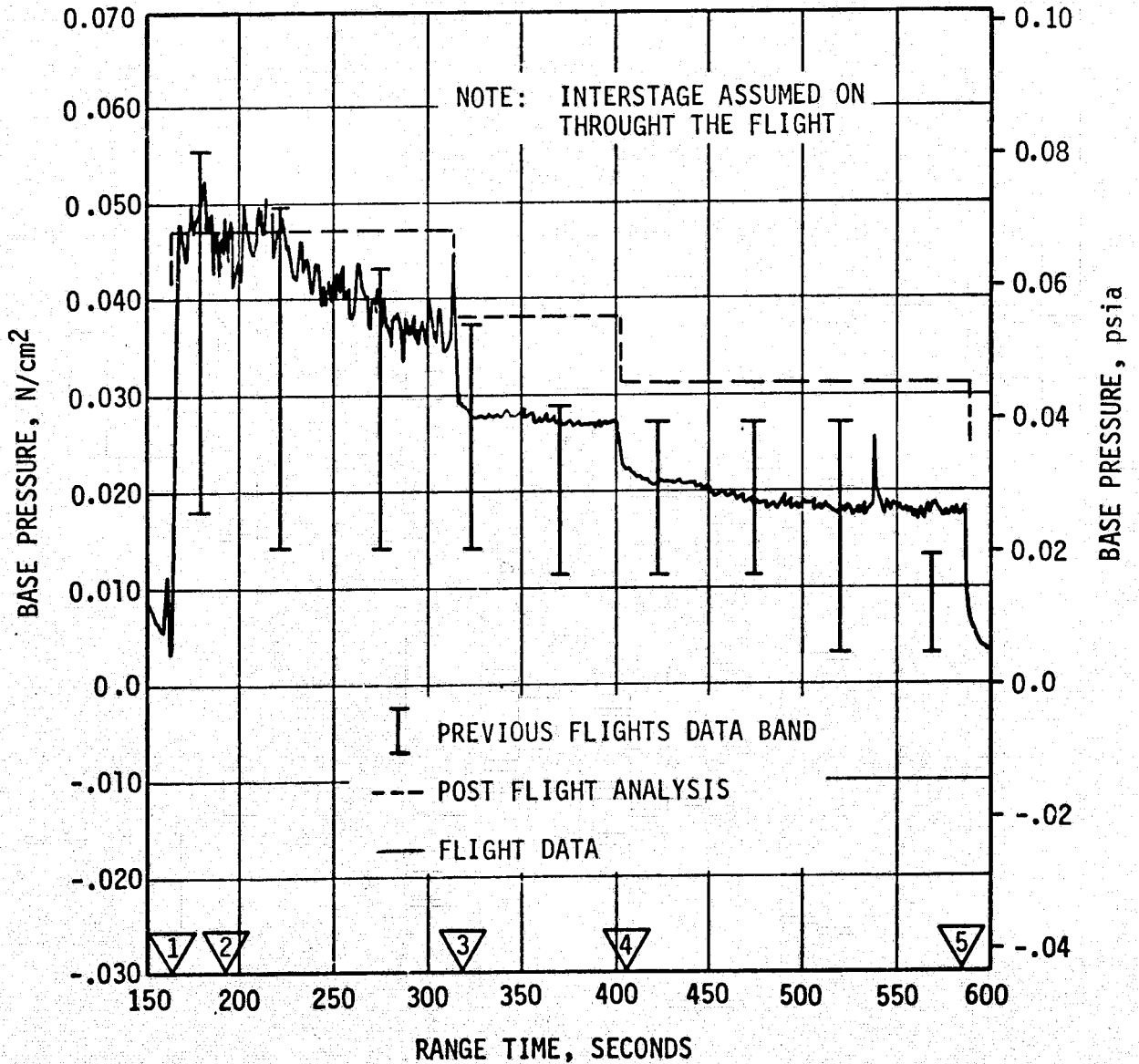
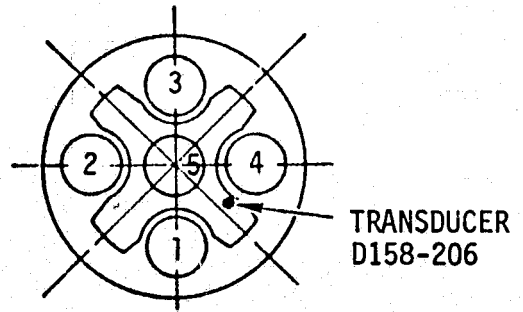


Figure 11-4. S-II Heat Shield Aft Face Pressure

1 MACH 1

2 MAXIMUM DYNAMIC PRESSURE

— FLIGHT DATA
- - - POST-FLIGHT ANALYSIS (PREDICTED -NO LEAK)

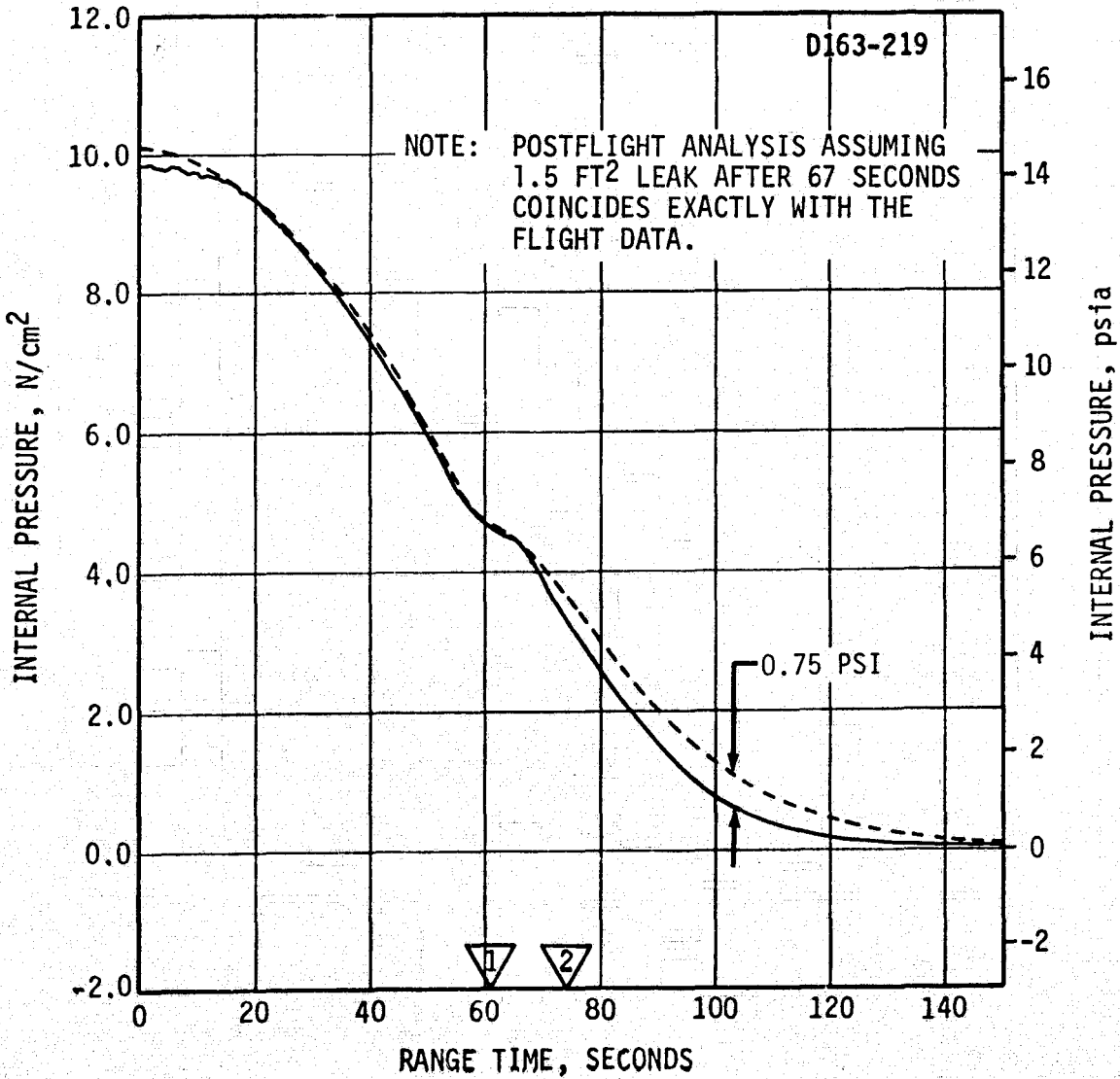


Figure 11-5. S-II/OWS Interstage Pressure

The figure shows that the measured and predicted pressures agree quite well until about 67-68 seconds into the flight when the measured pressure starts falling more rapidly than expected. From about 85 to 100 seconds, the measured pressures are about 0.75 psi less than the post-flight analytical values. This difference between the measured and predicted pressures is larger than the corresponding discrepancies obtained on the previous Apollo Saturn V launches.

The sudden change in the slope of the measured pressure decay curve at 67-68 seconds suggests an increase in vent area at about this time. An analysis was conducted to determine possible size and location of this anomalous vent area. It was found that the measured internal pressure could be matched by adding more vent area to either the S-II/OWS frustum or the S-II forward skirt. The use of an equivalent vent area of approximately 288 in² at vehicle station 2604 (frustum) or 108 in² at vehicle station 2507 on the S-II forward skirt, assumed to open at 68 seconds into the flight, closely matches the measured data, as shown in Figure 11-5. Note that the added vent area could be the sum of several small holes or one larger hole. Also, the locations assumed in the analysis are not the only possible ones. This would indicate a good probability that skin damage from OWS debris (reference Section 17).

The greater than expected pressure levels measured on the forward face of the heat shield and thrust cone surface following the time of S-II second plane separation are indications that the S-IC/S-II interstage did not separate. This anomaly is discussed in greater detail in Paragraph 9.5.2.

11.4 S-IC/S-II SEPARATION PRESSURES

There are no environmental pressure measurements in the forward skirt of the S-IC, however, since the S-IC/S-II separation was close to nominal the pressures in this area should be well below maximum allowable values.

The S-II base region pressure transducer (D00158-206, see Figure 11-4) exhibits normal response during the engine start transient, indicating that the S-II base region pressures were lower during S-IC/S-II separation than during full thrust operations.

SECTION 12

VEHICLE THERMAL ENVIRONMENT

12.1 SUMMARY

The SA-513 S-IC base region environment was similar to that experienced on Apollo flights.

The SA-513 S-II base region thermal environment was expected to be about the same as that experienced on Apollo flights. However, the S-IC/S-II interstage failed to separate; consequently, the thrust cone region temperatures following scheduled time of separation were greater than experienced during Apollo flights.

Aerodynamic heating environments were not measured on SA-513.

Since the S-IC/S-II separation dynamics for SA-513 were nominal, the heating rates to the S-IC forward dome and S-II base area during separation were well below maximum allowable values.

12.2 S-IC BASE HEATING

The S-IC base region thermal environments for the SA-513 flight were indicated by two total calorimeters and two gas temperature probes located on the base heat shield. The sensing surface of the total calorimeters (C26-106 and C149-106) were mounted flush with the aft surface of the heat shield. The gas temperature sensing surfaces were mounted at 0.25 inch (C50-106) and 2.50 inches (C52-106) aft of the heat shield surface. Data from these instruments are compared with Apollo flight data and are presented in Figure 12-1 and 12-2.

The SA-513 S-IC base region environments have trends and magnitudes similar to Apollo flight data. The maximum recorded total heating rate was approximately 24 Btu/ft²-sec and occurred at an altitude of 11 n mi, and the maximum gas temperature was approximately 1718°F recorded 2.5 inches aft of the heat shield at an altitude of 11 n mi. In general, center engine cutoff (CECO) produced a spike in the environmental data with a magnitude and duration similar to that seen in Apollo flight data.

Ambient gas temperatures under the engine cocoons (monitored by C0242-101 through C0202-105) were within the band of previous Apollo flight data. These temperatures are shown in Figure 12-3.

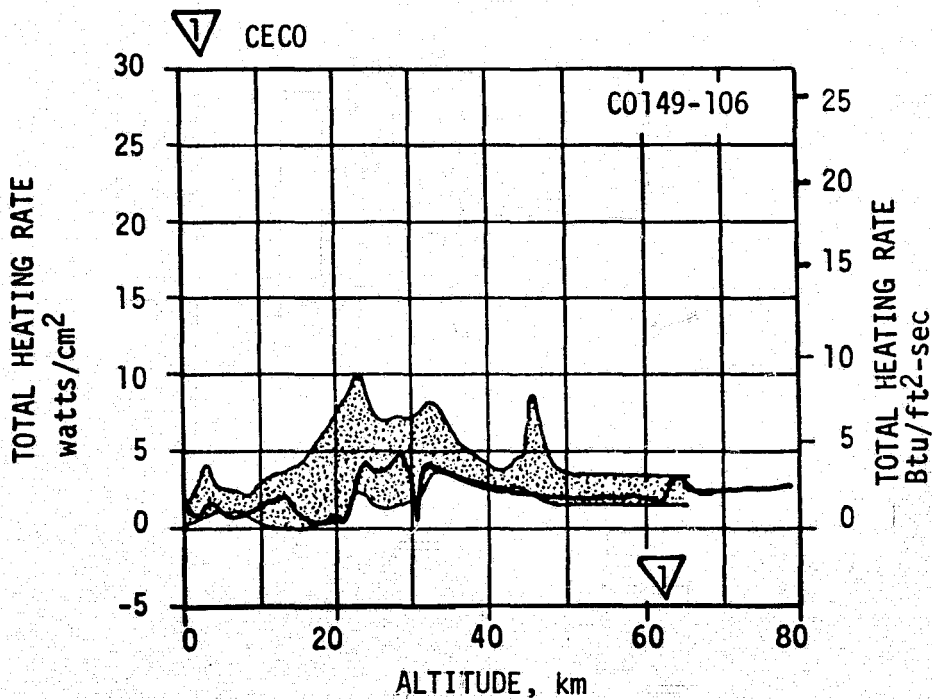
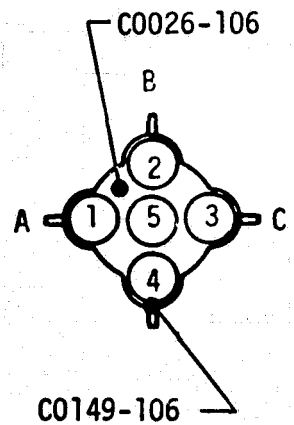
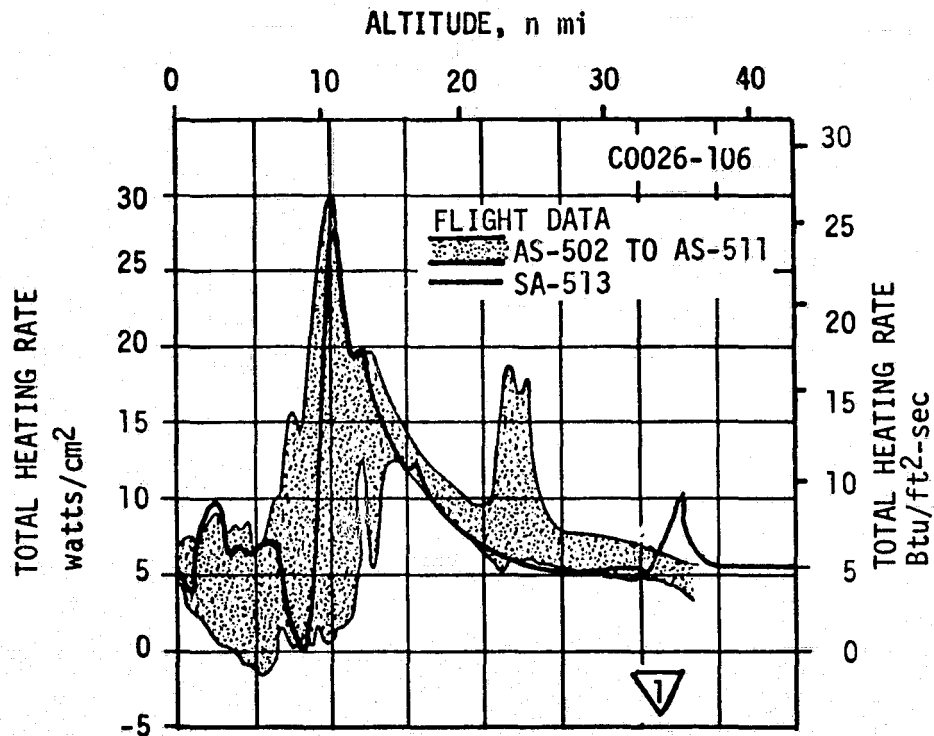


Figure 12-1. S-IC Base Region Total Heating Rate

ALTITUDE, n mi

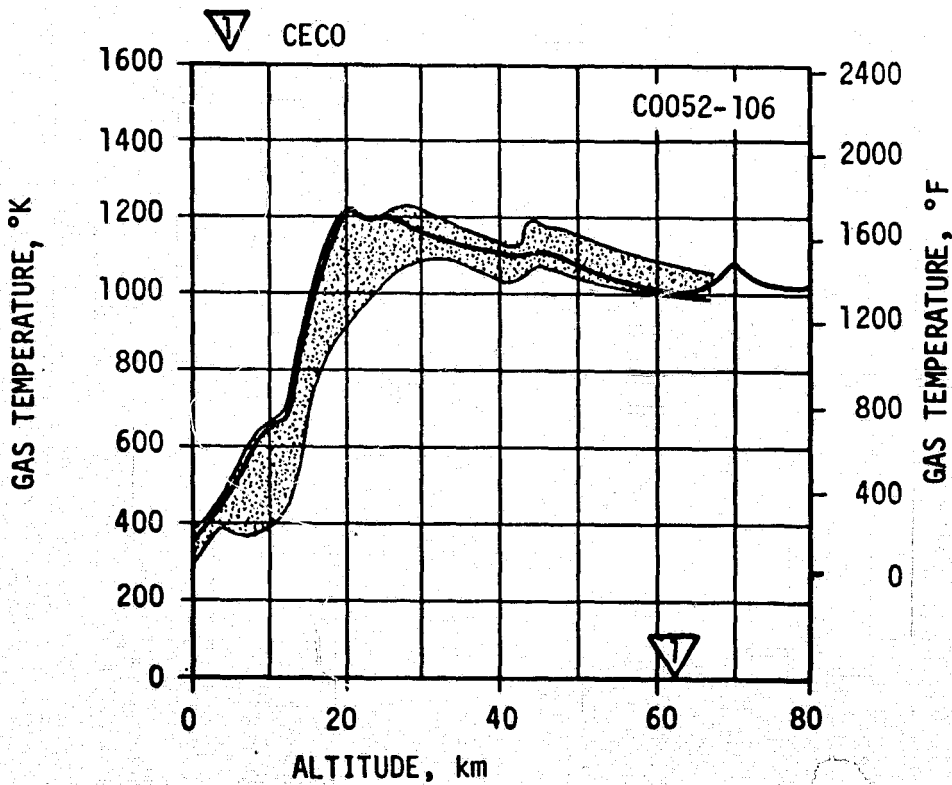
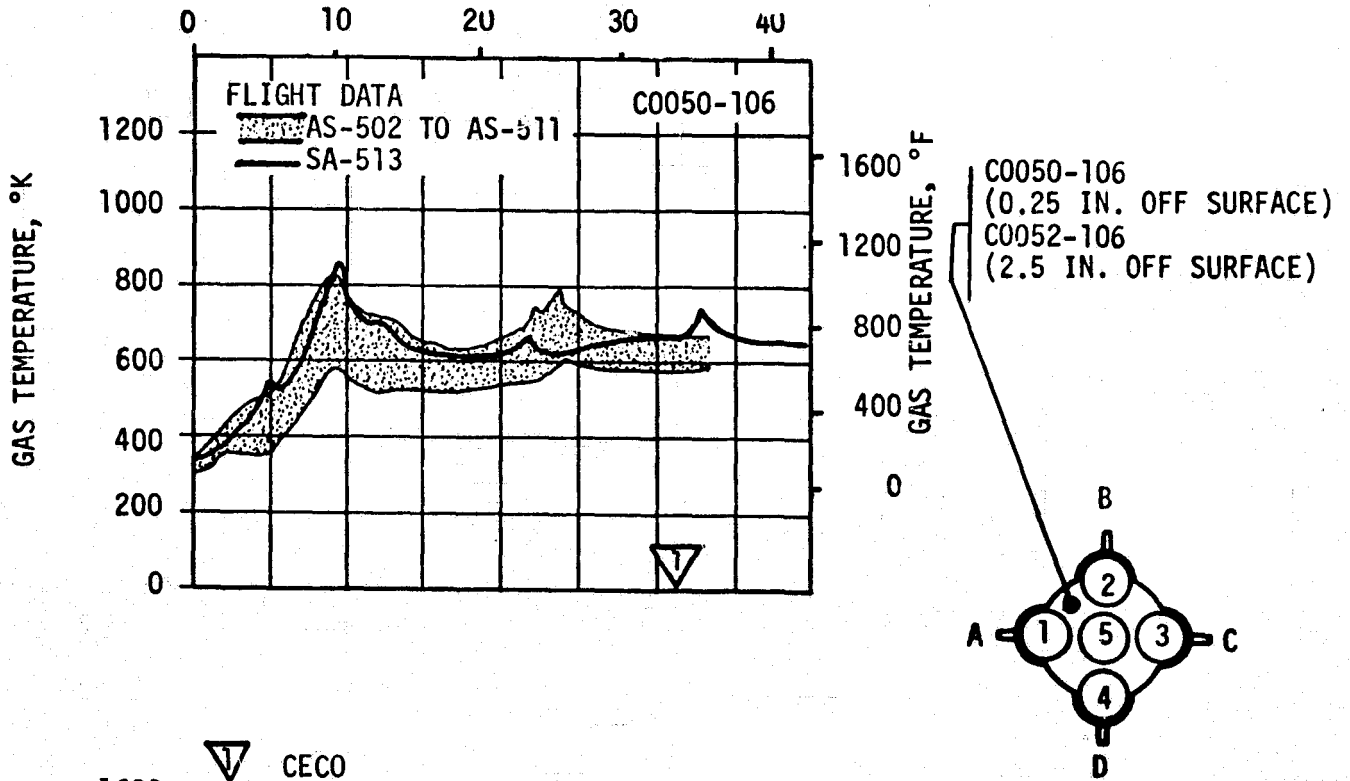


Figure 12-2. S-IC Base Region Gas Temperature

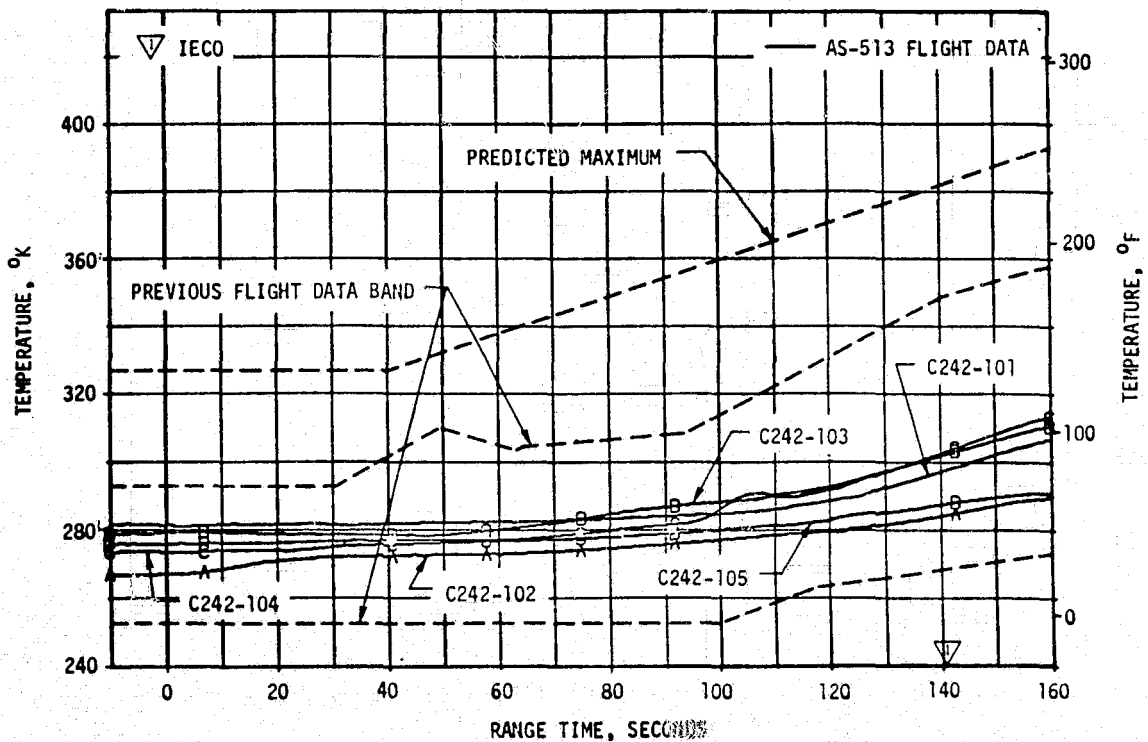


Figure 12-3. S-IC Thermal Environments Ambient Gas Temperature Under Engine Cocoon

12.3 S-II BASE HEATING

The SA-513 S-II base region thermal environment was expected to be the same as that experienced during the Apollo flights. The heat shield aft face total heating rate (C0722-206) measured during the S-II flight is presented in Figure 12-4 together with the post-flight analytical values, based on wind tunnel data and post-flight trajectory, and the data band of previous Apollo flights. It is seen that prior to CECO the flight heating rates fall slightly below the data band of the Apollo flights, and considerably below the post-flight analytical values. The heating rate increase at CECO during this flight was greater than that noted on previous flights. This could be due to the S-IC/S-II interstage remaining on throughout the S-II flight (see paragraph 9.5.2, Controls and Separation) which affects the center-engine-out reverse flow pattern and hence the heat shield heating rates.

The S-II heat shield aft side gas recovery temperature (C0731-206) flight history is presented in Figure 12-5 together with the post-flight analytical output. The previous Apollo flight data band is also shown for comparison. It is seen from the figure that the probe indicated temperatures are in agreement with the Apollo flight data prior to CECO. Because

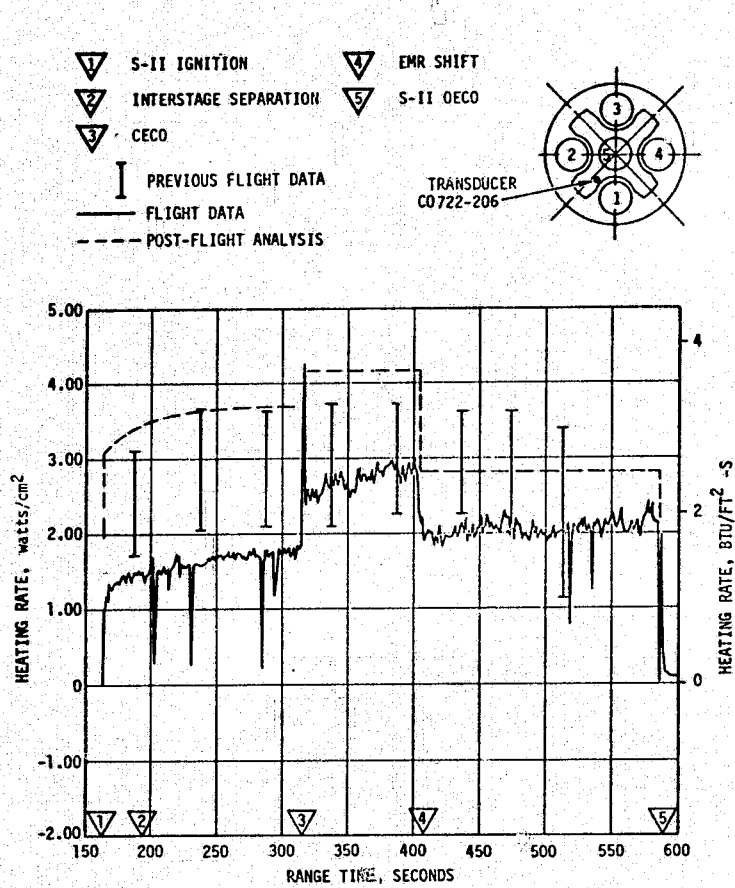


Figure 12-4. S-II Heat Shield Aft Heat Rate

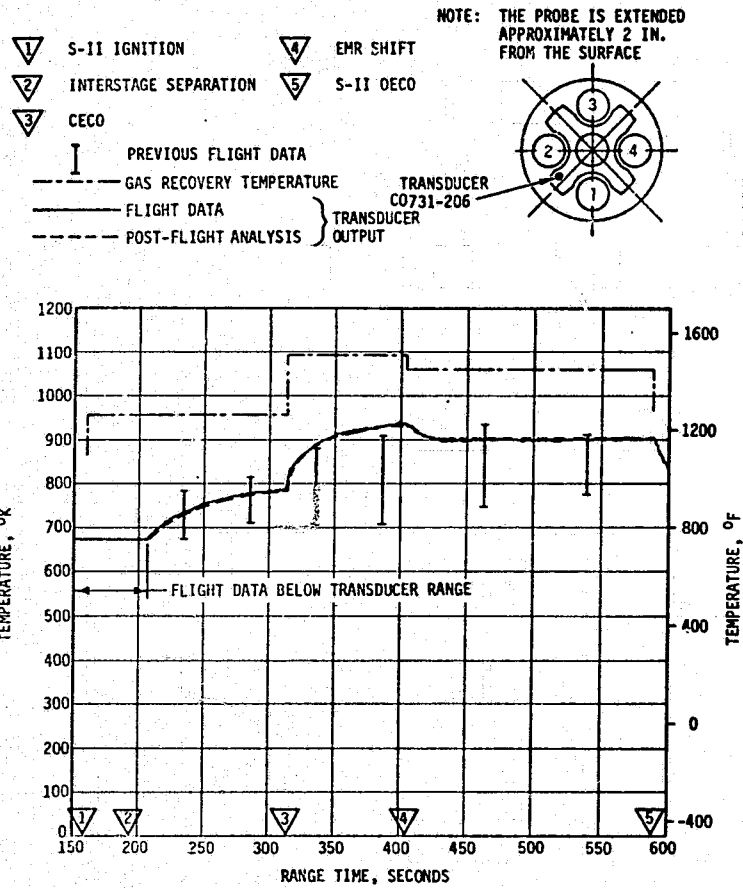


Figure 12-5. S-II Heat Shield Recovery Temperature

of the longer period between CECO and the Engine Mixture Ratio (EMR) shift on SA-513, the indicated temperatures during this period fall on the high side of the Apollo flight data band.

The heat shield aft side gas temperature was 1265°F, 1520°F, and 1460°F prior to CECO, after CECO and after EMR shift, respectively. These values are about 200°F higher than the corresponding average values experienced during the Apollo flights.

Figure 12-6 presents the SA-513 flight and post-flight analytical values of the radiometer (C0692-206) indicated radiative heat flux to the heat shield aft face. Also shown is the post-flight analytical values of the actual incident radiative heat flux at the same location. It is seen that the SA-513 flight radiometer output falls on the low side of the Apollo flight data band. The discrepancy between the radiometer indicated output and the incident radiative heat flux is due to the heating of the radiometer quartz window by convection and long wave plume radiation with the result that the radiometer sensor receives additional heat from the quartz window by radiation and convection across the air gap between the window and the sensor.

There were no structural temperature measurements on the base heat shield. In order to evaluate the structural temperatures experienced on the aft surface of the heat shield, a maximum post-flight predicted temperature was determined for the aft surface using maximum post-flight predicted base heating rates for the SA-513 flight. The predicted maximum post-flight temperature was 983°F which is comparable to the maximum post-flight temperatures predicted for Apollo flights, and was well below the maximum design temperature of 1460°F for no engine out and 1550°F for one control engine out. However, all three thrust cone forward surface temperature measurements were considerably higher than recorded on previous Apollo flights. The maximum temperature recorded by any of the three thrust cone forward surface temperature transducers was by measurement C0241-206 (see Figure 12-7) which exceeded the upper measurement limit of 150°F. Extrapolation of the recorded data indicates a maximum temperature of about 165°F at the time of S-II outboard engine cutoff. The maximum temperature recorded on Apollo flights was 30°F. The thrust cone forward surface temperature measurements were not located in the region of maximum base heating, and a post-flight analysis was conducted to predict the maximum SA-513 thrust cone temperatures with interstage-on. The maximum predicted temperatures for SA-513, shown in Figure 12-8, were calculated using post-flight predicted base heat rates, and are in the same range as the maximum allowable temperatures for a factor of safety of 1.0 indicating a marginal structural capability for the thrust cone.

S-II-13 measured heat shield curtain forward gas temperatures closely followed the upper range of previously recorded flight data up to S-II interstage separation time. Two of the five measurements are shown in Figures 12-9 and 12-10, indicating a continued rise until CECO rather than a sharp decrease after the scheduled interstage separation event. A

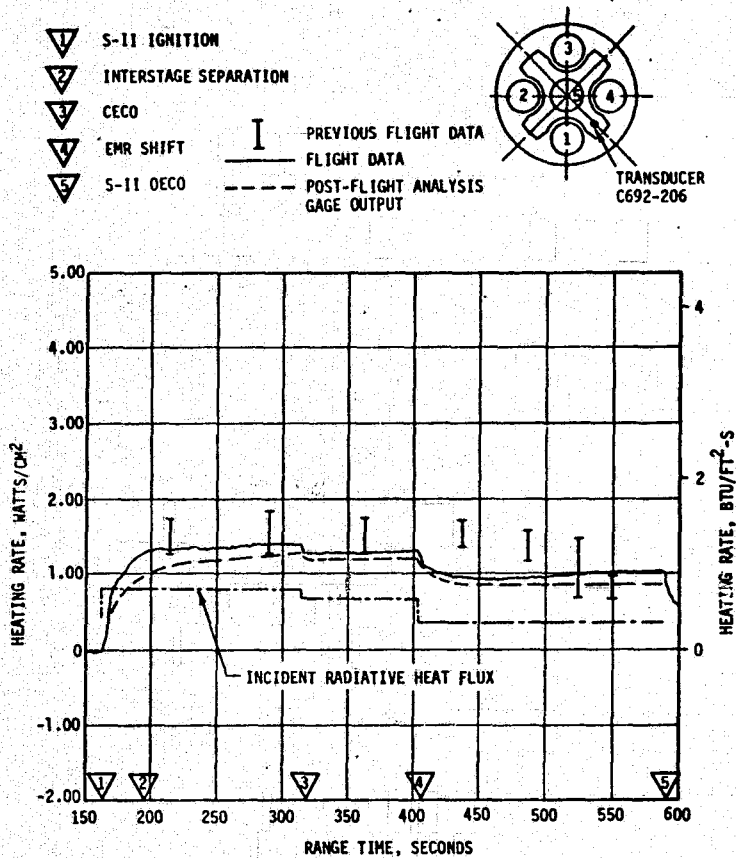


Figure 12-6. S-II Heat Shield Aft Radiation Heat Rate

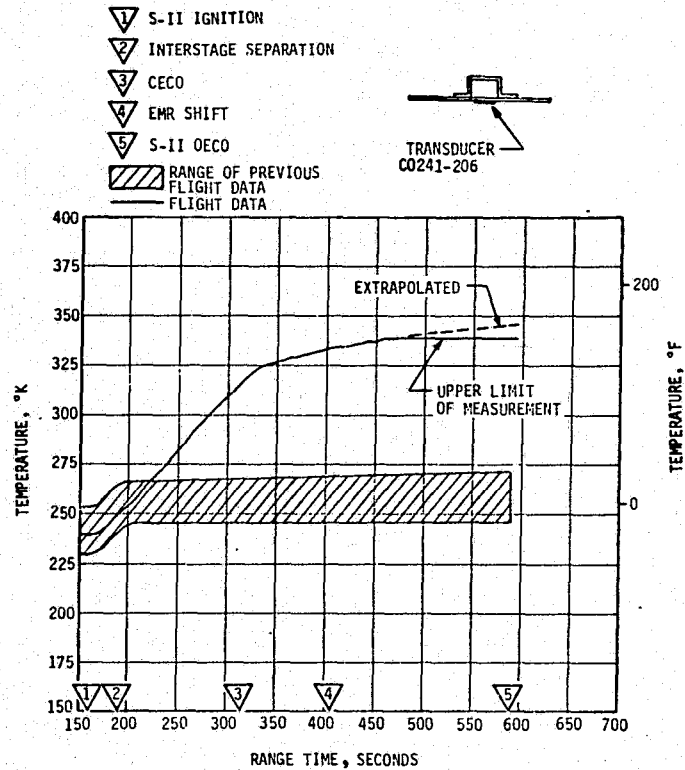


Figure 12-7. S-II Thrust Cone Forward Surface Temperature

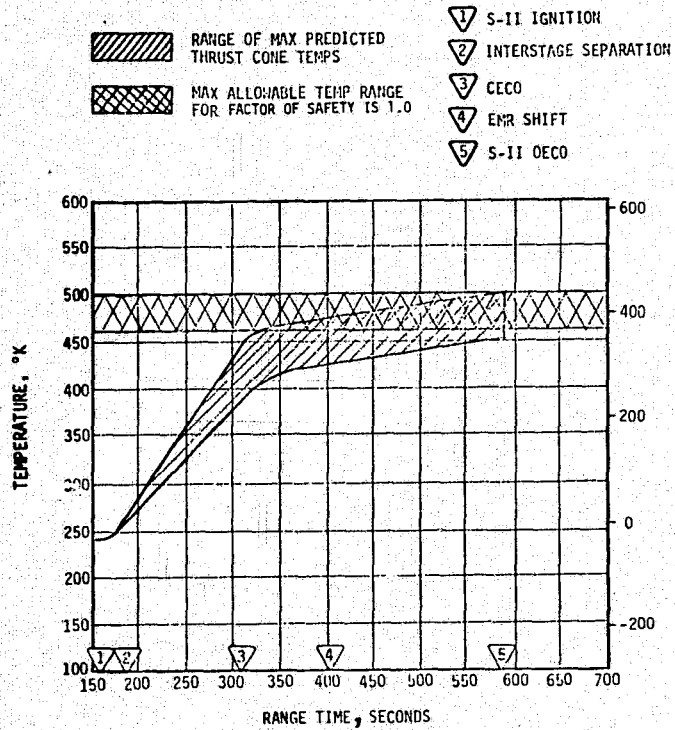


Figure 12-8. Estimate of Maximum Predicted S-II Thrust Cone Temperatures

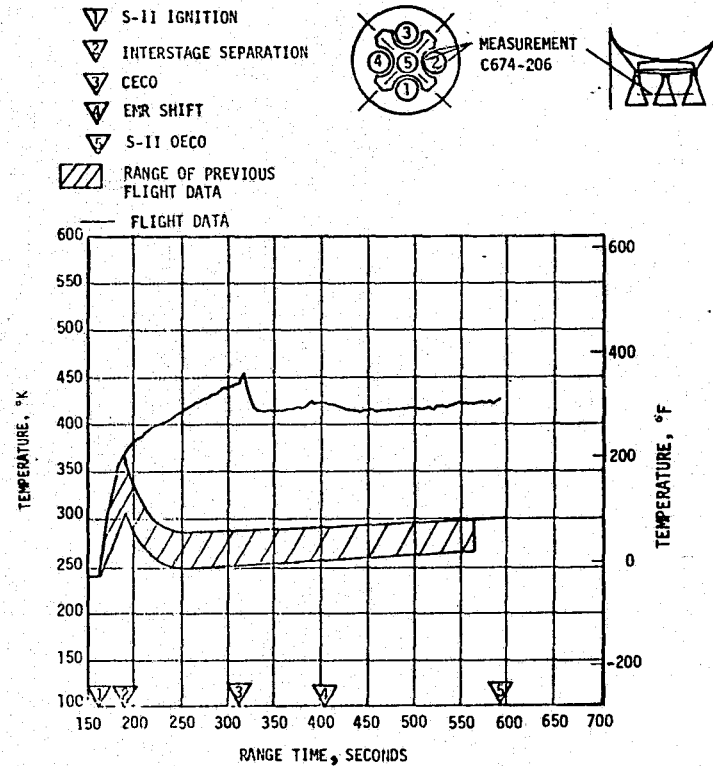


Figure 12-9. S-II Engine Compartment Gas Temperature (C674-206)

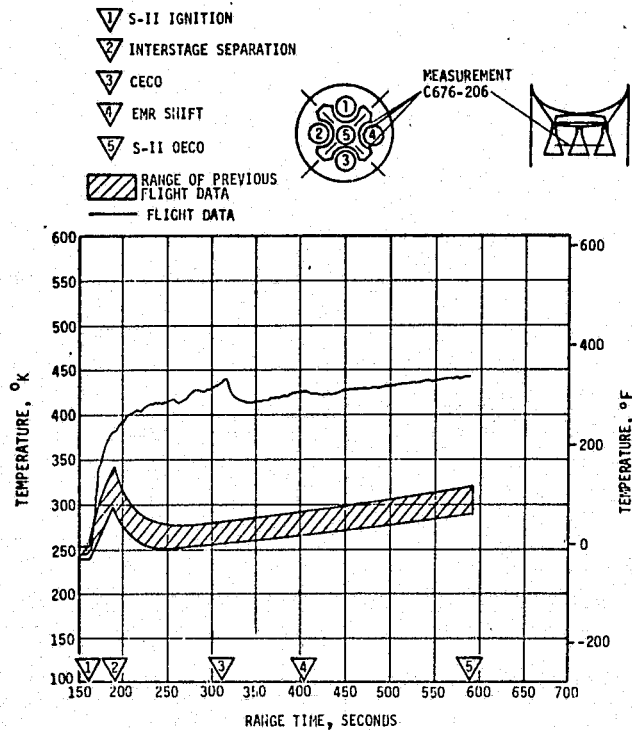


Figure 12-10. S-II Engine Compartment Gas Temperature (C676-206)

typical engine actuation system reservoir oil temperature is shown in Figure 12-11, also showing a more rapid increase than on previous flights. This base environment is attributed to the failure of the S-II interstage to separate (see paragraph 9.5.2).

The greater than expected temperatures measured in the engine compartment following the time of S-II second plane separation are indications that the S-IC/S-II interstage failed to separate. This along with other supporting data is presented in paragraph 9.5.2 with the conclusion that S-IC/S-II interstage separation did not occur.

12.4 VEHICLE AEROHEATING THERMAL ENVIRONMENT

Aerodynamic heating environments were not measured on the SA-513 S-IC stage. The trajectory for SL-1 was slightly different than that for the Apollo flights which causes the aerodynamic heating environments to be less severe. Ground optical data were not available to measure plume induced flow separation (PIFS) because of cloud interference. An estimate of the forward point of flow separation based on Apollo flight data adjusted to the SA-513 flight trajectory is shown in Figure 12-12. This estimate shows the flow separation point to be farther up the vehicle at equivalent Apollo flight times because of the different trajectory. The step function change in the forward point of flow separation at CECO occurs later in flight for SA-513

- ▽ S-II IGNITION
- ▽ 2 INTERSTAGE SEPARATION
- ▽ 3 CECO
- ▽ 4 EMR STEP
- ▽ 5 OECO

▨ RANGE OF PREVIOUS FLIGHT DATA
 — FLIGHT DATA

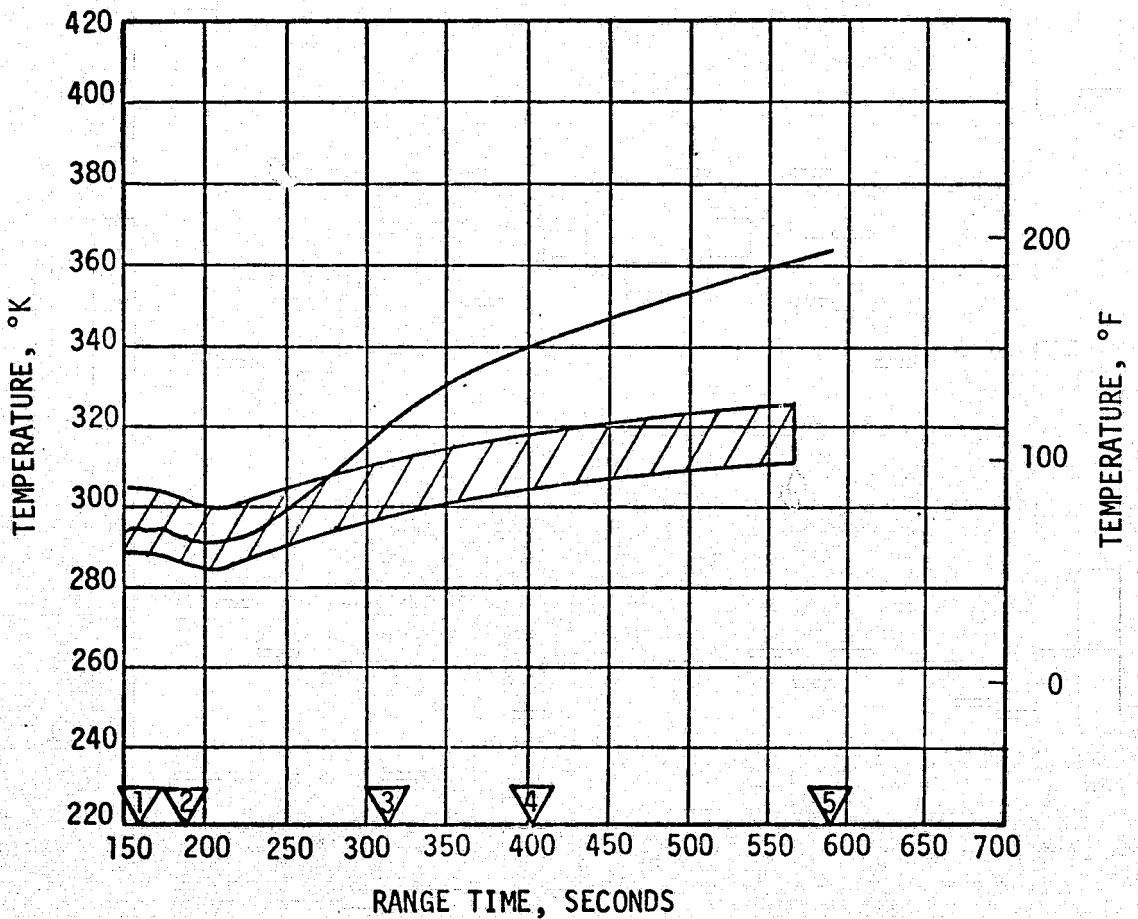


Figure 12-11. S-II Engine Actuation System Reservoir Oil Temperature (Engine 4 Typical)

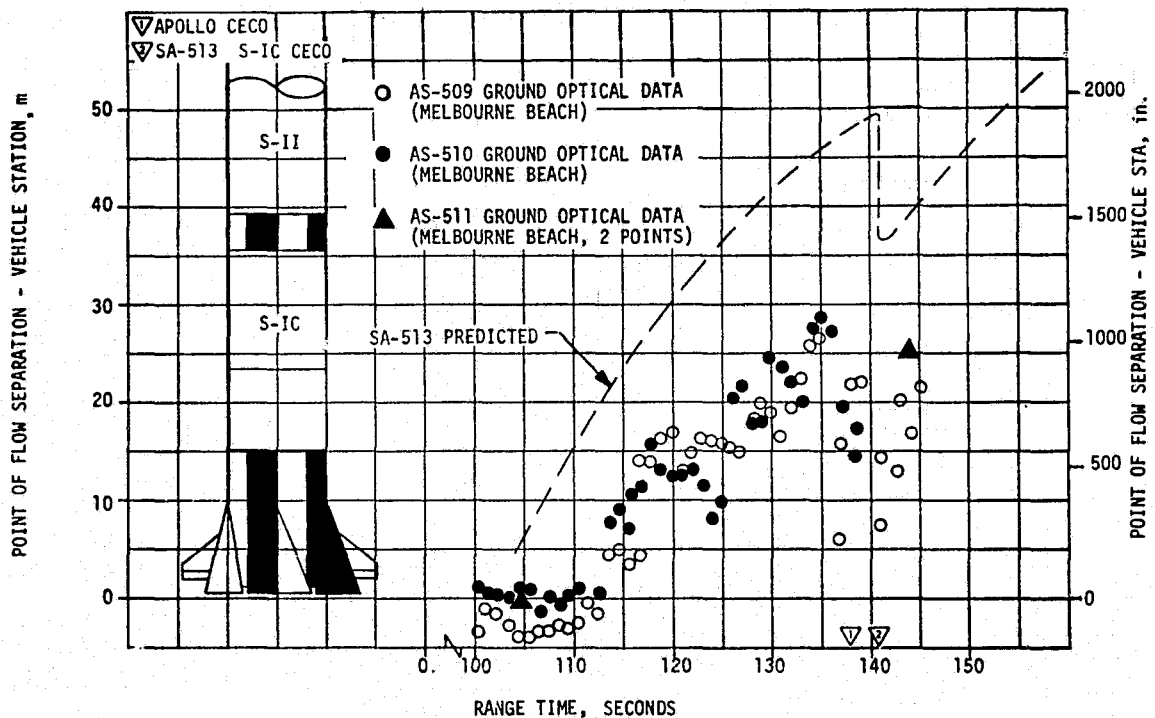


Figure 12-12. SA-513 Predicted Location of Separated Flow

than on Apollo flights, as shown in Figure 12-12. It is to be expected that PIFS heating would be slightly more severe than that experienced on Apollo because the exposure to this environment was about six seconds longer.

12.5 S-IC/S-II SEPARATION THERMAL ENVIRONMENT

Post-flight reconstruction of the S-IC/S-II separation (see paragraph 9.5.1) indicates a slower separation than the nominal prediction but within the 3-sigma band. The pressure and heating environments of the S-IC LOX tank dome should, therefore, be slightly higher than the pre-flight nominal predictions but less than the 3-sigma values and within the design limits. Since there are no environmental measurements in this area on the flight vehicle, no further analysis of the staging environment is planned for this flight.

The S-II base region heating rate transducer (C0722-206, see Figure 12-4) exhibits normal response during the engine start transient, indicating that the base region thermal environment is less severe during S-IC/S-II separation than that corresponding to nominal flight conditions.

SECTION 13

ENVIRONMENTAL CONTROL SYSTEMS

13.1 SUMMARY

The S-IC stage forward compartment and aft compartment thermal environments were adequately maintained throughout the launch countdown and S-IC boost phase.

The S-II stage engine compartment conditioning system maintained the ambient temperature and thrust cone surface temperatures within design ranges throughout the launch countdown. The system also maintained an inert atmosphere within the compartment.

The IU stage Environmental Control System (ECS) exhibited satisfactory performance for the duration of the IU mission. Coolant temperatures, pressures, and flowrates were continuously maintained within the required ranges and design limits.

13.2 S-IC ENVIRONMENTAL CONTROL SYSTEM

The S-IC ECS performance was satisfactory and maintained temperatures within the required limits during launch countdown and S-IC boost.

The most severe prelaunch forward compartment thermal environment typically occurs during J-2 engine chilldown. The lowest ambient temperature measured during SA-513 J-2 engine chilldown was -83.2°F . The lowest temperature measured during the flight was -130°F at instrument location C206-120.

The aft compartment environmental conditioning system performed satisfactorily during countdown. After the initiation of LOX loading, the temperature (12K10) in the vicinity of the batteries decreased to 65°F which is within the battery qualification limits of 35 to 95°F . The temperature increased to 76°F at liftoff. Just prior to liftoff, the other ambient temperatures in the aft compartment ranged from 69.8°F at measurement C203-115 to 82.4°F at measurement C205-115. During flight, the lowest temperature recorded was 52.7°F and was at measurement C203-115.

13.3 S-II ENVIRONMENTAL CONTROL

The engine compartment conditioning system maintained the ambient temperature and thrust cone surface temperatures within design ranges throughout the launch countdown. The system also maintained an inert atmosphere within the compartment as evidenced by the absence of H₂ or O₂ indications on the hazardous gas monitor.

The ambient temperature measurements external to the equipment containers indicated that temperatures within the containers were satisfactory and since there were no problems with the equipment in the containers, it is assumed that the thermal control system performed adequately.

13.4 IU ENVIRONMENTAL CONTROL

The IU Environmental Control System (ECS) performance was satisfactory and maintained temperatures, pressures and flowrates within the required limits for the duration of the IU mission.

13.4.1 Thermal Conditioning System (TCS)

Performance of the TCS was satisfactory throughout the mission, including modifications made because of the absence of an S-IVB Stage on this flight (Ref. Appendix B). The temperature of the liquid coolant supplied to the coldplates and internally cooled components was continuously maintained within specification limits of 45° to 68°F for the required IU lifetime.

Sublimator performance parameters for the initial cycle are presented in Figure 13-1. The water supply valve opened as programmed, approximately 350 seconds after lift-off. The initial opening was delayed from the 180-second time, used on all previous vehicles to allow the pressure within the IU compartment to decay to the level necessary for proper sublimator start-up. This level occurs later because of the additional volume of gas in the compartments joined to the IU in the Skylab configuration which must exhaust through the same vent area. Significant cooling from the sublimator was not evident until about 675 seconds after lift-off, at which time the coolant supply temperature began to decrease rapidly. At the first thermal switch sampling (650 seconds) the coolant temperature was still above the actuation point, hence the water supply valve remained open. The second switch sampling occurred at approximately 950 seconds and the water valve was closed by switch selector command as programmed.

Effective with IU-513 and IU-514, the Ground Support Cooling Unit (GSCU) is shut down 47 seconds prior to launch by the Terminal Count Sequencer. This was reflected, as shown in Figure 13-1, by an initially rapid increase in coolant supply temperature (C15-601) from the stabilized pre-shutoff value, followed by a more gradual increase through liftoff and the first 60 seconds of flight. This event is similar to that initiated at umbilical separation (lift-off) on all previous flights and does not, in itself, result in a significant change in overall system temperature levels. The

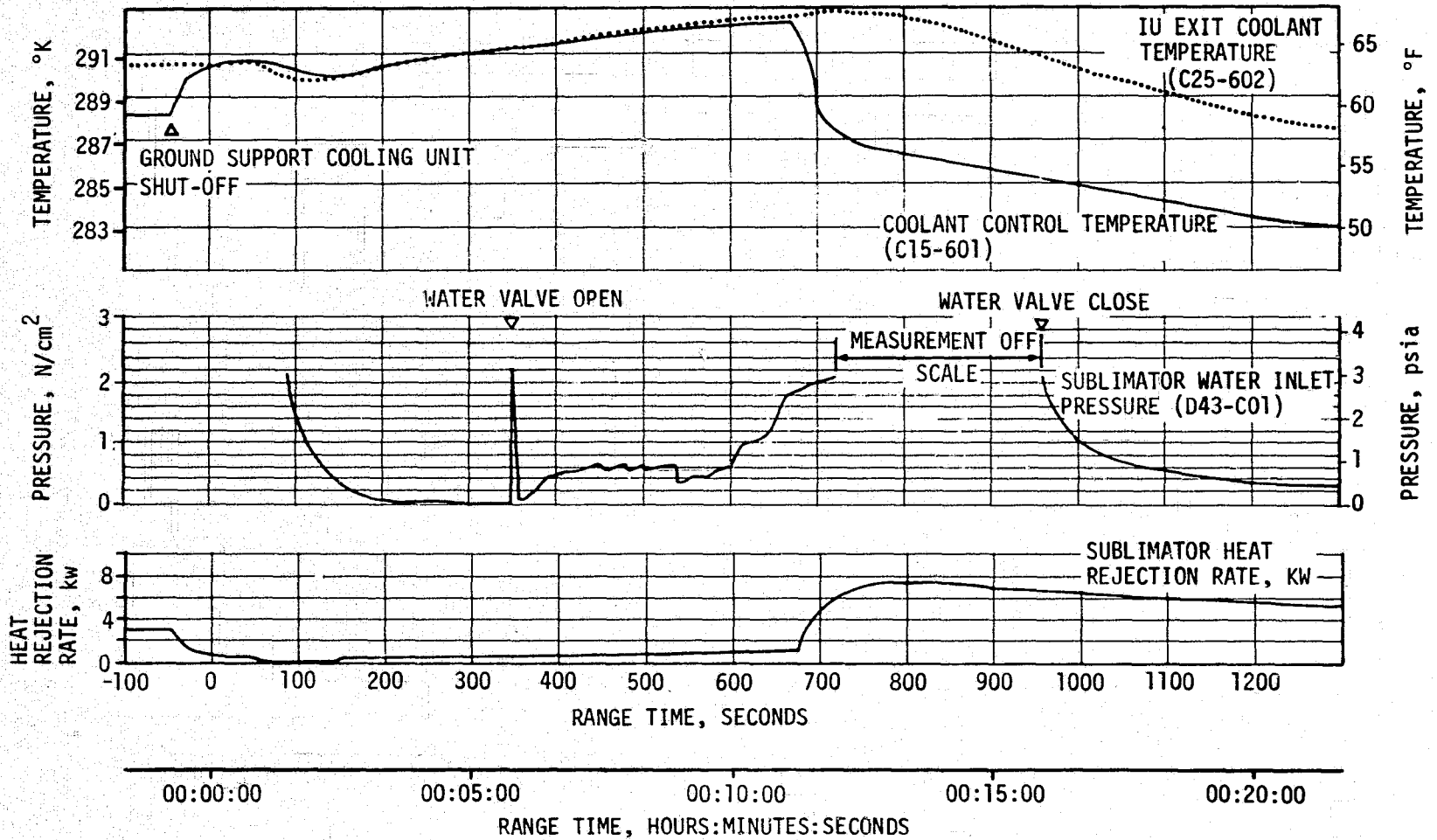


Figure 13-1. IU Sublimator Start-Up Parameters (Initial Cycle)

combination of early GSCU shut-off and delayed water valve opening more than doubled the interim period of no active cooling on SL-1, but system temperature response was moderate and within the conservative predictions.

Figure 13-2 shows temperature control parameters over the total time span for which data has been received. Sublimator cooling was nominal and the coolant control temperature (C15-601) was maintained within the allowable range of 45 to 68°F through 36,000 seconds. At approximately 35,640 seconds the LVDC logic controlling water supply valve operation was inhibited by DCS command with the valve in the open position. This resulted in the valve remaining open and continuous operation of the sublimator. This event was undertaken based on a real-time decision to attempt to extend the IU operating lifetime. In the nominal case, a major restriction in operational lifetime of the IU is over-heating of the electronic components. This occurs when coolant circulation ceases due to 6D40 battery depletion. By forcing the sublimator to operate continuously prior to this time a "subcooling" effect is achieved, and thus when circulation does cease, the time to reach an over-heated condition is extended.

The average system heat load on IU-513 was significantly higher than on previous missions. This was due primarily to the solar inertial attitude and resulted in more frequent sublimator cycling and increased water consumption. A lack of sufficient data prevents an exact determination, but it is estimated that the average net system heat load in orbit was approximately 2.4 kilowatts. The total mass of water consumed through the operating lifetime of the TCS is similarly estimated to be 120 pounds. Water accumulator capacity at lift-off is about 145 pounds, leaving an estimated residual of 25 pounds.

Hydraulic performance of the TCS is indicated by the parameters shown in Figure 13-3. Operation was nominal with system flowrate and pressure relatively constant through 42,000 seconds. At this time, output from the battery powering the pump began to decay through normal depletion, causing a corresponding decrease in pump outlet pressure and flowrate. Fluid circulation ceased altogether at approximately 48,600 seconds when the pump outlet pressure becomes equal to that at the pump inlet.

The TCS GN₂ supply sphere pressure decay, which is indicative of GN₂ usage rate, was normal and is presented in Figure 13-4.

TCS pressurization as indicated by the coolant pump inlet pressure, D24-601, was maintained at the required level of 16 \pm 0.5 psia through 67,000 seconds, at which time the inlet pressure to the First Stage regulator had decayed to less than 200 psia.

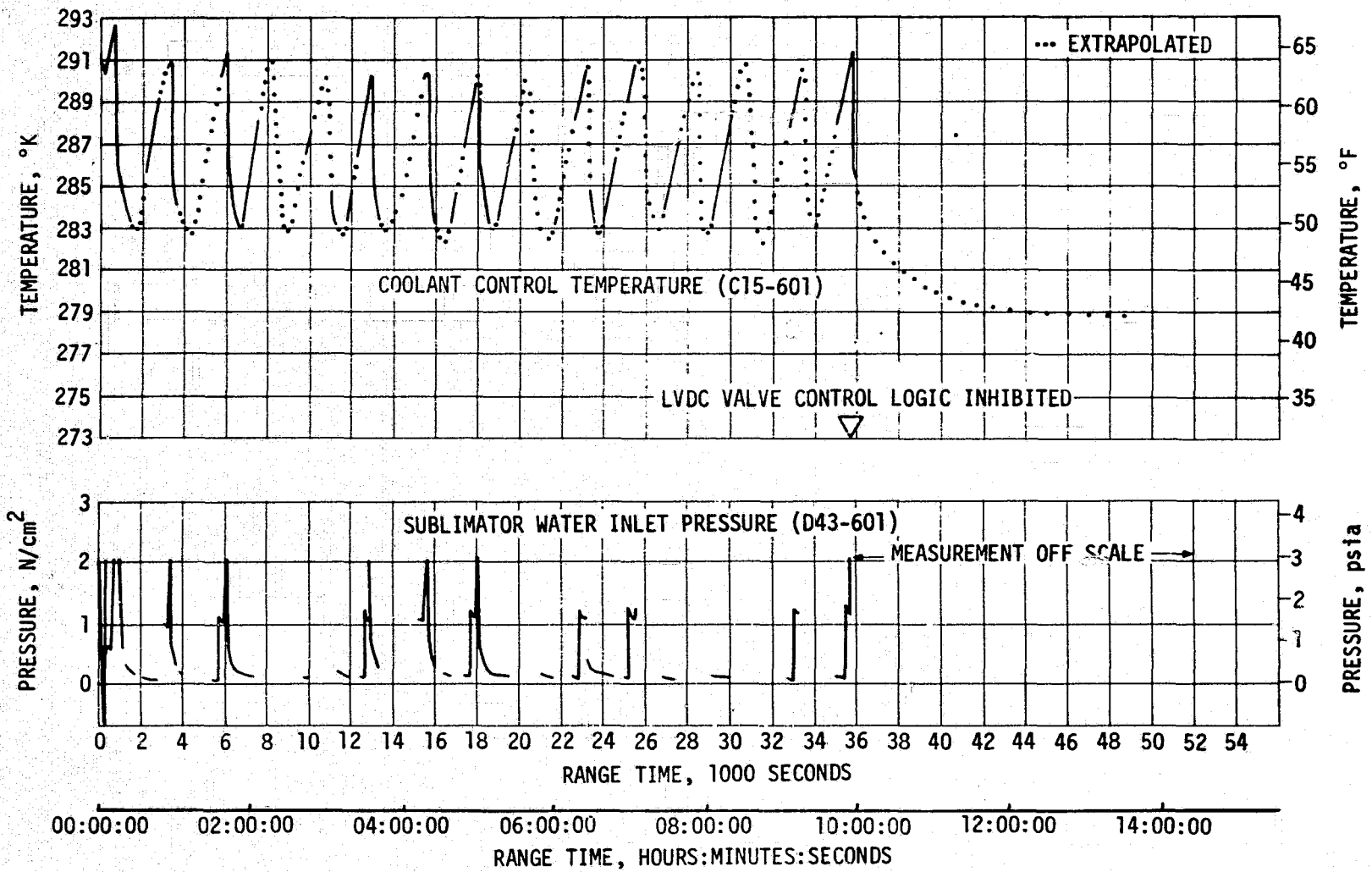


Figure 13-2. IU TCS Coolant Control Parameters

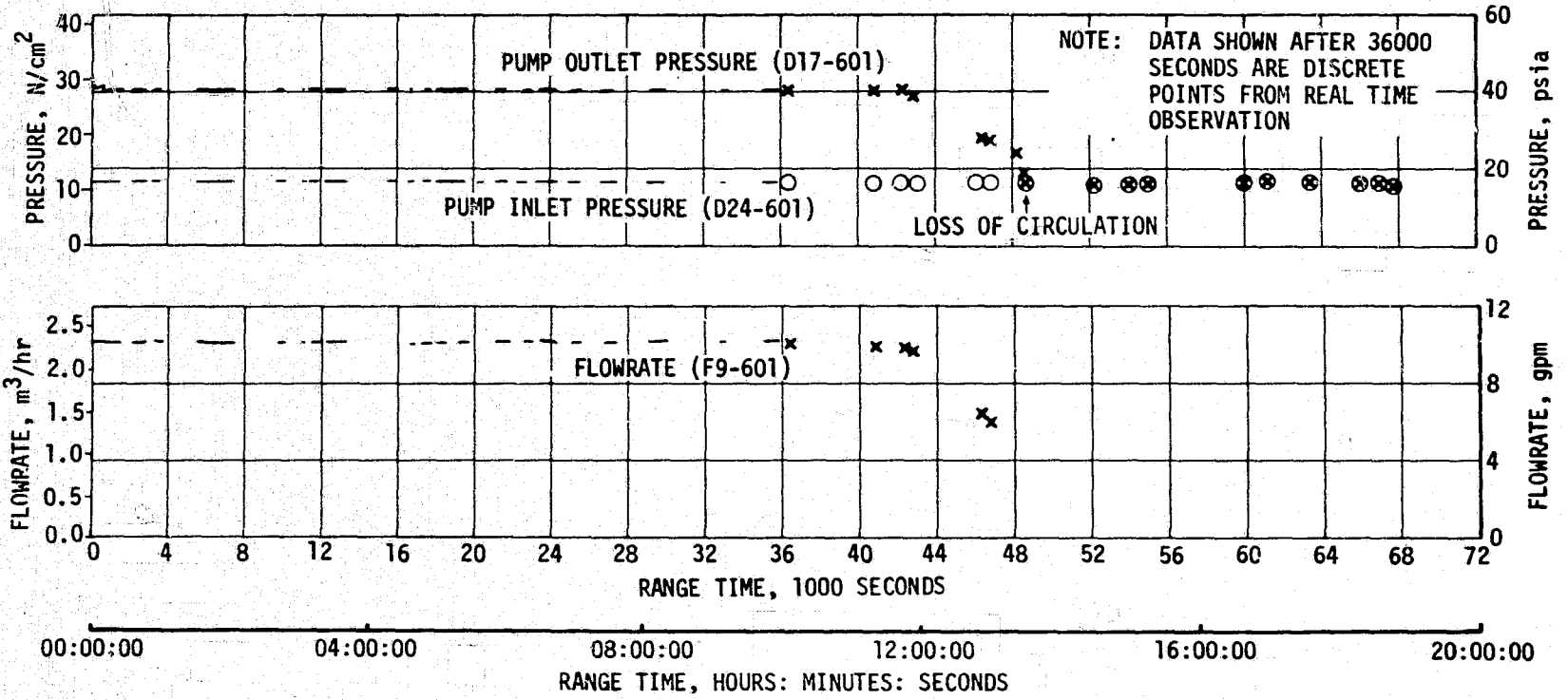


Figure 13-3. IU TCS Hydraulic Performance

13-7

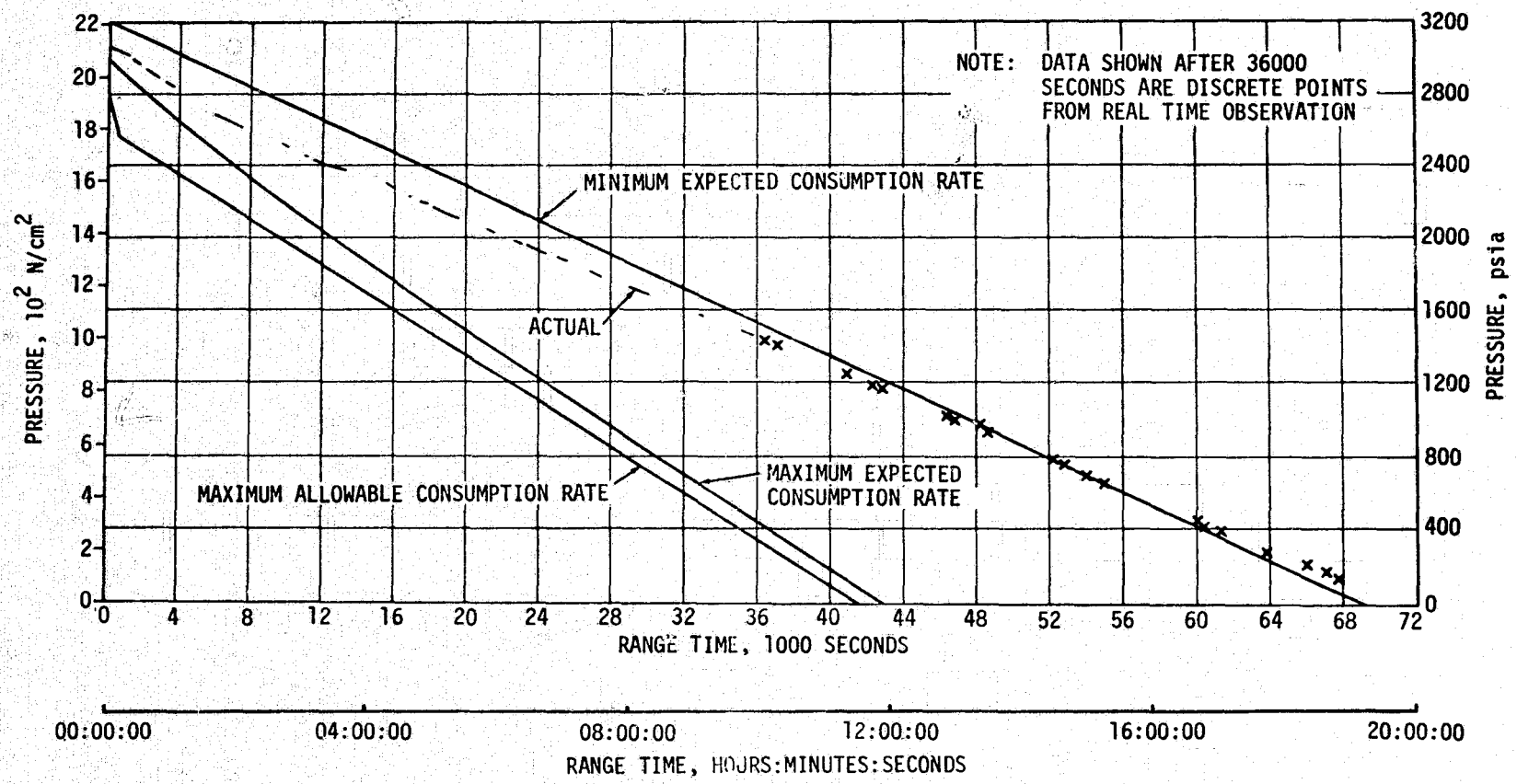


Figure 13-4. IU TCS GN₂ Sphere Pressure (D25-603)

13.4.2 Gas Bearing System Performance

Gas Bearing System (GBS) operation was nominal throughout the IU-513 mission. Figure 13-5 shows platform pressure differential (D11-603) and internal ambient pressure (D12-603). The differential pressure remained constant and within specification limits through 56,000 seconds. In the 56,000 to 60,000 second time frame both differential and ambient (reference) pressures began to decay as expected as a result of GN₂ depletion. At this time the supply pressure to the gas bearing regulator dropped below the minimum level for proper operation of the regulator (300 psia). The GBS GN₂ supply sphere pressure decay is depicted in Figure 13-6. GN₂ consumption was as expected.

13.4.3 Component Temperatures

All component temperatures remained within expected ranges throughout the primary mission (Figures 13-7 and 13-8) and until loss of coolant circulation. As stated previously, continuous sublimator operation was initiated at about 35,640 seconds to "subcool" the electronics and thus extend the operational lifetime. This operation was successful in lowering component temperatures as shown in Figures 13-7 and 13.8. The lower temperatures were maintained until loss of circulation, whereupon the components generally began an immediate and continued temperature increase until eventual loss of system power. The component temperature profiles during this period of no active cooling are virtually the same as was observed previously on S-IU-508 under the same general circumstances.

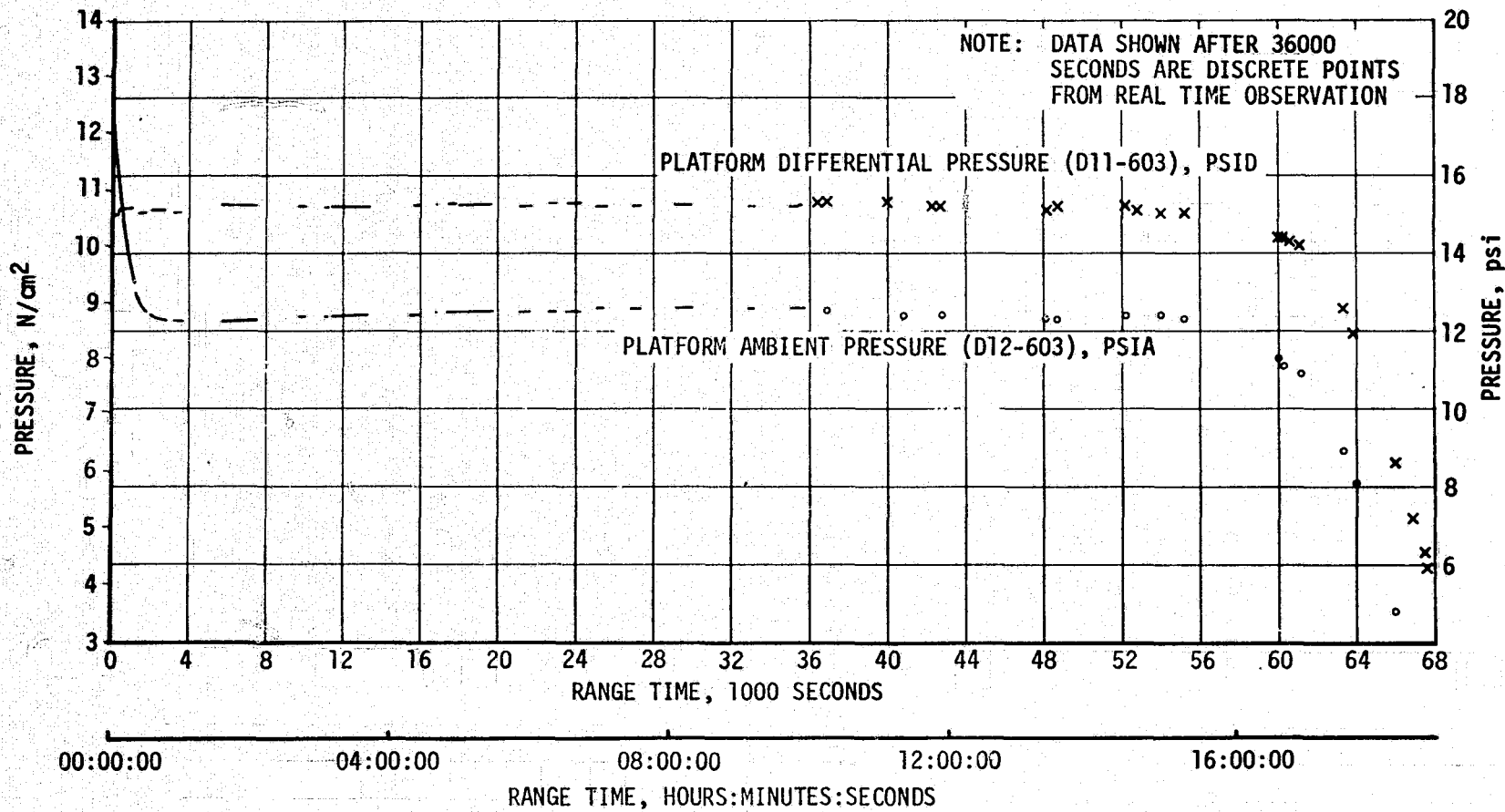


Figure 13-5. IU Inertial Platform GN₂ Pressures

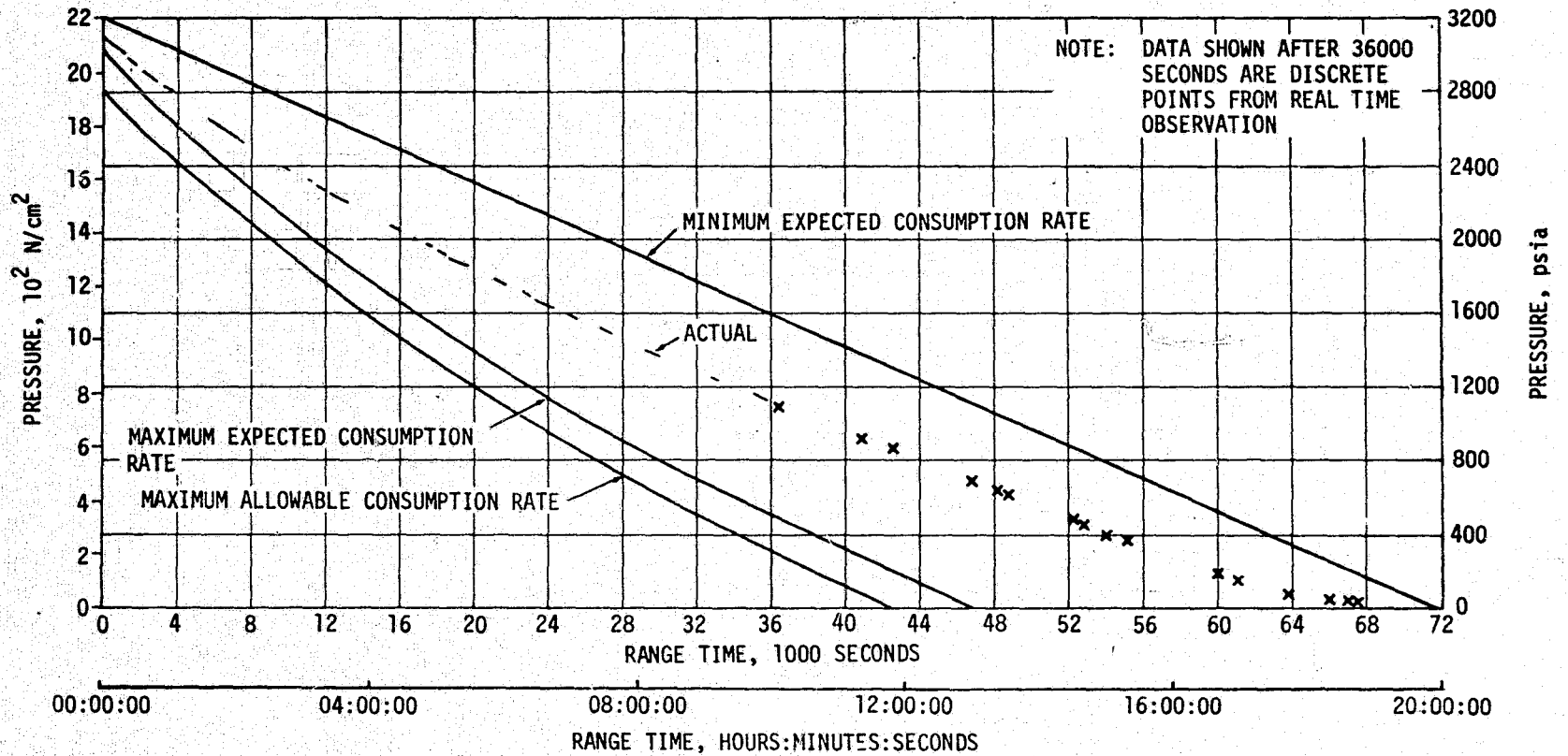


Figure 13-6. IU GBS GN_2 Sphere Pressure (D10-603)

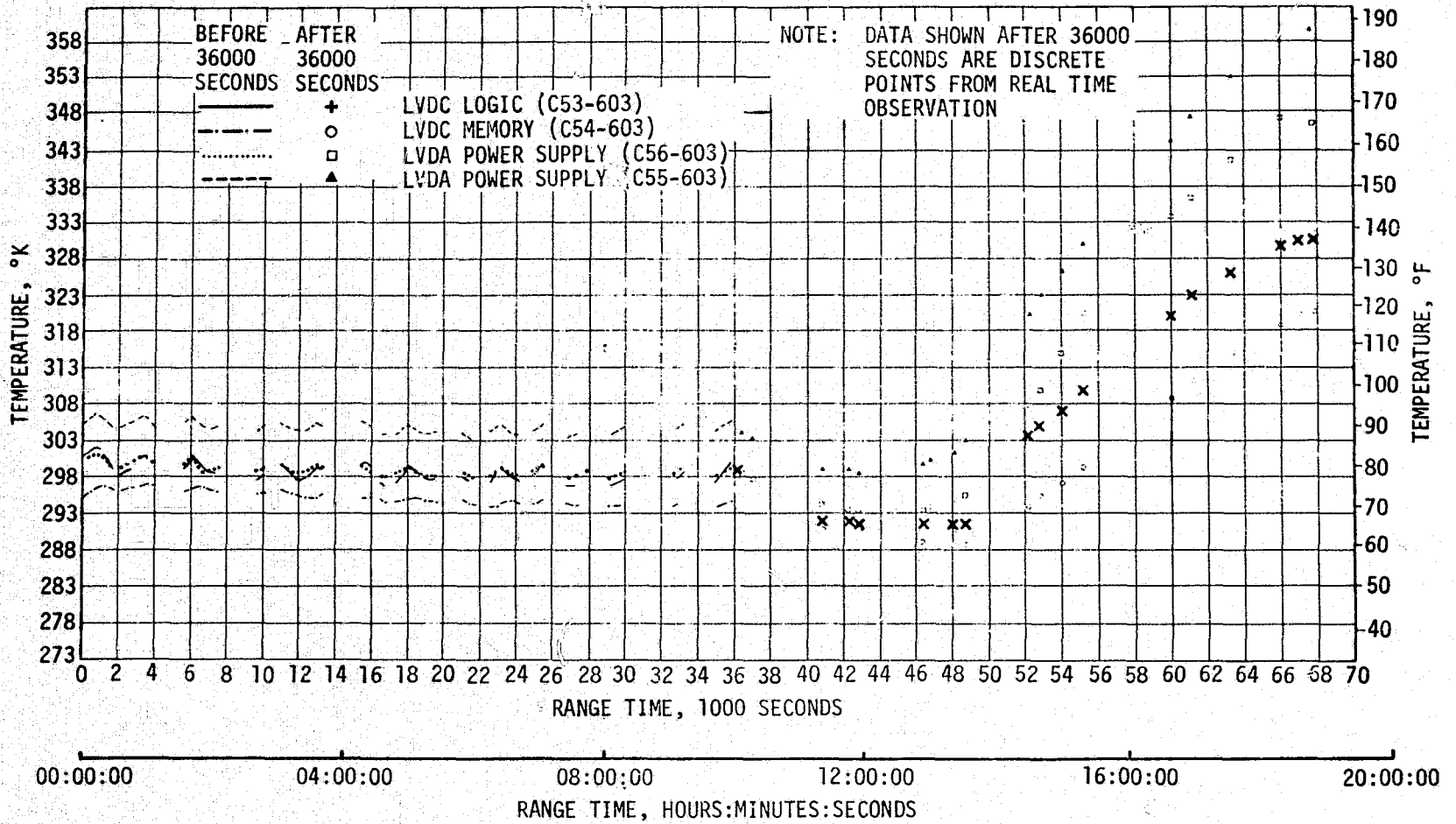


Figure 13-7. IU Selected Component Temperatures

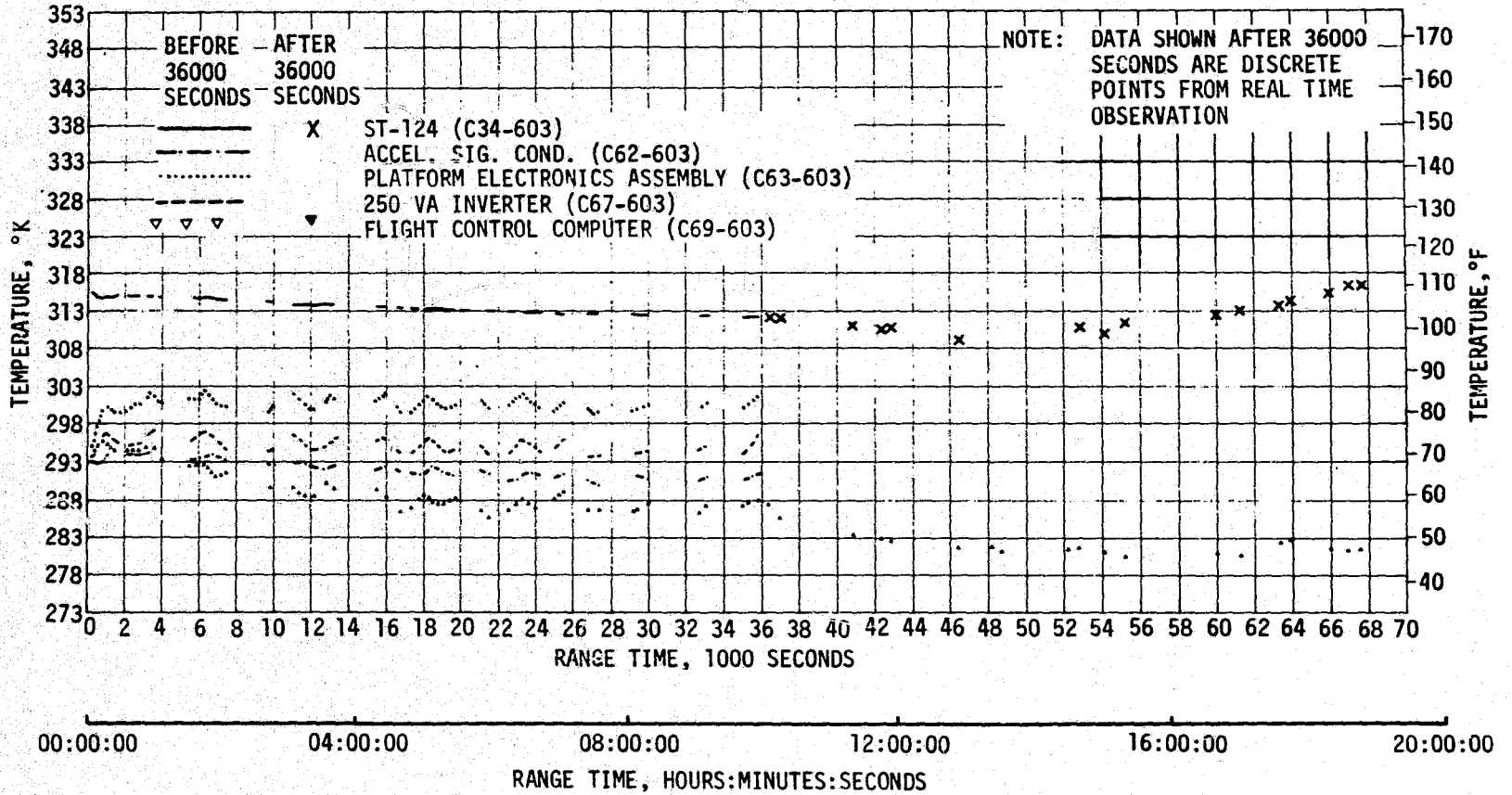


Figure 13-8. IU Selected Component Temperatures

SECTION 14

DATA SYSTEMS

14.1 SUMMARY

All data systems performed satisfactorily throughout the flight. Flight measurements from onboard telemetry were 99.7 percent reliable.

Telemetry performance was satisfactory and no hardware anomalies were observed during any phase of the Skylab (SL)-1. Radio Frequency (RF) propagation was satisfactory, though the unusual interference due to flame effects and staging was experienced. Usable Very High Frequency (VHF) data were received until 67,620 seconds (18:47:00). Signal strength variations coincident with the 63-second anomaly were observed. The Secure Range Safety Command Systems (SRSCS) on the S-IC and S-II stages were ready to perform their functions properly, on command, if flight conditions during launch phase had required destruct. The system properly safed the S-II destruct system on a command transmitted shortly after completion of powered flight (589 seconds). The performance of the Command and Communications System (CCS) was satisfactory from liftoff through 151,200 seconds (42:40:45). Good tracking data were received from the C-Band radar, with Hawaii (HAW) indicated last record of interrogation at 16,915 seconds (4:41:55). In general, ground engineering camera coverage was good; however, there was no coverage of the 63 second anomaly because of cloud coverage.

14.2 VEHICLE MEASUREMENT EVALUATION

The SA-513 launch vehicle had 1093 measurements scheduled for flight; one measurement was waived prior to start of the automatic countdown sequence leaving 1092 measurements active for flight. Three measurements failed during flight, resulting in an overall measurement system reliability of 99.7 percent.

A summary of measurement reliability is presented in Table 14-1 for the total vehicle and for each stage. The waived measurements, failed measurements, partially failed measurements, and questionable measurements are listed by stage in Tables 14-2, 14-3 and 14-4. None of these listed failures had any significant impact on postflight evaluation.

14.3 AIRBORNE VHF TELEMETRY SYSTEMS EVALUATION

Performance of the seven VHF telemetry links provided good data from liftoff until battery depletion. Data degradation and dropouts were

Table 14-1. SA-513 Measurement Summary

MEASUREMENT CATEGORY	S-IC STAGE	S-II STAGE	INSTRUMENT UNIT	TOTAL VEHICLE
Scheduled	294	571	228	1093
Waived	0	1	0	1
Failed	1	1	1	3
Partial Failed	0	2	0	2
Questionable	0	1	0	1
Reliability, Percent	99.7	99.8	99.6	99.7

experienced at various times during launch and earth orbit as on previous flights, due to the attenuation of RF signals. Signal attenuation was caused by S-IC stage flame effects, S-IC Center Engine Cutoff (CECO) and retro-motor effects at S-IC/S-II separation. The main engine flame effect was very prominent from 100 to 126 seconds and was observed earlier than on previous Saturn V launches. Flame attenuation, combined with the relatively bad look angles at Merritt Island Launch Area (MILA), caused an unexpected, long data dropout from 111.7 to 117.5 seconds. Flame attenuation effects were much less severe at Central Instrumentation Facility (CIF). The effects at S-IC/S-II separation and S-II engine start resulted in approximately 1.2 seconds of data dropout. Flame impingement on the jettisoned S-II aft interstage has produced signal dropout in all previous Saturn V launches. This expected signal deviation did not occur because the S-II aft interstage did not separate (reference Paragraph 9.5.2).

The performance of the S-II VHF telemetry systems was normal through second revolution. The performance of IU VHF telemetry systems was normal during the entire earth orbit operation. A summary of available VHF telemetry coverage showing Acquisition of Signal (AOS) and Loss of Signal (LOS) for each station is shown in Figure 14-1 and Figure 14-2. The last VHF telemetry data was received at approximately 67,620 seconds (18:47:00) at Madrid (MAD).

14.4 C-BAND RADAR SYSTEM EVALUATION

The C-Band radar subsystem operated satisfactorily during this mission with the only problems experienced occurring in the ground stations. A summary of the C-Band radar coverage showing AOS and LOS for each station is shown in Figure 14-3.

Table 14-2. SA-513 Flight Measurements Waived Prior to Flight

MEASUREMENT NUMBER	MEASUREMENT TITLE	NATURE OF FAILURE	REMARKS
S-II STAGE			
D012-201	E1 Helium Regulator Outlet Pressure	Measurement read ambient pressure in the low RACS mode rather than ambient plus 1 VDC.	Waiver NR 13-1

Table 14-3. SA-513 Measurement Malfunctions

MEASUREMENT NUMBER	MEASUREMENT TITLE	NATURE OF FAILURE	TIME OF FAILURE (RANGE TIME)	DURATION SATISFACTORY OPERATION	REMARKS
MEASUREMENT FAILURES, S-IC STAGE					
C003-102	Temperature, Turbine Manifold, Engine 2	Measurement pegged off scale high	Liftoff	0 Seconds	Probable transducer failure
MEASUREMENT FAILURES, S-II STAGE					
E339-206	Normal Vibration Thrust Cone	No response	Liftoff	0 Seconds	Probable open coaxial cable
MEASUREMENT FAILURES, INSTRUMENT UNIT					
B1-601	Acoustic, Flush MTG	No output except noise during periods of vibration	Prior to liftoff	0 Seconds	Probable open circuit in cable or connector
PARTIAL MEASUREMENT FAILURES, S-II STAGE					
C004-202	E2 LOX Turbine Inlet Temperature	Measurement pegged off scale high	264 seconds	Prior to 264 seconds	Probable transducer failure
G007-203	E3 Hydraulic Reservoir Piston Position	Measurement pegged off scale low	484 seconds	Prior to 484 seconds	Probable transducer failure

Table 14-4. SA-513 Questionable Flight Measurements

MEASUREMENT NUMBER	MEASUREMENT TITLE	REASON QUESTIONED	REMARKS
S-II STAGE			
C001-204	E4 Fuel Pump Discharge Temperature	Changed by 1/2°F over an 8 second period after 285 seconds. Did not reflect engine performance.	2% of full scale

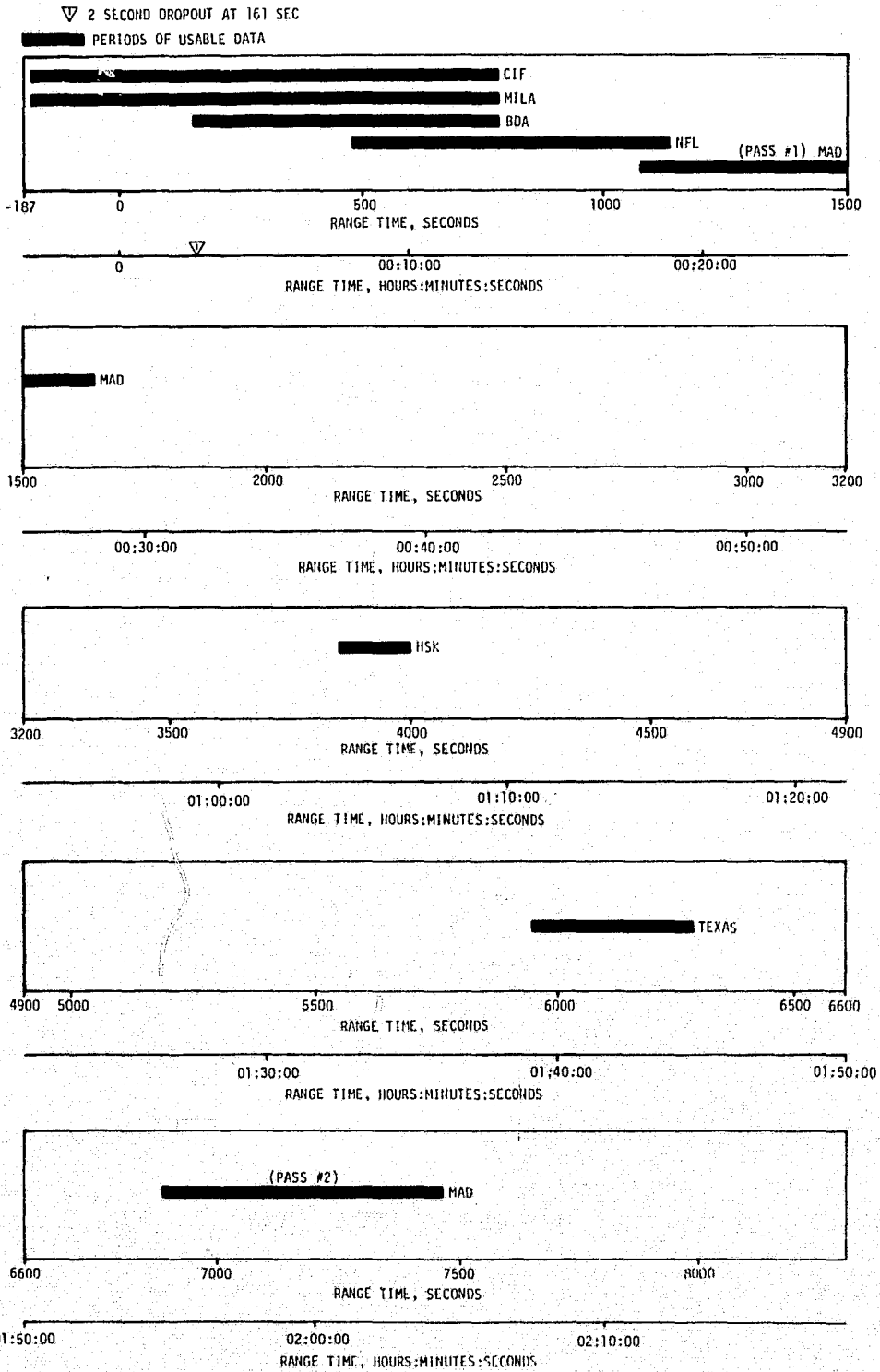


Figure 14-1. S-II Stage VHF Telemetry Ground Station Coverage Time

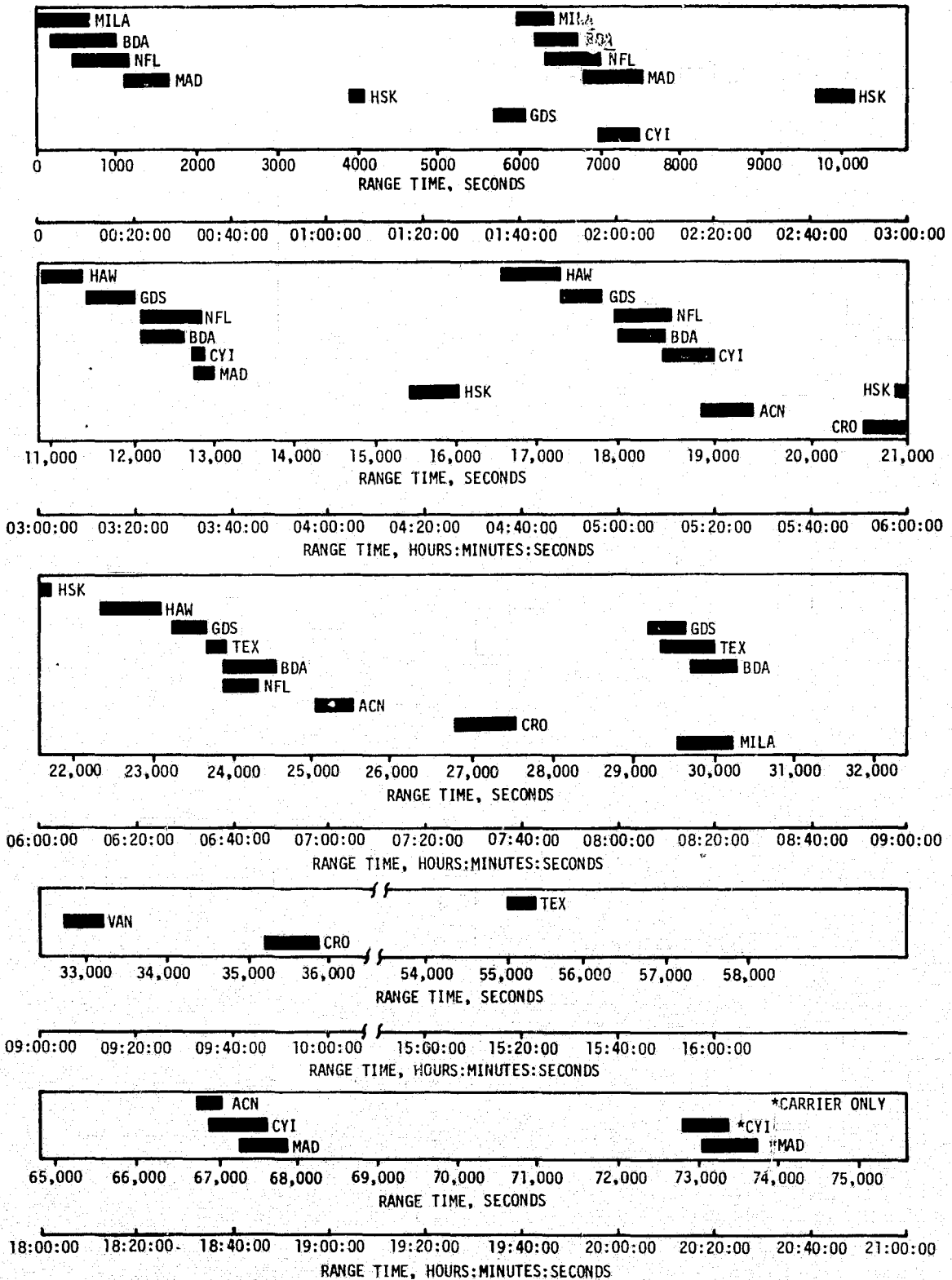


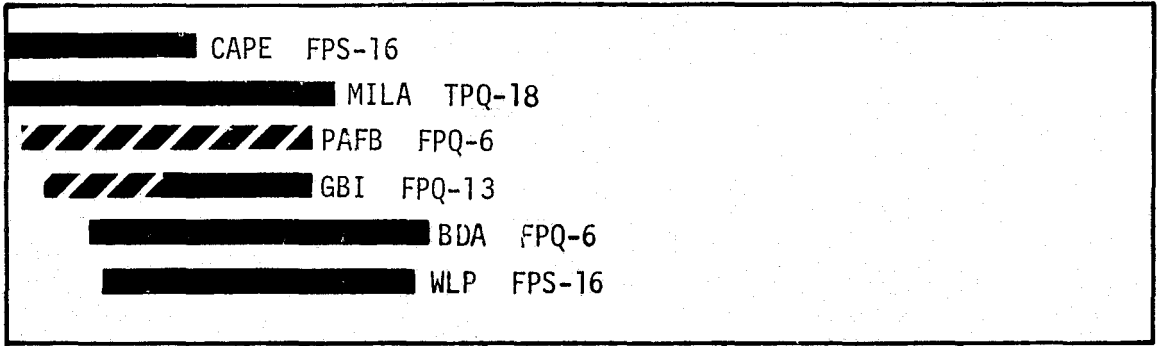


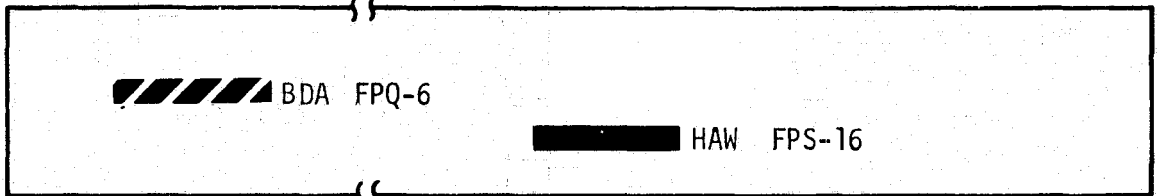
Figure 14-2. Instrument Unit VHF Telemetry Ground Station Coverage Time

 BEACON TRACK
 SKIN TRACK



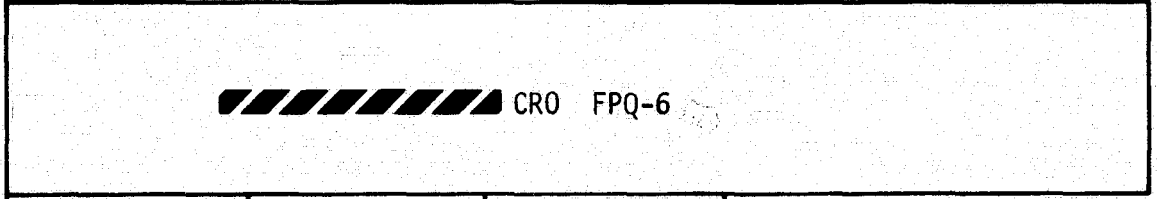
0 500 1000 1500 2000
RANGE TIME, SECONDS

0 00:10:00 00:20:00 00:30:00
RANGE TIME, HOURS:MINUTES:SECONDS



6000 6500 16,500 17,000 17,500
RANGE TIME, SECONDS

01:40:00 01:50:00 04:40:00 04:50:00
RANGE TIME, HOURS:MINUTES:SECONDS



28,000 28,500 29,000 29,500
RANGE TIME, SECONDS

07:50:00 08:00:00 08:10:00
RANGE TIME, HOURS:MINUTES:SECONDS

Figure 14-3. C-Band Acquisition and Loss Times

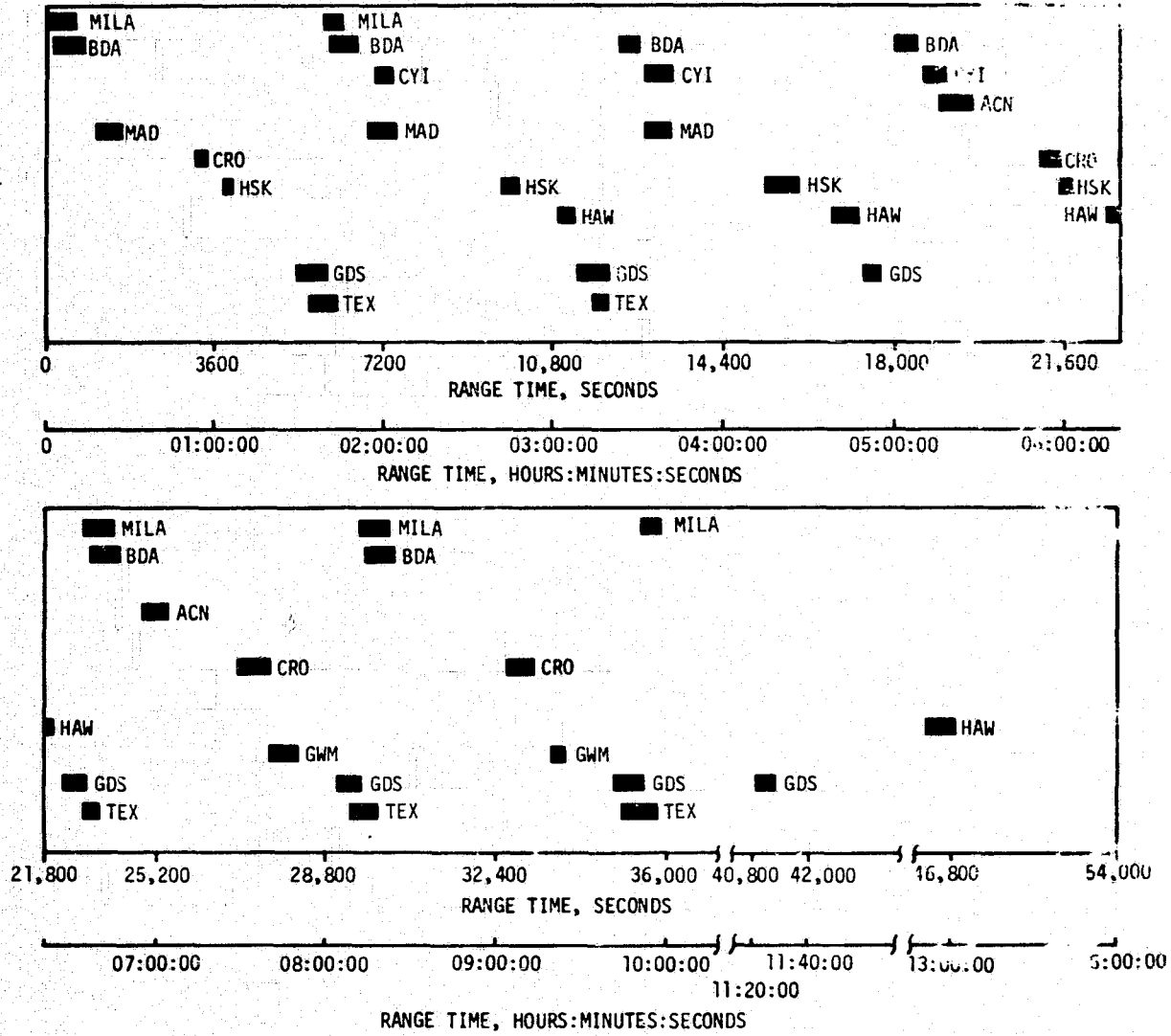


Figure 14-4. CCS Coverage (Sheet 1 of 3)

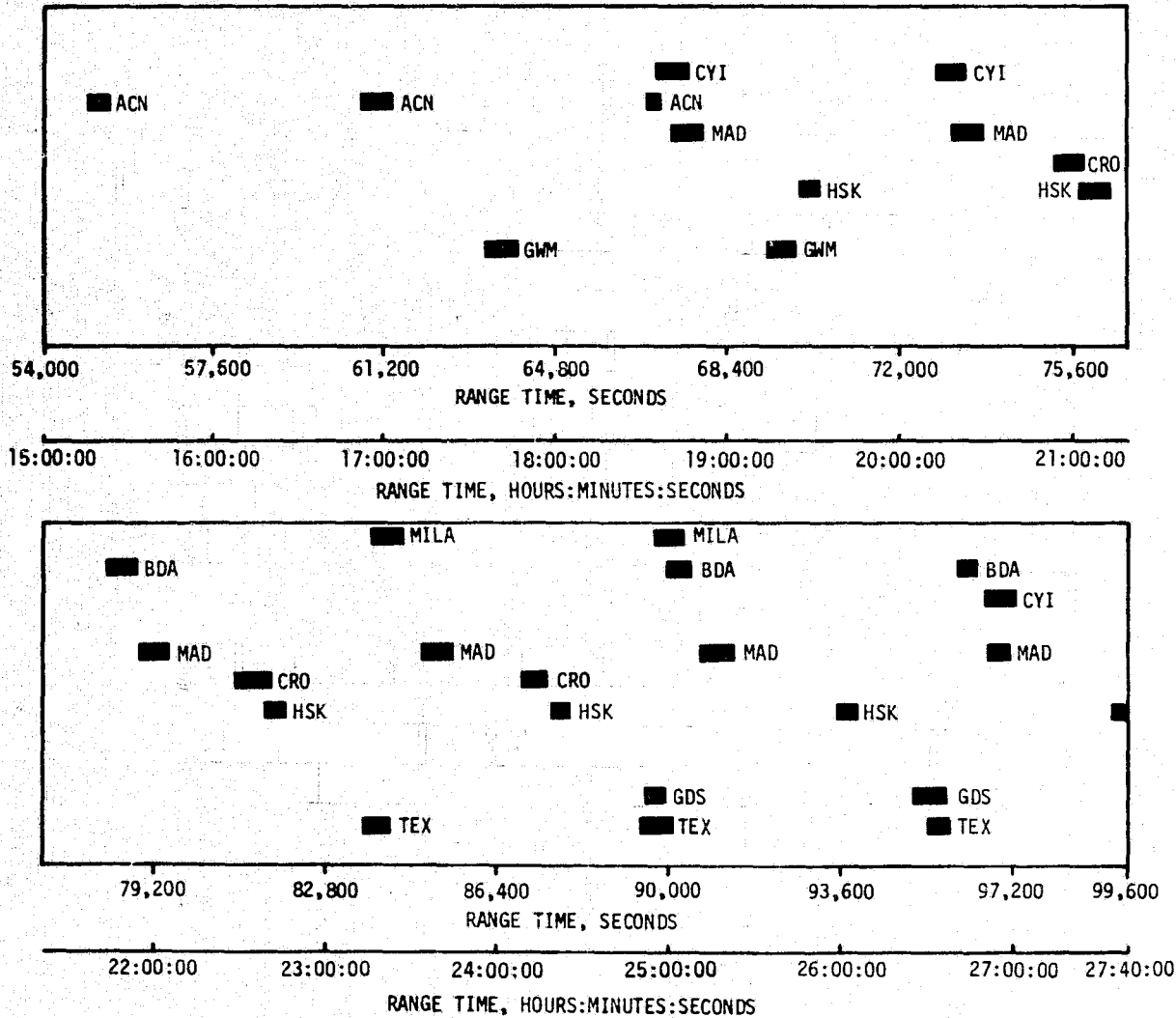


Figure 14-4. CCS Coverage (Sheet 2 of 3)

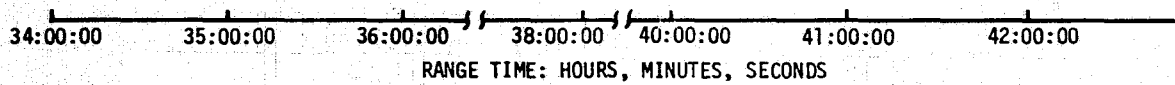
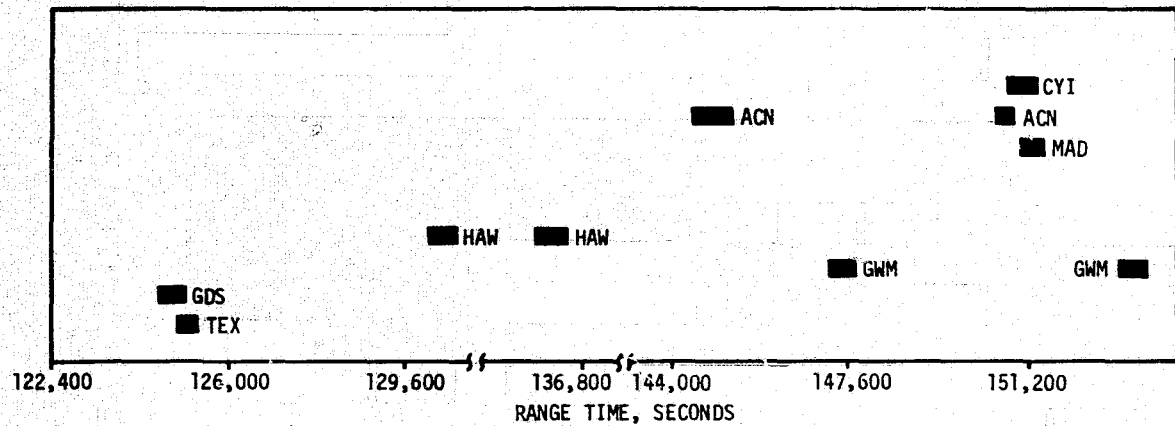
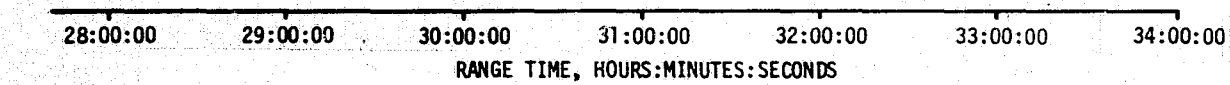
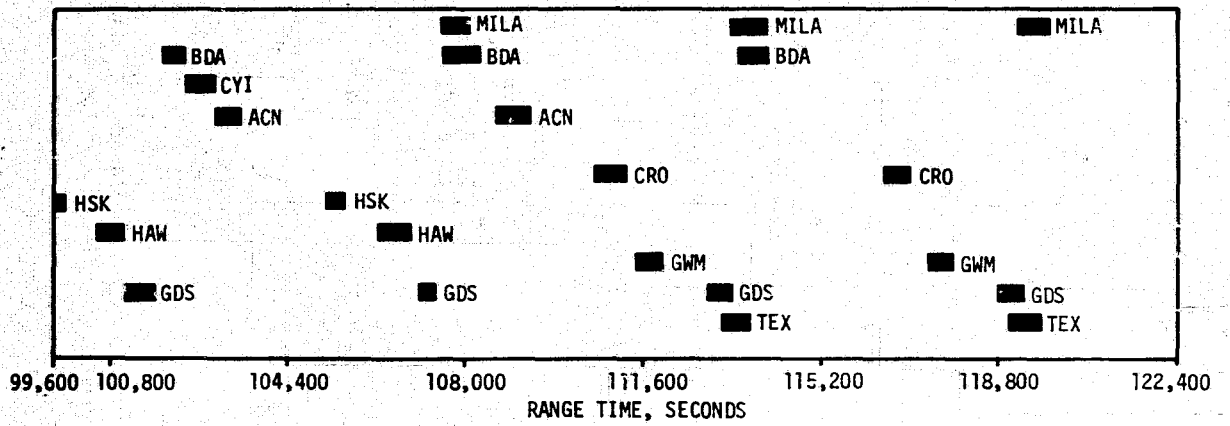


Figure 14-4. CCS Coverage (Sheet 3 of 3)

Table 14-5. SA-513 Launch Vehicle Telemetry Links

LINK	FREQUENCY (MHZ)	MODULATION	STAGE	FLIGHT PERIOD (RANGE TIME, SEC)	PERFORMANCE SUMMARY
AF-1	256.2	FM/FM	S-IC	0 to 517.4	Satisfactory
AP-1	244.3	PCM/FM	S-IC	0 to 517.4	Data Dropouts Range Time (sec) Duration (sec) 97.2 .2 142.2 .9 163.2 .8
BF-1	241.5	FM/FM	S-II	0 to 7461	Satisfactory
BF-2	234.0	FM/FM	S-II	0 to 7461	Data Dropouts
BP-1	248.6	PCM/FM	S-II	0 to 7461	Range Time (sec) Duration (sec) 161.0 1.2
DF-1	250.7	FM/FM	IU	0 to 67,620	Satisfactory
DP-1	245.3	PCM/FM	IU	0 to 67,620	Data Dropouts Range Time (sec) Duration (sec) 111.7 5.8

Phase front disturbances were experienced at the Cape between 300 and 400 seconds, at Grand Bahama Island (GBI) between 300 and 733 seconds, and at MILA between 300 and 690 seconds. Phase front disturbances have been experienced during boost on almost all previous missions. They occur when the pointing information is erroneous as a result of sudden antenna nulls or distorted beacon returns.

Telemetry data showed that several ground stations interrogated the transponders during boost. However, according to the telemetry data and ground station logs, radar contacts after Bermuda (BDA) LOS at 885 seconds were in the skin track mode with the exception of third revolution from 16,600 seconds to 16,915 seconds when HAW used beacon tracking. The transponder operated normally during the HAW track.

14.5 SECURE RANGE SAFETY COMMAND SYSTEMS

Telemetered data indicated that the command antennas, receivers/decoders, Exploding Bridge Wire (EBW) networks, and destruct controllers on each powered stage functioned properly during flight. They were in the required state-of-readiness if flight conditions during the launch had required vehicle destruct. Since no arm/cutoff or destruct commands were required, all data except receiver signal strength remained unchanged during the flight. The S-II range safety receiver signal strength measurements indicated that each receivers went out of saturation twice between 260 and 370 seconds and receiver Number 2 went out again at 520 seconds. However, because of the redundant nature of the range safety system, the system was in the required state-of-readiness

if flight conditions during the launch had required vehicle destruction. Power to the S-II stage range safety command systems was cutoff shortly after completion of powered flight by ground command, thereby deactivating (safing) the systems.

14.6 COMMAND AND COMMUNICATIONS SYSTEM EVALUATION

14.6.1 Summary of Performance

The CCS data indicate excellent performance of the onboard subsystem. No flight equipment malfunctions occurred during the flight. Ground station coverage times through CCS battery depletion are shown in Figure 14-4.

Events occurring during boost caused a degradation of the CCS received signal strength at MILA as expected. S-IC stage flame attenuated the signal from 94 to 126.5 seconds. The minimum signal strength during this period was -105 dbm. S-IC CECO caused a drop in received signal strength from 142 to 144 seconds with the minimum value being -100 dbm. Very slight, (almost negligible) signal fluctuations were noted at 160 seconds during S-IC/S-II separation and retro-motors burn. These fluctuations were much less severe than experienced on previous flights because of the higher altitude at the time of occurrence. The usual signal strength fluctuations resulting from S-II aft interstage separation were not discernible on this flight because the aft interstage failed to separate. No dropouts occurred at MILA during launch except during handover to BDA at 450 seconds.

The CCS was tracked until it ceased to transmit due to battery depletion. During the entire flight, the only dropouts occurring were at interrogating station handovers. There were several stations that received fluctuating signals. These signal fluctuations appeared on both the uplink and downlink signals and were caused by vehicle maneuvers. The most severe signal fluctuations occurred over MAD during the first revolution from 1245 to 1490 seconds when the vehicle was maneuvering to solar inertial attitude. The lowest downlink signal during this time period was -140 dbm. Although this low signal was sufficient to maintain carrier lock, telemetry data was lost.

Five commands were transmitted and all five were accepted. A detailed list of all commands initiated by MCC-Houston is shown in Table 14.6.

14.7 GROUND ENGINEERING CAMERAS

In general, ground camera coverage was good. Forty-seven items (43 from fixed cameras and four from tracking cameras) were received from KSC and evaluated. Two items did not operate, two items did not have coded range time, and three items were obscured due to frost and ice. As a result of these seven failures, system efficiency was 85 percent. The short range tracking cameras tracked until the vehicle was lost in clouds

Table 14-6. Command and Communication System Command History, SA-513

RANGE TIME		TRANS. STATION	COMMANDS	NO. OF WORDS TRANS.	REMARKS
SECONDS	HRS:MIN:SEC				
11,037	3:03:57	HAW	AM Deploy Busses Off	3	Accepted
34,984	9:43:04	GDS	Rate Measurement Switch	3	Accepted
35,549	9:52:29	TEX	ECS Logic Inhibit	1	Accepted
46,849	13:00:49	HAW	Terminate	1	Accepted
48,375	15:26:15	VAN	Water Valve Open	3	Accepted

at approximately 30 seconds. One camera reacquired the vehicle at approximately 85 seconds and tracked through 135 seconds. However, this camera had a 40-inch focal length lens and provided little usable data. The long range (500-inch focal length lens) tracking camera was not operated due to cloud coverage.

An extensive and thorough analysis was performed on all Skylab-1 engineering film. The analysis centered around the anomaly of the meteoroid shield being torn from the vehicle at approximately +63 seconds. Particles (debris) were first observed on engineering film item E-46 (400 frames per second) where a light colored and a dark colored particle were tentatively identified as coming from the vehicle. The white particle was observed and timed at 13.8 seconds for a period of 10 frames. The dark particle was observed at 15.4 seconds for a period of 31 frames.

Subsequent analysis of other engineering film items identified numerous particles falling from the tower. These particles were identified as carpet, panels from swing arms, plastic bags, boxes, a loud speaker, tape, etc. No particles were identified as coming from the vehicle during ignition, liftoff, and flight of the Skylab-1 vehicle through the +63 second time period that onboard instrumentation indicated the anomaly. Uprange tracking cameras did not acquire the vehicle during the anomaly period due to cloud coverage. Therefore, optically there was no coverage of the meteoroid shield anomaly.

A search of the pad area turned up items of debris such as those mentioned above. The debris seen falling through the camera field of view was not a result of ground support equipment malfunction since all GSE appeared to operate satisfactorily during ignition and liftoff.

SECTION 15

MASS CHARACTERISTICS

15.1 SUMMARY

Total vehicle mass, determined from post-flight analysis, was within 1.91 percent of prediction from ground ignition through S-II stage shutdown. This larger than anticipated difference was due mainly to the S-IC/S-II large interstage not separating as expected. Had the S-II stage residuals and OWS not been 4900 lbs. less than predicted, this percentage would have been greater.

15.2 MASS EVALUATION

Post-flight mass characteristics are compared with final predicted mass characteristics (MSFC Memorandum S&E-SAE-73-38)) and the operational trajectory (MSFC Memorandum S&E-AERO-MFT-14-73).

The post-flight mass characteristics were determined from an analysis of all available actual and reconstructed data from S-IC ignition through S-II/OWS separation. Dry weights of the launch vehicle are based on actual stage weighings and evaluation of the weight and balance log books (MSFC Form 998). Propellant loading and utilization was evaluated from propulsion system performance reconstructions.

Differences in dry weights of the inert stages and the loaded spacecraft were all within 0.72 percent of predicted, which was well within acceptable limits.

During S-IC burn phase, the total vehicle mass was less than predicted by 3464 kilograms (7637 lbm) (0.11 percent) at ignition, and less than predicted by 6465 kilograms (14253 lbm) (0.86 percent) at S-IC/S-II separation. These differences are due collectively to: S-IC stage dry weight (103 lbm), S-IC LOX loading (+1866 lbm), S-IC RP-1 loading (-6956 lbm), spacecraft (-975 lbm), S-II stage and interstage (-1695 lbm), S-IC residuals at separation (-10541 lbs) and loss of meteoroid shield from OWS during S-IC flight (-1153 lbs). S-IC burn phase vehicle mass is shown in Tables 15-1 and 15-2.

During S-II burn phase, the total vehicle mass was less than predicted by 1211 kilograms (2670 lbm) (0.29 percent) at ignition, and greater than predicted by -2758 kilograms (6080 lbm) (1.91 percent) at S-II/OWS separation. These large deviations in mass are due to: S-IC dry weight (-96 lbm), S-IC/S-II large interstage dry weight (-91 lbm), S-II LOX loading (-1604 lbm), S-II fuel loading (+96 lbm), OWS at S-II ignition (-2128 lbs), S-II stage residuals at separation (-2688 lbm) and no S-IC/S-II large interstage separation (+10992 lbm).

Total vehicle mass for the S-II burn phase is shown in Tables 15-3 and 15-4.

A summary of mass utilization and loss, both actual and predicted, from S-IC stage ignition through OWS separation is presented in Table 15-5. A comparison of actual and predicted mass, center of gravity, and moment of inertia is shown in Table 15-6.

Table 15-1. Total Vehicle Mass--S-IC Burn Phase--Kilograms

EVENTS	GROUND IGNITION		HOLDDOWN ARM RELEASE		CENTER ENGINE CUTOFF		OUTBOARD ENGINE CUTOFF		S-IC/S-II SEPARATION	
	PRED	ACT	PRED	ACT	PRED	ACT	PRED	ACT	PRED	ACT
RANGE TIME--SEC	-6.90	-6.80	0.20	0.20	140.60	140.70	158.15	158.16	159.90	159.90
DRY STAGE	130406.	130453.	130406.	130453.	130406.	130453.	130406.	130453.	130406.	130453.
LOX IN TANK	1479230.	1480077.	1447830.	1444345.	129035.	125615.	1009.	647.	612.	481.
LOX BELOW TANK	21115.	21123.	21875.	21883.	21859.	21666.	15853.	13224.	13479.	10501.
LOX ULLAGE GAS	190.	190.	236.	226.	3014.	3053.	3357.	3404.	3364.	3411.
FUEL IN TANK	636636.	633481.	626483.	621666.	64769.	62779.	8255.	6618.	6806.	5089.
FUEL BELOW TANK	4313.	4313.	5996.	5996.	5996.	5996.	5958.	5958.	5958.	5958.
FUEL ULLAGE GAS	43.	46.	43.	48.	226.	228.	245.	249.	247.	251.
N2 PURGE GAS	36.	36.	36.	36.	19.	19.	19.	19.	19.	19.
HELIUM IN BOTTLE	288.	288.	288.	284.	105.	104.	86.	84.	84.	82.
FROST	635.	635.	635.	635.	340.	340.	340.	340.	340.	340.
RETROCKET PROP.	1026.	1026.	1026.	1026.	1026.	1026.	1026.	1026.	1026.	1026.
OTHER	239.	239.	239.	239.	239.	239.	239.	239.	239.	239.
TOTAL STAGE	2274162.	2271909.	2235098.	2226842.	357039.	351723.	166798.	162266.	162586.	157854.
TOTAL S-IC/S-II IS	5649.	5608.	5649.	5608.	5649.	5608.	5649.	5608.	5649.	5608.
TOTAL S-II STAGE	483619.	482891.	493619.	482891.	483397.	482670.	483397.	482670.	483397.	482670.
TOT S-II/S-IVB IS	3453.	3453.	3453.	3453.	3453.	3453.	3453.	3453.	3453.	3453.
TOTAL SPACECRAFT	89539.	89096.	89539.	89096.	89539.	88573.	89539.	88573.	89539.	88573.
TOTAL UPPERSTAGE	582260.	581049.	582260.	581049.	582039.	580305.	582039.	580305.	582039.	580305.
TOTAL VEHICLE	2856423.	2852959.	2817358.	2807892.	939078.	932029.	748636.	742511.	746625.	738160.

Table 15-2. Total Vehicle Mass--S-IC Burn Phase--Pounds

EVENTS	GROUND IGNITION		HOLDDOWN ARM RELEASE		CENTER ENGINE CUTOFF		OUTBOARD ENGINE CUTOFF		S-IC/S-II SEPARATION	
	PRED	ACT	PRED	ACT	PRED	ACT	PRED	ACT	PRED	ACT
RANGE TIME--SEC	-6.90	-6.80	0.20	0.20	140.60	140.70	158.15	158.16	159.90	159.90
DRY STAGE	287498.	287601.	287498.	287601.	287498.	287601.	287498.	287601.	287498.	287601.
LOX IN TANK	3261145.	3263011.	3191920.	3184237.	284474.	276934.	2225.	1427.	1349.	1060.
LOX BELOW TANK	46552.	46568.	48227.	48243.	48190.	48206.	34950.	29155.	29718.	23151.
LOX ULLAGE GAS	419.	419.	520.	499.	6646.	6732.	7401.	7505.	7417.	7521.
FUEL IN TANK	1403543.	1396587.	1381159.	1370540.	142791.	138405.	18201.	14591.	15005.	11219.
FUEL BELOW TANK	9509.	9509.	13219.	13219.	13219.	13219.	13136.	13136.	13136.	13136.
FUEL ULLAGE GAS	95.	98.	95.	107.	498.	505.	541.	549.	545.	553.
N2 PURGE GAS	80.	80.	80.	80.	43.	43.	43.	43.	43.	43.
HELIUM IN BOTTLE	636.	636.	636.	627.	232.	231.	189.	185.	185.	181.
FROST	1400.	1400.	1400.	1400.	750.	750.	750.	750.	750.	750.
RETROCKET PROP	2264.	2264.	2264.	2264.	2264.	2264.	2264.	2264.	2264.	2264.
OTHER	528.	528.	528.	528.	528.	528.	528.	528.	528.	528.
TOTAL STAGE	5013671.	5008704.	4927548.	4909348.	787136.	775418.	367728.	357735.	358441.	346010.
TOTAL S-IC/S-II IS	12455.	12364.	12455.	12364.	12455.	12364.	12455.	12364.	12455.	12364.
TOTAL S-II STAGE	1066197.	1054593.	1066197.	1064593.	1065709.	1064105.	1065709.	1064105.	1065709.	1064105.
TOT S-II/S-IVB IS	7613.	7613.	7613.	7613.	7613.	7613.	7613.	7613.	7613.	7613.
TOTAL SPACECRAFT	197400.	196425.	197400.	196425.	197400.	195272.	197400.	195272.	197400.	195272.
TOTAL UPPERSTAGE	1283665.	1280995.	1283665.	1280995.	1283177.	1279354.	1283177.	1279354.	1283177.	1279354.
TOTAL VEHICLE	6297336.	6289699.	6211213.	6190343.	2070314.	2054773.	1630906.	1637090.	1641619.	1627365.

Table 15-3. Total Vehicle Mass--S-II Burn Phase--Kilograms

EVENTS	S-IC IGNITION		S-II IGNITION		S-II MAINSTAGE		S-II ENGINE CUTOFF		S-II/OWS SEPARATION	
	PRID	ACT	PRED	ACT	PRED	ACT	PRED	ACT	PRED	ACT
	RANGE TIME--SEC	-6.90	-6.80	161.60	161.60	163.60	163.60	588.32	588.99	588.50
S-IC/S-II SMALL IS	622.	622.	0.	0.	0.	0.	0.	4985.	0.	4985.
S-IC/S-II LARGE IS	5027.	4985.	5027.	4985.	5027.	4985.	0.	4985.	0.	4985.
S-IC/S-II PROPELLANT	0.	0.	0.	0.	0.	0.	0.	0.	0.	0.
TOTAL S-IC/S-II IS	5649.	5608.	5027.	4985.	5027.	4985.	0.	4985.	0.	4985.
DRY STAGE	36697.	36653.	36697.	36653.	36697.	36653.	36697.	36653.	36697.	36653.
LOX IN TANK	372943.	372216.	372943.	372216.	372483.	371755.	8586.	7536.	8488.	7407.
LOX BELOW TANK	737.	737.	737.	737.	800.	800.	787.	787.	787.	767.
LOX ULLAGE GAS	176.	176.	176.	176.	179.	179.	1991.	1991.	1996.	1996.
FUEL IN TANK	72651.	72695.	72645.	72689.	72431.	72475.	2810.	2666.	2758.	2620.
FUEL BELOW TANK	104.	104.	110.	110.	127.	127.	123.	123.	123.	123.
FUEL ULLAGE GAS	37.	37.	38.	38.	39.	39.	798.	798.	800.	800.
INSULATION PURGE GAS	17.	17.	0.	0.	0.	0.	0.	0.	0.	0.
FROST	204.	204.	0.	0.	0.	0.	0.	0.	0.	0.
START TANK	13.	13.	13.	13.	2.	2.	2.	2.	2.	2.
OTHER	34.	34.	34.	34.	34.	34.	34.	34.	34.	34.
TOTAL S-II STAGE	483619.	482891.	483397.	482670.	482796.	482068.	51834.	50594.	51689.	50420.
TOT S-II/OWS IS	3453.	3453.	3453.	3453.	3453.	3453.	3453.	3453.	3453.	3453.
TOTAL SPACECRAFT	89535.	89036.	89539.	88573.	89539.	88573.	89462.	88497.	89462.	88497.
TOTAL UPPER STAGE	92992.	92550.	92992.	92027.	92992.	92027.	92915.	91950.	92915.	91950.
TOTAL VEHICLE	582260.	581049.	581417.	579683.	580815.	579081.	144750.	145330.	144605.	147363.

Table 15-4. Total Vehicle Mass--S-II Burn Phase--Pounds

EVENTS	S-IC IGNITION		S-II IGNITION		S-II MAINSTAGE		S-II ENGINE CUTOFF		S-II/OWS SEPARATION	
	PRED	ACT	PRED	ACT	PRED	ACT	PRED	ACT	PRED	ACT
	RANGE TIME--SEC	-6.90	-6.80	161.60	161.60	163.60	163.60	588.32	588.99	588.50
S-IC/S-II SMALL IS	1372.	1372.	0.	0.	0.	0.	0.	10992.	0.	10992.
S-IC/S-II LARGE IS	11083.	10992.	11083.	10992.	11083.	10992.	0.	10992.	0.	10992.
S-IC/S-II PROPELLANT	0.	0.	0.	0.	0.	0.	0.	0.	0.	0.
TOTAL S-IC/S-II IS	12455.	12364.	11083.	10992.	11083.	10992.	0.	10992.	0.	10992.
DRY STAGE	80904.	80808.	80904.	80808.	80904.	80808.	80904.	80808.	80904.	80808.
LOX IN TANK	822200.	820596.	822200.	820596.	821185.	819581.	18935.	16616.	18715.	16331.
LOX BELOW TANK	1625.	1625.	1625.	1625.	1764.	1764.	1736.	1736.	1736.	1736.
LOX ULLAGE GAS	390.	390.	390.	390.	395.	395.	4391.	4391.	4402.	4402.
FUEL IN TANK	160170.	160266.	160156.	160252.	159684.	159781.	6197.	5878.	6081.	5777.
FUEL BELOW TANK	231.	231.	244.	244.	282.	282.	272.	272.	272.	272.
FUEL ULLAGE GAS	83.	83.	84.	84.	86.	86.	1760.	1760.	1765.	1765.
INSULATION PURGE GAS	38.	38.	0.	0.	0.	0.	0.	0.	0.	0.
FROST	450.	450.	0.	0.	0.	0.	0.	0.	0.	0.
START TANK	30.	30.	30.	30.	5.	5.	5.	5.	5.	5.
OTHER	76.	76.	76.	76.	76.	76.	76.	76.	76.	76.
TOTAL S-II STAGE	1066197.	1064593.	1065709.	1064105.	1064383.	1062779.	114276.	111542.	113956.	111172.
TOT S-II/OWS IS	7613.	7613.	7613.	7613.	7613.	7613.	7613.	7613.	7613.	7613.
TOTAL SPACECRAFT	197400.	196425.	197400.	195272.	197400.	195272.	197231.	195103.	197231.	195103.
TOTAL UPPER STAGE	205013.	204038.	205013.	202885.	205013.	202885.	204844.	202716.	204844.	202716.
TOTAL VEHICLE	1283665.	1280995.	1281805.	1277982.	1280479.	1276556.	319120.	325230.	318830.	324880.

Table 15-5. Flight Sequence Mass Summary

MASS HISTORY	PREDICTED		ACTUAL	
	KG	LBM	KG	LBM
S-IC STAGE, TOTAL	2274162.	5013671.	2271909.	5008704.
S-IC/S-II IS, TOTAL	5649.	12455.	5608.	12364.
S-II STAGE, TOTAL	483618.	1066197.	482891.	1064593.
S-II/S-IVB IS, TOTAL	3453.	7613.	3453.	7613.
SPACECRAFT, TOTAL	89539.	197400.	89096.	196425.
1ST FLT STG AT IGN THRUST BUILDUP	2856422. -39064.	6297336. -86123.	2852958. -45067.	6289699. -99356.
1ST FLT STG AT HDAR FROST	2817358. -294.	6211213. -650.	2807891. -294.	6190343. -650.
MAINSTAGE	-2066744.	-4556393.	-2062971.	-4548076.
N2 PURGE GAS	-16.	-37.	-16.	-37.
THRUST DECAY-IE	-1053.	-2321.	-1102.	-2431.
ENG EXPENDED PROP	-189.	-418.	-187.	-418.
S-II INSUL PURGE	-17.	-38.	-17.	-38.
S-II FROST	-204.	-450.	-204.	-450.
OWS MET SHIELD	0.	0.	-522.	-1153.
1ST FLT STG AT OECO THRUST DECAY MS	748838. -4212.	1650906. -9287.	742571. -4411.	1637090. -9725.
1ST FLT STG AT SEP STG AT SEPARATION	744625. -162586.	1641619. -358441.	738160. -157854.	1627365. -348010.
S-IC/S-II SMALL IS	-622.	-1372.	-622.	-1372.
2ND FLT STG AT SSC	581417.	1281805.	579683.	1277982.
2ND FLT STG AT IGN THRUST BUILDUP	581417. -590.	1281805. -1301.	579683. -590.	1277982. -1301.
START TANK	-11.	-25.	-11.	-25.
2ND FLT STG AT MS MAINSTAGE	580815. -430907.	1280479. -949989.	579081. -431414.	1276656. -951106.
OWS VENT	-76.	-169.	-76.	-169.
S-IC/S-II LARGE IS	-5027.	-11083.	0.	0.
TD & ENG PROP	-53.	-118.	-59.	-130.
2ND FLT STG AT COS THRUST DECAY	144750. -145.	319120. -320.	147530. -167.	325250. -370.
2ND FLT STG AT SEP STG AT SEPARATION	144605. -51689.	318800. -113956.	147363. -55412.	324880. -122164.
S-II/OWS IS DRY	-2972.	-6553.	-2972.	-6553.
S-II/OWS PROP	-480.	-1060.	-480.	-1060.
OWS AFT FRAME	-21.	-48.	-21.	-48.
OWS DET PKG	-1.	-3.	-1.	-3.
SKYLAB IN ORBIT	89439.	197180.	88474.	195052.

Table 15-6. Mass Characteristics Comparison

EVENT	MASS		LONGITUDINAL C.G. (X STA.)		RADIAL C.G.		ROLL MOMENT OF INERTIA		PITCH MOMENT OF INERTIA		YAW MOMENT OF INERTIA	
	KILO POUNDS	O/O DEV.	METERS INCHES	DELTA	METERS INCHES	DELTA	KG-M2 X10-6	O/O DEV.	KG-M2 X10-6	O/O DEV.	KG-M2 X10-6	O/O DEV.
S-IC STAGE DRY	PRED	130407. 287498.	9.316 366.8		0.0651 2.5632		2.543		16.486		16.426	
	ACTUAL	130454. 287601.	9.387 369.6	0.071 2.79	0.0651 2.5632	0.0000 0.0000	2.544	0.04	16.492	0.04	16.432	0.04
S-IC/S-II INTER-STAGE TOTAL	PRED	5649. 12455.	41.656 1640.0		0.1223 4.8166		0.139		0.083		0.083	
	ACTUAL	5608. 12364.	41.656 1640.0	0.000 0.00	0.1223 4.8166	0.0000 0.0000	0.138	-0.72	0.082	-0.72	0.083	-0.72
S-II STAGE, DRY	PRED	36697. 80904.	47.922 1886.7		0.1613 6.3505		0.601		2.012		2.025	
	ACTUAL	36654. 80808.	47.759 1880.3	-0.162 -6.40	0.1613 6.3505	0.0000 0.0000	0.600	-0.11	2.010	-0.11	2.022	-0.11
S-II/OVS INTER-STAGE TOTAL	PRED	3453. 7613.	66.415 2614.8		0.0727 2.8635		0.061		0.040		0.041	
	ACTUAL	3453. 7613.	66.415 2614.8	0.000 0.00	0.0727 2.8635	0.0000 0.0000	0.061	0.00	0.040	0.00	0.041	0.00
SPACECRAFT, TOTAL	PRED	89539. 197400.	83.596 3291.2		0.0942 3.7121		0.551		6.040		6.070	
	ACTUAL	89097. 196425.	83.619 3292.1	0.022 0.89	0.0920 3.6235	-0.0022 -0.0886	0.547	-0.69	6.007	-0.55	6.040	-0.48
1ST FLIGHT STAGE AT IGNITION	PRED	2856423. 6297336.	29.210 1150.0		0.0007 0.0300		4.004		746.189		746.205	
	ACTUAL	2852959. 6289699.	29.215 1150.2	0.005 0.19	0.0007 0.0282	-0.0000 -0.0017	3.997	-0.15	743.429	-0.36	743.405	-0.37
1ST FLIGHT STAGE AT HOLDDOWN ARM RELEASE	PRED	2817359. 6211213.	29.138 1147.1		0.0007 0.0300		4.039		745.067		745.083	
	ACTUAL	2807892. 6190342.	29.138 1147.1	0.000 0.00	0.0009 0.0360	0.0001 0.0060	4.032	-0.15	741.391	-0.42	741.866	-0.42

15-6

Table 15-6. Mass Characteristics Comparison (Continued)

EVENT	MASS		LONGITUDINAL C.G. (X STA.)		RADIAL C.G.		ROLL MOMENT OF INERTIA		PITCH MOMENT OF INERTIA		YAW MOMENT OF INERTIA	
	KILO POUNDS	O/O DEV.	METERS INCHES	DELTA	METERS INCHES	DELTA	KG-M2 X10-6	O/O DEV.	KG-M2 X10-6	O/O DEV.	KG-M2 X10-6	O/O DEV.
1ST FLIGHT STAGE AT OUTBOARD ENGINE CUTOFF SIGNAL	PRED	748838. 1650905.	43.812 1724.9		0.0026 0.1044		4.024		381.334		381.354	
	ACTUAL	742571. 1637089.	43.973 1731.2	0.160 6.33	0.0027 0.1077	0.0000 0.0033	4.011	-0.33	374.295	-1.84	374.275	-1.85
1ST FLIGHT STAGE AT SEPARATION	PRED	744625. 1641618.	44.001 1732.3		0.0029 0.1170		4.023		376.558		376.578	
	ACTUAL	738160. 1627364.	44.176 1739.2	0.175 6.89	0.0027 0.1077	-0.0002 -0.0093	4.009	-0.34	369.113	-1.97	369.092	-1.98
2ND FLIGHT STAGE AT START SEQUENCE COMMAND	PRED	581417. 1281806.	53.651 2112.2		0.0084 0.3310		1.349		110.193		110.240	
	ACTUAL	579683. 1277983.	53.609 2110.6	-0.042 -1.66	0.0084 0.3312	0.0000 0.0001	1.336	-0.92	109.671	-0.46	109.718	-0.46
2ND FLIGHT STAGE AT MAINSTAGE	PRED	580816. 1280479.	53.650 2112.2		0.0084 0.3310		1.351		110.181		110.229	
	ACTUAL	579081. 1276656.	53.607 2110.5	-0.043 -1.70	0.0084 0.3312	0.0000 0.0001	1.338	-0.92	109.661	-0.46	109.708	-0.46
2ND FLIGHT STAGE AT CUTOFF SIGNAL	PRED	144750. 319120.	70.203 2763.9		0.0363 1.4294		1.226		51.555		51.602	
	ACTUAL	147531. 325250.	69.373 2731.2	-0.829 -32.67	0.0330 1.3024	-0.0032 -0.1269	1.337	9.07	54.892	6.47	54.940	6.47
2ND FLIGHT STAGE AT SEPARATION	PRED	144605. 318800.	70.227 2764.8		0.0363 1.4294		1.226		51.468		51.515	
	ACTUAL	147363. 324880.	69.401 2732.3	-0.826 -32.55	0.0330 1.3024	-0.0032 -0.1269	1.337	9.07	54.795	6.46	54.842	6.46
SPACECRAFT SEPARATED	PRED	89439. 197180.	83.608 3291.6		0.0942 3.7121		0.551		6.033		6.067	
	ACTUAL	88474. 195052.	83.678 3294.4	0.070 2.75	0.0931 3.6674	-0.0011 -0.0447	0.559	-2.07	5.955	-1.25	5.968	-1.28

15-7/15-8

SECTION 16

SATURN WORK SHOP SUMMARY

The Saturn Work Shop (SWS) was launched from Kennedy Space Center, Florida at 13:30:00 Eastern Daylight Time (17:30:00 Universal Time) on May 14, 1973. At approximately 63 seconds into the flight the meteoroid shield structurally failed resulting in premature release of the Orbital Work Shop (OWS) solar array wing No. 2 (refer to Section 17). S-II stage retro motor exhaust plume impingement on partially deployed solar array wing No. 2, at about 593 seconds, caused the wing to be torn from the OWS.

The SWS was inserted into a near circular Earth orbit of 235 n. mi. altitude at an inclination of 50 degrees. The payload shroud was jettisoned, and the Apollo Telescope Mount (ATM) and its solar array were deployed as planned during the first orbit. The OWS solar array wing No. 1 released as planned during the first orbit but stopped after only a few degrees of movement. This array was restrained from further movement by debris from the meteoroid shield. The remainder of the planned Skylab system activation and deployment functions occurred as scheduled with transfer of attitude control from the IU to the ATM at approximately 4 hours and 50 minutes.

The SWS was maneuvered into a solar inertial attitude with the solar arrays at right angles to the Sun for maximum electrical power generation. The work shop area temperatures then rose above operating limits due to increased exposure to solar heat flux since the meteoroid shield was also designed to provide thermal protection. The SWS was pitched up toward the Sun at 13 hours into the flight to reduce the solar heat flux on the work shop area. This attitude further reduced the power generation capability which had already been severely limited by the loss of the work shop solar array wing No. 2 and the failure of wing No. 1 to deploy. A continuous adjustment of SWS attitude was necessary to keep the power and temperature within acceptable limits. Constraints to maintain adequate heat in other critical areas of the Skylab and to optimize the operation of the attitude control system in an off-nominal mode of operation added further complications. This delicate balance continued for approximately 10 days.

The electrical power available from the ATM solar array was further reduced by the requirement to cycle certain power regulator modules on and off to prevent over-heating caused by the unplanned vehicle attitudes. Although considerably below the total design capability, power was sufficient for the critical loads. Many components and systems were turned off or were cycled as required to remain within the power

generation capability. These maneuvers and attitude control during several docking attempts caused a much larger usage of the attitude control thruster impulse capability than predicted. Sufficient propellant remained, however, for the three manned missions that were planned.

Due to the high internal temperatures that were reached in the work shop there was concern that outgassing of some materials would be hazardous to the crew. Prior to the crew arrival, the habitation area was depressurized and repressurized four times to purge the internal atmosphere of any hazardous outgassing products. This cycle was started approximately 4 days into the mission with internal pressure reduced to approximately 0.6 psia and then repressurized to 2.0 psia with nitrogen for each cycle. The habitation area was repressurized with the proper oxygen/nitrogen mixture prior to the first crew entry. The crew later tested this atmosphere and no hazardous outgassing products were found.

The SWS was originally planned to be manned on May 15, 1973, the day after launch) by the first of three astronaut crews. The manned launch, Skylab-2 (SL-2) was delayed 10 days for analysis of the SWS thermal and electrical power problems. This delay permitted analysis of mission impacts on SWS, the development of special repair hardware, and the time for crew training in repair methods. Necessary revisions to the flight plan were also developed.

The first astronaut crew arrived at the SWS on May 25, 1973. After a flyaround inspection and a soft docking, the crew undocked and attempted to free the solar array wing No. 1 using special tools while standing in the open command module hatch. This activity was not successful. A later attempt on mission day 14 using Skylab extravehicular activity facilities was successful in deploying the wing which subsequently operated normally and relieved the electrical power shortage.

The thermal problem was relieved when the crew deployed a parasol sun shade through a work shop scientific airlock. This also allowed the Skylab to be returned to solar inertial attitude which increased the electrical power output and returned the SWS to a nominal attitude control mode.

The crew proceeded to complete the SWS activation as planned. The environmental control system operated satisfactorily; however, it was several days before the excess heat within the cabin was removed. On mission day 11 the air temperature was down to 76.5°F which was still above the 70°F planned. The SWS operated after activation approximately as planned with some electrical power limitations until the solar array wing No. 1 was deployed.

The exterior contamination, based on measurements available, was indicated to be acceptable and within the range predicted. Some visible deposition appeared on the exterior surfaces of windows, no serious optical contamination has been reported by any of the several investigators.

The overall experiment program was executed essentially as planned although two experiments had to be cancelled because the parasol occupied the solar scientific airlock. Some experiments were performed using the other scientific airlock as a contingency method. The solar experiments of the telescope mount were performed every day subsequent to mission day 4 and a total of 11 photography passes were made with the Earth resources experiment group. An observation of typhoon Ava was made on mission day 13.

The crew completed the deactivation procedures and left the SWS on June 22, 1973, after a stay of 28 days.

SECTION 17

63 AND 593 SECOND ANOMALIES

17.1 SUMMARY

Skylab-1 launch vehicle instrumentation recorded unusual disturbances at approximately 63 and 593 seconds during flight. The first possible evidence of anomalous behavior was an increase in S-II stage antenna reflected power beginning at 59.87 seconds. At 62.76 seconds the Orbital Work Shop (OWS) film vault vibration measurement recorded a structural transient which propagated up and down the space vehicle. At approximately 593 seconds, immediately after S-II/Saturn Work Shop (SWS) separation, another transient was indicated by the IU and SWS instrumentation.

The cause of the transient at 63 seconds was structural failure and release of the OWS meteoroid shield, and premature fracture of the OWS Solar Array System (SAS) Wing No. 2 tie down fittings (modules), permitting Wing No. 2 to partially deploy.

The 593 second transient was caused by the partially deployed SAS Wing No. 2 being rotated past its fully deployed position and torn from its hinges by impingement from the S-II retro motor plume.

The origin of these anomalies was in a unique payload and external to the launch vehicle; therefore, no launch vehicle corrective action is necessary.

The vehicle reacted properly to the external disturbance originating at the OWS with no significant effect except for damage to the S-II second plane separation system.

17.2 63 SECOND ANOMALY

17.2.1 Initial Vehicle Response

Review of data has shown the first evidence of anomalous behavior was an increase in S-II stage antenna reflected power (N035-225) possibly indicating a vehicle/ground-plane shape change beginning at 59.87 seconds. At 62.76 seconds the OWS film vault vibration measurement (E7000-436) recorded a transient. This structural transient propagated up and down the space vehicle from the OWS as shown by the sequence of events depicted in Figure 17-1. The vehicle also responded to a counter-clockwise (CCW) [all attitude references are defined looking forward] roll torque beginning at 62.04 seconds (see Figure 17-2), reducing the

roll rate from .85 deg/s to .7 deg/s. This type of small roll activity has been seen on previous flights as response to the Mach 1 (61.1 seconds) environment and thus could be attributed to either an early indication of the anomaly or normal Mach 1 aerodynamics. If the small CCW roll torque was related to the anomaly, it was probably due to the shield segment between the main tunnel and the auxiliary tunnel lifting into the air stream. The captured air flow would be deflected toward the main tunnel causing the observed torque. At 62.8 seconds, an abnormal clockwise torque was applied which increased the roll rate to 2.4 deg/s. This torque was probably due to the failing shield applying a sudden force to SAS Wing No. 2. The resultant impulse partially deployed Wing 2 and rolled the vehicle.

17.2.2 Initial Orbital Work Shop (OWS) Measurement Response

A detailed review of pertinent OWS measurements (as shown in Figure 17-3) points to an anomalous condition occurring between 62.0 and 62.78 seconds in the OWS meteoroid shield and solar array panels. The exact time is indeterminate due to the low data sampling rate. The first indications were loss of meteoroid shield temperature measurements C7011 and C7012. C7011 was active when sampled at 61.9791 seconds and open at 62.7791 seconds. C7012 was active when sampled at 62.0863 and open at 62.8863. These two measurements sense the external temperature of the Meteoroid Shield (MS) at Positions I and II, respectively, as shown in Figure 17-4. The instrumentation cabling runs are shown in Figure 17-5. From the failure of temperature measurement indication C7011 it can be assumed that the anomaly was locally in progress no later than 62.7791 seconds. The good readings at this time from the MS tension straps K7010, K7011, and K7012, the SAS Wing No. 2 indication K7211, and temperature measurement C7013, indicate the disturbance was still confined to the vehicle position I/II quadrant and that the major failure of the MS had not begun.

17.2.3 Meteoroid Shield Structural Failure

During the time period between the 62.760 seconds OWS film vault vibration transient and the 62.779 seconds MS temperature measurement C7011 loss, the launch vehicle experienced no measurable transient effects from the initial OWS disturbance and the OWS was in the configuration as illustrated by Figure 17-6a.

At about 62.8 seconds the launch vehicle began to react to the OWS disturbance and the major failure is believed to have started. Table 17-1 presents a MS failure event correlation summary.

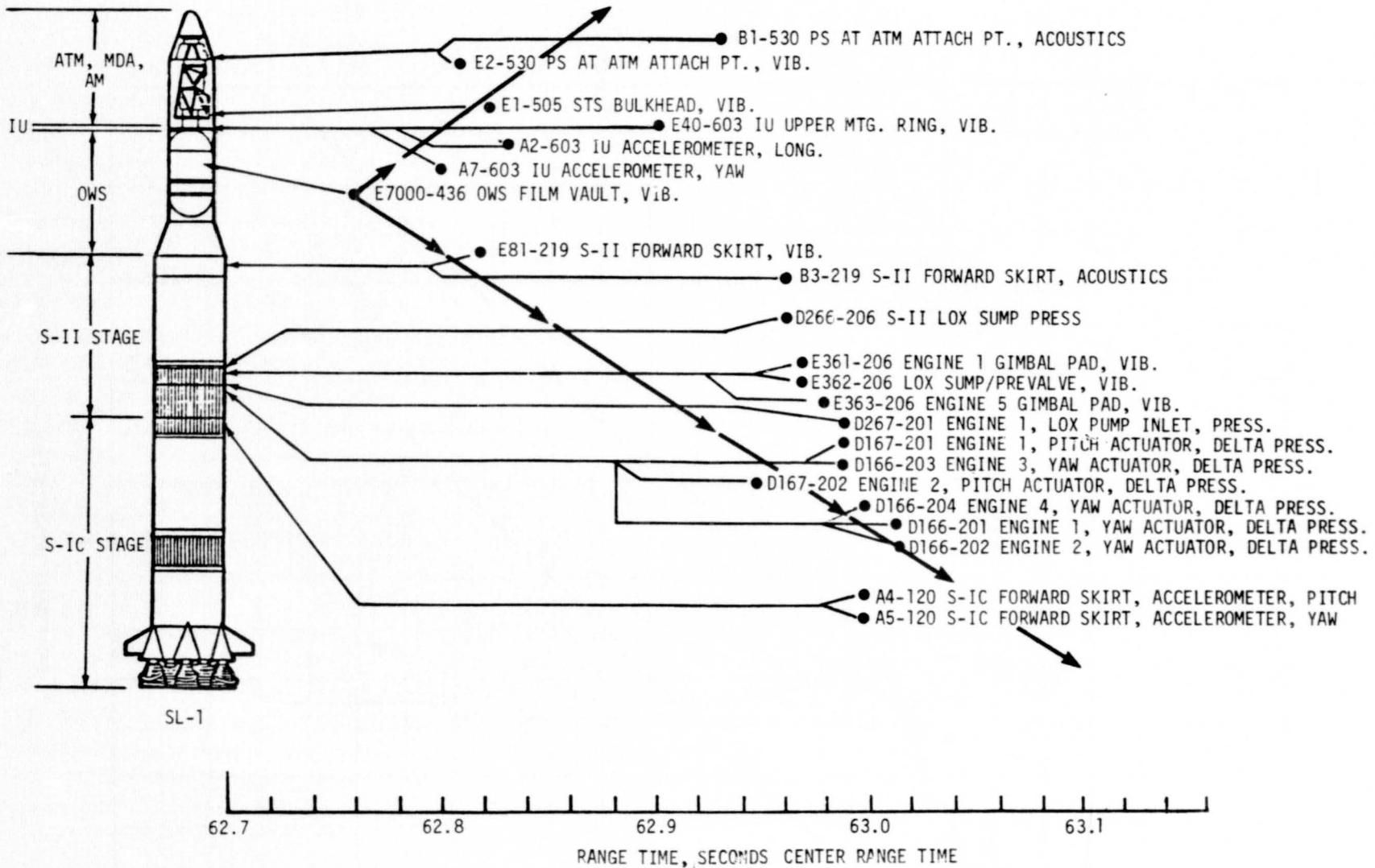


Figure 17-1. Propagation of the 63-Second Transient

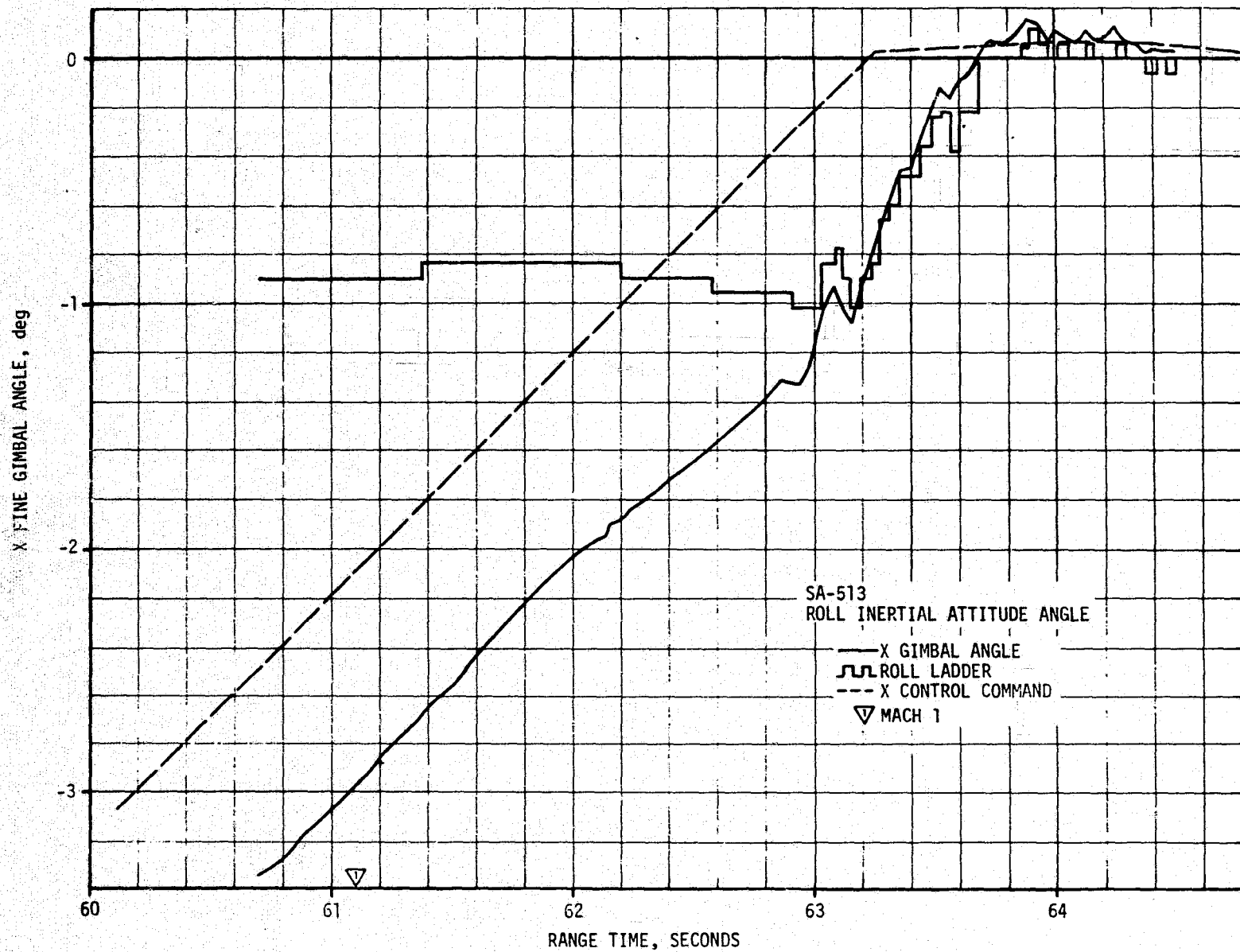


Figure 17-2. SA-513 Roll Inertial Attitude Angle Transients During 63 Second Anomaly

LEGEND: NORMAL ● --- UNKNOWN --- ● LOST

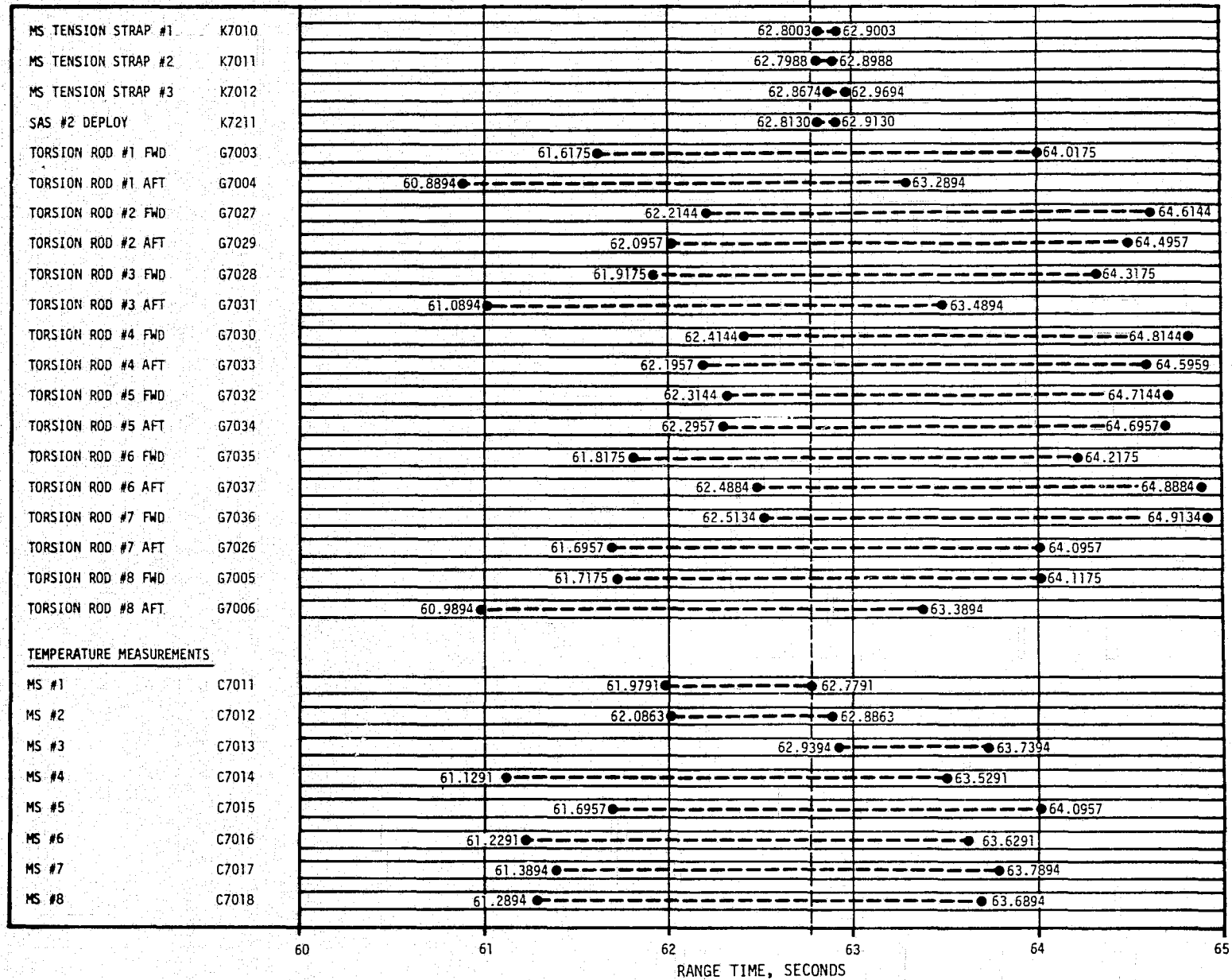
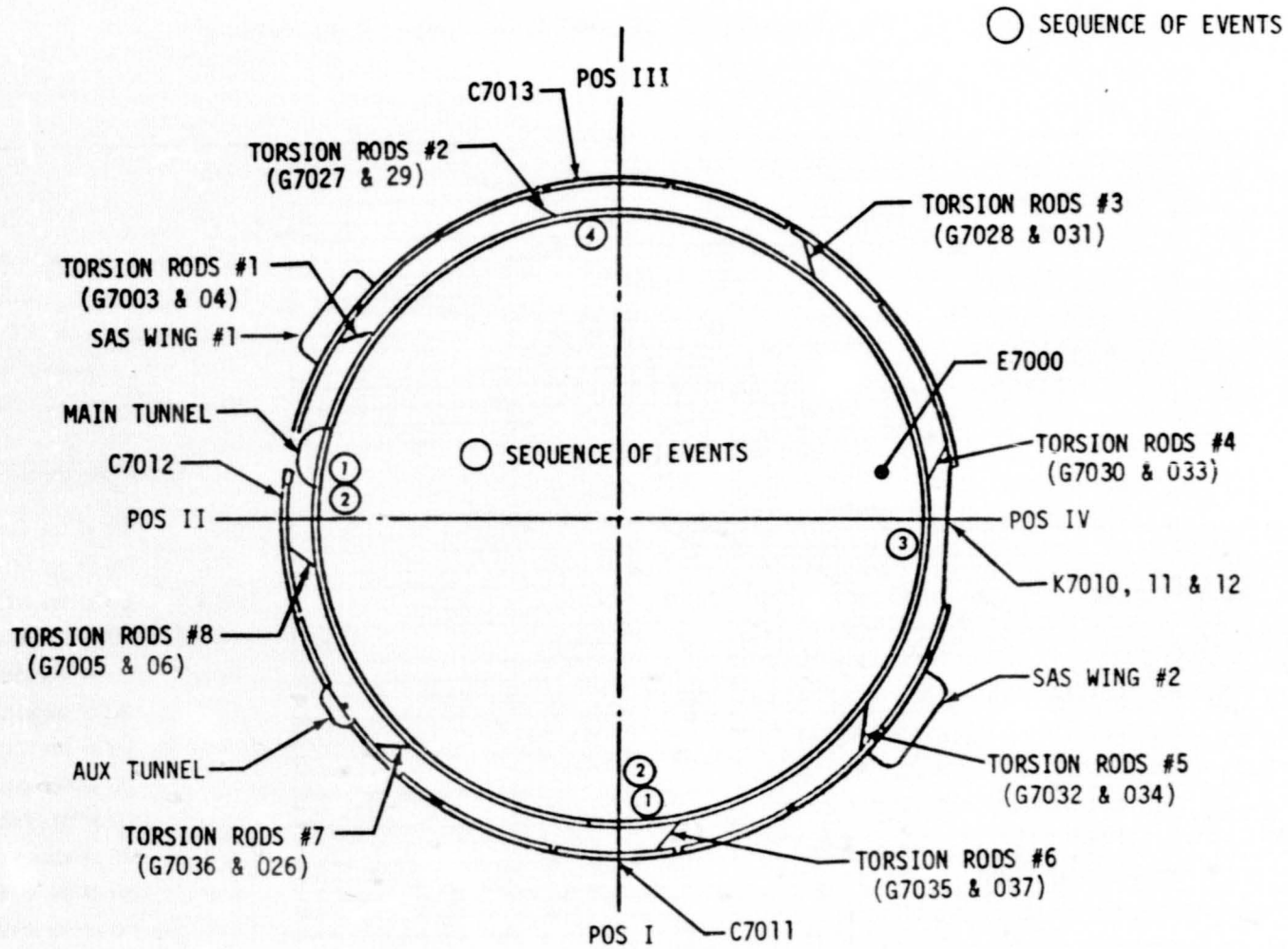


Figure 17-3. OWS Instrumentation Timeline for 63 Second Anomaly

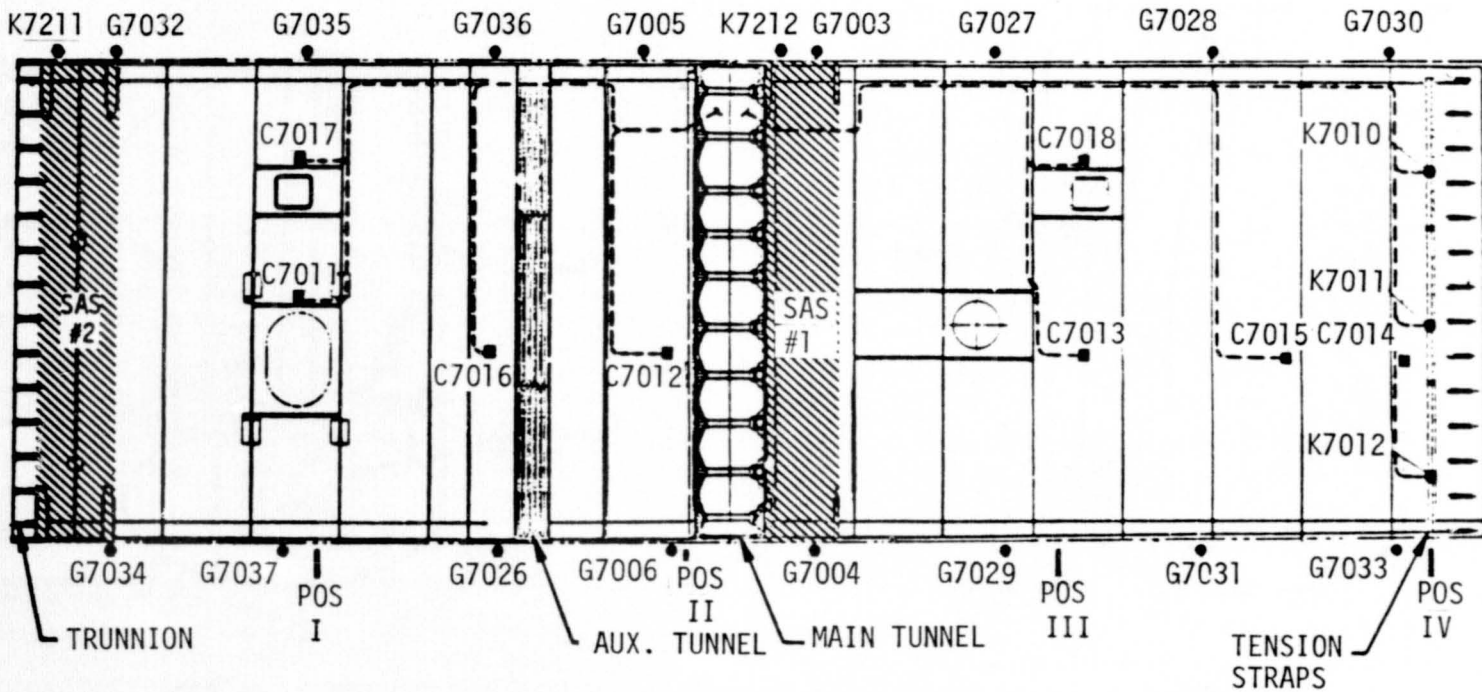
17-5



VIEW LOOKING FWD

OWS Instrumentation Location

Figure 17-4. OWS Instrumentation Location



TENSION STRAPS

K7010
K7011
K7012

SAS DEPLOY

K7211
K7212

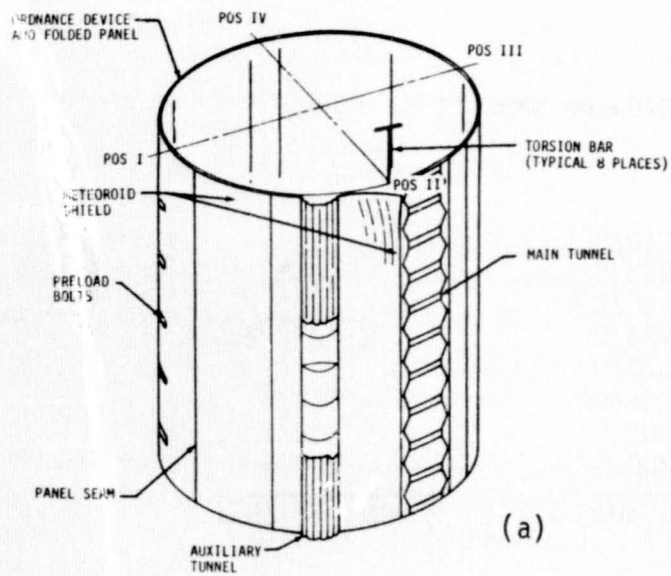
TORSION RODS

G7002 G7032
G7004 G7034
G7027 G7035
G7029 G7037
G7028 G7036
G7031 G7026
G7030 G7005
G7033 G7006

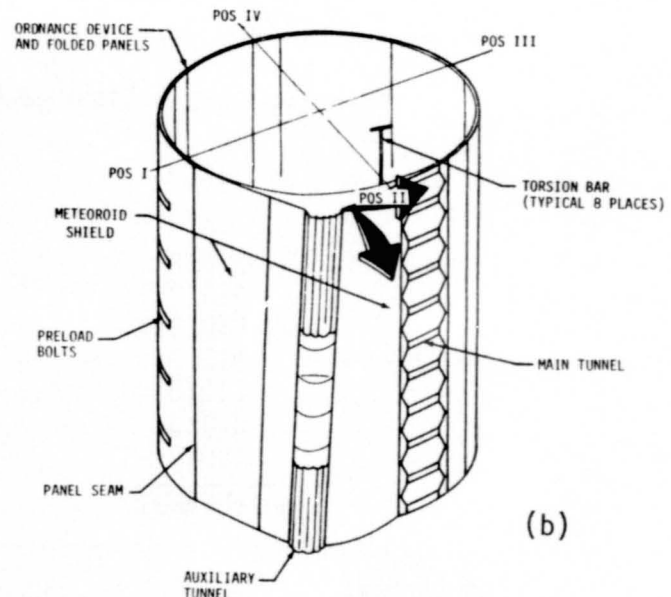
TEMPERATURES

C7011
C7012
C7013
C7014
C7015
C7016
C7017
C7018

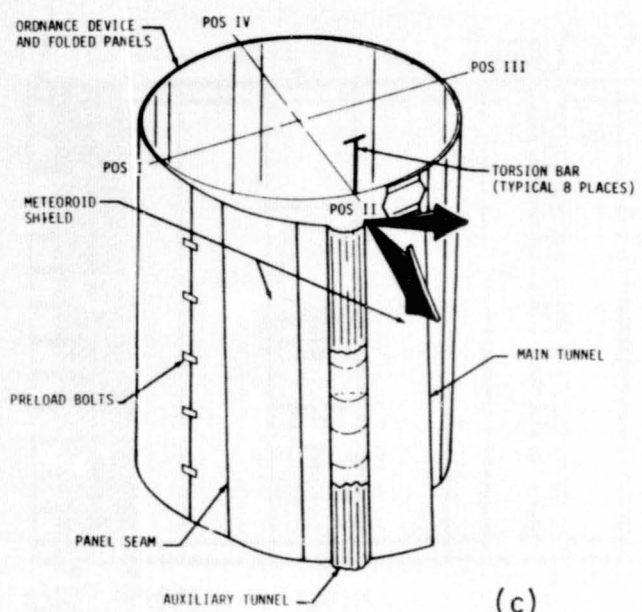
Figure 17-5. OWS Meteoroid Shield Instrumentation External View



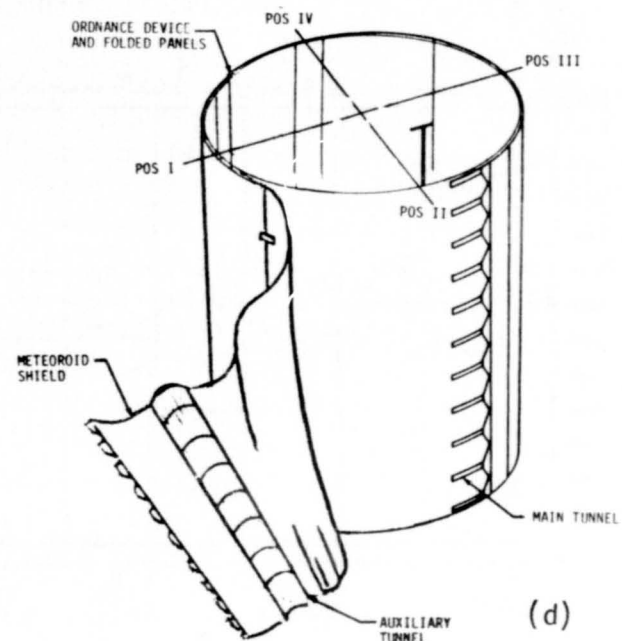
(a)



(b)



(c)



(d)

Figure 17-6. OWS Configuration During Meteoroid Shield Structure Failure (Artist Concept)

Table 17-1. Meteoroid Shield Failure Event Correlation

EVENT	LOCAL INDICATION (SEC)	LV INDICATION (SEC)	MOST PROBABLE TIME OF OCCURRENCE
First Structural Response	62.760-62.779 (E-7000, C-7011)	Inconclusive	62.760
Major Failure Begun	62.760-62.899 (E-7000, K-7011)	62.797-62.807 (S-II EAS*, IU Roll)	62.800
Front Shield Separated	62.867-62.899 (K-7010, K-7011, K-7012)	62.857-62.887 (S-II EAS*)	62.882
Shield/Wing 2 Interference	Inconclusive	62.887-62.907 (S-II EAS*)	62.902
Wing 2 Aft Separation	62.813-62.913 (K-7211)	62.907-62.937 (S-II EAS*)	62.910
Shield/Wing 2 Cleared	Inconclusive	62.917-62.937 (S-II EAS*)	62.925
Event Complete	62.939-63.289 (C-7013, G-7004)	62.957-62.977 (S-II EAS*)	62.965

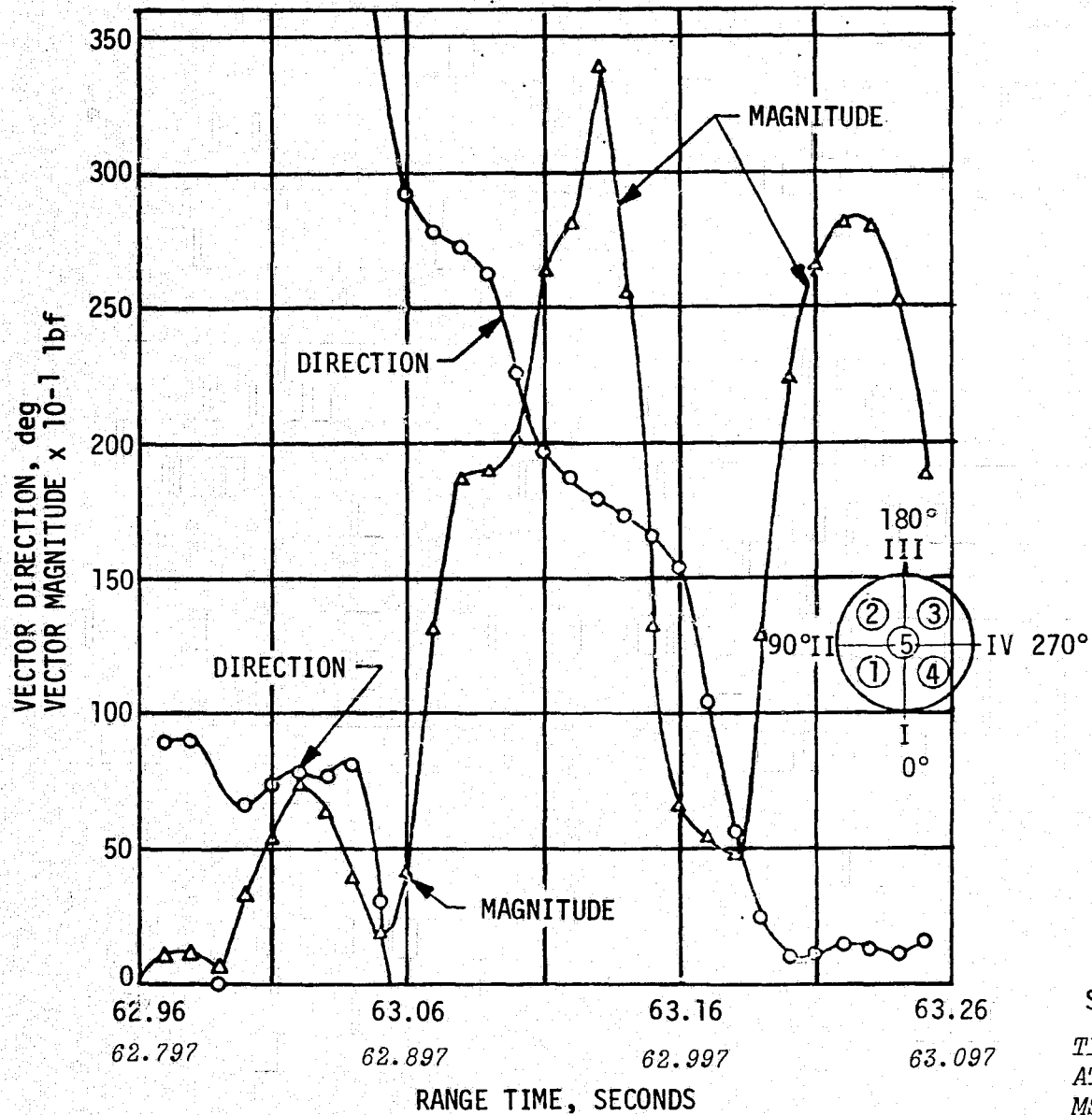
*163 millisecond delay for structural transmission of transient from Work Shop to EAS has been removed to allow direct comparison of OWS and EAS data.

At 62.807 seconds the vehicle reacted to an abnormal clockwise torque which increased the roll rate to 2.4 deg/s (Figure 17-2). At 62.797 seconds, the the S-II engine actuation system (EAS) responded to a force in the outboard direction between vehicle positions I and II (Figure 17-4 and 17-7). Figure 17-6b depicts the OWS configuration at about 62.8 seconds.

At 62.899 seconds the first MS tension strap (K7011, Figure 17-3) was indicated failed. The S-II EAS (Figure 17-7) also indicates that the first significant force was applied to the vehicle in an outward direction, beginning at 62.83 seconds. The initial force peak occurred at 62.857 seconds at about 80° from Position I toward Position II. Figure 17-6c depicts the OWS configuration at this time. It is believed that this force buildup caused the MS to slip around the OWS, releasing the tension strap indications. At the same time the MS began to peel away from the OWS as indicated by the reduction in magnitude from 62.857 to 62.887 seconds and direction change from 80° toward 0° (Figure 17-7).

A closeup photograph of the OWS exterior, taken during the SL-2 CSM fly-around, is shown in Figure 17-8. The gold coated mylar covering, which is exposed because of the missing MS, shows surface markings that could have been made by circumferential movement of the MS during structural failure.

At 62.887 seconds the amplitude of the force begins to increase with the direction changing from vehicle Position I toward Position IV. This is probably the result of the MS continuing to peel around the OWS as depicted in Figure 17-6d. Between 62.907 and 62.937 seconds the MS encounters the SAS Wing No. 2 causing premature deployment. At approximately 62.925 seconds the MS cleared SAS Wing No. 2 and continued to peel toward Position III. At 62.939 seconds temperature measurement C7013, located at Position III, was still normal.



S-II EAS RAW DATA
 TIME OF APPLIED FORCE
 AT OWS (REFLECTS 163
 MSEC TIME DELAY FOR
 STRUCTURAL TRANSMISSION)

Figure 17-7. S-II Stage Engine No. 1 Actuator Response to the 63-Second Transient

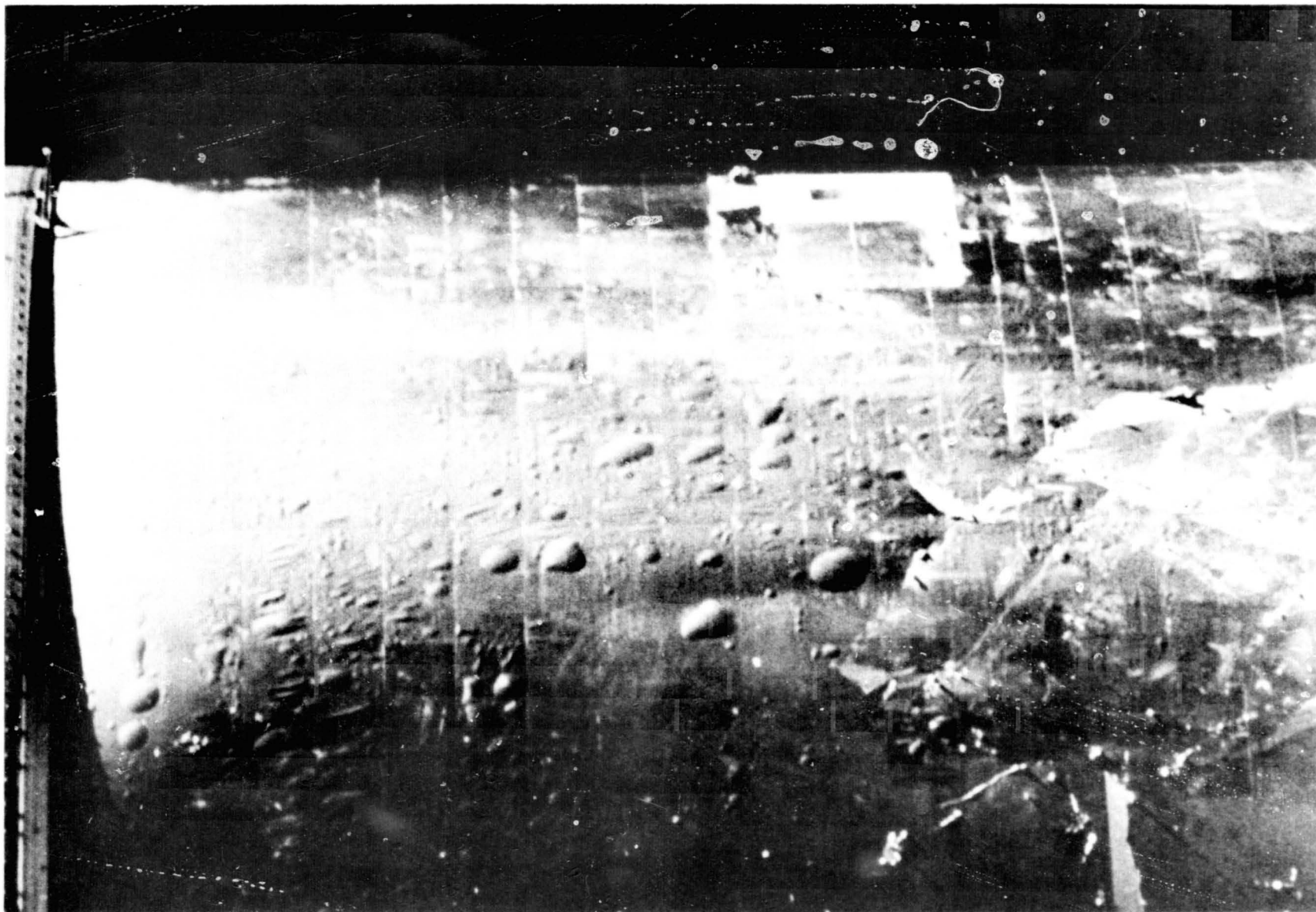


Figure 17-8. OWS Exterior During SL-2 CSM Flyaround Inspection

The MS continued to peel counterclockwise around the vehicle with the force peaking at 62.951 seconds at Position III (Figure 17-7). This peak was probably due to the tearing away of 75 percent or more of the deployed MS by the air stream. This tearing probably occurred between torsion rods 2 and 3. Afterwards the vehicle continued a 4 Hz damped response to the third bending mode, which is highly sensitive to radial excitation in the OWS area (refer to paragraph 7.2.4).

The total extent of the damage was almost certainly achieved prior to 63.289 seconds as indicated by the anomalous torque reading on aft torsion rod #1 located between Position III and Position II (Figure 17-4). The partially deployed positions of torsion rods #1 forward (8°), #1 aft (18°) and #2 forward (85°) at 65 seconds also indicate that the tearing occurred around Position III and that a portion of the MS remained between Position III and II, probably as a result of being entangled with SAS Wing No. 1. The tearing of the shield occurring at Position III accounts for the fact that SAS Wing No. 1 was not prematurely released as was SAS Wing No. 2. Insufficient portions of the shield remained to apply the required force to cause premature deployment. Table 17-2 is a listing of the position of the MS torsion rods at 65 seconds.

Table 17-3 is a sequential summary listing of events occurring throughout the space vehicle and OWS that might be related to the 63 second anomaly.

An estimate of the disturbing forces to produce the observed IU body mounted accelerometer measurements was developed using a dynamic simulation. The best estimate of force and total impulse which provides a simulation match with the observed data is shown in Figure 17-9. This supports Figure 17-7 which indicated that the peak forces started in the area of SAS Wing No. 2. This is a tangential force located at SAS Wing No. 2 of approximately 290,000 N (65,200 lbf) with a total impulse of 26,100 N-sec (5870 lb sec). Figures 17-10 and 17-11 show a comparison of the measured and simulated data for the pitch and yaw acceleration and the roll rate. These figures show a good agreement between the trends of the measured data and simulation results. Some of the differences in the pitch acceleration appear to be due to higher modes and possibly some beating between adjacent modes.

17.3 593 SECOND DISTURBANCE

At approximately 593 seconds, following S-II/SWS separation, another transient was indicated on the IU and OWS instrumentation. Table 17-4 is

Table 17-2. OWS Meteoroid Shield Torsion Rod Indicated Positions

FORWARD TORSION ROD	INDICATED POSITION PRIOR TO 60 SEC (DEG)	INDICATED POSITION AT 65 SEC (DEG)	DESIGN POSITION WHEN FULLY DEPLOYED (DEG)
1	0	8	148
2	0	85	145
3	0	173	156
4	0	175	163
5	0	-	163
6	0	165	156
7	0	170	145
8	0	145	148
AFT TORSION ROD			
1	0	18	148
2	0	160	145
3	0	165	156
4	0	180	163
5	0	165	163
6	0	163	156
7	0	165	145
8	0	135	148

Table 17-3. Sequential Summary of Events Related to 63-Second Anomaly

MEASUREMENT NUMBER	EVENT, MEASUREMENT DESCRIPTION AND LOCATION	TIME OF INDICATION, SECONDS		PEAK AMPLITUDE	REMARKS
		1ST IND.	PEAK		
N034-225	S-II ANTENNA REFLECTED POWER INCREASE	59.87			REFLECTED POWER INCREASED
G7008-432	POSITION - SOLAR ARRAY SYSTEM, WING 1	60.87			7% CHANGE DOWN (1 SAMPLE ONLY)
	POSITION - SOLAR ARRAY SYSTEM, WING 1	65.67			3% CHANGE DOWN (1 SAMPLE ONLY)
	MACH 1	61.1			
E7000-436	VIBRATION ORBITAL WORK SHOP (OWS) FILM VAULT LONGITUDINAL	62.76	63.0	+0.35 G	
C7011-434	TEMPERATURE - METEOROID SHIELD, EXTERIOR, NUMBER 1	62.78		MID TO DOWN	PEGGED
A2-603	(IU) ACCELERATION LONGITUDINAL	62.83	63.1	+0.07 G	
A7-603	(IU) ACCELERATION YAW	62.80	63.1	+0.38 G	
R6-602	ANGULAR VELOCITY ROLL CONTROL (IU)	62.80			10 SPS
E2-530	VIBRATION, X-AXIS, PAYLOAD SHROUD AT ATM ATTACH POINT	62.81	63.1	+0.2 G	
E1-505	VIBRATION, X-AXIS, STRUCTURAL TRANSITION SECTION, AFT BULKHEAD STRINGER 23, (MDA)	62.82	63.2	+0.2 G	
E81-219	RADIAL VIBRATION FORWARD SKIRT STRINGER (S-II)	62.82	63.09	+12G	
R4-602	ANGULAR VELOCITY PITCH CONTROL (IU)	62.87			12 SPS
H10-603	Z ACCELEROMETER PICKUP ST-124M (IU)	62.85	63.2	+0.4°	
H12-603	Y ACCELEROMETER PICKUP ST-124M (IU)	62.85	62.9	+0.4°	
D167-204	ENGINE 4 PITCH, ACTUATOR DELTA PRESSURE (S-II)	62.85			
C7012-434	TEMPERATURE - METEOROID SHIELD, EXTERIOR, NUMBER 2	62.89			
B1-530	ACOUSTIC, INTERNAL, PAYLOAD SHROUD AT ATM ATTACH POINT	62.93	63.0	0.004 PSI	LITTLE DEVIATION FROM NORMAL

Table 17-3. Sequential Summary of Events Related to 63-Second Anomaly (Continued)

MEASUREMENT NUMBER	EVENT, MEASUREMENT DESCRIPTION AND LOCATION	TIME OF INDICATION, SECONDS		PEAK AMPLITUDE	REMARKS
		1ST IND.	PEAK		
K7011-434	EVENT - METEOROID SHIELD, TENSION STRAP 2, SECURED	62.90			FULL SCALE SHIFT
E40-603	VIBRATION, UPPER MOUNTING RING, LOCATION 21, PERPENDICULAR	62.90	63.2	+9 G	
K7010-434	EVENT - METEOROID SHIELD TENSION STRAP 1, SECURED	62.90			FULL SCALE SHIFT
H11-603	X ACCELEROMETER PICKUP ST-124M (IU)	62.91	63.2	+0.2°	
K7211-426	EVENT - SOLAR ARRAY SHIELD WING 2, FAIRING, SECURED	62.91			120 SPS
D167-201	ENGINE 1, PITCH, ACTUATOR, DELTA PRESSURE (S-II)	62.99			FULL SCALE SHIFT
D167-202	ENGINE 2, PITCH, ACTUATOR, DELTA PRESSURE (S-II)	62.95			120 SPS
B3-219	ACOUSTIC, FORWARD SKIRT BOUNDARY LAYER (S-II)	62.96	63.1	.27 PSI	
D266-206	LOX SUMP PRESSURE (S-II)	62.96	63.06	20 PSIA	
E361-206	VIBRATION, ENGINE 1 GIMBAL PAD, LONGITUDINAL (S-II)	62.97	63.07	-3.4 G	
E363-206	VIBRATION, LOX/SUMP PREVALVE, LONGITUDINAL (S-II)	62.97	63.10	+8 G	
K7012-434	EVENT - MS, TENS STRAP 3, SECURED	62.97	63.05	-10 G	FULL SCALE SHIFT
E363-206	VIBRATION, ENGINE 5 THRUST PAD, LONGITUDINAL (S-II)	62.98			

Table 17-3. Sequential Summary of Events Related to 63-Second Anomaly (Continued)

MEASUREMENT NUMBER	EVENT, MEASUREMENT DESCRIPTION AND LOCATION	TIME OF INDICATION, SECONDS		PEAK AMPLITUDE	REMARKS
		1ST IND.	PEAK		
D166-204	ENGINE 4, YAW, ACTUATOR, DELTA PRESSURE (S-II)	63.00			120 SPS
D267-201	ENGINE 1, LOX PUMP INLET PRESSURE (S-II)	62.99	63.5		
D166-201	ENGINE 1, YAW ACTUATOR, DELTA PRESSURE (S-II)	63.01	63.5		
A4-120	ACCELERATION, PITCH (S-IC)	63.00	63.6	+0.42 G	
R5-602	ANGULAR VELOCITY YAW CONTROL (IU)	63.05			10 SPS
D166-202	ENGINE 2, YAW, ACTUATOR DELTA PRESSURE (S-II)	63.11			12 SPS
D167-203	ENGINE 3, PITCH, ACTUATOR DELTA PRESSURE (S-II)	63.15			12 SPS
E23-115	VIBRATION, UPPER THRUST RING, LONGITUDINAL (S-IC)		63.34	+8 G	NO CLEAR FIRST INDICATION.
C7014-434	TEMPERATURE - METEOROID SHIELD, EXTERIOR, NUMBER 4	63.53		MID TO UP	PEGGED
C7016-434	TEMPERATURE - METEOROID SHIELD, EXTERIOR, NUMBER 6	63.63		MID TO DOWN	PEGGED
C7018-434	TEMPERATURE - METEOROID SHIELD, EXTERIOR, NUMBER 8	63.69		MID TO DOWN	PEGGED
C7013-434	TEMPERATURE - METEOROID SHIELD, EXTERIOR NUMBER 3	63.74		MID TO DOWN	PEGGED
C7013-434	TEMPERATURE - METEOROID SHIELD, EXTERIOR NUMBER 7	63.79		MID TO DOWN	PEGGED
C7015-434	TEMPERATURE - METEOROID SHIELD, EXTERIOR NUMBER 5	64.09		MID TO UP	PEGGED

17-17

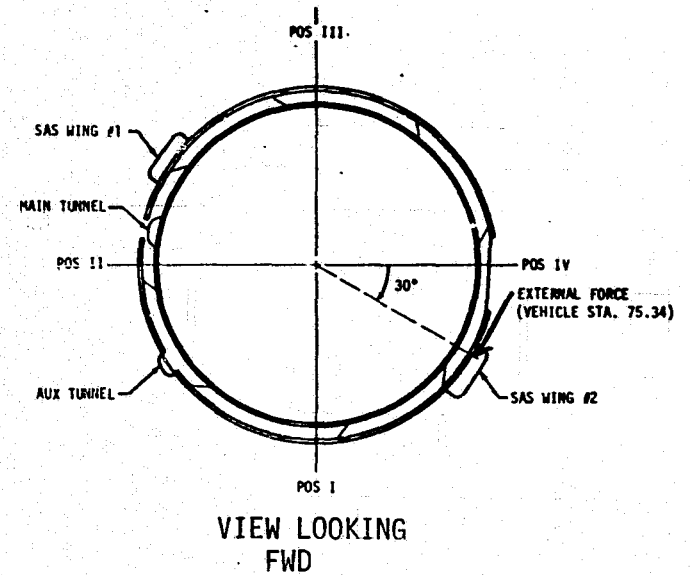
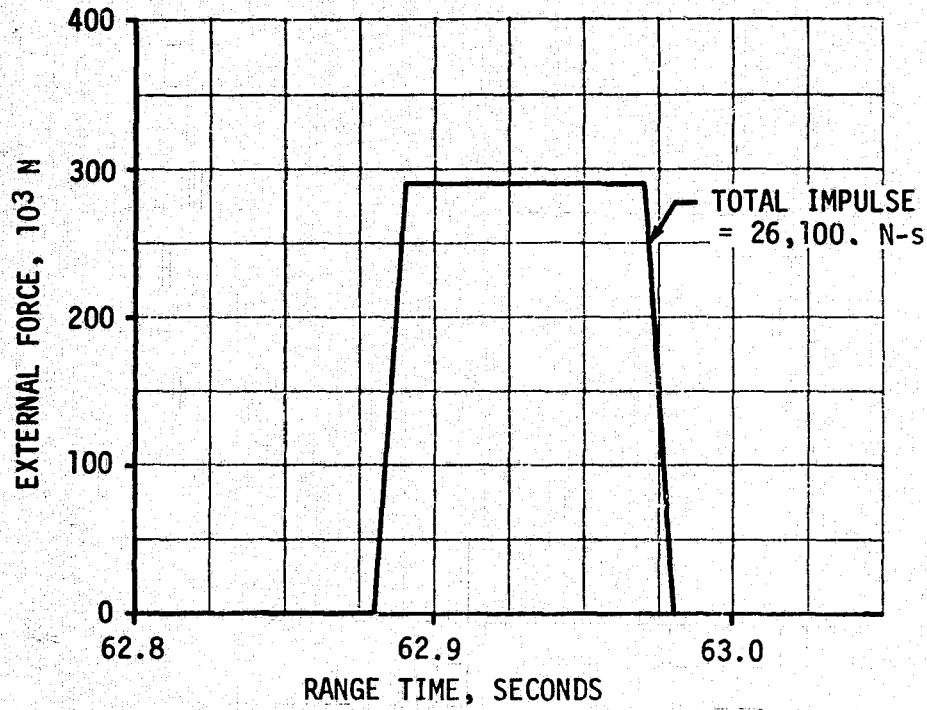


Figure 17-9. Simulated Force and Total Impulse

- ▽ SIMULATED FORCE INTRODUCED, 62.88 SECONDS
- ▽ SIMULATED FORCE REMOVED, 62.98 SECONDS
- ▽ END ROLL MANEUVER

— ACTUAL (RAW DATA WITH BIASES REMOVED)
 - - - SIMULATED

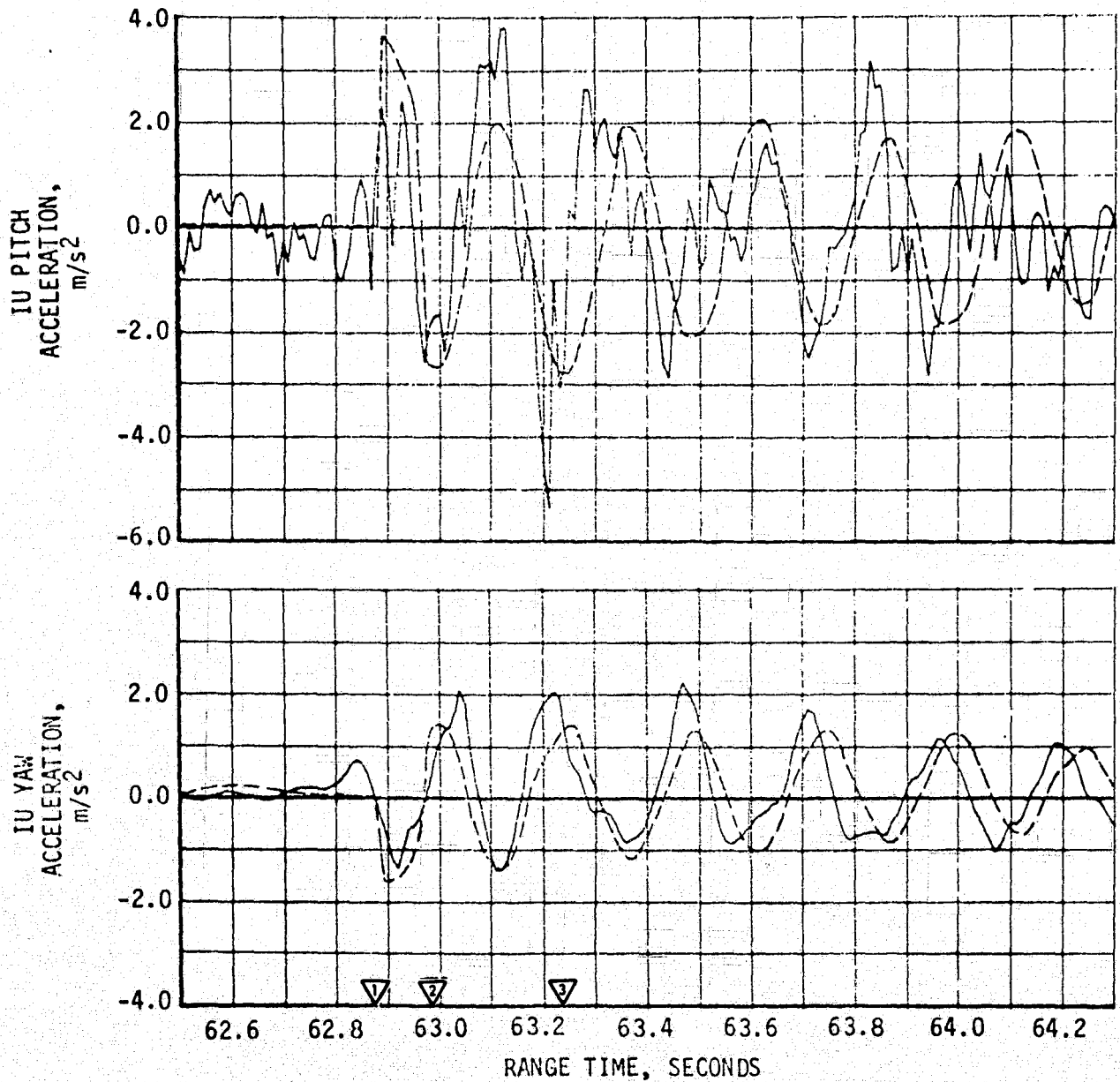


Figure 17-10. Comparison of Actual and Simulated Lateral IU Acceleration During 63-Second Anomaly

- ▽ SIMULATED FORCE INTRODUCED, 62.88 SECONDS
- ▽ SIMULATED FORCE REMOVED, 62.98 SECONDS
- ▽ END ROLL MANEUVER

- ACTUAL (RAW DATA WITH BIAS REMOVED)
- - - ACTUAL DATA FILTERED TO 1.0 HZ
- · · · · SIMULATED

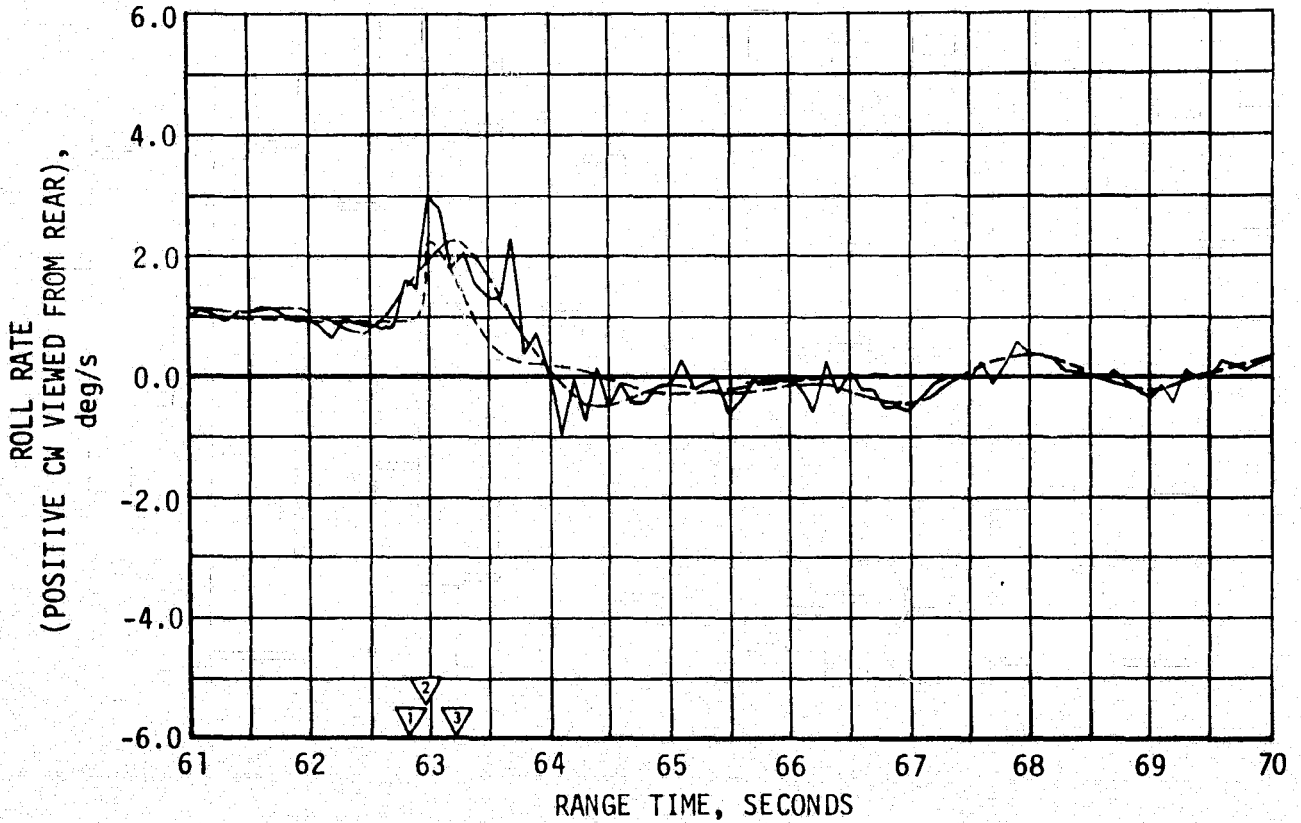


Figure 17-11. Comparison of Actual and Simulated Roll Rate During 63-Second Anomaly

Table 17-4. Sequential Summary of Events Related to 593-Second Anomaly

MEASUREMENT NUMBER	MEASUREMENT DESCRIPTION AND LOCATION	TIME OF INDICATION, SECONDS		PEAK AMPLITUDE	REMARKS
		1ST IND.	PEAK		
R5-602	IU YAW CONTROL	591.2			
R4-602	IU PITCH CONTROL	591.2			
E1-505	VIBRATION, X-AXIS, STRUCTURAL TRANSITION SECTION AFT BULKHEAD, STRINGER 23 PAYLOAD (MDA)	592.7		+0.1 G	NO AMPLITUDES OF SIZE
R6-602	IU ROLL RATE	592.5			
A7-603	IU YAW ACCELERATION	592.72	593.1		
A2-603	IU LONGITUDINAL ACCELERATION	592.8			
A6-603	IU PITCH ACCELERATION	592.82	593.5	+0.46 G	120 SPS
E40-603	VIBRATION, UPPER MOUNTING RING, LOCATION 21, PERPENDICULAR (IU)	592.83	593.05	+17 G	
E2-530	VIBRATION, X-AXIS, PAYLOAD SHROUD AT ATM ATTACH POINT	593.05		+0.3 G	NO AMPLITUDE CHANGE OF SIGNIFICANCE
H10-603	Z ACCELEROMETER PICKUP ST-124M (IU)	593.05	593.07		
H12-603	Y ACCELEROMETER PICKUP ST-124M (IU)	593.05	593.09		
H11-603	X ACCELEROMETER PICKUP ST-124M (IU)	593.06	593.1		
E7000-436	VIBRATION, ORBITAL WORK SHOP (OWS) FILM VAULT LONGITUDINAL	593.06			VERY SMALL AMPLITUDES
C7243-433	TEMPERATURE - SOLAR ARRAY SYSTEM, WING 2, SECTION 1, PANEL 3	593.1	593.75	MID TO UP	PEGGED AT 593.75
C7249-433	TEMPERATURE - SOLAR ARRAY SYSTEM, WING 2, SECTION 3, PANEL 3	594.0		MID TO DOWN	PEGGED
C7245-433	TEMPERATURE - SOLAR ARRAY SYSTEM, WING 2, SECTION 2, PANEL 3	595.1		MID TO DOWN	PEGGED
G7008-433	POSITION - SOLAR ARRAY SYSTEM, WING 1, SECTION 1	603.25			9% CHANGE

a sequential listing of events that may be related to this anomaly. Rate gyros in the IU indicated pitch, yaw, and roll disturbances. The roll rate increase started about 592.5 seconds, 1.38 seconds after the structure was severed, approximately at the end of nominal retro-motor burn, and continued for approximately one second. At 592.83 seconds a severe shock was experienced by the IU, with approximately +17 g amplitude measured by E40-603 which is located near the root of the SAS Wing No. 2. About this time, probably between 593 and 594 seconds, all electrical signals from SAS Wing No. 2 were lost (Figure 17-12).

▽ RETRO FIRE 591.10
 ▽ S-II/SWS SEPARATION 591.1

LEGEND: NORMAL ●---UNKNOWN---● LOST

17-21

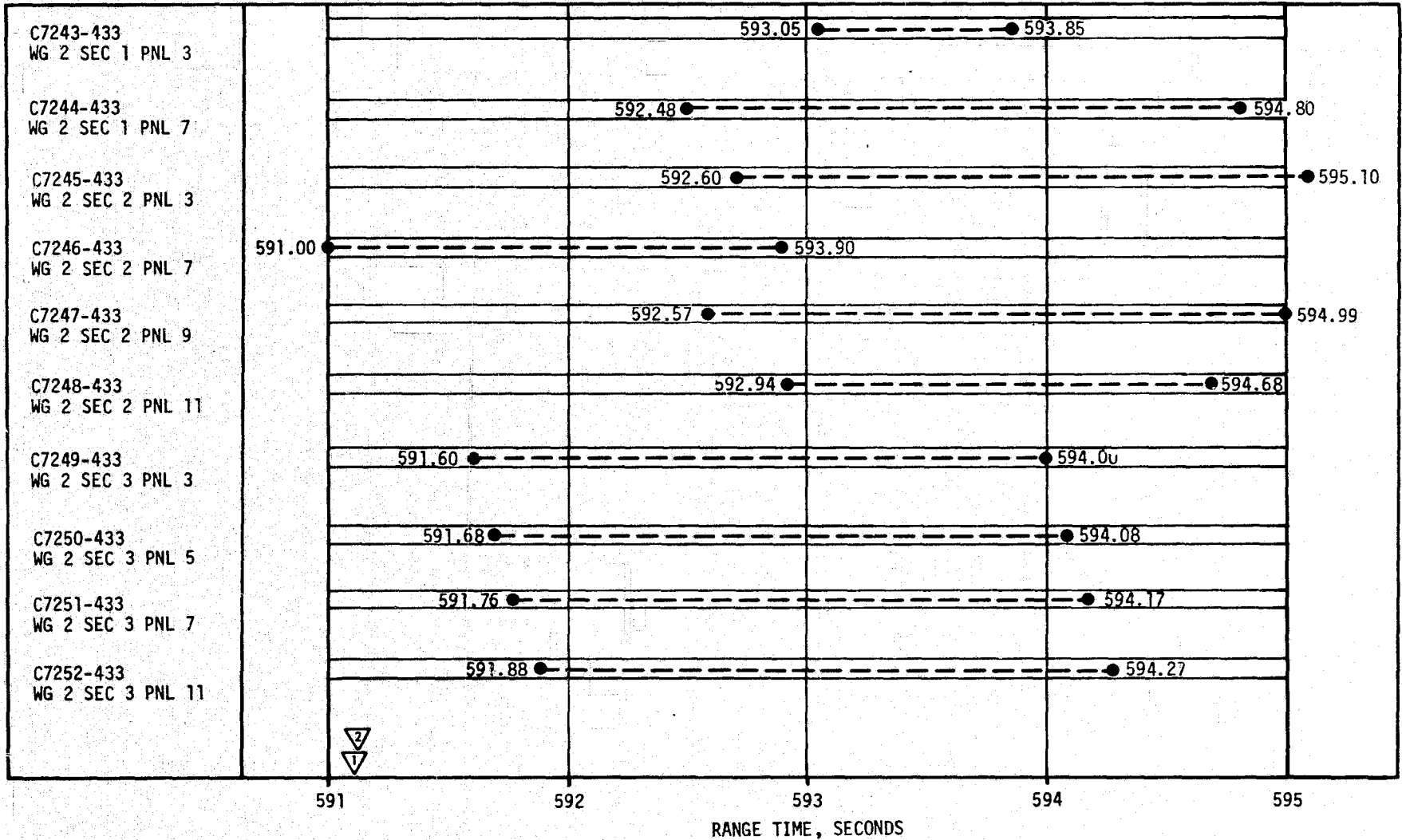


Figure 17-12. SAS Wing 2 Instrumentation Timeline for 593 Second Anomaly

Figure 17-13 presents the location of pertinent IU instrumentation and the general configuration of the OWS at the 593 second time period. Figure 17-14 shows the sequence of events during the 593 second anomaly as interpreted from measured vehicle motions and analyses of the aerodynamic forces acting on the vehicle during retro-fire. The following sequence of events is believed to have occurred. At 591.18 the retro-fire command was initiated and plume impingement caused a positive yaw rate buildup and a reduction in the positive pitch rate.

At 592.3 SAS Wing No. 2 deployed into the plume of the retro-motor in I-IV Quadrant, and began to affect rigid body rates causing a large negative roll rate and a small negative pitch rate increment. This impingement force deformed the arm as a cantilever beam in the -Z direction and produced a negative yaw rate which overcame the positive rate previously induced by plume impingement on the OWS. The retro impingement also accelerated the deployment rate of SAS Wing No. 2. These retro exhaust plume impingement forces are shown in Figure 17-13.

At 593.0 retro-fire ceased and basic rigid body rates became constant. The release of the side force on SAS Wing No. 2 which had stored strain energy in the SAS Wing No. 2 arm (and in the support point) in the direction normal to the hinge line, caused local structural dynamic activity. This shows up as oscillations in the roll, pitch, and yaw rates. The IU accelerometers, located at Position IV, also pickup a local transient at this time. The SAS Wing No. 2 arm continued to deploy.

At 593.4 a transient occurred in the yaw direction. This was possibly caused by the SAS Wing No. 2 arm as it progressed through its hinge stops.

At 593.9 the SAS Wing No. 2 arm transferred momentum to the SWS causing a negative increment in yaw rate and a smaller positive increment in pitch rate. The SAS Wing No. 2 was torn away from the OWS at this time. All electrical communication with SAS Wing No. 2 was lost at that time. Correlatable structural oscillations were observed in pitch and roll rates, and smaller oscillations in yaw rate. Yaw is primarily in the direction of the hinge, roll and pitch primarily normal to the hinge. The local structural dynamics were also picked up by the IU accelerometers at this time.

17.4 METEOROID SHIELD FAILURE

The suspected cause of the structural breakup of the meteoroid shield is air flow through the open areas of the auxiliary tunnel aft boot. Figures 17-15 and 17-16 show the initial and second phase responses of the auxiliary tunnel system to externally applied pressures causing inward air flow at the aft rubber boot as well as through the open areas of the aft fairing. The result of the air flow at the aft boot is to change the loading condition from a crushing pressure along the entire length of the

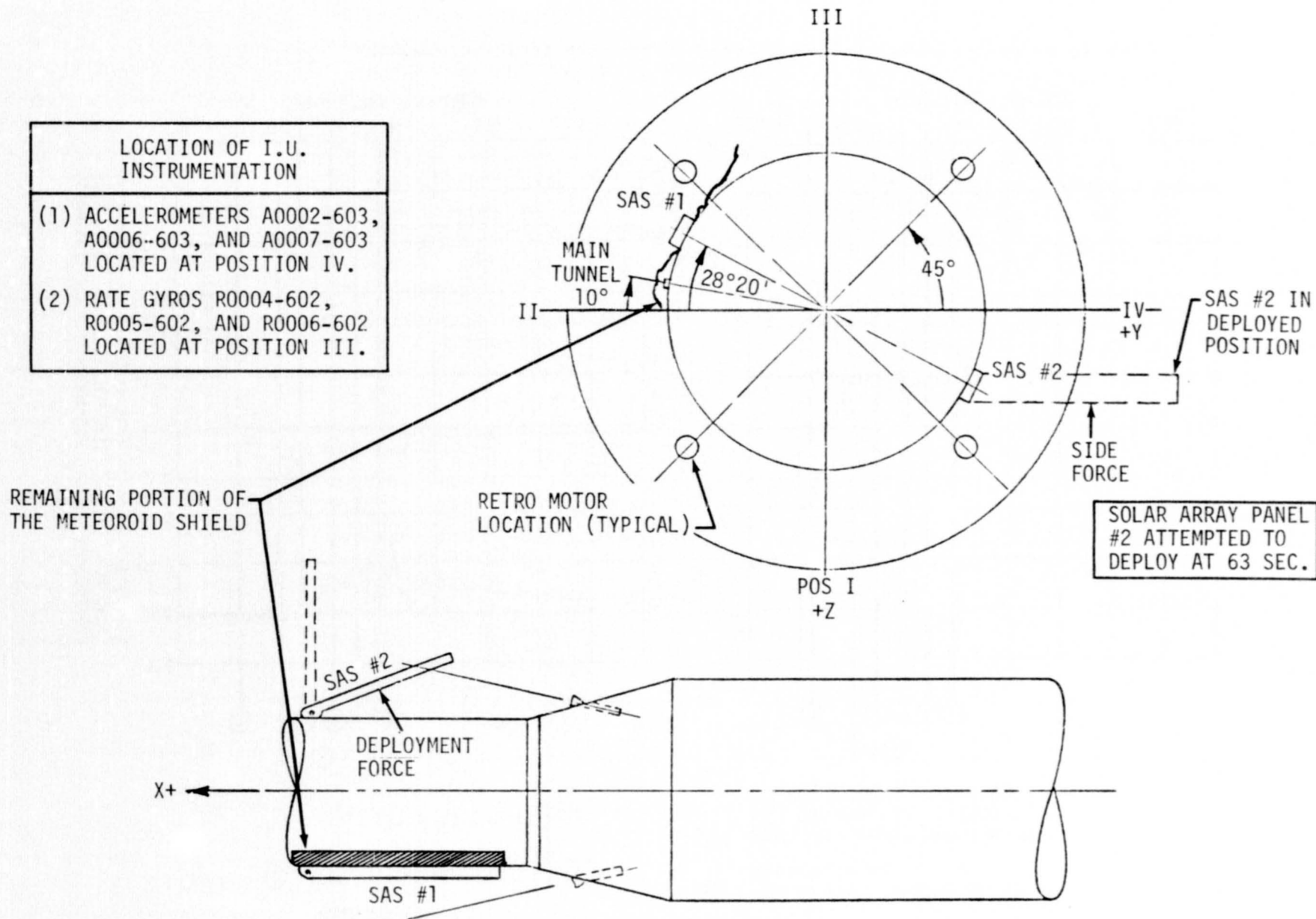


Figure 17-13. Instrumentation Location and OWS Configuration Near 593 Seconds

- ① (591.2) S-II RETRO FIRE COMMAND AND PLUME IMPINGEMENT ON FRAGMENTS IN QUADRANT II-III
- ② (592.3) SAS #2 DEPLOYED INTO RETRO PLUME AND EXERTS FORCE ON SWS
- ③ (593) END OF S-II RETRO FIRE
- ④ (593.4) INITIAL TRANSFER OF SAS MOMENTUM TO SWS
- ⑤ (593.9) FINAL TRANSFER OF SAS MOMENTUM TO SWS
- ⑥ (592) TACS SYSTEM OPERATING TO NULL OUT RATES AND ATTITUDES INDUCED BY RETRO IMPINGEMENT

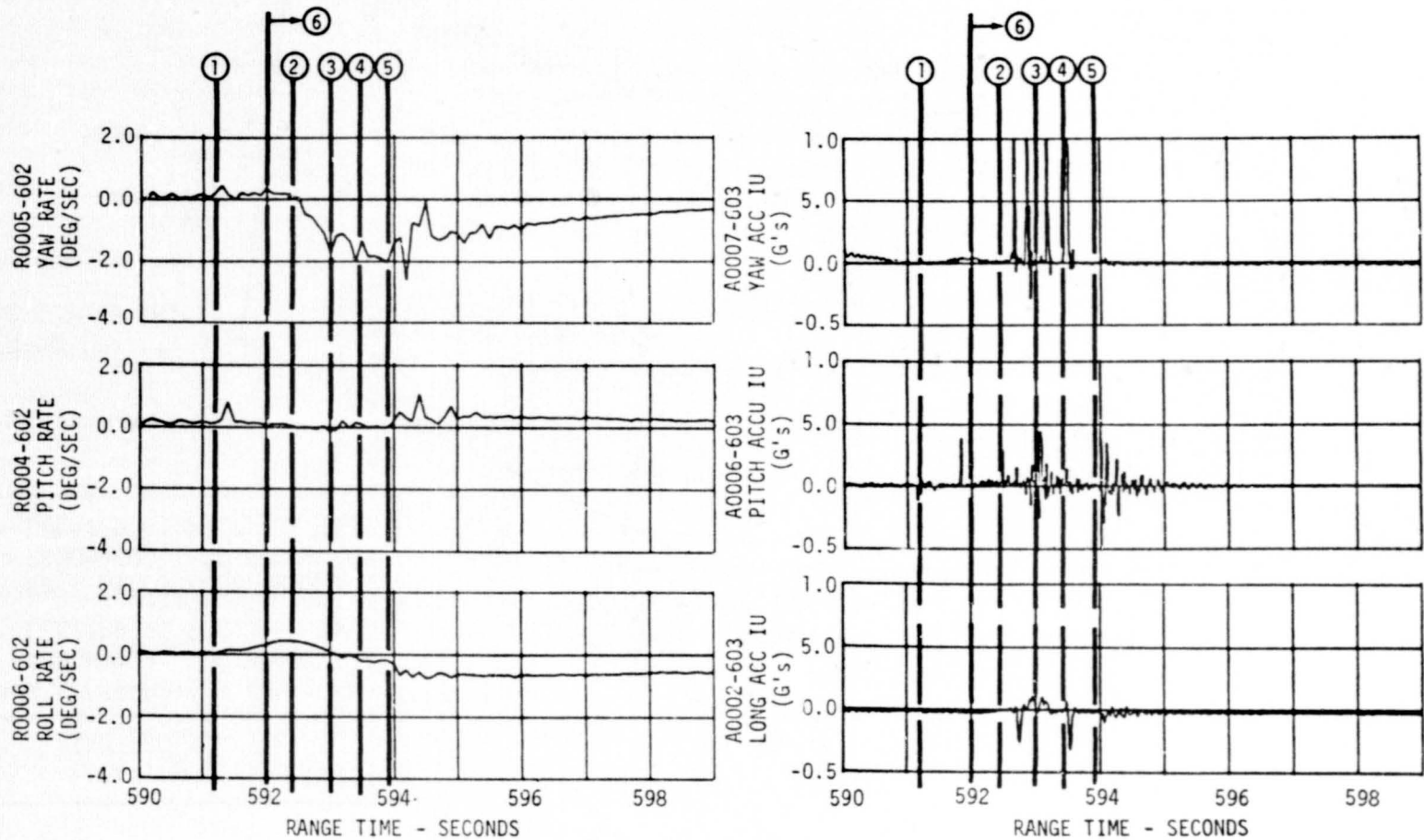


Figure 17-14. Interpretation of IU Control Measurements During 593-Second Period

INITIAL PHASE

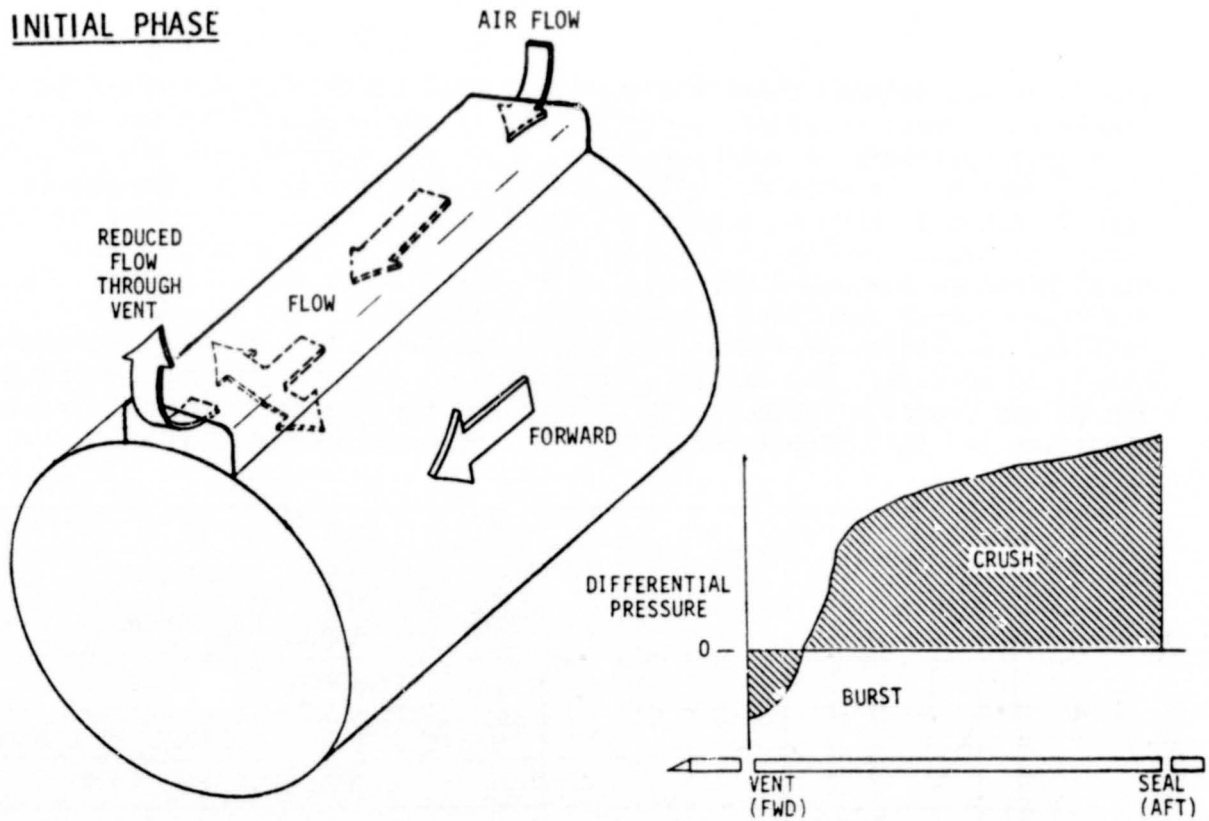


Figure 17-15. Meteoroid Shield-Flow Through Auxiliary Tunnel

SECOND PHASE

- FLOW THROUGH GAP - UNDER SHIELD
- UNSTABLE AEROELASTIC CONDITION

- Tunnel Unseats
- Shield/Tank Separates
- Pressure Fills Shield/Tank Cavity
- Deflection-Pressure Relationship Diverges
- Meteoroid Shield Ruptures

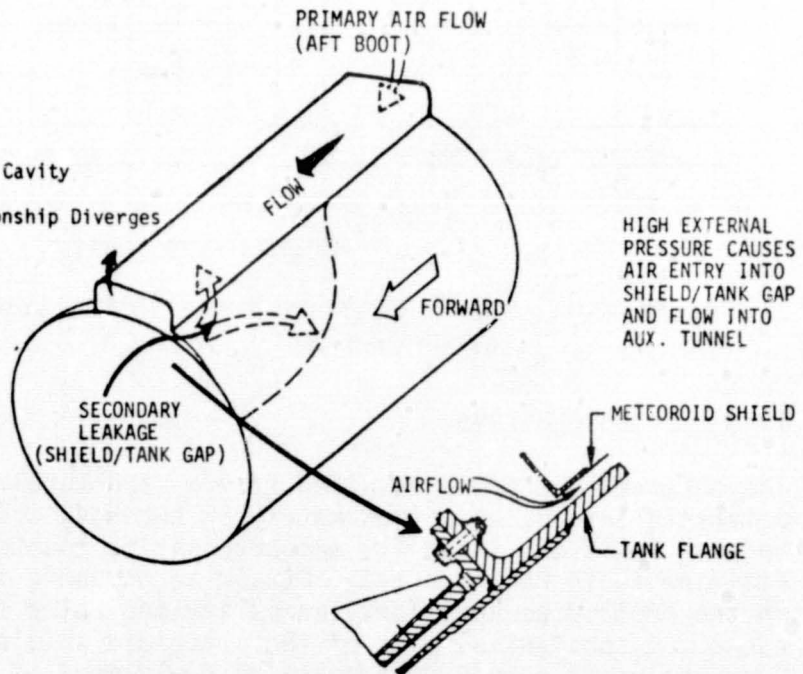


Figure 17-16. Meteoroid Shield Response

tunnel to a condition where the forward tunnel section is subjected to a significant burst pressure. Only 0.2 psi is required to lift the shield. An average pressure of approximately 1.1 psi was applied over the forward 2 to 3 feet of the shield. This force is sufficient to lift the shield edge 2 inches or more as determined by structural test. Figure 17-17 shows the Auxiliary Tunnel Pressure Distribution at 63 seconds (Design Burst Pressure Maximum 0.025 psid). The air flow at the aft end of the auxiliary tunnel permitted a burst pressurization of the tunnel and resulted in lifting of the shield toward the free air stream at approximately 63 seconds. Ram air at approximately 1.05 Mach entered underneath the MS and caused a rapid pressurization and the divergent load-deflection condition led to a structural failure of the meteoroid shield.

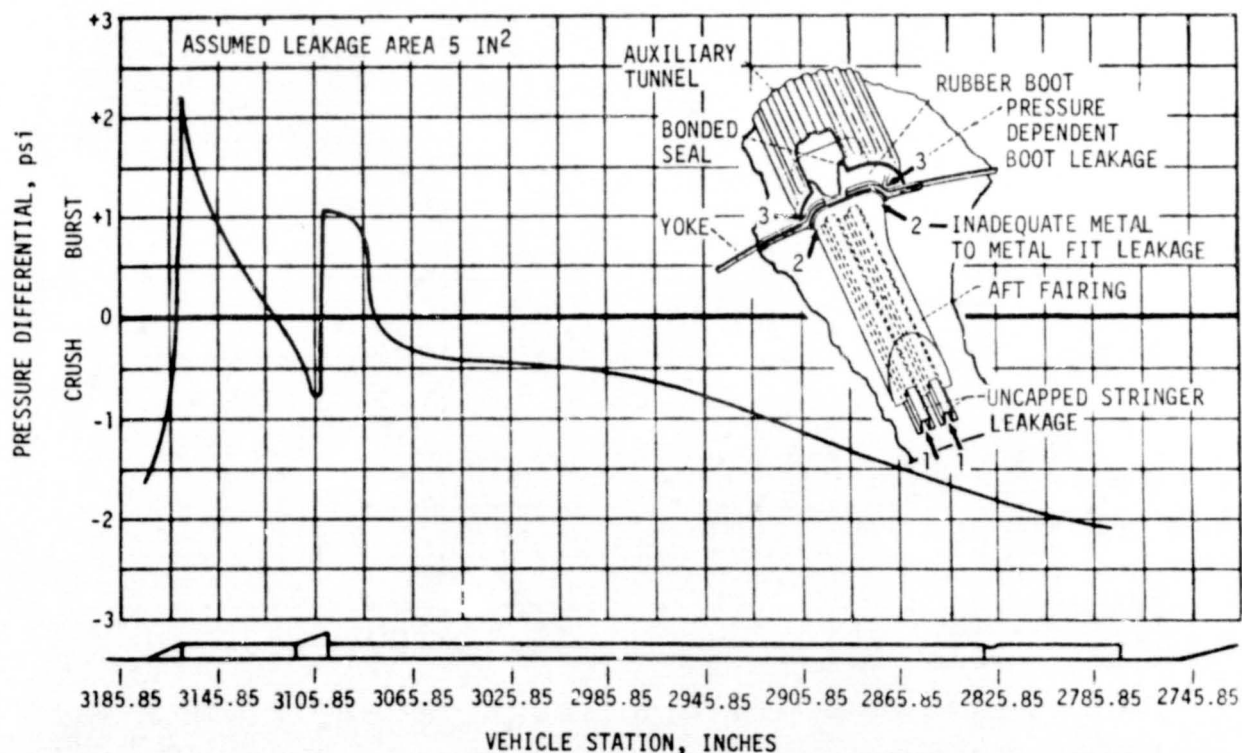


Figure 17-17. SL-1 Auxiliary Tunnel Calculated Pressure Distribution at 63 Seconds

17.5 CONCLUSIONS

The observed phenomena resulted from a structural failure of the OWS meteoroid shield, at approximately 63 seconds, originating in the Quadrant between Positions I and II, and propagating counter-clockwise through Position IV to Position III. Static aerodynamic forces near Mach 1 acting on the protruding auxiliary tunnel are indicated to be the most probable cause. A substantial part of the meteoroid shield apparently separated from the vehicle and forced partial deployment of SAS Wing No. 2. A

portion of the meteoroid shield remains between Positions II and III. These findings are confirmed by on-orbit pictures taken by the crew of Skylab-2. After S-II/SWS separation, the exhaust from the retro-motor in the I-IV Quadrant apparently impinged on the partially deployed SAS Wing No. 2 forcing it to the fully deployed position. As it hit the hinge stops, the vehicle experienced a +17 g shock, the wing sheared off, and electrical connections were severed.

Visual observation during rendezvous with the SWS by the Skylab-2 crew substantiated the conclusion from boost phase data that the OWS was operating with most of the meteoroid shield and all of SAS Wing No. 2 missing. It was also observed (verifying boost data) that SAS Wing No. 1 was being prevented from total deployment by the remaining portion of the meteoroid shield. The most probable cause of the failure was the application of burst pressure to the meteoroid shield which was designed for crush pressure only. The crush pressure only criteria would probably have been valid provided the aft end of the auxiliary tunnel had been sealed. An examination of the auxiliary tunnel aft boost design indicates that it was never intended to be an effective seal.

17.6 IMPACT OF ANOMALIES ON LAUNCH VEHICLE

The launch vehicle reacted properly to the external disturbance with no significant effect except for damage to the S-II second plane separation system. This failure is discussed in paragraph 9.5.2. The origin of the 63 and 593 second anomalies were in a unique payload and external to the launch vehicle; therefore, no launch vehicle corrective action is necessary.

17.7 INVESTIGATING COMMITTEE

On May 22, 1973, Dr. Fletcher, NASA Administrator, appointed Mr. Bruce T. Lundin, Director of Lewis Research Center, as chairman of a board to investigate the anomalies which occurred during the launch of Skylab-1. On May 18, 1973, Rocco A. Petrone, MSFC Director, authorized the Saturn Flight Evaluation Working Group (FEWG) to collect and analyze all flight data relative to the OWS meteoroid shield and solar array system anomalies during the launch phase of Skylab-1. The initial findings of the FEWG were submitted to the SL-1 Investigating Board on June 12, 1973, for consideration. The findings of the Investigating Board are documented in "NASA Investigation Board Report on the Initial Flight Anomalies of Skylab-1 on May 14, 1973," dated July 13, 1973.

The descriptions of the meteoroid shield failure contained in this document and the Investigating Board's Report are substantially the same. The differences are minor and are primarily due to refinement of the timed sequence of events. These differences can be attributed to MSFC and contractor analyses received by the FEWG after the Board's investigation had been completed.

APPENDIX A

ATMOSPHERE

A.1 SUMMARY

This appendix presents a summary of the atmospheric environment at launch time of the SA-513. The format of these data is similar to that presented on previous launches of Saturn vehicles to permit comparisons. Surface and upper level winds, and thermodynamic data near launch time are given.

A.2 GENERAL ATMOSPHERIC CONDITIONS AT LAUNCH TIME

During the launch of Skylab-1, the Cape Kennedy launch area was experiencing cloudy conditions with warm temperatures and gentle surface winds. These conditions resulted from a warm air mass covering most of Florida. This warm air was separated from a cold air mass over the rest of the South by a quasi-stationary front oriented east northeast - south southwest with its nearest point being about 90 miles northwest of KSC. Although the stationary front was weak, it still produced overcast conditions over Cape Kennedy prior to and during launch time (see Figure A-1). Surface winds in the Cape Kennedy area were light with a southerly component as shown in Table A-1. Wind flow aloft is shown in Figure A-2 (500 millibar level). The maximum wind belt was located north of Florida, giving less intense wind flow aloft over the Cape Kennedy area.

A.3 SURFACE OBSERVATIONS AT LAUNCH TIME

At launch time, total sky cover was 10/10, consisting of scattered cumulus at 0.7 kilometers (2,400 feet), scattered stratocumulus at 1.5 kilometers (5,000 feet), broken altocumulus at 3.7 kilometers (12,000 feet) and cirrus at 7.0 kilometers (23,000 feet). Surface ambient temperature was 303°K (86.0°F). During ascent the vehicle did pass through the cloud layers. No lightning was observed in the Cape Kennedy area. All surface observations at launch time are summarized in Table A-1. Solar radiation data for the day of launch is not available, due to miscalibration of the instruments.

A.4 UPPER AIR MEASUREMENTS

Data were used from three of the upper air wind systems to compile the final meteorological tape. Table A-2 summarizes the wind data systems used. Only the Rawinsonde and the Super Loki Dart meteorological rocket data were used in the upper level atmospheric thermodynamic analyses.

A.4.1 Wind Speed

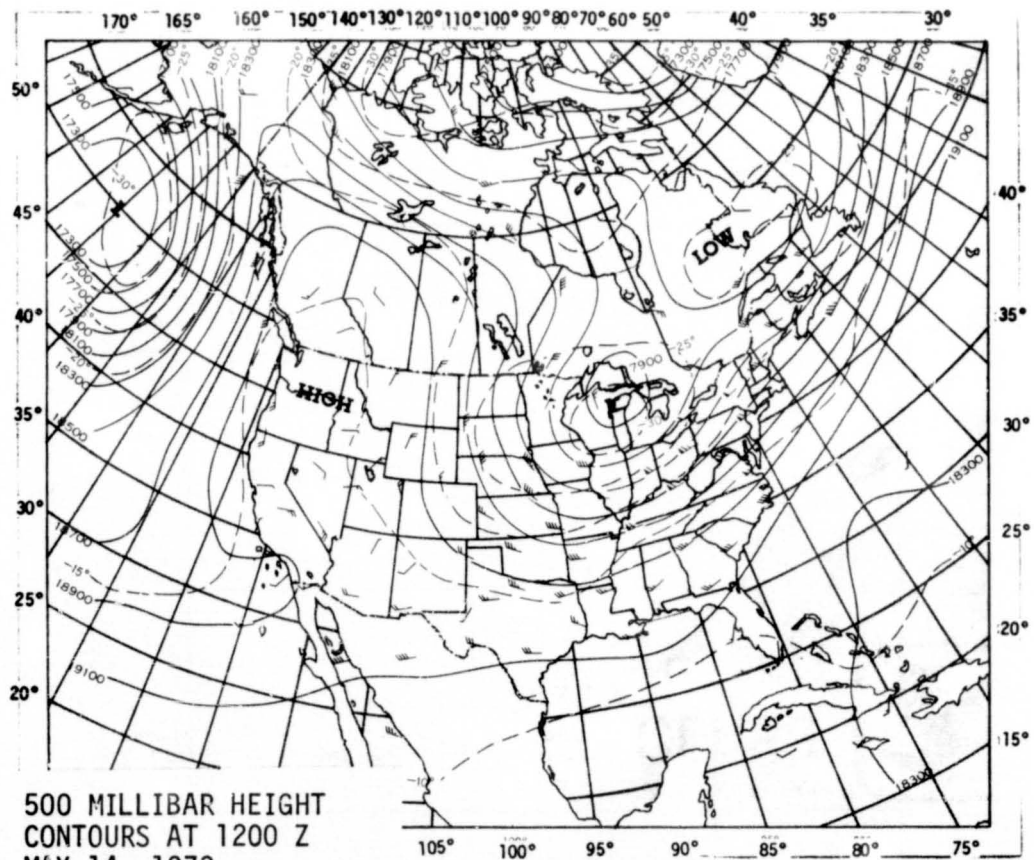
Wind speeds were light, being 3.0 m/s (5.8 knots) at the surface and

Table A-1. Surface Observations at SA-513 Launch Time

LOCATION	TIME AFTER T-0 (MIN)	PRES-SURE N/CM ² (PSIA)	TEM-PERATURE °K (°F)	DEW POINT °K (°F)	RELA-TIVE HUMID-ITY (%)	VISI-BILITY KM (STAT MI)	SKY COVER			WIND*	
							CLOUD AMOUNT (TENTHS)	CLOUD TYPE	HEIGHT OF BASE METERS (FEET)	SPEED M/S (KNOTS)	DIR (DEG)
NASA 150 m Ground Wind Tower. Winds measured at 10 m (32.8 ft)**	0	10.171 (14.75)	303.2 (86.0)	291.5 (65.0)	53	16 (10)	3	Cumulus	732 (2400)	2.5# (5.0)	262#
							3	Strato-cumulus	1524 (5000)		
							6	Alto-cumulus	3658 (12,000)		
							5	Cirrus	7010 (23,000)		
							10###				
Cape Kennedy AFS*** Surface Measurements	150	10.166 (14.74)	300.6 (81.3)	294.9 (71.1)	71	--	--	--	3.0## (6.0)	140##	
Pad 39A Lightpole SE 18.3 m (60.0 ft)**	0	--	--	--	--	--	--	--	5.1 (10.0)	155	
Pad 39A LUT E 161.5 m (530 ft)**	0	--	--	--	--	--	--	--	5.1 (10.0)	177	

* Instantaneous readings at T-0, unless otherwise noted.
 ** Above natural grade.
 *** Balloon release site.
 # 10 Minute average about T-0.
 ## 1 minute average about T-0.
 ### Total sky cover.

A-3



500 MILLIBAR HEIGHT
 CONTOURS AT 1200 Z
 MAY 14, 1973

CONTINUOUS LINES INDICATE HEIGHT CONTOURS IN
 FEET ABOVE SEA LEVEL. DASHED LINES ARE ISO-
 THERMS IN DEGREES CENTIGRADE. ARROWS SHOW
 WIND DIRECTION AND SPEED AT THE 500 MB LEVEL.
 (ARROWS SAME AS ON SURFACE MAP).

Figure A-2. 500 Millibar Map Approximately 5 1/2 Hours Before Launch of SA-513

Table A-2. Systems Used to Measure Upper Air Wind Data for SA-513

TYPE OF DATA	RELEASE TIME		PORTION OF DATA USED			
	TIME (UT)	TIME AFTER T-0 (MIN)	START		END	
			ALTITUDE M (FT)	TIME AFTER T-0 (MIN)	ALTITUDE M (FT)	TIME AFTER T-0 (MIN)
FPS-16 Jimsphere	1745	15	125 (410)	15	14,725 (48,310)	64
Rawinsonde	2000	150	14,750 (48,392)	198	24,750 (81,200)	231
Super Loki Dart	1800	30	62,500 (205,050)	30	25,000 (82,020)	56

A-5

increasing to a peak of 34.4 m/s (66.8 knots) at 12.70 kilometers (41,666 feet). The winds began decreasing above this altitude, becoming relatively calm at 34.25 kilometers (112,367 feet). Above this level, winds increased again to a peak of 41.0 m/s (79.7 knots) at 54.50 km (178,804 feet) altitude as shown in Figure A-3. Maximum dynamic pressure occurred at 12.03 kilometers (39,459 feet). At max Q altitude, the wind speed and direction was 24.2 m/s (47.0 knots), from 264 degrees. SL-1 pad 39A wind data is available in MSFC memorandum S&E-AERO-YT-19-73.

A.4.2 Wind Direction

At launch time, the surface wind direction was from 140 degrees. The wind direction was southwesterly throughout the lower and middle troposphere, becoming westerly throughout the upper troposphere and lower stratosphere. Above 20 kilometers (65,616 feet) easterly flow prevailed. Figure A-4 shows the complete wind direction versus altitude profile. As shown in Figure A-4, wind directions were quite variable at altitudes with low wind speeds.

A.4.3 Pitch Wind Component

The pitch wind velocity component (component parallel to the horizontal projection of the flight path) at the surface was a tailwind of 0.5 m/s (0.9 knots). The maximum tailwind, in the altitude range of 8 to 16 kilometers (26,247 to 52,493 ft), was 26.2 m/s (50.9 knots) observed at 13.03 kilometers (42,732 feet) altitude. See Figure A-5.

A.4.4 Yaw Wind Component

The yaw wind velocity component (component normal to the horizontal projection of the flight path) at the surface was a wind from the right of 3.0 m/s (5.8 knots). The peak yaw wind velocity in the high dynamic pressure region was from the left of 24.9 m/s (48.3 knots) at 12.68 kilometers (41,584 feet). See Figure A-6.

A.4.5 Component Wind Shears

The largest component wind shear ($\Delta h = 1,000$ m) in the max Q region was a pitch shear of 0.0139 sec^{-1} at 14.05 kilometers (46,095 feet). The largest yaw wind shear, at these lower levels, was 0.0107 sec^{-1} at 9.25 kilometers (30,347 feet). See Figure A-7.

A.4.6 Extreme Wind Data in the High Dynamic Region

A summary of the maximum wind speeds and wind components is given in Table A-3. A summary of the extreme wind shear values ($\Delta h = 1,000$ meters) is given in Table A-4.

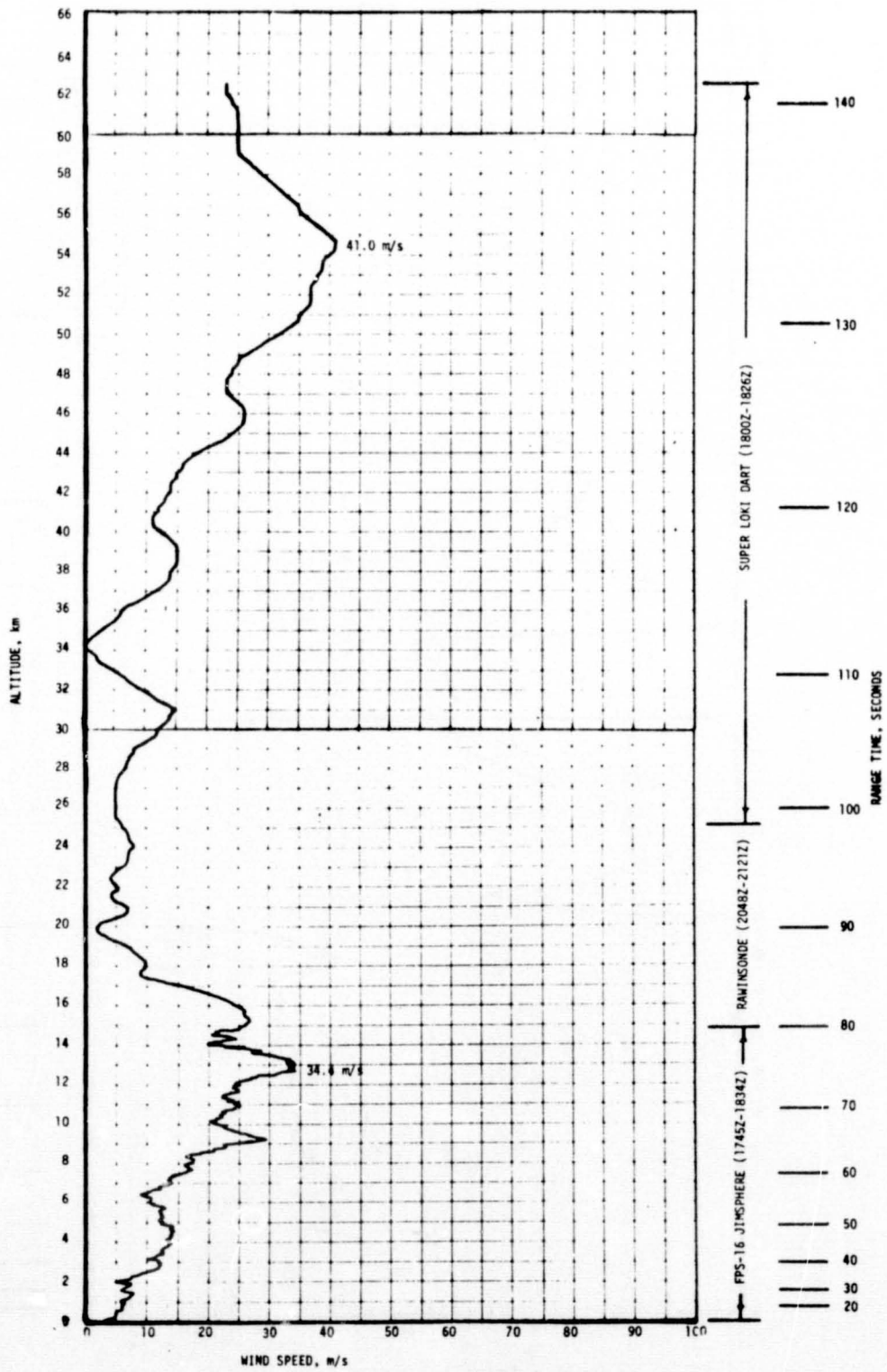


Figure A-3. Scalar Wind Speed at Launch Time of SA-513 (SL-1)

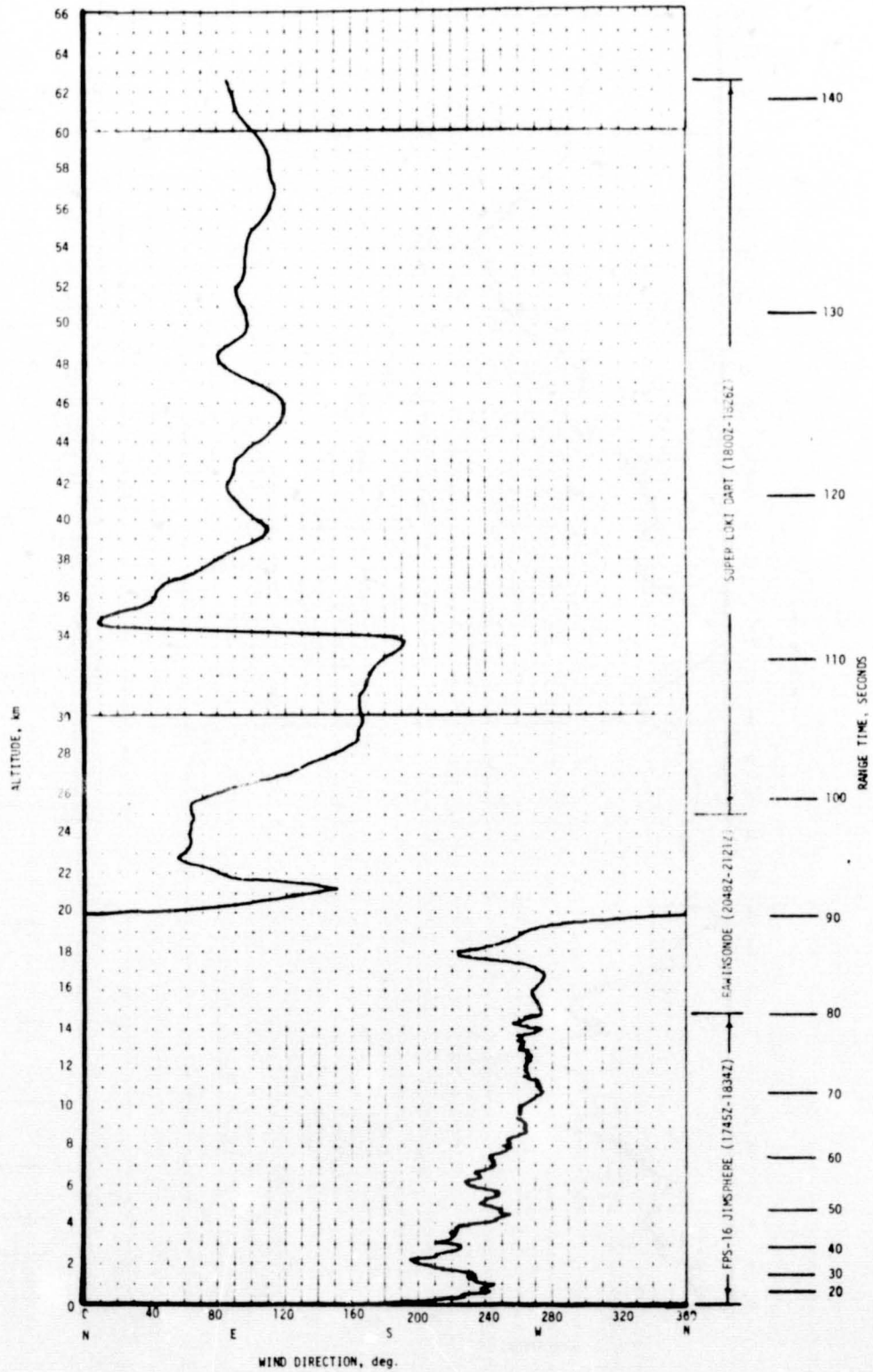


Figure A-4. Wind Direction at Launch Time of SA-513 (SL-1)

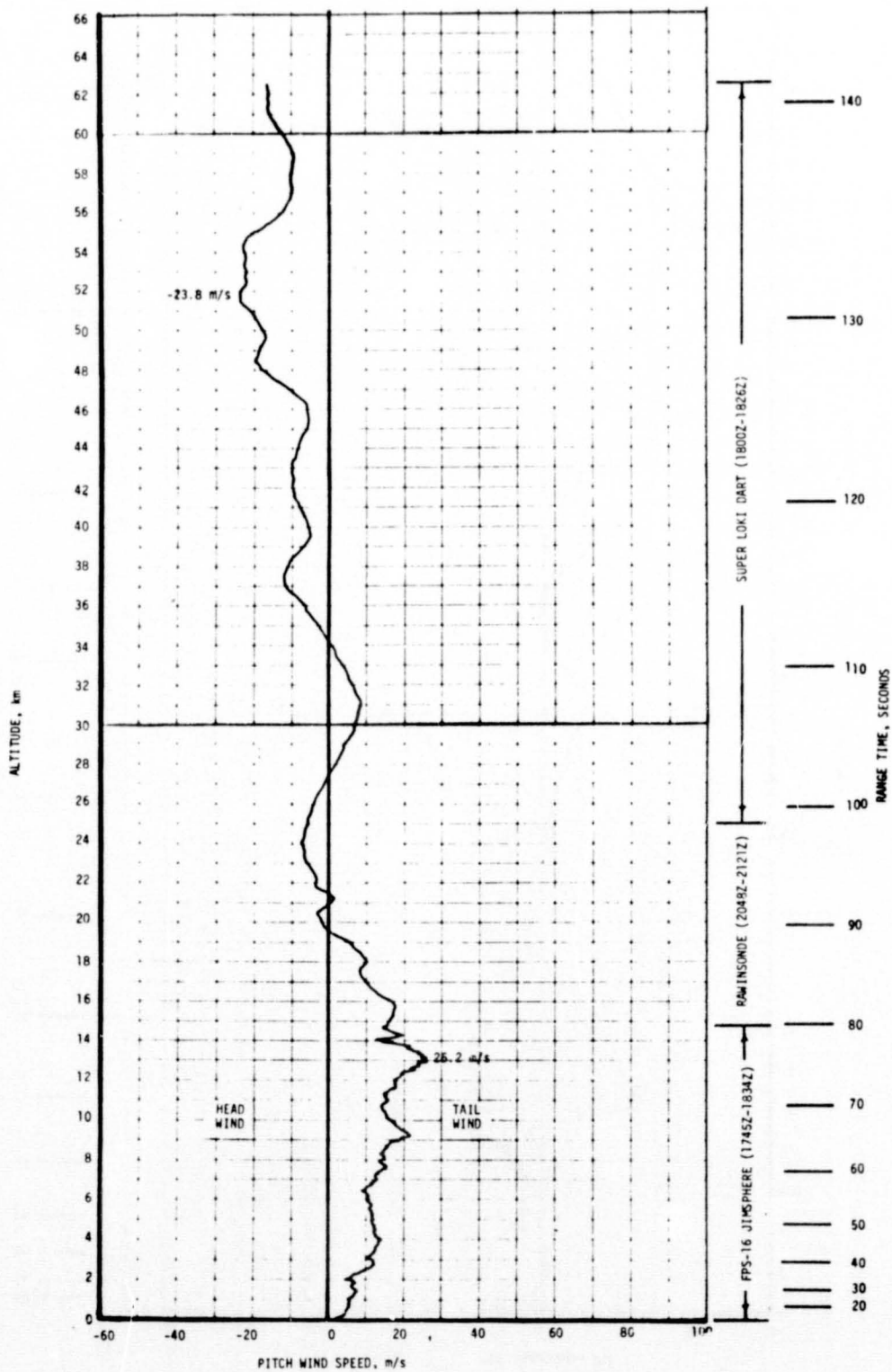


Figure A-5. Pitch Wind Velocity Component (W_x) at Launch Time of SA-513 (SL-1)

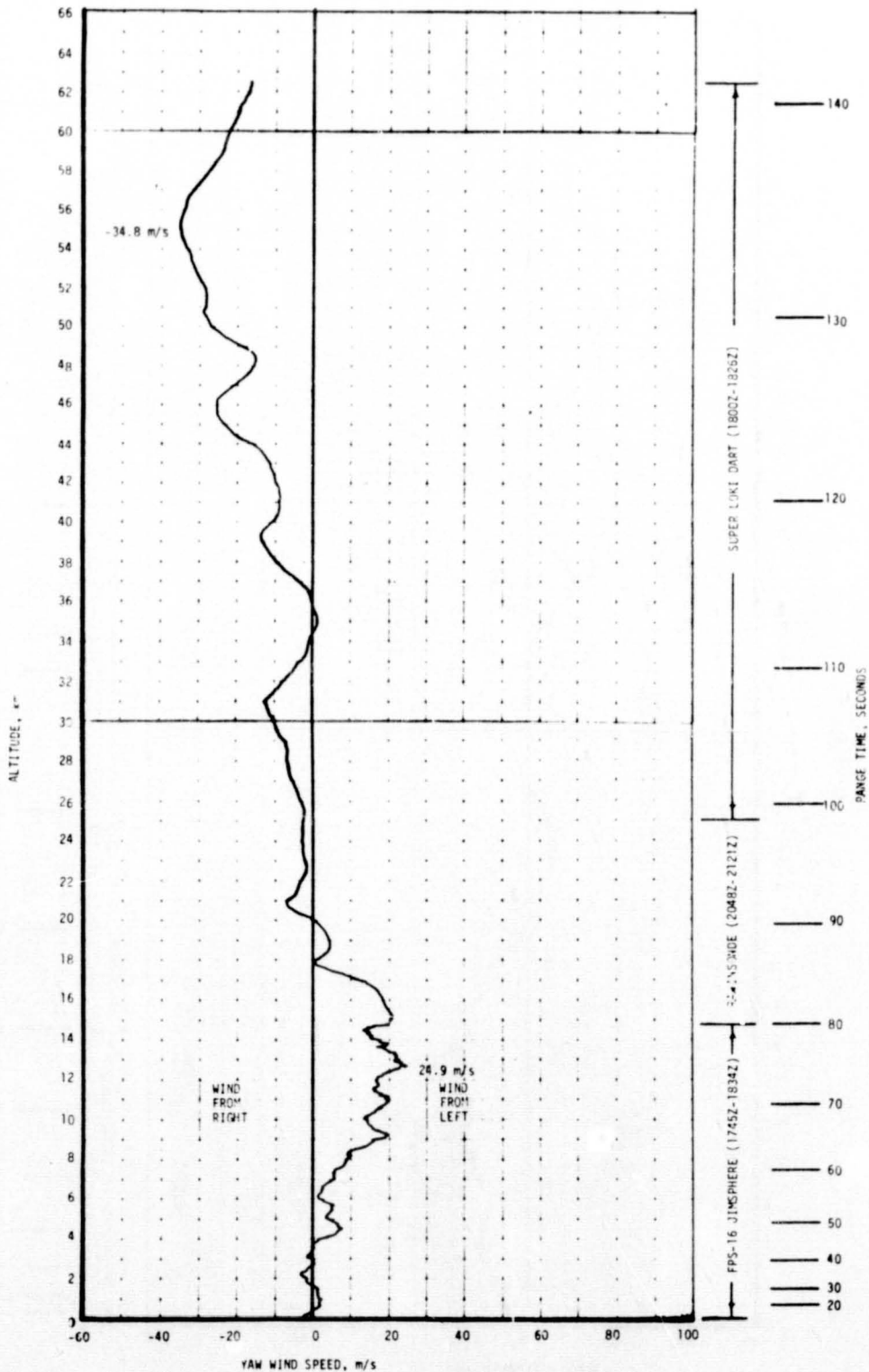


Figure A-6. Yaw Wind Velocity Component (W_z) at Launch Time of SA-513 (SL-1)

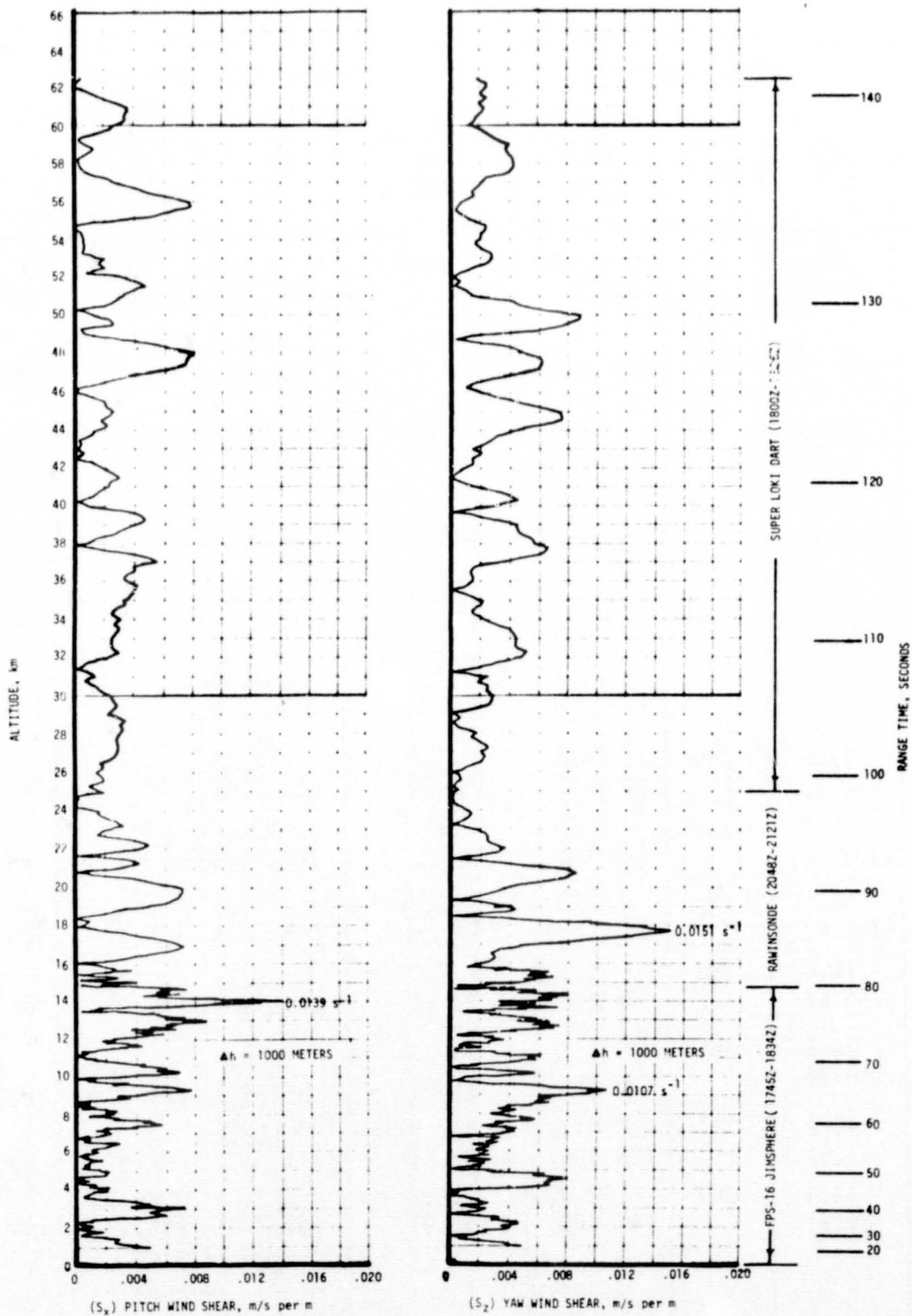


Figure A-7. Pitch (S_x) and Yaw (S_z) Component Wind Shears at Launch Time of SA-513 (SL-1)

Table A-3. Maximum Wind Speed in High Dynamic Pressure Region for Apollo/Saturn 501 through Saturn 513 Vehicles

VEHICLE NUMBER	MAXIMUM WIND			MAXIMUM WIND COMPONENTS			
	SPEED M/S (KNOTS)	DIR (DEG)	ALT KM (FT)	PITCH (W _x) M/S (KNOTS)	ALT KM (FT)	YAW (W _z) M/S (KNOTS)	ALT KM (FT)
SA-501	26.0 (50.5)	273	11.50 (37,700)	24.3 (47.2)	11.50 (37,700)	12.9 (25.1)	9.00 (29,500)
SA-502	27.1 (52.7)	255	13.00 (42,650)	27.1 (52.7)	13.00 (42,650)	12.9 (25.1)	15.75 (51,700)
SA-503	34.8 (67.6)	284	15.22 (49,900)	31.2 (60.6)	15.10 (49,500)	22.6 (43.9)	15.80 (51,800)
SA-504	76.2 (148.1)	264	11.73 (38,480)	74.5 (141.8)	11.70 (38,390)	21.7 (42.2)	11.43 (37,500)
SA-505	42.5 (82.6)	270	14.18 (46,520)	40.8 (79.3)	13.80 (45,230)	18.7 (36.3)	14.85 (48,720)
SA-506	9.6 (18.7)	297	11.40 (37,400)	7.6 (14.8)	11.18 (36,680)	7.1 (13.8)	12.05 (39,530)
SA-507	47.6 (92.5)	245	14.23 (46,670)	47.2 (91.7)	14.23 (46,670)	-19.5 (-37.9)	13.65 (44,780)
SA-508	55.6 (108.1)	252	13.58 (44,540)	55.6 (108.1)	13.58 (44,540)	15.0 (29.1)	12.98 (42,570)
SA-509	52.8 (102.6)	255	13.33 (43,720)	52.8 (102.6)	13.33 (43,720)	24.9 (48.5)	10.20 (33,460)
SA-510	18.6 (36.2)	063	13.75 (45,110)	-17.8 (-34.6)	13.73 (45,030)	7.3 (14.2)	13.43 (44,040)
SA-511	26.1 (50.7)	257	11.85 (38,880)	26.0 (50.5)	11.85 (38,880)	12.5 (24.2)	15.50 (50,850)
SA-512	45.1 (87.6)	311	12.18 (39,945)	34.8 (67.6)	12.18 (39,945)	29.2 (56.8)	11.35 (37,237)
SA-513	34.4 (66.8)	267	12.70 (41,666)	26.2 (50.9)	13.03 (42,732)	24.9 (48.3)	12.68 (41,584)

Table A-4. Extreme Wind Shear Values in the High Dynamic Pressure Region
For Apollo/Saturn 501 through Saturn 513 Vehicles

($\Delta h = 1000 \text{ m}$)				
VEHICLE NUMBER	PITCH PLANE		YAW PLANE	
	SHEAR (SEC ⁻¹)	ALTITUDE KM (FT)	SHEAR (SEC ⁻¹)	ALTITUDE KM (FT)
SA-501	0.0066	10.00 (32,800)	0.0067	10.00 (32,800)
SA-502	0.0125	14.90 (48,900)	0.0084	13.28 (43,500)
SA-503	0.0103	16.00 (52,500)	0.0157	15.78 (51,800)
SA-504	0.0248	15.15 (49,700)	0.0254	14.68 (48,160)
SA-505	0.0203	15.30 (50,200)	0.0125	15.53 (50,950)
SA-506	0.0077	14.78 (48,490)	0.0056	10.30 (33,790)
SA-507	0.0183	14.25 (46,750)	0.0178	14.58 (47,820)
SA-508	0.0166	15.43 (50,610)	0.0178	13.98 (45,850)
SA-509	0.0201	13.33 (43,720)	0.0251	11.85 (38,880)
SA-510	0.0110	11.23 (36,830)	0.0071	14.43 (47,330)
SA-511	0.0095	13.65 (44,780)	0.0114	15.50 (50,850)
SA-512	0.0177	7.98 (26,164)	0.0148	10.65 (34,940)
SA-513	0.0139	14.05 (46,095)	0.0107	9.25 (30,347)

A.5 THERMODYNAMIC DATA

Comparisons of the thermodynamic data taken at SA-513 launch time with the annual Patrick Reference Atmosphere, 1963 (PRA-63) for temperature, pressure, density, and Optical Index of Refraction are shown in Figures A-8 and A-9, and are discussed in the following paragraphs.

A.5.1 Atmospheric Temperature

Atmospheric temperature differences were small, generally deviating less than 3 percent from the PRA-63, below 63 kilometers (206,690 feet) altitude. Temperatures did deviate to 2.5 percent of the PRA-63 value at 14.50 km (47,572 feet). Air temperature was warmer than the PRA-63 at the surface and oscillated about the PRA-63 above this level. See Figure A-8 for the complete profile.

A.5.2 Atmospheric Pressure

Atmospheric pressure deviations were slightly greater than the PRA-63 pressure values from the surface through 26 kilometers (85,301 feet) altitude. The peak deviation of 1.1 percent occurred at 17.85 kilometers (58,562 feet) altitude. See Figure A-8.

A.5.3 Atmospheric Density

Atmospheric density deviations were also small, being within 3 percent of the PRA-63 below 35 kilometers (114,828 feet) altitude. The density deviation reached a maximum of 3.0 percent greater than the PRA-63 value at 18.25 kilometers (59,875 feet) as shown in Figure A-9.

A.5.4 Optical Index of Refraction

The Optical Index of Refraction at the surface was 10.4×10^{-6} units lower than the corresponding value of the PRA-63. The deviation then became less negative with altitude, and approximated the PRA-63 at high altitudes, as is shown in Figure A-9. The maximum value of the Optical Index of Refraction was 1.39×10^{-6} units greater than the PRA-63 at 13.25 kilometers (43,471 feet).

A.6 COMPARISON OF SELECTED ATMOSPHERIC DATA FOR SATURN V LAUNCHES

A summary of the atmospheric data for each Saturn V launch is shown in Table A-5.

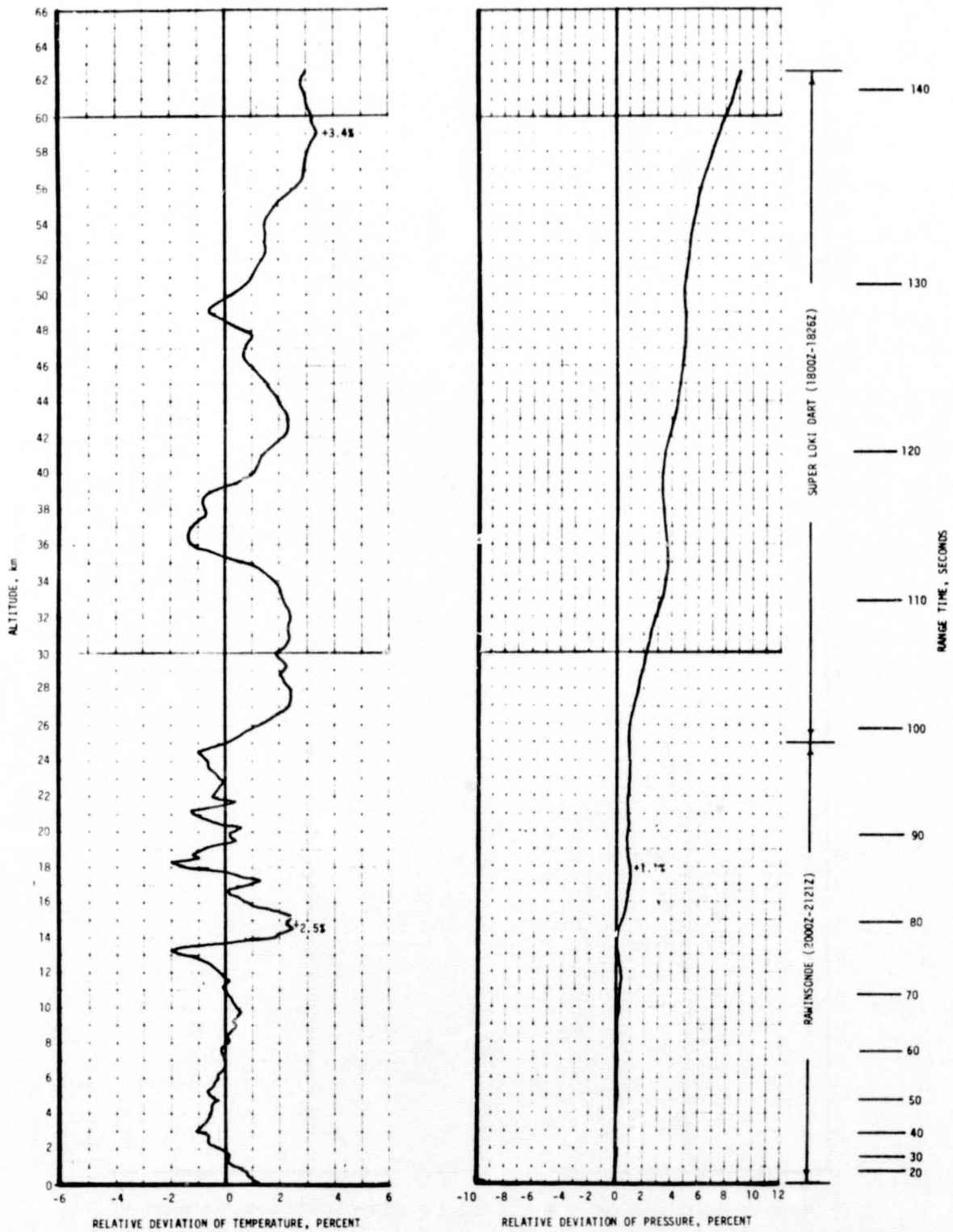


Figure A-8. Relative Deviation of Temperature and Pressure from the PRA-63 Reference Atmosphere, SA-513 (SL-1)

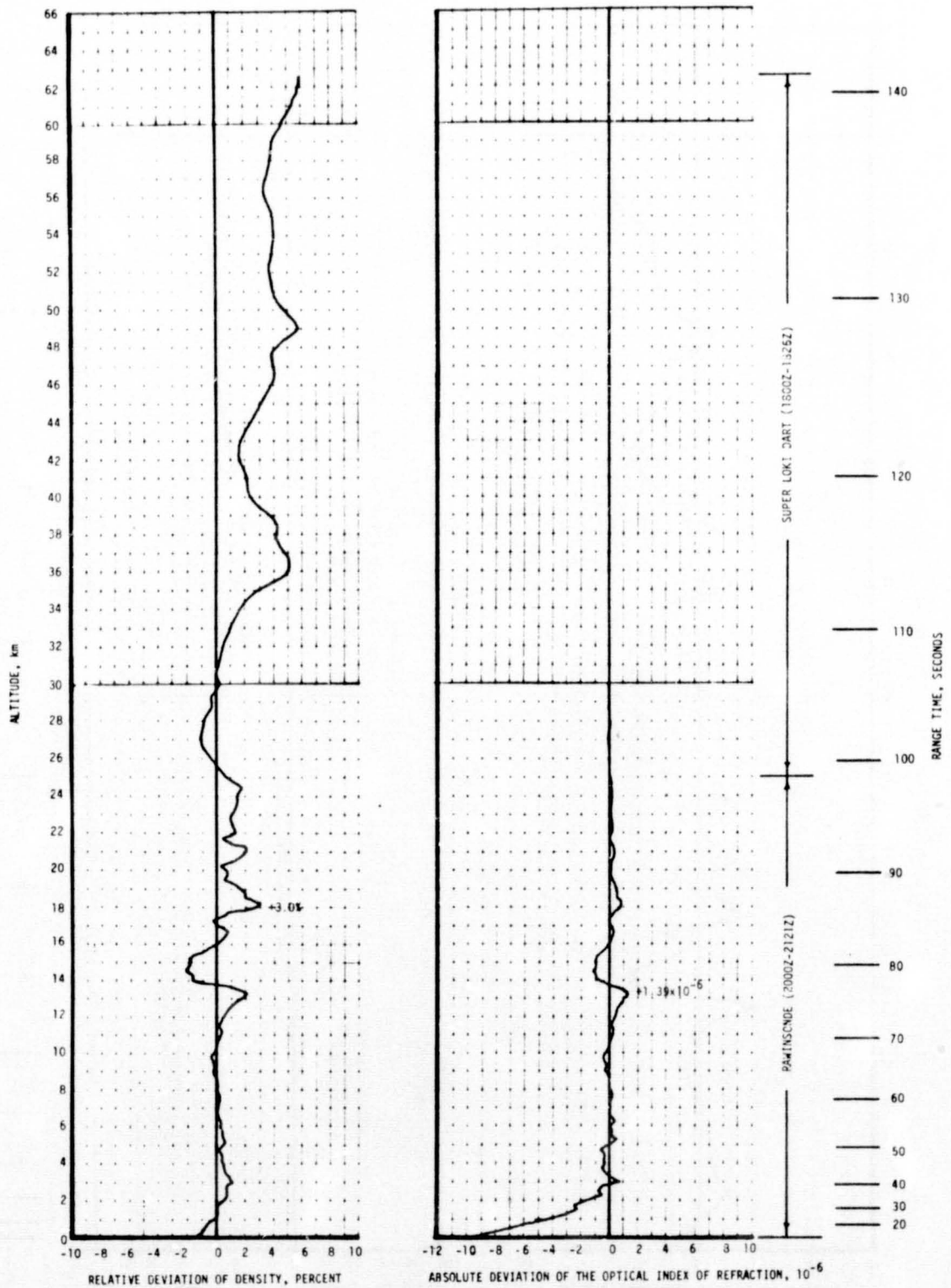


Figure A-9. Relative Deviation of Density and Absolute Deviation of the Index of Refraction From the PRA-63 Reference Atmosphere, SA-513 (SL-1)

Table A-5. Selected Atmospheric Observations for Apollo/Saturn 501 through Saturn 513 Vehicle Launches at Kennedy Space Center, Florida

VEHICLE NUMBER	VEHICLE DATA			SURFACE DATA						INFLIGHT CONDITIONS		
	DATE	TIME NEAREST MINUTE	LAUNCH COMPLEX	PRESSURE N/CM ²	TEMPERATURE °C	RELATIVE HUMIDITY PERCENT	WIND*		CLOUDS	MAXIMUM WIND IN 8-16 KM LAYER		
							SPEED M/S	DIRECTION DEG		ALTITUDE KM	SPEED M/S	DIRECTION DEG
SA-501	9 Nov 67	0700 EST	39A	10.261	17.6	55	8.2**	070**	4/10 stratocumulus	11.50	26.0	273
SA-502	4 Apr 68	0700 EST	39A	10.200	20.9	83	5.4**	132**	5/10 stratocumulus, 1/10 cirrus	13.00	27.1	255
SA-503	21 Dec 68	0751 EST	39A	10.207	15.0	88	5.7**	348**	4/10 cirrus	15.22	34.8	284
SA-504	3 Mar 69	1100 EST	39A	10.095	19.6	61	6.9	160	7/10 stratocumulus, 10/10 altostratus	11.73	76.2	264
SA-505	18 May 69	1249 EDT	39B	10.190	26.7	75	9.8	142	4/10 cumulus, 2/10 altocumulus, 10/10 cirrus	14.18	42.5	270
SA-506	16 Jul 69	0932 EDT	39A	10.203	29.4	73	3.3	175	1/10 cumulus, 2/10 altocumulus, 9/10 cirrostratus	11.40	9.6	297
SA-507	14 Nov 69	1122 EST	39A	10.081	20.0	92	6.8	280	10/10 stratocumulus with rain	14.23	47.6	245
SA-508	11 Apr 70	1413 EST	39A	10.119	24.4	57	6.3	105	4/10 altocumulus 10/10 cirrostratus	13.58	55.6	252
SA-509	31 Jan 71	1603 EST	39A	10.102	21.7	86	5.0** 8.5**	255** 275**	7/10 cumulus 2/10 altocumulus	13.33	52.8	255
SA-510	26 Jul 71	0934 EDT	39A	10.196	29.8	68	5.1** 5.4**	156** 158**	7/10 cirrus	13.75	18.6	063
SA-511	16 Apr 72	1254 EST	39A	10.183	31.2	44	6.3 5.1	269 256	2/10 cumulus	11.85	26.1	257
SA-512	7 Dec 72	0033 EST	39A	10.201	21.1	93	4.1 5.4	005 335	2/10 stratocumulus, 5/10 cirrus	12.18	45.1	311
SA-513	14 May 73	1330 EDT	39A	10.171	30.0	53	5.1 5.1	155 177	3/10 cumulus 3/10 stratocumulus 6/10 altocumulus 5/10 cirrus	12.70	34.4	267

*Instantaneous readings from charts at T-0 (unless otherwise noted) from anemometers on launch pad 39 (A & B) light pole at 18.3 m (60.0 ft). Beginning with AS-509, wind measurements were required at the 161.5 m (530 ft) level from anemometer charts on the LUT. These instantaneous LUT winds are given directly under the listed pad light pole winds. Heights of anemometers are above natural grade.

**Not instantaneous, but one minute average about T-0.

APPENDIX B

SL-1/SA-513 SIGNIFICANT CONFIGURATION CHANGES

B.1 INTRODUCTION

The Skylab-1 (SL-1) space vehicle consisting of the SA-513 Launch Vehicle and the Saturn Work Shop (SWS) is the first to be launched in the Skylab series. The SA-513 Launch Vehicle booster is comprised of Saturn V hardware as follows: S-IC-13 stage for initial boost; S-II-13 stage for final boost into a near circular earth orbit; and IU-513 stage, located in the SWS, to provide sequencing and guidance commands for the space vehicle during launch, ascent and payload orbital insertion. The SWS is the orbital payload of SL-1 and is comprised of the Payload Shroud, Orbital Work Shop, Airlock Module, Multiple Docking Adapter, and Apollo Telescope Mount and IU stage. The IU stage, structurally a part of the Saturn Work Shop, provides initial sequencing and attitude control commands to the SWS in addition to being a functional part of the SA-513 Launch Vehicle. Figure B-1 shows the Skylab Space Vehicle configuration.

B.2 S-IC STAGE

B.2.1 S-IC Configuration

The S-IC Stage, as shown in Figure B-2, is a cylindrical structure designed to provide the initial boost for the Saturn V/Skylab-1 vehicle. This booster stage is 138 feet long and has a diameter of 33 feet. The basic structures of the S-IC are the thrust structure, fuel (RP-1) tank, intertank section, LOX tank, and the forward skirt. Attached to the thrust structure are the five F-1 engines which produce a combined nominal sea level thrust of 7,610,000 lbf. Four of these engines are spaced equidistantly about a 30.33 foot diameter circle. The four outboard engines are attached so they have a gimbaling capability. Each outboard engine can move in a 5 degree, 9 minute square pattern to provide pitch, yaw, and roll control. The fifth engine is mounted on the stage centerline. In addition to supporting the engines, the thrust structure also provides support for the base heat shield, engine accessories, engine fairings and fins, propellant lines, retro motors, and environmental control ducts. The intertank structure provides structural continuity between the LOX and fuel tanks, which provide propellant storage; and the forward skirt provides structural continuity with the S-II stage.

B.2.2 S-IC Systems

Systems on the S-IC include:

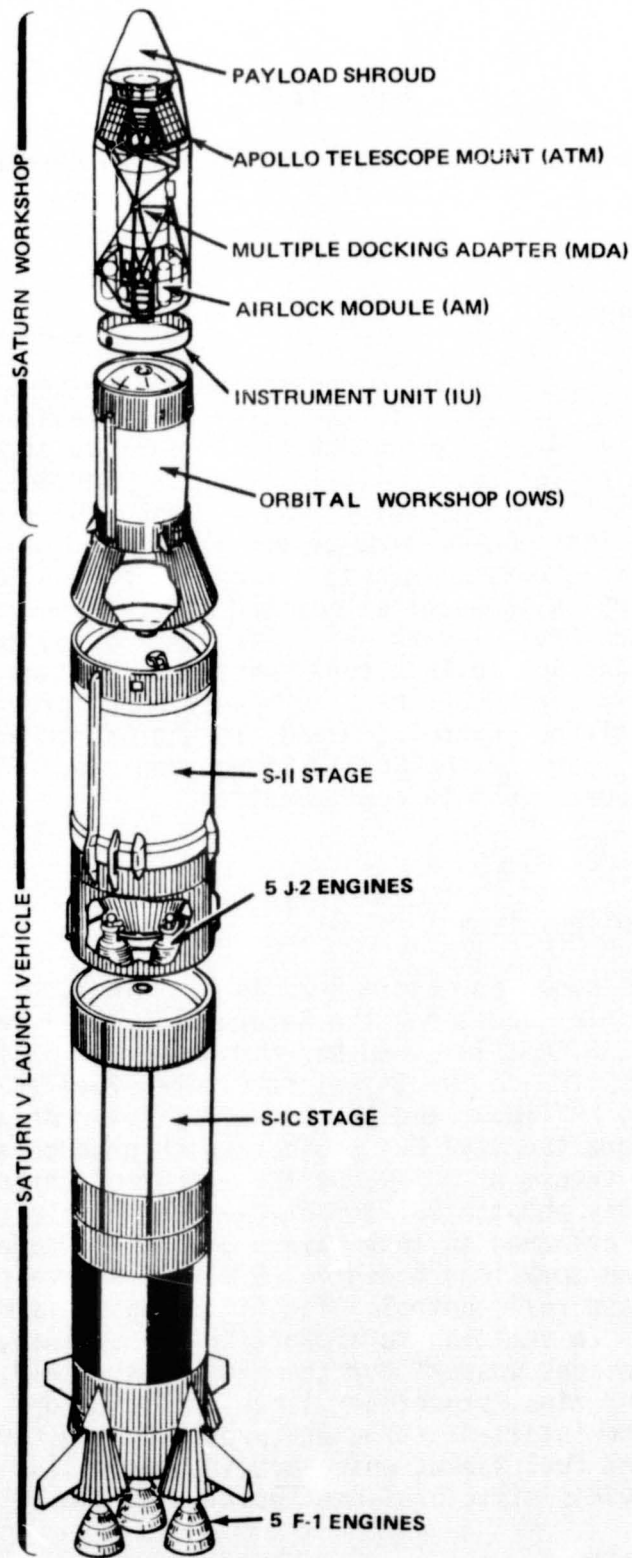


Figure B-1. Skylab Space Vehicle Configuration

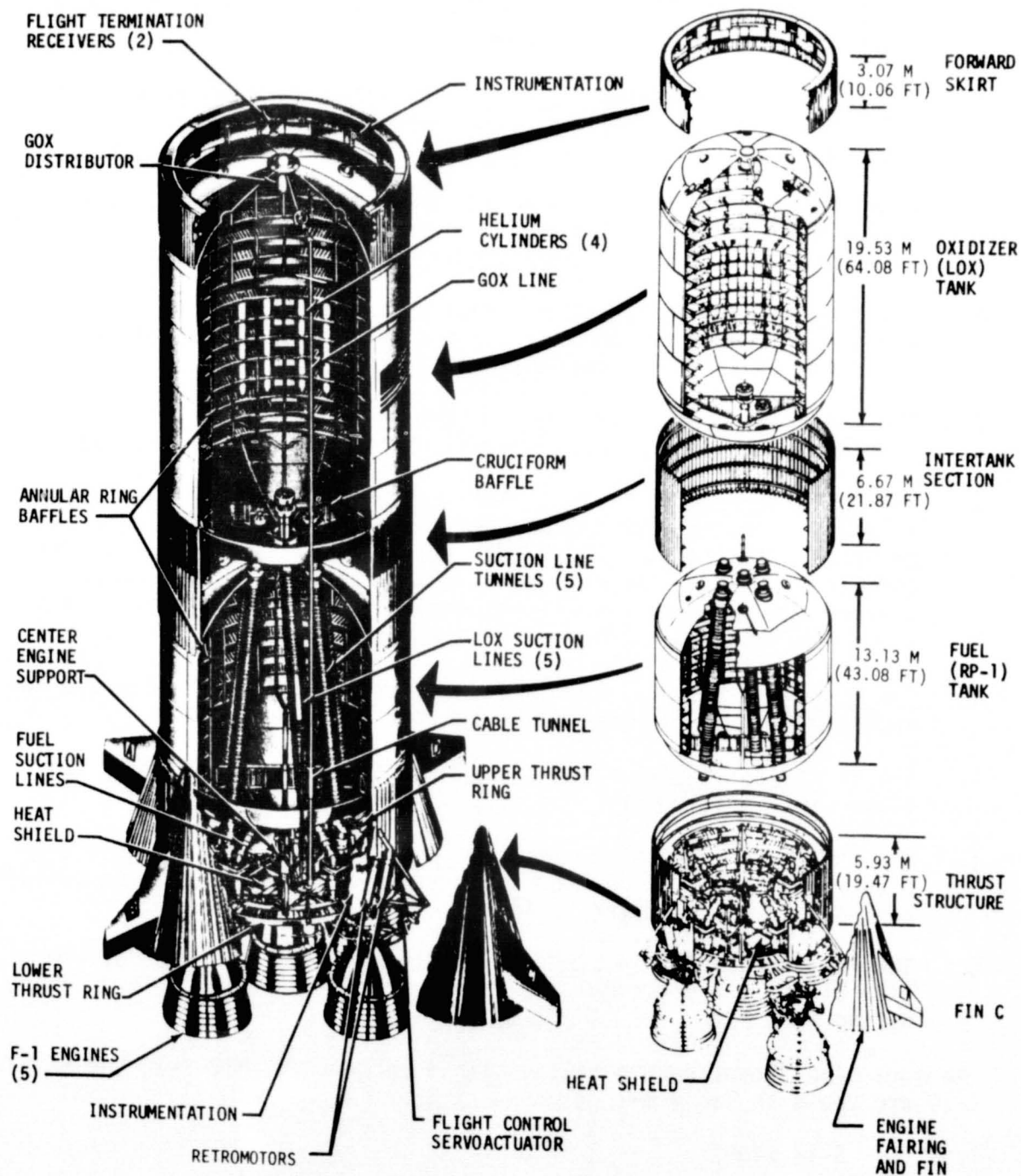


Figure B-2. S-IC Stage Configuration

- a. Propulsion System as discussed in paragraph B.2.1.
- b. Propellant Storage and Delivery System. The fuel tank, with 29,301 ft³ capacity, supplies RP-1 and the oxidizer tank, with 47,369 ft³ capacity, supplies LOX to the engines.
- c. Propellant Pressurization System. Maintains required propellant inlet pressure to the engine turbopumps and provides for tank venting.
- d. Retro Motor System. Eight solid propellant retro motors, located inside the four outboard engine fairings and attached to the thrust structure, provide separation thrust after S-IC burnout.
- e. Purge System. This system provides pressurized nitrogen to various engine subsystems and cocoons to reduce concentration of hazardous gases or for thermal conditioning.
- f. The Pneumatic Control Pressure System which provides a pressurized nitrogen supply for command operations of various pneumatic valves.
- g. The POGO Suppression System. This system provides gaseous helium to a cavity in each of the LOX prevalues of the four outboard engine suction lines. These gas filled cavities act as a "spring" and serve to lower the natural frequency of the feed system and thereby prevent coupling between engine thrust oscillations and the first longitudinal mode of the vehicle structure.
- h. The Hydraulic System. This system distributes power to operate the engine valves and thrust vector control system.
- i. The Electrical System. This system distributes and controls the stage electrical power.
- j. The Environmental Control System (ECS). This system protects the S-IC stage compartments from temperature extremes, excessive humidity and hazardous gas concentrations.
- k. The Instrumentation System. This system monitors functional operation of the stage systems and provides signals for vehicle tracking during S-IC burn.

The more significant configuration changes between AS-512 S-IC and SA-513 S-IC are shown in Table B-1.

B.3 S-II STAGE

B.3.1 S-II Configuration

The S-II Stage, as shown in Figure B-3, is a cylindrical structure

Table B-1. S-IC Significant Configuration Changes

SYSTEM	CHANGE	REASON
F-1 Engines	Provide 1-2-2 Engine Cutoff Sequence	To avoid exceeding structural design limits of the Apollo Telescope Mount (ATM) at outboard engine cutoff.

designed to provide second stage boost of the Skylab payload into earth orbit. This booster stage is 81.5 feet long and 33 feet in diameter. Propulsive power is provided by five J-2 engines with a combined nominal thrust of 1,158,279 lbf. The four outboard engines are provided with gimbaling capability to provide attitude control in pitch, roll and yaw during powered flight. The fifth engine is mounted on the stage centerline.

The S-II stage is made up of five major units: (1) aft interstage, (2) aft skirt thrust structure, (3) liquid oxygen tank, (4) liquid hydrogen tank, and (5) forward skirt.

B.3.2 S-II Systems

Systems on the S-II include:

- a. Propulsion System as discussed in paragraph B.3.1.
- b. Propellant Storage and Delivery System. The fuel tank with 37,737 ft³ capacity supplies LH₂ and the oxidizer tank with 12,745 ft³ capacity supplies LOX to the engines. The two tanks are separated by a common bulkhead.
- c. Propellant Pressurization System. Maintains required propellant inlet pressure to the engine turbopumps and provides for tank venting.
- d. Purge System. This system provides for thermal control of equipment containers in the forward and aft S-II skirt areas, S-II engine compartment, and S-II/S-IC interstage during launch operations.
- e. Pneumatic System. This system provides a pressurized nitrogen supply for operation of stage pneumatic valves.
- f. Safing System. This system provides for non-propulsive venting of propellant tanks and gas storage bottles after end of powered flight.
- g. Flight Control Subsystem. The flight control subsystem incorporates

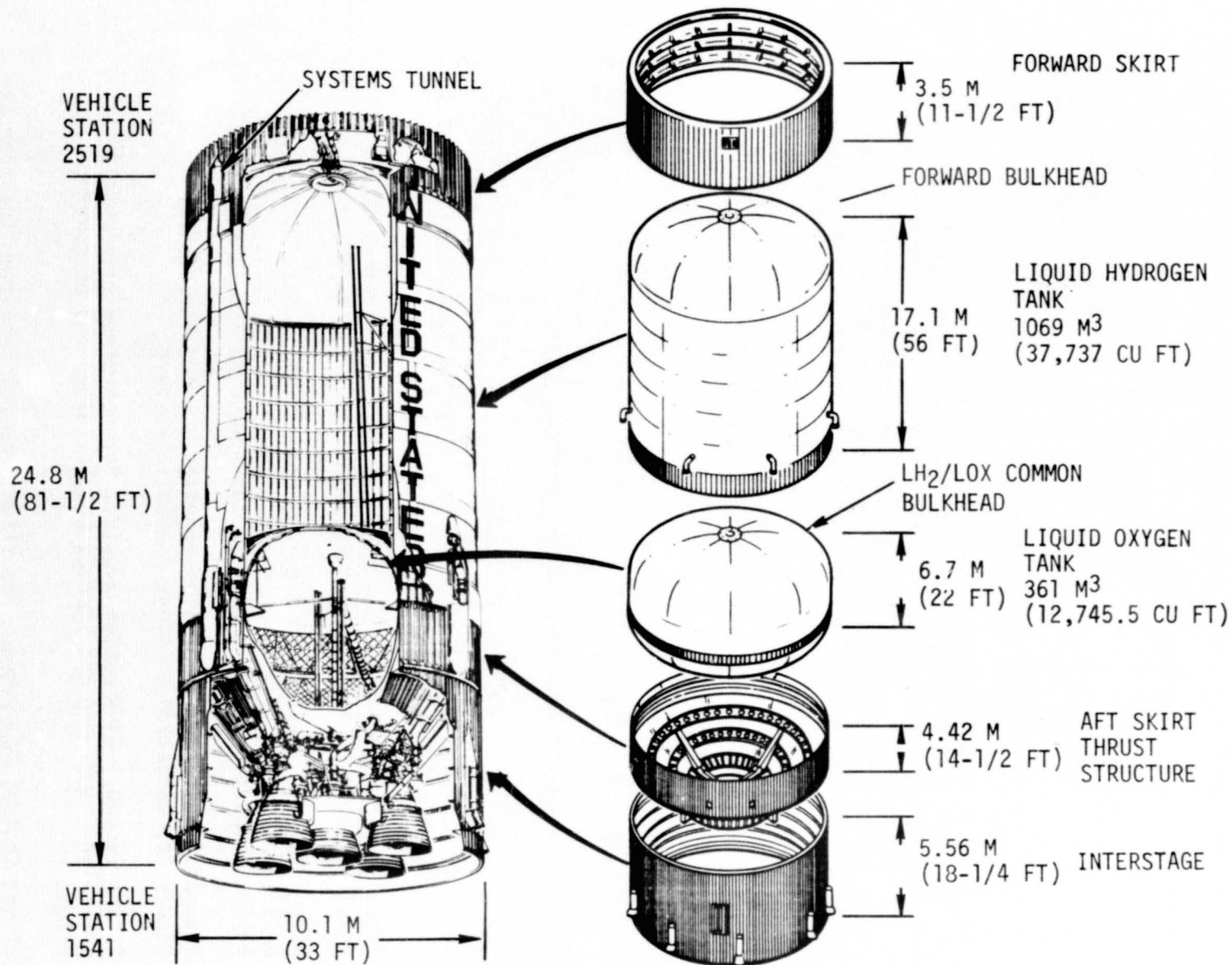


Figure B-3. S-II Stage Configuration

a self-contained hydraulic system for gimbal control of the engines. A continuously operating closed-loop hydraulic system is provided for each outboard engine to control engine gimbaling.

- h. Instrumentation. The instrumentation system acquires and transmits data associated with vehicle performance and its environment. The system consists of transducers, signal conditioners, telemetry equipment, and RF equipment.
- i. Electrical Subsystem. The electrical power system contains battery power to supply inflight electrical power and distributes the power to various equipment containers and other major subsystems.
- j. Environmental Control Subsystems. The environmental control subsystems consist of two basic subsystems: the thermal control system for thermal protection of equipment containers on the ground including containers in forward and aft skirt and engine compartment conditioning system for purging and temperature control of the S-II/S-IC interstage during launch operations.

Significant configuration changes between S-II-12 and S-II-13 are shown in Table B-2.

Table B-2. S-II Significant Configuration Changes

SYSTEM	CHANGE	REASON
Structure	<p>Increase the effective venting area of the S-II forward skirt by 46 square inches.</p> <p>Addition of closures and sealant to aft ends of S-II fairings.</p> <p>Modify the engine heat shield flexible curtains by use of improved materials.</p> <p>Addition of 2400 pounds of lead ballast bolted to the interior support structure of the S-II interstage.</p>	<p>To regulate internal skirt pressure during ascent within the S-II skirt and OWS interstage design limits</p> <p>To minimize S-IC plume-induced flow separation heating on ordnance and propellant lines under fairings.</p> <p>To protect thrust structure and stage/engine components during increased base heating from larger nominal engine deflections with one engine out.</p> <p>To decrease the collision probability between engines and interstage during separation with one engine out.</p>
Propulsion	<p>Installation of non-propulsive overboard vent lines for the LOX and LH₂ propellant tanks.</p> <p>Use of existing engine and stage systems to vent engine helium and hydrogen tanks.</p>	<p>To achieve equal force venting from two diametrically opposed nozzles for each tank. Propellant tank venting is required for S-II stage safing, sequenced after S-II/SWS separation.</p> <p>To reduce engine tank pressures during stage safing, sequenced after S-II/SWS separation.</p>
Electrical	<p>Addition of circuitry, timers, and ordnance for sequencing stage safing functions.</p> <p>Addition of instrumentation measurements in safing circuitry and non-propulsion vent systems.</p> <p>Addition of redundant commands for S-II interstage separation and for S-II/SWS separation events.</p>	<p>To sequence stage safing functions and provide ordnance for actuating the LOX and LH₂ non-propulsive valves.</p> <p>To monitor systems performance.</p> <p>To increase reliability of arming and triggering these functions</p>

B.4 INSTRUMENT UNIT (IU)

B.4.1 IU Configuration

The IU, as shown in Figure B-4, is a short cylinder fabricated from an aluminum alloy honeycomb sandwich material and although functionally a

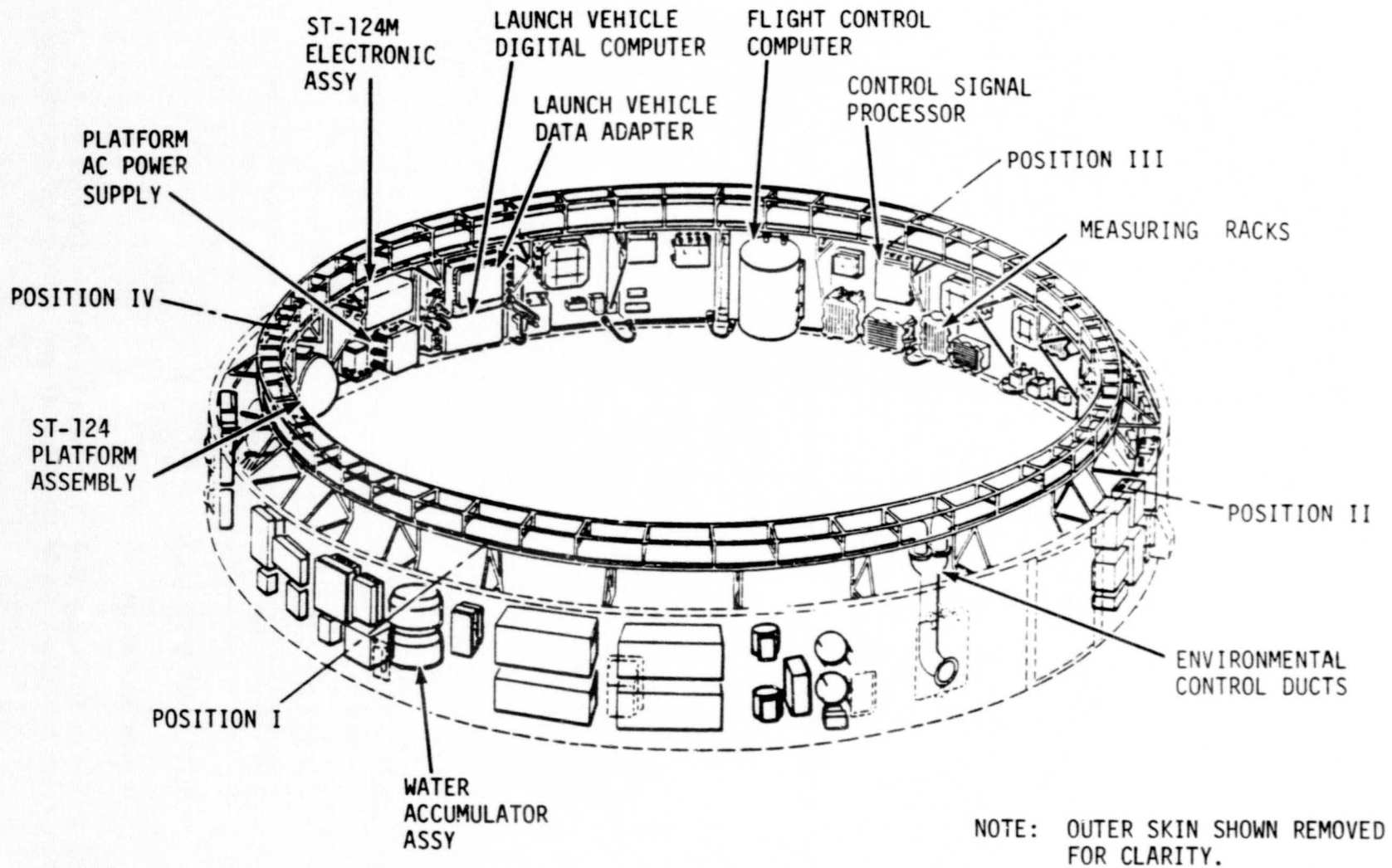


Figure B-4. Instrument Unit Configuration

a part of the booster vehicle, is structurally a part of the Saturn Work Shop. The IU provides sequencing commands for both the booster and Saturn Work Shop and provides guidance, navigation, and control commands to the booster. The IU has a diameter of 21.6 feet and a length of 3 feet. The cylinder is manufactured in three 120 degree segments which are joined by splice plates into an integral load bearing unit. The top and bottom edges of the cylinder are made from extruded aluminum channels bonded to the honeycomb sandwich material. Cold plates are attached to the interior of the cylinder which serve both as mounting structure and thermal conditioning units for the electrical/electronic equipment.

B.4.2 IU Systems

Systems on the IU are:

- a. The Environmental Control System (ECS) which maintains an acceptable environment for the IU equipment.
- b. The electrical system which supplies and distributes electrical power to the various systems.
- c. The navigation, guidance, and control system.
- d. The measurements and telemetry system which monitors and transmits signals to ground monitoring stations.
- e. The flight program which controls the LVDC from seconds before liftoff until the end of the launch vehicle mission.

The more significant configuration changes between AS-512 IU and SA-513 IU are shown in Table B-3.

B.5 SATURN WORK SHOP (SWS)

B.5.1 SWS Configuration

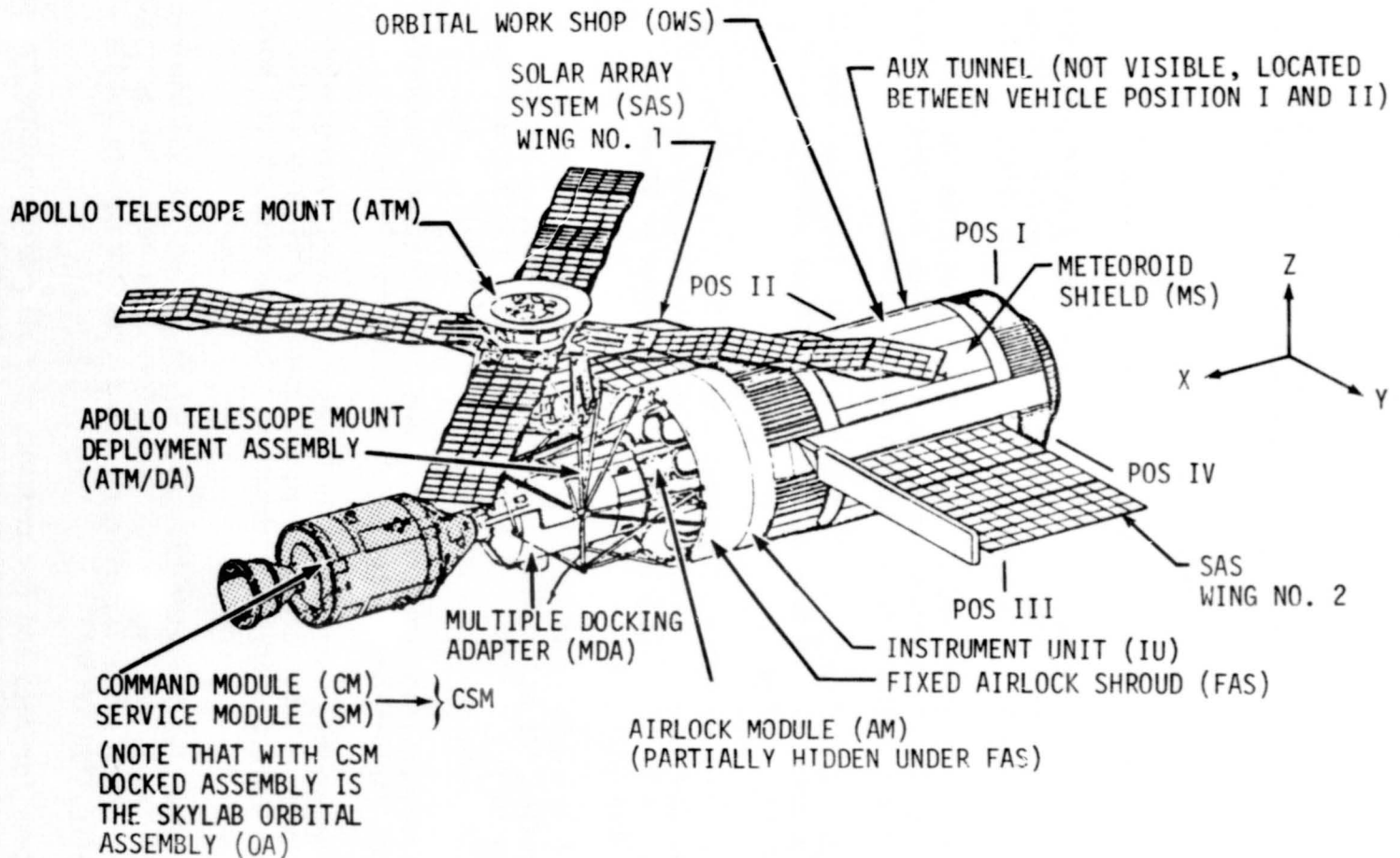
The SWS, shown in Figure B-5 in the deployed configuration with the Command and Service Module docked, is composed of an Orbital Work Shop (OWS); an Airlock Module (AM); a Multiple Docking Adapter (MDA); a Saturn V Instrument Unit; an Apollo Telescope Mount (ATM); and a Payload Shroud.

The Orbital Work Shop is a modified S-IVB Stage which has been fitted out to be suitable for manned habitation, and for the performance of experiments in orbit, and provides:

- a. A habitable environment, with crew provisions and consumables;
- b. A capability for experiment installation and storage before launch and operational space during manned phases;

Table B-3. IU Significant Configuration Differences Between IU-512 and IU-513

SYSTEM	CHANGE	REASON
Environmental Control	<p>Early shutdown of GSCU to permit partial drainage of secondary coolant loop.</p> <p>Modify TCS</p> <ul style="list-style-type: none"> o Delete provision of cooling to S-IVB stage forward skirt o Add S-IVB simulation loop in IU to represent the deleted S-IVB TCS <p>Delete IU hazardous gas system sampling capability.</p> <p>Delay initial water valve opening from liftoff +180 seconds to liftoff +350 seconds.</p>	<p>Temperature levels anticipated would result in pressures beyond proven capability of secondary coolant loop system.</p> <p>Absence of an S-IVB forward skirt cooling system requires coolant lines simulating S-IVB TCS to maintain IU TCS performance characteristics.</p> <p>No requirement to sense for hazardous gases within OWS/ IU area of SL-1.</p> <p>Necessary to delay water solenoid valve opening until internal compartment pressure is below maximum level necessary for adequate sublimator operation.</p>
Structures	<p>Modify cork exterior surface insulation and configuration.</p> <p>Add reinforcing plates to all aft interface bolt holes to provide load safety factor of 1.25.</p> <p>Relocate thermal expansion chamber to coldplate 11. Paint exterior of IU white at location 7 to reduce coolant manifold absorbed heat.</p>	<p>Potential contamination of critical optical systems required reduction of outgassing from cork insulation.</p> <p>Analysis showed that SL-1 tension loads could result in yielding of aft interface flange.</p> <p>Heat load from constant solar attitude of SWS would result in over-pressurization of the secondary coolant loop of the thermal conditioning system.</p>
Instrumentation and Communications	<p>Move CCS components from solar illuminated side of vehicle to shaded side. Delete coaxial switch and directional antenna. Add electrical load.</p>	<p>Solar inertial attitude maintained by Skylab results in excessive CCS component temperatures after ECS operation ceases. Directional antenna not required for orbital mission. Electrical load needed to ensure passivation of CCS battery (6020).</p>
Navigation, Guidance & Control	<p>Modify the Flight Control Computer (FCC) control gains and shaping networks to satisfy S-IU-513 design requirements.</p>	<p>Provide satisfactory stability and response characteristics for SA-513.</p>
Networks	<p>Provide expulsion control of battery electrolyte through use of a battery covering pad and a membrane filter.</p> <p>Modify IU/S-IVB electrical interface.</p> <p>Provide an open loop EDS.</p> <p>Provide S-II engine out interrupt to LVDA.</p> <p>Delete Q-Ball.</p>	<p>Normal battery venting could cause expulsion of battery electrolyte.</p> <p>Change of S-IVB stage to Saturn Work Shop.</p> <p>Skylab-1 will be launched unmanned.</p> <p>Redundant indications of S-II engine out needed for LVDA timing functions due to S-II velocity cutoff in lieu of S-II fuel depletion cutoff.</p> <p>Q-Ball previously required for manned missions - not required for SL-1.</p>
LVDC	<p>Used a fixed (prestored) acceleration profile in place of the downrange (Z) and crossrange (Y) accelerometer output for the first 10 seconds of flight.</p> <p>Added a combined X_y and X_z maneuver as opposed to a X_z only maneuver to steer the vehicle away from the launch umbilical tower.</p> <p>Provide capability for both X_y and X_z commands during S-IC stage burn. Computer X_y and X_z as a tabular function of time.</p> <p>Provide scale factors which produce an effective attitude error deadband of 3° of roll and 2° in both pitch and yaw.</p> <p>Maintain attitude hold (Chi freeze) from T4+0 until T4+10 seconds.</p> <p>Compute commands to maneuver to payload shroud jettison attitude (local vertical maneuver nose down.)</p> <p>Computer commands to maneuver to solar inertial attitude.</p> <p>Compute the minor loop guidance command rate limits as a function of the attitude error in each axis such that the root-sum-squares do not exceed 0.3°/second.</p>	<p>Reduce the possibility of introducing large errors in navigation due to vibration near liftoff.</p> <p>Improve tower avoidance capability for SL-1.</p> <p>Improve vehicle stability.</p> <p>Requires less TACS for deadband control.</p> <p>Necessary to accomplish SL-1 guidance functions.</p> <p>To limit vehicle command rate to deployed Skylab structural limitations.</p>



B-11

Figure B-5. Saturn Work Shop (SWS) in Orbital Configuration

- c. Cold gas attitude control system for varying the attitude of the cluster;
- d. A solar array power source, mounting provision for the array and routing of power to an electrical power management and distribution system;
- e. Storage of cluster waste material.

The habitable portion of the Work Shop is shown in Figure B-6.

Six cold gas thrusters are mounted in two diametrically opposed locations on the aft end of the Work Shop to provide attitude control augmenting the three control moment gyros located in the Apollo Telescope Mount.

Solar arrays, consisting of two wings, are mounted outside the Work Shop to generate electrical power in conjunction with the power generated by the solar arrays mounted on the Apollo Telescope Mount.

A meteoroid shield deploys some six inches radially from the outer surface of the Work Shop to provide thermal radiation shielding and protection from meteoroids.

The Airlock Module provides a structural support for the modules located forward of the Work Shop, provides a habitable passageway between the Work Shop and the Multiple Docking Adapter, and contains an airlock for astronaut EVA activities.

The structural assembly consists of a tunnel section, a structural transition section for attachment to the MDA, truss assemblies for support of the tunnel section and gas supply containers, the deployment assembly for the ATM, and the Fixed Airlock Shroud (FAS).

Electrical power, environmental control, and communications support provided by the Airlock Module to Skylab includes the following:

- a. Eight rechargeable batteries with individual charger/regulator units provide a total average output capability of 3830 watts. The batteries are charged by the solar array on the Orbital Work Shop.
- b. An active/passive radiator thermal control system (16,000 Btu/hour heat rejection), umbilical provisions for extra-vehicular activity, and the cluster's 5 psia, nitrogen and oxygen atmosphere supply and air purification systems.
- c. VHF systems for data and for command, and also delayed-time (recorded) voice operating with redundant deployable antennas.

The Multiple Docking Adapter provides docking facilities for the Command

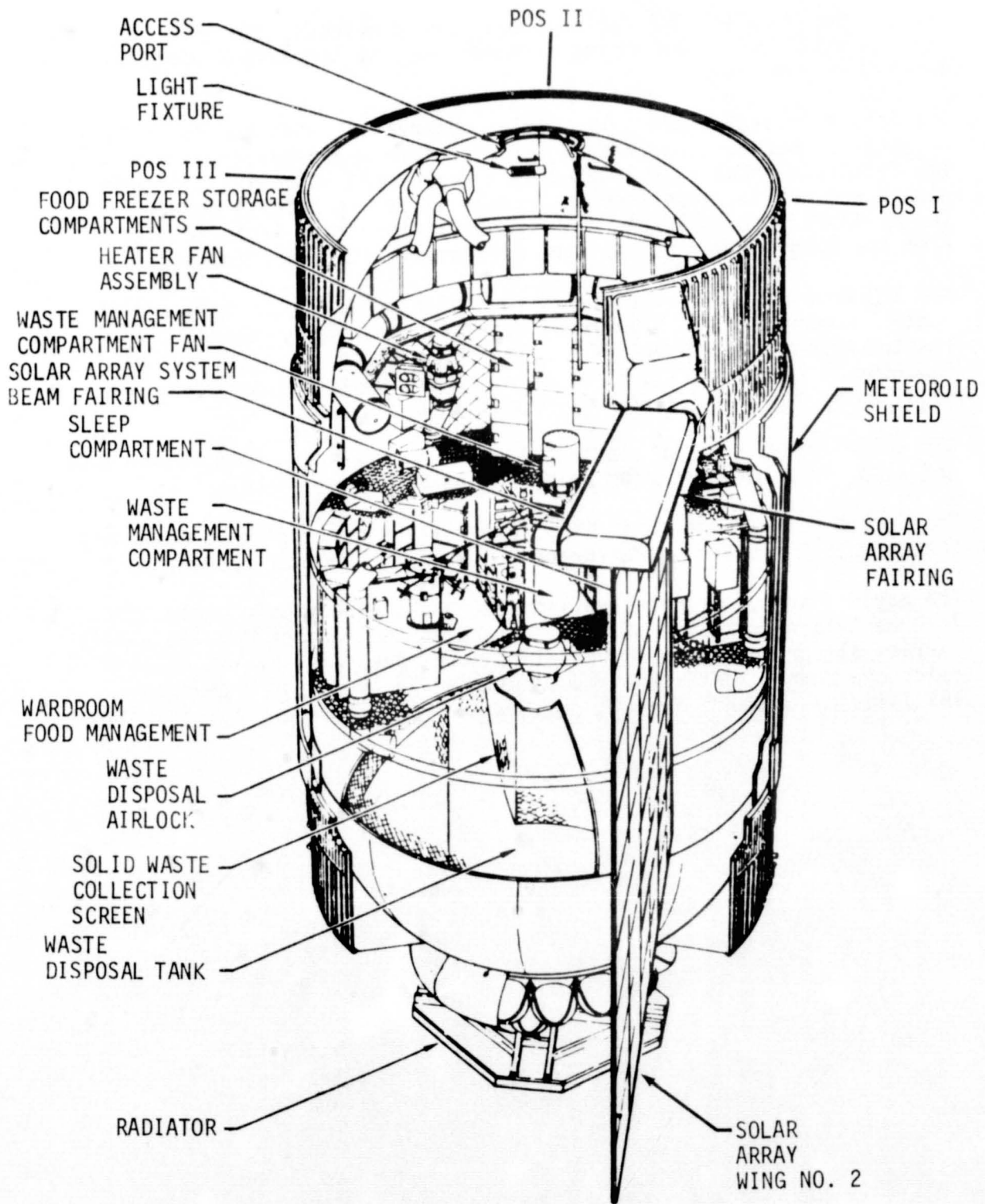


Figure B-6. Saturn Work Shop Habitable Area

and Service Module. Two docking ports are provided: the prime docking port is axially located on the forward end, and the backup port is located on the side.

The Apollo Telescope Mount is a solar observatory with the capability to observe, monitor, and record the structure and behavior of the Sun. The Telescope Mount is supported by a deployment assembly. Throughout launch and orbital insertion the module is stowed axially forward of the Multiple Docking Adapter. After orbit insertion it is rotated 90°, from the longitudinal axis of the cluster, to its operating position.

The ATM provides primary attitude control for the Skylab by means of control moment gyros. Experiment pointing control is provided, to a limited extent independent of the Skylab attitude, as a "fine tuning" function in order to assure the pointing orientation and accuracies required by the solar astronomy experiments.

ATM solar arrays provide electrical power to Telescope Mount systems, and also, in a power sharing role, to the Skylab as a whole.

The Saturn V Instrument Unit is structurally a part of the Saturn Work Shop and is discussed in Paragraph B.4.1 of the booster description.

The payload shroud provides environmental and aerodynamic protection for the Saturn Work Shop modules forward of the Airlock Module, and it carries all ground and powered flight loads generated by the Apollo Telescope Mount. Jettison is accomplished by pyrotechnic devices initiated by commands from the Instrument Unit after orbital insertion.

APPROVAL

SATURN V LAUNCH VEHICLE FLIGHT EVALUATION REPORT

SA-513, SKYLAB-1

By Saturn Flight Evaluation Working Group

The information in this report has been reviewed for security classification. Review of any information concerning Department of Defense or Atomic Energy Commission programs has been made by the MSFC Security Classification Officer. The highest classification has been determined to be unclassified.

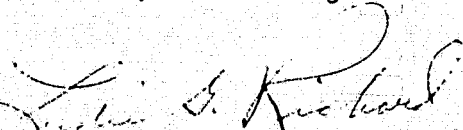


Stanley L. Fragge
Security Classification Officer

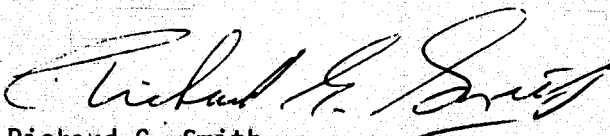
This report has been reviewed and approved for technical accuracy.



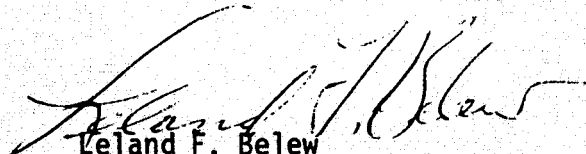
George H. McKay, Jr.
Chairman, Saturn Flight Evaluation Working Group



Herman K. Weidner
Director, Science and Engineering



Richard G. Smith
Saturn Program Manager



Leland F. Belew
Skylab Program Manager